FACULTY OF ENGINEERING
AND ARCHITECTURE

Development of Dry EEG Textrodes for Brain Activity Monitoring

Granch Berhe Tseghai

Doctoral dissertation submitted to obtain the academic degree of
Doctor of Materials Engineering

Supervisors

Prof. Lieva Van Langenhove, PhD - Benny Malengier, PhD

Department of Materials, Textiles and Chemical Engineering
Faculty of Engineering and Architecture, Ghent University

September 2022

GHENT
UNIVERSITY

FACULTY OF ENGINEERING AND ARCHITECTURE

Development of Dry EEG Textrodes for Brain Activity Monitoring

Granch Berhe Tseghai

Doctoral dissertation submitted to obtain the academic degree of
Doctor of Materials Engineering

Supervisors
Prof. Lieva Van Langenhove, PhD - Benny Malengier, PhD
Department of Materials, Textiles and Chemical Engineering
Faculty of Engineering and Architecture, Ghent University

September 2022

GHENT UNIVERSITY

ISBN 978-94-6355-628-6
NUR 971, 959
Wettelijk depot: D/2022/10.500/69

Members of the Examination Board

Chair

Prof. Em. Luc Taerwe, PhD, Ghent University

Other members entitled to vote

Prof. Evelien Carrette, PhD, Ghent University
Kinde Anlay Fante, PhD, Jimma University, Ethiopia
Prof. Patrick Segers, PhD, Ghent University
Prof. Jan Vanfleteren, PhD, Ghent University

Supervisors

Prof. Lieva Van Langenhove, PhD, Ghent University
Benny Malengier, PhD, Ghent University

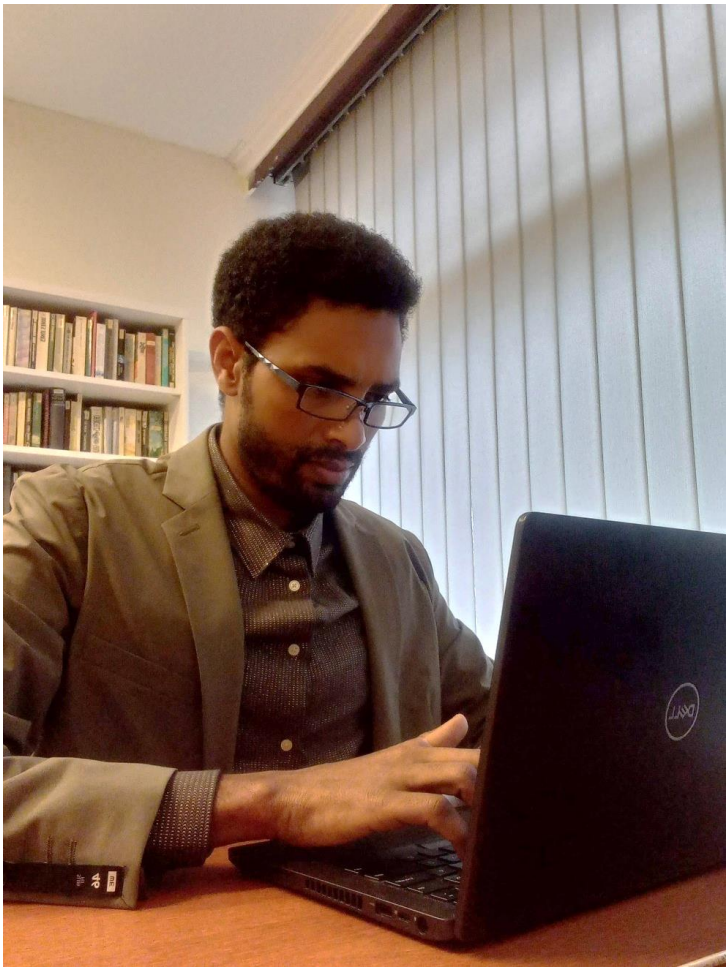

Spring 2022

Preface

I spent the whole of my childhood living in a community that frequently use the word 'Doctor" and "Engineer' to bless and applaud kids. In primary school, my teachers used to call me 'Doctor', although I had not much knowledge of what exactly doctors do. At that age, a 'Doctor' for me was, someone who examines the health of humans, so the medical doctor. Then in high school, one of my technical drawing teachers applauded me 'you will be a great engineer'. I was fine with the applause but later it occurred to me that then I would not be a 'doctor'. With this state of confusion, I joined a university and studied an engineering field. It was there I learned that the rank 'Doctor' is not given only to a medical doctor, but rather anyone who studied a Ph.D. is also called a Doctor.

While I was studying for a master's, Professor R. B. Chavan, my professor, wisely approached me out of class and dropped a suggestion. 'Granch', he said, 'after this master's, look for a Ph.D. abroad, you have the potential, and getting the opportunity would definitely make you a substantial researcher'. He even promised to guide me on how and to be a reference. After I completed my master's study, although I had to serve the then my home university, Wollo university as a lecturer, the advice of Prof R.B. Chavan always used to run in my mind. Fortunately, IUPPEPE posted a call for a homegrown Ph.D. supported by KU Leuven, Belgium, and Bahir Dar University. I applied and was selected. However, later KU Leuven announced that my research area was much more relevant at UGent, Department of Materials, Textiles and Chemical Engineering. Then, I was automatically transferred from KU Leuven to UGent. This gave me the opportunity to meet Professor Lieva Van Langenhove. After some email communications, I clearly let Professor Lieva Van Langenhove know that a homegrown Ph.D. would not suit me as the topic I was proposing was in smart materials where no one can give me advice, and lab facilities are not available domestically. The response of Professor Lieva Van Langenhove was, 'I let you come to Ghent and we will discuss'. The result of that process is here in front of you!

It was the start of a new adventure, research in a totally different culture! I was so eager and energetic to refine my topic for the Ph.D., thanks to Prof. Lieva Van Langenhove, who suggested I think of a smart textile application in health. I was fascinated by the theme. The next week, I came up with the topic EEG textrode for brain activity monitoring. After some technical questions and comments, Professor Lieva Van Langenhove gave me the go-ahead.

I understood that there was clearly a need for textile-based sensors. And, I engaged myself in literature reading and writing on a specific topic. Through time, I got the experience and the knowledge of how to develop EEG electrodes and of course EEG measurement techniques and tools. We bought an OpenBCI board with its kits. Under the close coaching of Dr. Benny Malengier, I produced a conductive fabric and developed an EEG electrode from it. Then, validation of the EEG electrodes was a challenge, but we developed ballistic gelatin and textile-based head phantom, so the challenge was perfectly tackled. However, this EEG textrode was flat and could not be used on a hairy scalp. Then, it was up to me to look for a solution for this. In the end, I found a conductive hook fabric!

Therefore, in this book, you find a comprehensive review of smart textiles, EEG textrodes, conductive fabric development, EEG electrode construction and validation, textile-based head phantoms, and an EEG cap that works without shaving the head. The EEG measurements were conducted at lab and clinic levels.

Granch Berhe Tseghai

Ghent, September 2022

Acknowledgment

I would like to express my sincere gratitude and appreciation to my supervisor Professor Dr. Ir. Lieva Van Langenhove, for suggesting to me an inspiring research theme and motivational start-up support and for providing me assistance throughout my research work. Most of all, she was by my side in difficult times, especially during the COVID-19 outbreak and the devastating war that Ethiopians and Eritreans waged on Tigray, where my family resides. On top of these, a deep family yearning was unthinkable to manage. However, I was fortunate to work with someone who felt my innermost feelings. Without her support, I would never have come this far.

I extend my special gratitude to my co-supervisor Dr. Benny Malengier, I can say my close friend, who helped me a lot in the experiments, paper write-ups, and this dissertation as well. I thank you, Benny, for being with me all the time when I was in need. His attitude, quick response, and unwavering work ethic were a source of inspiration for me. The speed with which the comments, edits, and proofreads came back to me was unbelievable. He also taught me software like Inkscape and Arduino IDE.

I'm also grateful to those who have made a noteworthy contribution to my work by providing necessary inputs as well as motivations from the Department of Materials, Chemicals, and Textile Engineering, Ghent University. I would also like to thank NASCERE and IUPEPPE projects and Global Minds Fund for the sponsorship that enabled me to study and complete the Ph.D. program. My gratitude also goes to Ingegno Maker Space owner, Dr. Maria-Cristina Ciocci, for providing me with digital fabrication laboratory facilities anytime I needed them.

I would also like to thank Prof. Dr. Evelien Carrette for her permission and guidance during EEG measurements at the Department of Neurology in UZ Gent, Ghent University Hospital.

I also have great respect and appreciation for Belgium as a whole; it was a safe haven for me at a time when my fellow Tigriyans in Ethiopia were being murdered, thrown into concentration camps, and starved to death as a result of government-sponsored, institutionalized genocide by Ethiopia and Eritrea. My parents and family, including my son, are unfortunately among the victims.

Exclusively, nothing would have been possible without my family, who have been providing me their perspicuous courage and potency; were close with me all the time from far, and unavoidably own a gigantic share of this success. Thanks for their indispensable patience living in a war region under total siege!!!

Unfortunately, I may have forgotten some people, but no doubt I appreciate what they have done! But I dedicate this book to my son, Natna, who has missed his father's natural embrace and care closely because of this Ph.D. study!

Granch Berhe Tseghai

Ghent, September 2022

To my son,

Natna Granch

Table of Contents

List Abbreviations

BCI	Brain-Computer Interface
BTCA	1,2,3,4-Butanetetracarboxylic Acid
CBT	Cognitive-Behavioral Therapy
CBs	Carbon Blacks
CE	Counter Electrode
CNTs	Carbon Nanotubes
CI	Confidence Interval
CP	Conductive Polymer
CPC	Conductive Polymer Composite
ECG	Electrocardiography
EEG	Electroencephalography
EMG	Electromyography
EOG	Electrooculography
ERSP	Event-Related Spectral Perturbation
fMRI	Functional Magnetic Resonance Imaging
FT-IR	Fourier Transform Infrared
GO	Graphene Oxide
GUI	Graphical User Interface
ITC	Inter-Trial Coherence
MEG	Magnetoencephalography
PDMS	Polydimethylsiloxane
PANI	Polyaniline
PEDOT	PEDOT:PSS Poly(3,4-ethylenedioxythiophene)
PET	Polyethylene Terephthalate
PLA	Polylactic Acid
PSD	Power Spectral density
PSS	Polystyrene Sulfonate
PPy	Polypyrrole
PU	Polyurethane
RE	Reference Electrode
SEM	Scanning electron Microscope
SFIT	Smart Fabrics and Interactive Textiles
SNR	Signal to Noise Ratio
SSMPS	Single-Source Multipolar Stimulation
SSPs	Stimuli Sensitive Polymers
WE	Working Electrode

List of Publications

A1 Publications

1. Granch Berhe Tseghai, Benny Malengier, Kinde Anlay Fante, and Lieva Van Langenhove. 2021. "Validating Poly(3,4-ethylene dioxythiophene) Polystyrene Sulfonate-Based Textile Electroencephalography Electrodes by a Textile-Based Head Phantom." *POLYMERS* 13 (21). doi.org/10.3390/polym13213629.

2. Granch Berhe Tseghai, Benny Malengier, Kinde Anlay Fante, and Lieva Van Langenhove. 2021. "Dry Electroencephalography Textrode for Brain Activity Monitoring." IEEE SENSORS JOURNAL 21 (19). doi.org/10.1109/JSEN.2021.3103411.

3. Granch Berhe Tseghai, Benny Malengier, Kinde Anlay Fante, and Lieva Van Langenhove. 2021. "A Long-Lasting Textile-Based Anatomically Realistic Head Phantom for Validation of EEG Electrodes." *SENSORS* 21 (14). doi.org/10.3390/s21144658

4. Granch Berhe Tseghai, Benny Malengier, Kinde Anlay Fante, Abreha Bayrau Bayrau Nigusse, and Lieva Van Langenhove. 2020. "Development of a Flex and Stretchy Conductive Cotton Fabric via Flat Screen Printing of PEDOT : PSS/PDMS Conductive Polymer Composite." *SENSORS* 20 (6). doi:10.3390/s20061742.

5. Granch Berhe Tseghai, Desalegn Alemu Mengistie, Benny Malengier, Kinde Anlay Fante, and Lieva Van Langenhove. 2020. "PEDOT : PSS-Based Conductive Textiles and Their Applications." SENSORS 20 (7). doi:10.3390/s20071881.

6. Granch Berhe Tseghai, Benny Malengier, Kinde Anlay Fante, and Lieva Van Langenhove. 2021. "The Status of Textile-Based Dry EEG Electrodes." *AUTEX RESEARCH JOURNAL* 21(1). doi.org/10.2478/aut-2019-0071.

7. Granch Berhe Tseghai, Benny Malengier, Kinde Anlay Fante, Abreha Bayrau Bayrau Nigusse, and Lieva Van Langenhove. 2020. "Integration of Conductive Materials with Textile Structures : An Overview." *SENSORS* 20 (23). doi:10.3390/s20236910.

8. Abreha Bayrau Nigusse, Benny Malengier, Desalegn Alemu Mengistie, Granch Berhe Tseghai, and Lieva Van Langenhove. 2020. “Development of Washable Silver Printed Textile Electrodes for Long-Term ECG Monitoring.” *SENSORS* 20 (21). doi:10.3390/s20216233.

9. Abreha Bayrau Nigusse, Desalegn Alemu Mengistie, Benny Malengier, Granch Berhe Tseghai, and Lieva Van Langenhove. 2021. “Wearable Smart Textiles for Long-Term Electrocardiography Monitoring—A Review.” SENSORS 21 (12). doi.org/10.3390/s21124174.

B2 Book Chapter

1. Granch Berhe Tseghai, Hasan Riaz Tahir, Benny Malengier, Carla Hertleer, Kinde Anlay Fante, Lieva Van Langenhove. 2022. “Smart Textiles.” *Reference Module in Biomedical Sciences, ELSEVIER*. ISBN 9780128012383. doi.org/10.1016/B978-0-12-822548-6.00121-7.

C1/P1 Publications

1. Granch Berhe Tseghai, Benny Malengier, Kinde Anlay Fante, and Lieva Van Langenhove. 2022. "Velcro Hook Electroencephalogram Textrode for Brain Activity Monitoring," *In 2022 IEEE International Conference on Flexible and Printable Sensors and Systems (FLEPS), 10-13 July 2022*. Austria, Vienna. IEEE Xplore. doi.10.1109/FLEPS53764.2022.9781526.
2. Granch Berhe Tseghai, Benny Malengier, Kinde Anlay Fante, and Lieva Van Langenhove. 2021. “A Dry EEG Textrode from a PEDOT:PSS/PDMS-coated Cotton Fabric for Brain Activity Monitoring.*” In 2021 IEEE International Conference on Flexible and Printable Sensors and Systems (FLEPS), 20-23 June 2021.* Manchester, United Kingdom. IEEE Xplore. doi.org/10.1109/FLEPS51544.2021.9469840.
3. Granch Berhe Tseghai, Benny Malengier, Kinde Anlay Fante, Abreha Bayrau Bayrau Nigusse, Bulcha Belay Etana, and Lieva Van Langenhove. 2020. “PEDOT:PSS/PDMS-Coated Cotton Fabric for ECG Electrode.*” In 2020 IEEE International Conference on Flexible and Printable Sensors and Systems (FLEPS), 16-19 August 2020.* Manchester, United Kingdom. IEEE Xplore. doi:10.1109/fleps49123.2020.9239526.

4. Granch Berhe Tseghai, Benny Malengier, Desalegn Alemu Mengistie, Kinde Anlay Fante, and Lieva Van Langenhove. 2020. “Knitted Cotton Fabric Strain Sensor by In-Situ Polymerization of Pyrrole.” In *7th International Conference on Intelligent Textiles & Mass Customisation 13-15 November 2019.* Marrakech, Morocco. Vol. 827. IOP Science. doi:10.1088/1757-899x/827/1/012041.

5. Malengier, Benny, Granch Berhe Tseghai, Maria-Cristina Ciocci, D A Mengistie, and Lieva Van Langenhove. 2020. "Functional Shoe for the Detection of Walking Pattern Anomalies." In *7th International Conference on Intelligent Textiles & Mass Customisation 13-15 November 2019.* Marrakech, Morocco. Vol. 827. IOP Science. doi:10.1088/1757-899x/827/1/012002.

6. Granch Berhe Tseghai, Benny Malengier, Kinde Anlay Fante, and Lieva Van Langenhove. 2021. "PEDOT:PSS/PDMS-Coated Cotton Fabric for Strain and Moisture Sensors." In *International Conference on the Challenges, Opportunities, Innovations and Applications in Electronic Textiles (E-Textiles 2020), 4 November 2020.* Virtual Venue, UK. PROCEEDINGS. Vol. 68. MDPI. doi:10.3390/proceedings2021068001.

7. Granch Berhe Tseghai, Benny Malengier, Abreha Bayrau Bayrau Nigusse, and Lieva Van Langenhove. 2018. "Development and Evaluation of Resistive Pressure Sensors from electro-conductive Textile Fabric." In *Proceedings of the Second International Forum on Textiles for Graduate Students*, 651–657. Tianjin, Xiqing District, China, 300384: Tianjin Polytechnic University.

8. Hasan Riaz Tahir, Granch Berhe Tseghai, Benny Malengier, and Lieva Van Langenhove. 2022. "Self-Powered PEDOT:PSS-PDMS-Printed Textile Woven Textile for Moisture Sensing." In *Proceedings of the 7th International Symposium : Technical Textiles : Present and Future 12 November 2021.* Iasi, Romania. SCIENDO. doi:10.2478/9788366675735-001.

9. Hasan Riaz Tahir, Benny Malengier, Granch Berhe Tseghai, and Lieva Van Langenhove. 2022. "Sensing of Body Movement by Stretchable Triboelectric Embroidery Aimed at Healthcare and Sports Activity Monitoring." In *3rd International Conference on the Challenges, Opportunities, Innovations and Applications in Electronic Textiles (E-Textiles 2021), 3–4 November 2021.* Manchester, UK. *ENGINEERING PROCEEDINGS.* Vol. 15. MDPI. doi.org/10.3390/engproc2022015004.

Summary

Nowadays, textile materials are relied upon to exhibit extra functionalities other than comfort and durability following the movement of electronic and computerized correspondence. Stretchable hardware is constructed from yarns, fabric textures, or other articles of clothing and has received extensive interest. A sensor is a device that acquires a physical quantity and converts it into a signal suitable for processing (mechanical, electrical, optical) to provide a usable output in response to a specific stimulus, and textile-based sensors are a booming buzzword in the field of smart textile materials.

The advancement in smart materials makes researchers seek smart textiles for wearable health monitoring due to their matching flexibility, being lightweight, and the possibility of washing. An e-textile can be developed by applying a conductive component on the surface of a textile substrate via plating, printing, coating, and other surface techniques, or by producing a textile substrate from metals and inherently conductive polymers via the creation of fibers and construction of yarns and fabrics with these. In addition, conductive filament fibers or yarns can be also integrated into conventional textile substrates during the fabrication like braiding, weaving, and knitting or as a post-fabrication of the textile fabric via embroidering.

As a conductive component, metal wires and conductive compounds can be employed. However, applying a pristine conductive component onto a textile structure results in a stiff fabric. The demand to produce electrically conductive fabrics that own normal characteristics of textile materials led to the emergence of conductive polymers and their composites.

The conductive polymer composites also increase the attachment of the conductive polymer to the textile, thereby increasing durability to washing and mechanical actions. A lot of conductive textiles have been used for the development of sensors, actuators, antennas, interconnections, energy harvesting, and storage devices.

The demand to produce flexible and lightweight electronics caused a rapid development in electronics technology and material science which in turn led to the emergence of smart textiles for healthcare applications. People are demanding to take active control of their health without compromising their comfort. Coming up with wearable health monitoring e-textiles would have a magnificent impact to monitor physiological activities such as electrocardiography (ECG), electroencephalography, electromyography, etc.

Therefore, it is sensible to develop a textile that must conduct electricity and owns the characteristics of normal textile materials.

As the aim of this dissertation was to develop a textile-based EEG electrode, a comprehensive review was made on the status of the textile-based dry EEG electrodes. Electroencephalogram (EEG) is the bio-potential recording of electrical signals generated by brain activity. It is useful for monitoring sleep quality and alertness, clinical applications, diagnosis, and treatment of patients with epilepsy and other neurological disorders, as well as continuous monitoring of tiredness/alertness in the field.

For this dissertation, the conductive polymer complex poly(3,4-ethylene dioxythiophene):polystyrene sulfonate (PEDOT:PSS), the most explored conductive polymer for conductive textiles applications, has been used. Since PEDOT:PSS is readily available in water dispersion form, it is convenient for roll-to-roll processing which is compatible with the current textile processing applications. The conductivity of PEDOT:PSS can be enhanced by several orders of magnitude using processing agents. However, neat PEDOT:PSS lacks flexibility and stretchability for wearable electronics applications. One way to improve the mechanical flexibility of conductive polymers is by making a composite with commodity polymers such as PDMS which have high extensibility and biocompatibility. So, conductive fabrics were produced by PEDOT:PSS/PDMS conductive polymer composite coating on a cotton fabric via screen printing.

From the experimental work, it was observed that the mechanical and electrical properties highly depend on the proportion of the polymers, which opens a new window to produce PEDOT:PSS-based conductive fabric with distinctive properties for different application areas. The bending length analysis proved that the flexural rigidity was lower with a higher PDMS to PEDOT:PSS ratio while tensile strength was increased. The SEM test showed that the smoothness of the fabric was better when PDMS is added compared to PEDOT:PSS alone. Fabrics with electrical resistance from 67.23 Ω/sq to 90.8 kΩ/sq have been obtained by varying the PDMS to PEDOT:PSS ratio. Moreover, the resistance increased with extension and washing. However, the change in surface resistance drops linearly at a higher PDMS to PEDOT:PSS ratio. As a proof of concept, the conductive fabrics were used to construct textile-based strain, moisture, and biopotential sensors depending upon their respective surface resistance.

As aforementioned, amongst the sensors, the main objective of this dissertation was to explore a washable and flexible textile-based dry EEG electrode that can detect the activities in the brain. This has been developed, and in-depth work was done on the development of PEDOT:PSS/PDMS-printed cotton fabric EEG

electrodes. The EEG electrodes were constructed from an electrically conductive cotton fabric with 67.23 Ω/sq. On human measurement, the skin-to-electrode impedance and signal quality were found comparable with commercial dry electrodes, which opens the door for long-term EEG monitoring. Moreover, the electrode can give clear and reliable EEG signals up to 15 washing cycles, 60 bending cycles, 10 multiple uses, and 8 hours of continued use.

Furthermore, an anatomically realistic long-lasting, and a low-weight textile-based head phantom was developed to validate the textile-based electrodes as keeping the human brain activity constant is hardly possible. A synthetic sine wave was generated using a function generator and digital oscilloscope injected into the phantom and measured back resulting in a performance similar to the commonly used ballistic gelatin-based head phantoms. While the textile-based phantom was designed for EEG, it can also be adapted to ECG, EMG, and other related studies as well. On the textile-based head phantom test, the PEDOT:PSS/PDMS-based electrodes gave a clear EEG signal similar to a commercial dry electrode.

In general, this work explored a textile-based EEG electrode from a PEDOT:PSS/PDMS-printed electrically conductive cotton fabric. However, it works only in a hair-free region and we still need to find ways in order to use it in the hairy part of the surface head. Besides, the performance stability of the electrode over time needs further improvement. For that reason, in this study, novel electrodes that can detect quality EEG signals without the need for conductive gels or skin treatments, or shaving the hair were fabricated from an electrically conductive hook fabric with 1 Ω/sq. A knitted net EEG bridge cap features a shutter mechanism that separates the hair and ensures good contact between the hook fabric electrode and the scalp, has also been constructed. Moreover, the electrode gives clear and reliable EEG signals up to 100 washing cycles and its functional performance is stable with time. In this way, the aim of this Ph.D. study was realized.

Samenvatting

Tegenwoordig wordt erop vertrouwd dat textielmaterialen extra functionaliteiten vertonen naast comfort en duurzaamheid, in analogie met de beweging van steeds meer elektronische en geautomatiseerde correspondentie. Rekbare hardware is gemaakt van garens, weefselstructuren of kledingstukken en heeft veel belangstelling gekregen. Een sensor is een apparaat dat een fysieke grootheid meet en omzet in een signaal dat geschikt is voor verwerking (mechanisch, elektrisch, optisch) om een bruikbare output te leveren als reactie op een specifieke stimulus, en op textiel gebaseerde sensoren zijn een booming modewoord op het gebied van slimme textielmaterialen.

De vooruitgang in slimme materialen zorgt ervoor dat onderzoekers op zoek gaan naar slim textiel voor draagbare gezondheidsmonitoring vanwege hun bijpassende flexibiliteit, laag gewicht en mogelijkheid om te wassen. Een e-textiel kan worden ontwikkeld door een geleidende component op het oppervlak van een textielsubstraat aan te brengen via bedrukken, coaten en andere oppervlaktetechnieken, of door een textielsubstraat te produceren uit metalen en inherent geleidende polymeren via het creëren van vezels en constructie van garens en stoffen hiermee. Bovendien kunnen geleidende filamentvezels of garens ook worden geïntegreerd in conventionele textielsubstraten tijdens de fabricage zoals tijdens vlechten, weven en breien of als een postfabricage van het textielweefsel via borduren.

Als geleidende component kunnen metaaldraden en geleidende verbindingen worden gebruikt. Het aanbrengen van een ongerepte geleidende component op een textielstructuur resulteert echter in een stugge stof. De vraag om elektrisch geleidend textiel te produceren dat de normale eigenschappen van textielmaterialen bezit, leidde tot de opkomst van geleidende polymeren en hun composieten.

De geleidende polymeercomposieten vergroten ook de hechting van het geleidende polymeer aan het textiel, waardoor de duurzaamheid bij wassen en mechanische acties wordt vergroot. Veel geleidend textiel is gebruikt voor de ontwikkeling van sensoren, actuatoren, antennes, verbindingen, energieoogst en energieopslagapparaten.

De vraag om flexibele en lichtgewicht elektronica te produceren zorgde voor een snelle ontwikkeling in elektronicatechnologie en materiaalwetenschap, wat op zijn beurt leidde tot de opkomst van slim textiel voor toepassingen in de gezondheidszorg. Mensen eisen actieve controle over hun gezondheid zonder afbreuk te doen aan hun comfort. Het bedenken van draagbaar e-textiel voor

gezondheidsmonitoring zou een geweldige impact hebben om fysiologische activiteiten zoals elektrocardiografie (ECG), elektro-encefalografie, elektromyografie, enz., textielmaterialen.

Aangezien het doel van dit proefschrift was om een op textiel gebaseerde EEG-elektrode te ontwikkelen, werd een uitgebreid overzicht gemaakt van de status van de op textiel gebaseerde droge EEG-elektroden. Elektro-encefalogram (EEG) is de bio-potentiële registratie van elektrische signalen die worden gegenereerd door hersenactiviteit. Het is nuttig voor het bewaken van de slaapkwaliteit en alertheid, klinische toepassingen, diagnose en behandeling van patiënten met epilepsie en andere neurologische aandoeningen, evenals het continu bewaken van vermoeidheid/alertheid in het veld.

Voor dit proefschrift is het geleidende polymeercomplex poly(3,4-ethyleendioxythiofeen): polystyreensulfonaat (PEDOT:PSS), het meest onderzochte geleidende polymeer voor geleidende textieltoepassingen, gebruikt. Aangezien PEDOT:PSS gemakkelijk verkrijgbaar is in de vorm van waterdispersie, is het handig voor rol-naar-rol verwerking die compatibel is met de huidige textielverwerkingstoepassingen. De geleidbaarheid van PEDOT:PSS kan met verschillende grootteordes worden verbeterd met behulp van verwerkingsstoffen. De pure PEDOT:PSS mist echter flexibiliteit en rekbaarheid voor draagbare elektronische toepassingen. Een manier om de mechanische flexibiliteit van geleidende polymeren te verbeteren, is het maken van een composiet met basispolymeren zoals PDMS die een hoge rekbaarheid en biocompatibiliteit hebben. Er werden daarom geleidende stoffen geproduceerd door PEDOT:PSS/PDMS geleidende polymeercomposietcoating op een katoenen stof aan te brengen via zeefdruk.

Uit het experimentele werk werd waargenomen dat de mechanische en elektrische eigenschappen sterk afhangen van het aandeel van de polymeren, wat een nieuw venster opent om op PEDOT:PSS gebaseerde geleidende stof te produceren met onderscheidende eigenschappen voor verschillende toepassingsgebieden. De analyse van de buiglengte toonde aan dat de buigstijfheid lager was met een hogere PDMS tot PEDOT:PSS-verhouding, terwijl de treksterkte toenam. De SEM-test toonde aan dat de gladheid van de stof beter was wanneer PDMS werd toegevoegd in vergelijking met PEDOT:PSS alleen. Stoffen met een elektrische weerstand van 67,23 Ω/sq tot 90,8 kΩ/sq zijn verkregen door de PDMS-naar-PEDOT:PSS-verhouding te variëren. Bovendien nam de weerstand toe met extensie en wassen. De verandering in oppervlakteweerstand daalt echter lineair bij hogere PDMS tot PEDOT:PSS-verhouding. Als proof of concept werden de geleidende stoffen gebruikt om op

textiel gebaseerde spannings-, vocht- en biopotentiaalsensoren te construeren, afhankelijk van hun respectieve oppervlakteweerstand.

Zoals eerder vermeld, was het hoofddoel van dit proefschrift het onderzoeken van een wasbare en flexibele op textiel gebaseerde droge EEG-elektrode die de activiteiten in onze hersenen kan detecteren, en er is diepgaand werk verricht aan de ontwikkeling van PEDOT:PSS/PDMS afgedrukt katoenen stof EEG-elektroden. De EEG-elektroden waren gemaakt van een elektrisch geleidende katoenen stof met 67,23 Ω/sq. Bij menselijke metingen werden de huid-naar-elektrode-impedantie en signaalkwaliteit vergelijkbaar gevonden met commerciële droge elektroden wat de deur opent voor langdurige EEG-monitoring. Bovendien kan de elektrode heldere en betrouwbare EEG-signalen geven tot 15 wascycli, 60 buigcycli, 10 meervoudig gebruik en 8 uur continu gebruik.

Bovendien werd een anatomisch realistische, duurzame en lichtgewicht op textiel gebaseerde hoofdfantoom ontwikkeld om de op textiel gebaseerde elektroden te valideren, aangezien het nauwelijks mogelijk is om het menselijk brein stabiel te houden. Een synthetische sinusgolf werd in het fantoom geïnjecteerd en teruggemeten, wat resulteerde in een prestatie die vergelijkbaar was met de veelgebruikte op ballistische gelatine gebaseerde hoofdfantomen. Hoewel het op textiel gebaseerde fantoom is ontworpen voor EEG, kan het ook worden aangepast aan ECG, EMG en andere gerelateerde onderzoeken. Bij de op textiel gebaseerde hoofdfantoomtest gaven de PEDOT:PSS/PDMS-gebaseerde elektroden een duidelijk EEG-signaal, vergelijkbaar met een commerciële droge elektrode.

Als conclusie onderzocht dit werk een op textiel gebaseerde EEG-elektrode van een PEDOT:PSS/PDMS-gecoate elektrisch geleidende katoenen stof. Het werkt echter alleen in een haarvrij gebied en we moeten dus nog manieren vinden om het op harige plaatsen te gebruiken. Bovendien moet de prestatiestabiliteit van de elektrode in de loop van de tijd verder worden verbeterd. Om die reden zijn in deze studie nieuwe elektroden die hoogwaardige EEG-signalen kunnen detecteren zonder de noodzaak van geleidende gels of huidbehandelingen en het scheren van het haar vervaardigd uit een elektrisch geleidende klittenbandhaak met 1 Ω/sq. Er is ook een gebreid net EEG-brugkapje met een sluitermechanisme dat het haar scheidt en zorgt voor een goed contact tussen de klittenbandhaakelektrode en de hoofdhuid. Bovendien geeft de elektrode duidelijke en betrouwbare EEG-signalen tot 100 wascycli en zijn functionele prestaties stabiel in de tijd. Op deze manier werd het doel van dit promotieonderzoek gerealiseerd.

1. Introduction

This chapter gives a general introduction to the doctoral dissertation, which consists of three sections i.e. background, the objective of the doctoral research, and the dissertation outline. In the background section, the motivation and relevance of the doctoral research thesis are introduced. The second section describes the general and specific objective of the doctoral research. And the last section is the dissertation outline.

Table of Contents

1.1. Background

The use of textiles has been essential to daily life since prehistoric times. Traditional textiles are composed of natural or synthetic fibers and filaments with certain properties and limited functionalities. Looking attractive and fitting comfortably are the basic requirements of textiles dictated by fashion. Recently, textiles are expected to exhibit additional functionalities besides making people warm or cool and comfortable in line with the progression of electronics and digital communication. This led to the development of electronic textiles (E-textiles) or smart textiles. E-textiles consist of fabric that provides advanced and special functions in the form of electronic features or interconnections [1], [2].

E-textiles can be categorized into two types [3], classical and integrated, where the electronic components are embedded into garments and directly integrated into textile substrates respectively. E-textiles have received significant attention as a new technology that can provide added value to existing wearable applications, including wearable sensors [4]. They have attracted attention in technical and socio-economic fields because of their ability to sense and respond to environmental stimuli [3], [1]. These textiles found ordinary, special, and critical applications almost in every sphere of human activities, serving as mechanically sensitive sensors, electronic skin, flexible transistors, and being used for energy harvesting and storage devices [1].

The recent advances in flexible and printed electronics have led to the widespread availability of new conductors that can be well suited to flexible, stretchable substrates like textiles. Smart textiles are good vehicles when unobtrusive sensing of brain activity, heart rate, breathing, muscle activity, temperature and motion tracking, etc. is required. They are the perfect mediums for the integration of electronics as everyone is in contact with textiles. Literature in the field of smart textiles indicates that smart textile materials and their application will drastically boom soon as the potential of textiles has been increasing with the emergence of new materials and innovative processing technologies. Flexible and lightweight sensors, (inter)connections, actuators, powering components, data processing units, and antennas are among the more eye-catching smart textiles components.

Clothes equipped with extra electronic components can improve the safety of the individual and ensure live monitoring of the health, location, and environment of the wearer [5]. As a result, it is gaining special attractiveness and profound potential in vital fields like healthcare, defense, space, and rescue operations.

Smart textiles are produced by direct integration of electronic and/or functional materials into textile end products. Ideally, such materials should be lightweight, robust, inexpensive, flexible, and easily integrable. Additional requirements are enforced when it comes to wearable and flexible applications. For example, in body-centric applications, the functional components must be biocompatible and compliant with health and safety requirements.

Various areas require smart textiles for critical usage. An example is epileptic patients on which the WHO February 2018 updated Fact Sheets indicated that epilepsy is one of the most common neurological diseases on the globe with nearly 50 million patients [6]. Epileptic patients should be equipped with clothes that sense the disorder and give a warning alarm to the victim before a seizure to be able to look for a healthier place and to communicate to the victim's family or doctor. Electronic functional components like sensors, actuators, conductive tracks, and antennas must be used to detect the critical condition of the patient and to communicate with whom it concerns. From the comfort and performance point of view, these should be an integral part of the fabric, flexible enough, and robust.

Neurological disorders that affect the brain and the central and autonomic nervous are, doubtlessly, among the most frightening illnesses that human beings face. One approach to treating primarily behavioral neurological issues is cognitive-behavioral therapy (CBT) which focuses on reorienting a patient's thoughts and behavior related to their disability. CBT has shown a considerable effect in the treatment of anxiety, mood disorders, and a range of primarily psychogenic impairments [7]. Another approach to treatment for brain disorders is medication. As a medication, for instance for epilepsy, anti-epileptic drugs (AEDs) are used. The effect of the drugs in pregnancy, interaction with alcohol, a consequence of overdose, and addiction become the main problems associated with neurological disease treatment. Developing an Electroencephalography (EEG) device that monitors brain activity would be a good way to assist the patients.

Electroencephalography relies heavily on so-called wet electrodes (e.g. Ag/AgCl electrodes) which require gel application to reduce skin-to-electrode impedance mismatch and skin preparation to operate properly. Skin preparation and gel application are time-consuming when a high number of electrodes are required. Wet electrodes need to be kept "wet" for optimal signal quality making it a very time-consuming and very specific task for only specifically trained nurses limiting the EEG recording to a hospital situation where this can be monitored and maintained over time. In extreme circumstances, very long-term monitoring

with cup-electrodes, the electrodes might sometimes leave a small scar, however, in most circumstances, EEG with wet-electrodes is a non-invasive, non-harmful investigation. But there are reports in the literature indicating continuous use of wet electrodes would cause skin irritation and leave skin lesions [8]. The application of conductive gel or paste may also cause an allergic reaction in some users. Thus, the demand for more comfortable and user-friendly electrodes has led to the development of an increasing number of dry electrodes that can overcome the limitations of wet electrodes.

The ideal monitoring device should be safe and easy to use for patients, families, and medical staff. It must be comfortable for patients, especially during sleep, and thus preferably wireless, miniaturized, and lightweight. If electrodes are used, they must be as small and few as possible since a significant percentage of patients are not willing to wear electrodes on a long-term basis[9]. The device should be unobtrusive and discrete. Uncomfortable cables, electrodes, lights, buttons, and sounds should be avoided as this disturbs the patient and family, even more so in the long term.

In addition to limited signal quality, some common limitations of the previously developed textile EEG electrodes and why outcomes remained on a shelf only as published research are inadequate flexibility, weight, and washability. This is mainly because metal-based conductors were used to coating the textile fabric. Therefore, the main objective of this work is to develop a textile-based EEG electrode from flexible conductive polymer composites and conductive hook textile fabric (such as sold by the commercial brand Velcro®).

1.2. The Objective of the Doctoral Research

The scientific objective of the Ph.D. study was to develop machine-washable and flexible EEG textrodes PEDOT:PSS/PDMS-printed cotton and conductive hook fabrics having good impedance match, flexibility, and washability that are used to measure brain activity.

Thus, the research work comprises;

- Developing a flexible PEDOT:PSS/PDMS-printed conductive cotton fabric via screen printing
- Designing and constructing a dry EEG textrode from PEDOT:PSS/PDMS-printed conductive cotton fabric and hook fabric, and comparing the two approaches

- Studying the robustness and reliability of the EEG textrodes on human and head phantom
- Designing an EEG cap from a conductive hook fabric for brain activity monitoring

In the end, this must lead to the possibility of the development of a machine washable and flexible dry EEG textrode capable of collecting brain waves comparable to commercially available dry EEG electrodes.

1.3. Sustainability Concerns of the Doctoral Research

Smart textiles are a boon and new niche products that are attaining wider market potential. Sustainable development in smart textiles gives future generations more capacity and opportunity to meet their requirements. From the perspectives of materials and product lifecycles, user behavior, and sociocultural and ethical considerations, this section will provide background information on the sustainability concerns and prospects for smart textiles in general and textile-based EEG electrodes in particular.

This research output has a great contribution to the critical need for using novel smart textiles. For example, the EEG textrodes for assisting brain disorder diseases will have a large benefit to the patients and their caretakers by monitoring live communication regarding the condition of the patient. Since the functional components are flexible, lightweight, and robust enough, the comfort of the user is not affected. The smart headband with EEG-textrode which is the outcome of the research might also be used for other brain disorders patients like dystonia, or sleep monitoring in normal cases, raising the potential benefit of the research. One way or the other, the EEG textrode would be incorporated to detect brain disorders at an early stage which in turn would minimize the probability of serious injury and death due to accidental seizure and falling. This has direct relevance with one of the UN SDG 3 (United Nations Sustainable Development Goals #Envision2030: Goal 3) targeted to ensure healthy lives and promote well-being for all of all ages.

Screen printing promises to be a low-cost technology allowing customized designs, as well as production close to the customer. Printing of electronic components on textiles and particularly for smart textiles is very promising. It provides the flexibility that is required for simpler textile configurations. The use of screen printing will have an environmental benefit by substituting the conventional techniques like weaving, knitting, and embroidery on which etching

is a mandatory process to obtain smooth wearable electrons. During etching small components are introduced which contribute a lot to environmental pollution. Thus, introducing printing techniques for this purpose will eliminate the aforementioned problems which are relevant to the UN SDG 12 targeted to ensure sustainable consumption and production patterns (United Nations Sustainable Development Goals #Envision2030: Goal 12) and also to UN SDG 9 (United Nations Sustainable Development Goals #Envision2030: Goal 9) focused on building resilient infrastructure, promoting inclusive and sustainable industrialization and fostering innovation

The raw material from which the EEG textrodes were constructed, as well as their structural design, set them apart from other commercial electrodes. Furthermore, they provide extra functions and applications thereof. Optimized EEG textrodes would give a sustainable benefit over commercial EEG electrodes. As the dissertation focuses on the development of textile-based EEG textrodes that replaces commercial wet and dry electrodes, their sustainability concerns can be discussed putting the following issues under consideration.

Comfort factor: Hundreds of electrodes are used during EEG measurement. Placing hundreds of heavy and stiff structure metal disks/cups, commercial EEG electrodes, might be used only at the clinical level but are not comfortable for long-term monitoring. Whereas textile-based electrodes are flexible and light in weight which makes them much more comfortable than heavy commercial dry EEG electrodes. At the clinical level, a conductive adhesive gel is used to bridge the EEG electrode with the skin/scalp. To apply the gel, skin preparation and scratching steps are compulsory which in turn consumes more time. In addition, the scratching of skin leaves skin lesions. Users may also be allergic to the gel. The gel must be washed off afterward. These novel textrodes completely avoid the use of conductive gel. The textrodes own normal textile substrate characteristics and thus comfort is not compromised.

Avoids shaving of hair: The velcro hook EEG textrode has hooks that keep it in the right area where it is placed as the hooks are entangled with the hair. The end tips of the hook stay in contact with the skin/scalp. Therefore, EEG measurement is performed without shaving the hair. Apparently, this is the factor that makes velcro hook EEG textrodes advantageous even over the textile-based PEDOT:PSS/PDMS-printed cotton EEG electrodes.

Monitoring Longevity: Although commercial dry flat electrodes are made of metal, their weight and rigidity make them unsuitable for portable purposes. The dry flat electrodes do not work on the hairy region. Although commercial

spike/comb electrodes made of metals and conductive plastics were later introduced for use in the hairy area, they are still heavy in weight and rigid in a structure that makes them unsuitable for portable purposes. In addition, they penetrate the skin and can cause infections. The Velcro hook electrode prevents the hair from shaving. In addition, it is light and flexible with a textile softness, making it a suitable candidate for long-term monitoring for wearable purposes.

Integrable to textile structures: The hook fabric electrodes can be easily integrated into textile structures, for example by sewing. Therefore, the electrodes are suitable for wearable purposes where people need them for their daily activities. The electrodes are also washable.

Versatile application: The textrodes can be used as EEG, ECG, or EMG electrodes. Moreover the PEDOT:PSS/PDMS-printed cotton EEG textrode can be used even as strain and moisture sensors as included in Chapter 4. The textrodes could also be used on humans and animals. This versatile application would certainly make them useful over existing electrodes.

Lesser environmental burden: Since a large proportion of their constituent is textiles with the potential to evolve from biodegradable substances and conductive polymers, the introduction of such textile-based electrodes would play a role in minimizing the burden of metallic electrode waste. Moreover, as gels are avoided, there will be gel leftovers and gel packages to be disposed to the environment.

Economic Factor: The price of a wet Gold cup EEG electrode is 4.5 Euro/electrode and the dry Silver/Silver chloride flat electrode is sold at 1.5 Euro/electrode. The price of A dry Silver/Silver chloride comb electrode is 1.5 Euro/electrode. However, the velcro hook EEG textrode can be produced at lower than 1 Euro/electrode. The PEDOT:PSS/PDMS-printed cotton EEG electrode can be produced at 0.5 Euro/electrode. For instance considering 25% profit, the selling price for the hook fabric and PEDOT:PSS/PDMS-printed cotton EEG electrodes would be 1.25 and 0.65 Euro/electrode. Therefore, the selling price would doubtlessly be cheaper than commercial electrodes. In addition, as a textile-based electrode, the EEG textrodes are simple to construct and give you more freedom to easily design the size and shape you want. Therefore, no special molding devices are required. Apart from that, the avoidance of gel and shaving of the hair avoid extra costs.

1.4. Thesis Outline

This Ph.D. dissertation is organized into 8 chapters as follows:

Chapter 1 is the general introduction of the doctoral research, including the background, objective of the doctoral research, and dissertation outline.

Chapter 2 describes a brief overview of smart textiles and addresses the conductive and responsive materials that can be used to develop smart textiles and the recent development of integration techniques into textile materials structure for smart textile applications. The review provides information on smart textile applications thereof, and prospects.

Chapter 3 addresses a brief overview of textiles-based EEG electrodes. The review gives information on the benefits of developing textile-based EEG electrodes.

Chapter 4 presents the experimental works on how to develop a conductive knitted cotton fabric with PEDOT:PSS/PDMS conductive polymer composite via screen printing. It also gives a brief overview of PEDOT:PSS/PDMS-based textiles and its application thereof in smart textiles, especially for bio-potential sensors.

Chapter 5 concerns developing an EEG electrode from a PEDOT:PSS/PDMS-printed cotton fabric. The performance of the textrode against a commercial dry electrode is studied. It also addresses the robustness and reliability performance stability of PEDOT:PSS/PDMS-printed cotton fabric. The effect of washing, bending, multiple uses, continuous uses, shape, and size are covered.

Chapter 6 addresses the validation of PEDOT:PSS/PDMS-printed cotton fabric EEG electrodes. A textile-based head phantom was introduced for the first time and compared with a ballistic gelatin head phantom. This chapter, thus, conveys an analysis of the performance of textile-based electrodes tested on a textile-based head phantom.

Chapter 7 focuses on the development of an EEG textrode from a conductive hook textile fabric for brain activity monitoring without shaving the head. A knitted net bridge EEG electrode was constructed to hold the hook fabric electrodes and indicate the position where the electrodes shall be placed.

Chapter 8 is the general conclusion that is derived from the previous chapters and presents future works.

Bibliography

[1] V. Kaushik *et al.*, "Textile-Based Electronic Components for Energy Applications: Principles, Problems, and Perspective," *Nanomaterials*, vol. 5, no. 3, pp. 1493–1531, 2015, doi: 10.3390/nano5031493.

[2] W. Weng, P. Chen, S. He, X. Sun, and H. Peng, "Smart electronic textiles," *Angew. Chem. - Int. Ed.*, vol. 55, no. 21, pp. 6140–6169, 2016, doi: 10.1002/anie.201507333.

[3] K. Cherenack, C. Zysset, T. Kinkeldei, N. Münzenrieder, and G. Tröster, "Woven electronic fibers with sensing and display functions for smart textiles," *Adv. Mater.*, vol. 22, no. 45, pp. 5178–5182, 2010, doi: 10.1002/adma.201002159.

[4] C. M. Choi, S. N. Kwon, and S. I. Na, "Conductive PEDOT:PSS-coated poly-paraphenylene terephthalamide thread for highly durable electronic textiles," *J. Ind. Eng. Chem.*, vol. 50, pp. 155–161, 2017, doi: 10.1016/j.jiec.2017.02.009.

[5] S. B. Roshni, M. P. Jayakrishnan, P. Mohanan, and K. P. Surendran, "Design and fabrication of an E-shaped wearable textile antenna on PVB-coated hydrophobic polyester fabric," *Smart Mater. Struct.*, vol. 26, no. 10, p. 105011, Oct. 2017, doi: 10.1088/1361-665X/aa7c40.

[6] World Health Organization, *Epilepsy: a public health imperative*. 2019. Accessed: Feb. 20, 2021. [Online]. Available: https://www.who.int/mental_health/neurology/epilepsy/report_2019/en/

[7] American Addiction Centers, "Cognitive Behavioral Therapy Techniques and Addiction Treatment," Mar. 10, 2020. https://americanaddictioncenters.org/cognitive-behavioral-therapy

[8] A. Schulze-Bonhage *et al.*, "Views of patients with epilepsy on seizure prediction devices," *Epilepsy Behav.*, vol. 18, no. 4, pp. 388–396, Aug. 2010, doi: 10.1016/j.yebeh.2010.05.008.

2. Smart Textiles

This chapter presents a comprehensive overview of smart textiles and the integration techniques of conductive and responsive materials with a textile structure. Many textile-based sensors are addressed for each integration technique. The applications and prospects of smart textiles are also discussed.

This chapter is redrafted from a published book chapter and journal papers:

G.B. Tseghai, H.R. Tahir, B. Malengier, C. Hertleer, K.A. Fante and L. Van Langenhove, "Smart Textiles", Reference Module in Biomedical Siences, Elsevier, ISBN 9780128012383, 2022. doi.org/10.1016/B978-0-12-822548-6.00121-7.

G.B. Tseghai, B. Malengier, K.A. Fante, and L. Van Langenhove, "Integration of Conductive Materials with Textile Structures, an Overview", Sensors, 20 (23): 6910, 2020. doi.org/10.3390/s20236910.

G.B. Tseghai, D.A. Mengistie, B. Malengier, K.A. Fante, and L. Van Langenhove, "PEDOT:PSS-Based Conductive Textiles and Their Applications*Sensors*, 20 (7): 1881, 2020. doi.org/10.3390/s20071881.

Table of Contents

2.1. Introduction

Anthropologists believe that humans first began to wear clothing after the last Ice Age i.e. 170,00 years ago, as humans migrated to new climates. Animal skins and vegetation were adapted into coverings to protect them from cold, heat, and rain [1]. Since then, methods of textile production have evolved continuously and the textiles available have influenced how people carried their possessions, clothed themselves, and decorated their surroundings. Because of modern technological advancements, knowledge of ancient textiles and clothing has grown in recent years.

Clothing has been one of the three basic human needs since the beginning of our species. In the primitive age, textile was used for clothing purposes and progressively extended to household and domestic applications. The textile was also used for technical applications such as sailcloth, tent, protective garments, ropes, etc., which leverage the textile properties to create a technical performance advantage. With the emergence of new fibers, fabrics and innovative processing technologies, the growth of the textile market has increased in recent years and has been instrumental in bringing about significant technological advances.

Starting with groundbreaking research on how to integrate conductive lines and circuits into textiles in the late 1990s [2], rigorous research resulted in sensor additions, actuators, user interfaces, and complicated textile circuits that could provide extra functionality to make smart textiles. Thus, electronic textiles (e-textiles) which are among the basic materials for the construction of smart textiles have received significant attention as a new technology that can provide added value to the existing wearable applications, including wearable sensors [3]. E-textiles can be categorized into two types [4], classical or integrated, in this the electronic components are embedded into garments, or directly integrated into textile substrates, respectively. They have attracted attention in technical and socio-economic fields because of their ability to sense and respond to environmental stimuli [4], [5]. These textiles found ordinary, special, and critical applications almost in every sphere of human activities such as mechanically sensitive sensors, electronic skin, flexible transistors, and energy-harvesting and storage devices [5]. Stretchable electronics are integrated with yarns, fabrics, or garments and have attracted considerable interest.

The insight of textile materials has shifted dramatically to include their use as a package for electronic components and drugs. People want textiles that conduct electricity while also having normal textile properties. This resulted in the

development of smart textiles. Smart textiles arose from the combination of textile materials with electronics, as well as collaboration between established electronics and textile engineering communities, resulting in a completely new class of large-area, flexible, conformable, and interactive systems known as smart fabrics and interactive textile (SFIT) [6]. These activities, which benefited from the textile industry's eagerness to develop new value-added textile products, yielded significant results in wearable smart systems, integrated multifunctional smart textiles, body sensor networks, and context-aware sensor systems for enabling a variety of applications in healthcare, protection, fashion, sport & military systems. In any of the aforementioned applications, the technological evolution of smart textiles can be divided into three stages: at first, a conventional sensor is simply attached to the textile. The sensor is then embedded in the textile, and the next generation of smart textiles turns the textile or garment itself into a sensor.

Smart textiles are materials and structures that sense and react to environmental conditions or stimuli, such as those from mechanical, thermal, chemical, electrical, magnetic, or other sources[7]. Textiles are materials that can react on themselves, unlike ordinary clothes. The expressions of "smart" and "intelligent" textiles or "wearable electronic" textiles are commonly used interchangeably. The term "smart textile" may refer to either a "smart textile material" or a "smart textile system". The definition is determined only by the context. Smart (intelligent) textile materials are functional textile materials actively interacting with their environment, i.e. responding or adapting to changes in the environment and smart (intelligent) textile systems are textile systems exhibiting an intended and exploitable response as a reaction either to changes in their surroundings/environment or to an external signal/input [8]. For instance, Steele et al. developed a bionic bra (Figure 2.1) using electro-material sensors and artificial muscle technology to detect the increase in breast motion and then respond with increased breast support to improve active living [9].

The first promising R&D prototypes used fabric strain sensors [10] and fabric electrodes to monitor electrocardiograms and respiration [11]. Further developments resulted in garment-based applications capable of recording biomechanical variables and physiological signals to monitor cardiovascular disease risk factors such as sleep disorders, physical activity, and post-events. Over the last two decades, the field has been evolving promisingly from a technology proof of concept and lab demonstrators to a new fashion/consumer experience and business paradigm, with smart textiles and wearables at the heart of the data economy. Smart textiles are now being used more widely in a

variety of applications, including workplace safety, productivity, and security, smart homes, healthcare, and banking. They are also regarded as tools for developing new forms of human-to-human and human-to-machine interaction and connection [12]. Recent prototypes focused on the advancement of smart fabrics and interactive textiles enabling interfacing, connectivity, and multi-parametric sensing, as well as integration toward fully functionalized garments, with a special emphasis on fully comfortable, multifunctional, reliable, low-power consumption, and cost-effective smart textiles, with a focus on interfacing, packaging, conformability, and robust interconnection.

Smart textiles integrate a high level of intelligence and can be classified into three subgroups: passive, active, and very active or intelligent smart textiles [13]. They can be made by incorporating electronic materials, conductive polymers, encapsulated phase change materials, shape memory polymers and materials, and other electronic sensors and communication equipment. As Dadi 2010 studied, these materials interact according to their designed feature with the stimuli in their environment [14]. As examples of very active smart textiles, the first generation of wearable motherboards which have sensors integrated inside garments and can detect injury and health information of the wearer, and transmit such information remotely to a hospital, has already been developed [15].

Understanding how smart textiles evolved over time will aid in predicting the direction and opportunities for future growth. Wu and Li claimed that smart textiles & apparel have evolved in three ways [16]: their smartness (intelligence), degree of integration, and self-sufficiency.

Based on their degree of smartness, smart textiles are characterized according to whether they can perform one or more of the following functions: sense, react and adapt [7], [17]. The working mechanism of a smart textile can be explained as shown in Figure 2.1. The sensors act as a sort of nerve system, picking up on any changes in signal strength. Processing is carried out by a controller, which analyzes and evaluates the input signals. Either directly or via a central control unit, actuators respond to the detected and evaluated signal.

Conventional textiles do not sense, react, or adapt to external stimuli but rather they give only functional advantages like protection and warmth. According to this classification, a smart textile needs to at least sense environmental conditions or an external stimulus to be considered even as “passive smart.” Examples of this class include ECG [18], [19], pressure [20]–[22], strain [23]–[25], pH [26]–[28], etc., sensing textiles. Possessing the further capability to react

after sensing qualifies it as "active smart." For instance, Bartkowiak et al. reported a shape-memory textile material made from a NiTi shape memory alloy wire in the form of spring for protection application which reacts with a martensitic transformation based on sensing heat that in turn led to shifting the thickness of a textile fabric [29]. Karpagam et al. reported on a chameleonic camouflage fabric made from thermochromic colorants that change its color upon heating and cooling [30]. If a smart textile can sense, react, and adapt, then it qualifies as "very smart." For instance, Steele et al. reported on a woven cotton fabric bionic bra, Figure 2.2a, that improves overall wear comfort by changing its properties in response to breast movement, and actuates to fit its size [31]. The bionic bra possesses polypyrrole-based tri-layers as a bending sensor, silver-coated nylon as a heating element, and acrylonitrile butadiene styrene-stimulant material as a housing of the textile-actuating. Zhang et al. [32] developed a smart material that can warm you up when you're cold and cool you down when you're hot [32], shown in Figure 2.2e. It is made of regular polymer fibers coated with carbon nanotubes, making them heat sensitive. During sweating in warm and humid conditions, the yarn contracts, allowing more infrared radiation to pass through. When it's cool and dry outside, the yarn expands and traps the same heat.

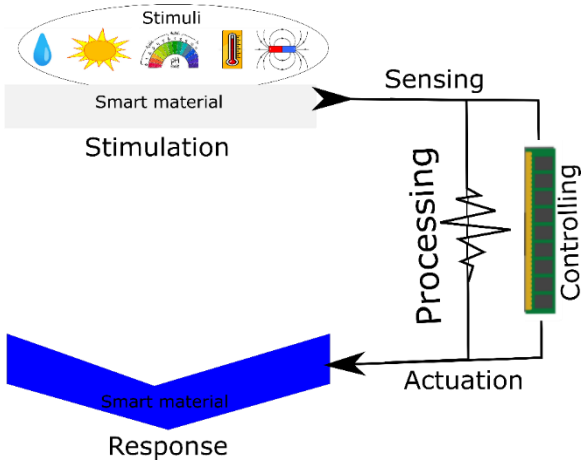

Figure 2.1: Working mechanism of smart textiles

Recently, some experts are also adding a fourth class called 'intelligent textiles' that achieve an even higher level of intelligence capable of responding or activating a function manually or pre-programmed. Wallace et al. reported a smart textile bra from conductive polymer-coated fabrics [33]. It is effective in preventing breast pain and sagging by tightening and loosening its straps or

stiffening and relaxing its cups to restrict breast motion. Data collected about how much strain the smart fabric is under can be used to adjust its elasticity. This means that it can stiffen or loosen its cups or straps instantly if it detects too much movement. Monitoring the comfort of a smart bra, for instance from mobile applications, even without any external stimuli, automatically makes it an intelligent smart textile.

The second classification of smart textiles is based on the degree of integration, which refers to the extent to which the component performing the "smart" function is embedded into the textile substrate. According to Hughes-Riley et al., there are three generations of smart and e-textiles: first generation, second generation, and third generation [34].

In first-generation smart textiles, a smart-functioning component is applied or attached to the surface of the textile through e.g. sewing, laminating, or embroidering. Some examples of first-generation smart textiles include microstrip patch antennas developed by Memon et al. where a copper sheet was attached to a spacer fabric [35] and embroidered silver-coated threads onto a neoprene fabric to develop a smart glove reported by Nolden et al. [36]. Kinnamon et al. [37] also developed first-generation influenza detecting smart textiles through a screen printing of graphene oxide on a textile fabric. This generation of smart textiles is more heavyweight, rigid in structure and bulky, and lacks drapability. In second-generation smart textiles, the smart-functioning component is integrated into the textile structure during the yarn or fabric production for example by incorporating conductive fibers or yarns during weaving or knitting. For instance, Husain et al. reported temperature sensing production by incorporating copper, nickel, and tungsten wire elements via a computerized flat-bed knitting machine [38]. Xu et al. [39] developed a woven fabric that detects a conductive liquid leakage. In this generation, smart textiles possess better flexibility than the first generation but still lack comfort and versatility. Third-generation smart textiles are considered the highest degree of integration where the fiber or yarn itself is innately smart-functioning and discretely exists within a textile design without interfering with the esthetic qualities and comfort level. Examples of this generation of smart fabrics are predominantly made by nanotechnology. For example, Salmon et al. [40] reported a color-changing artificial 'chameleon skin' powered by light-triggered nanoparticles made of tiny gold particles coated in a polymer shell and then squeezed into microdroplets of water in oil. When the material is exposed to heat or light, the particles stick together, causing the material's color to change as shown in Figure 2.2c.

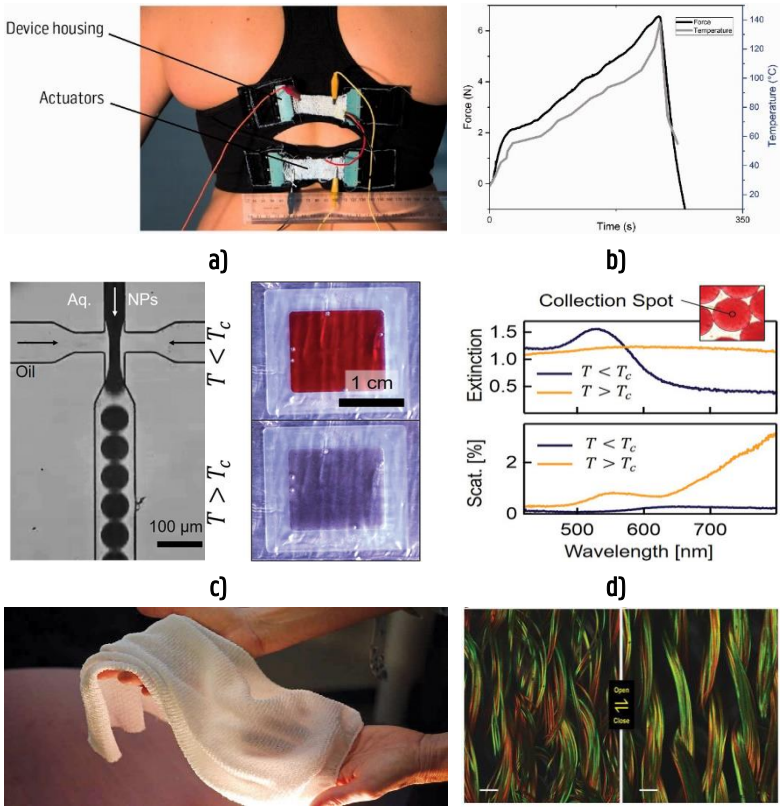

Figure 2.2: a) A typical example of a very smart textile, the bionic bra, under CC-NC by 4.0; **b**) force and temperature response curve for an actuating textile in the bionic bra. [31], under CC-NC by 4.0; **c**) Optical micrograph of the formation of chromatophore microdroplets at a flow-focusing microfluidic junction and camera images showing large area switching of the microdroplet chromatophores with temperature (Tc = 32 °C) in various lighting conditions, under CC BY 4.0; **d**) extinction and scattering spectra below and above Tc acquired from a 2 µm spot in the center of the droplets shown highlighted in the top-right inset [40], under CC BY 4.0; **e**) photograph of a thermoregulating fabric knitted from bimorph fibers, with permission; **f**) confocal fluorescent microscopy images showing the knitted fabric in the closed state, low humidity, and the open state, high humidity [32], with permission.

Jennifer and Li [16] extend the classification of smart textiles based on their integration, adding a "fourth generation" class, the potential next degree of integration that smart textiles are progressing towards and exist more as far

inspiring idealistic theories. In this class, the aspiration is fundamentally engineering the biological functions to form their own textiles. Growing genetically modified conductive fibers naturally could be an example of a "fourth-generation" concept. For example, increasing the absorption of metallic minerals in cotton and allowing them to accumulate in the seed. Metallic nanoparticles could also be added to cotton during the flowering and boll opening stages. At the moment, these are merely conceptual ideas that are unlikely to see commercial realization but a major breakthrough could happen in the future. They do, however, stretch the imagination in terms of the level of integration that clever textiles could in all likelihood gin in the future.

The third classification of smart textiles is based on the degree of self-sufficiency [41] which refers to the extent to which they can self-sufficiently perform their smart functionalities and sustain themselves environmentally friendly throughout their life cycle. The classes are denoted as past, present, and future. The "past" stage refers to smart textiles made from non-renewable or non-biodegradable raw materials and dependent on non-renewable energy resources from manufacturing to disposal. Examples are attaching LED or other commercially available electronics onto the textile structure regardless of their effect on the characteristics of the textile. The "present" stage factors in sustainability as not only an afterthought but an integral part of the development and life of smart textiles. The durability of the functioning component and its effect on the base substrate is considered. Examples are color-changing dyes integrated into textiles. The "future" stage that refers to the degree of self-sufficiency of smart textiles could involve an intelligently adapting feature and gradually improving its self-sufficient smart functions by learning from each experience such as producing self-healing agents in certain areas. These are idealistic concepts like the "fourth generation" of smart textiles but could be appeared in the future.

2.2. Building Blocks of a Smart Textile System

It may be worthwhile to consider why we require textiles as a substrate for the development of electronics and smart materials, particularly for wearable applications. People nowadays want wearable electronics for daily activities, and the electronics industry is always working to make electronics as flexible and lightweight as possible. Textile-based electronics are the obvious choice for meeting the requirements. Most importantly, textiles are versatile in terms of form, type, and characteristics, with the option of special after treatments to enhance or change the original properties for multi-functionality. Van

Langenhove's brief explanations [7] covered inherent, technological, and business reasons for choosing textiles. Textiles that can be customized to the level of property required, and are used as clothing that comes into contact with a significant portion of the body. Textiles are the interface between the wearer and the environment, with a large surface area and constant contact, making them ideal for long-term and large-scale monitoring. They are a material that is used by almost everyone in almost all activities. Producing smart textiles is not an expensive business. As technology advances, the components used in e-textiles have become significantly less expensive, allowing them to be produced and sold at a reasonable cost.

As a single-purpose textile, smart textiles with sensing [27] and actuating [42] capabilities have been developed. However, the entire smart textile system may include specific function building blocks such as a sensor, actuator, interconnection, a controlling unit, a communication device, and a power supply. Figure 2.3 shows a schematic representation of a complete smart textile system.

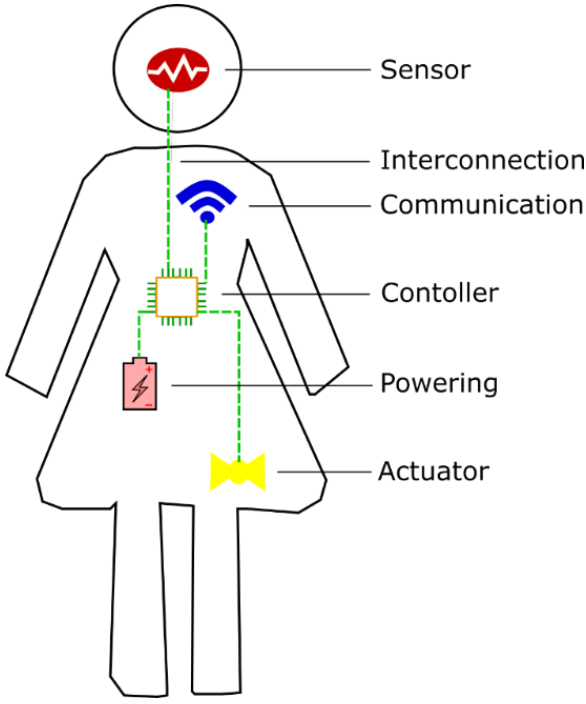

Figure 2.3: Building blocks of the smart textile system

2.2.1. Sensor

A sensor is an electronic element that detects physical tracks and records, indicates, or otherwise responds to them. The sensor converts one type of data or signal into another type of data or signal. It can only be read and executed by a specific reader. Biosignals such as heart and respiration rate, temperature, and motion can all be measured by sensors. Textile sensors for strain [47]–[51], electrocardiography [52]–[56], electromyography [57]–[59], electroencephalography [60]–[62], humidity [63]–[66], temperature [67], [68], pressure [68], [69], [21], light [70], [71], and molecule detection [72], [73] are among the well-studied smart textile functional components. A typical example of a textile-based pressure sensor integrated into a motorcycle glove that analyzes the biker's posture while riding, reported by Aigner et al. [43], is shown in Figure 2.4a.

2.2.2. Actuator

An actuator is a building component that has the ability to influence its surroundings. Actuators respond to the impulse result from sensors and change their form, shape, or size in response to external factors or on command from a controller. Other types of actuators generate light or sound. Organic light-emitting diodes [44]–[46], phase changing materials [14], [47], [48], temperature regulating textiles [49]–[51], and sound-generating textile [52]–[54] are examples of existing textile actuators. Shape memory textile materials are the most effective in this application. For instance, Buckner et al. [55] reported an emblematic textile-based robotic fabric with printed sensors and bending shape-memory ribbon actuators that could be used to create smart adaptable clothing and self-deployable shelters, as shown in Figure 2.4b.

2.2.3. Communication Device

A communication device is a unit that transmits and receives electronic data and/or information to and from another system. There can be numerous communication faces on smart clothing, it is used to transmit data from the individual elements of smart clothing as well as the environment, to the wearer's clothing. Various microstrip textile patch antennas [56]–[59]have been introduced. A typical example is a breathable microstrip textile patch antenna reported by Memon et al. [35], as shown in Figure 2.4c. The use of smart textiles

in WiFi tracking [60] and radio frequency identification (RFID) sensors [61] are also among the most promising technological innovations.

2.2.4. Interconnection

The interconnections are the elements that connect two or more functional components of the smart textile system to provide communication or current. A lot of conductive textiles have been introduced for interconnection purposes [13], [62], [63]. A silver-coated polyamide filament interconnection is shown in Figure 2.4d.

2.2.5. Control Unit

The control unit is an electric-powered circuit board that directs the processor's operation and is in charge of decoding sensor signals, commanding the actuator to react, and instructing the communication device to transmit vital messages. Specific examples of control units that can be integrated into a textile system are Arduino [64]–[66], OpenBCI board [67], etc. Traditional textile material does not have any computing power. However, e-textiles can be used to develop the circuit boards of a data processing unit entirely or partly in combination with other materials. For instance, Kim et al [68] reported a silkscreen wearable fabric computer. Yang et al. [69, p.] also fabricated a self-powered woven textile circuit board for wireless biomedical monitoring and early warning, shown in Figure 2.4e.

2.2.6. Power Supply

The entire smart textile system requires power to function; the component included to supply power to the system is the power supply unit. Because of their small size, lithium polymer (LiPo) batteries are commonly used in smart textiles. However, recently introduced textile-based energy harvesting devices [64], [70]–[72], and storage capacitors [73]–[76] could replace these for some applications. Many researchers are exploring state-of-the-art innovations in using the fiber to generate power, but in very small amounts, e.g. Sun et al. generated power from a woven thermoelectric fiber but this was only 0.07W/m^2 [77]. If this amount is enhanced to the capability of running the entire textile system, the use of smart textiles will expand much faster than it is now. A typical example of a textile battery [78] is shown in Figure 2.4f.

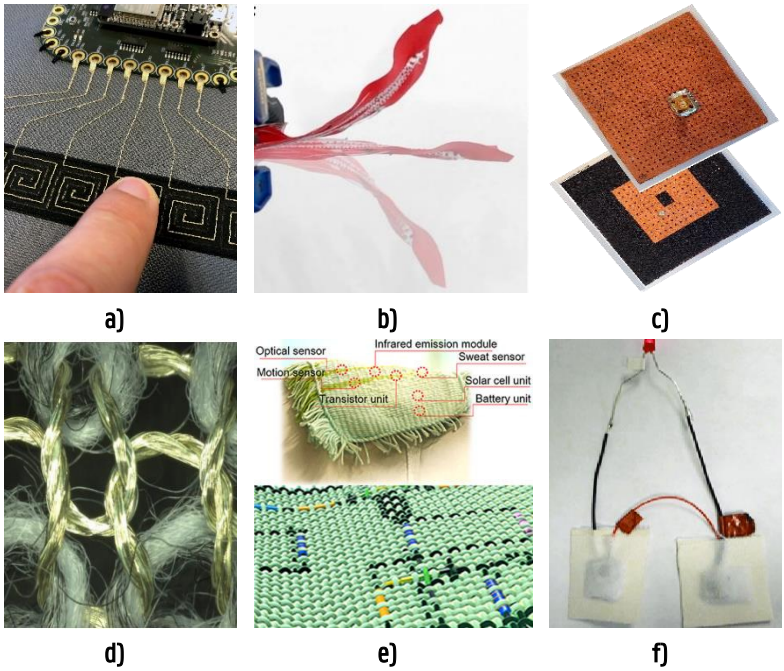

Figure 2.4: Building blocks of smart textile system; **a**) resistive pressure sensor [43], under CC-NC by 3.0; **b**) bending shape memory alloy ribbon actuator [55], under CC by 4; **c**) a breathable textile patch antenna **[35]**, under CC by 4.0; **d**) silver-coated polyamide filament interconnection [79], Under CC by 3.0; **e**) a woven textile integrated circuit board (Yang et al., 2021, p.), under CC by 4.0; **f**) a liquid activated textile battery [78], under CC by 3.0.

2.3. Conductive Materials for Smart Textiles

Electrical conductive textiles are used in many applications of smart textile materials. However conventional textile materials are usually insulating materials, where they cannot be used directly for smart textile applications that require electrical conductivity. Therefore, the primary step in smart textiles is making conductive textiles. It is possible to obtain electrically conductive textiles by integrating metallic wires, conductive polymers, or other conductive compounds into the textile structure at different stages, such as fiber construction, yarn spinning, or fabric creation stages. Non-textile metallic filament wires made of silver, stainless steel, nickel, aluminum, and copper can be inserted into the textile structure to add conductivity. Metals have high conductivity, which is important for some smart textile applications, but they add weight to the material and reduce its flexibility. Furthermore, some metals

corrode easily. Metal-based conductive textiles can also be created by coating metal ink on the surface of textile materials, but these have wash stability limitations. This necessitates the search for alternative conductive compounds in order to create more dependable conductive textiles with greater flexibility.

Generally, conductive textiles can be classified into bulk and surface conductive textiles [80]. Bulk conductive textiles include intrinsically conductive polymer textiles, textiles twisted/embedded with metallic filaments, and textiles filled with conductive additives such as carbon blacks (CBs), and carbon nanotubes (CNTs), or conductive polymers. Surface conductive textiles are textiles coated with conductive layers. The conductive coatings may consist of metals, conductive polymers, or other conductive materials such as CNTs or CBs. There are different kinds of conductive materials. In this, the conductive materials for textile materials are categorized as conductive inks, carbon-based conductive polymers, intrinsically conductive polymers, and conductive polymer composites. The choice of conductive material is one of the most important parameters in the development of different components of smart textiles. The materials should not only have good mechanical properties but also require environmental stability, good flexibility, and sometimes washability.

2.3.1. Conductive Inks

The success of inkjet printing for printed electronics has been attributed to the emergence of functional printable inks with different nanoscale sizes and structures. Usually, conductive metals are added to conventional inks to make them conductive. Conductive inks are usually used to make the circuit, switch or pressure pads on the smart textiles or to get conductivity at a specific area in garments. Based on their constituents, conductive inks can be categorized into three-dimensional nanostructured materials such as nanoparticles, nanowires, and nanotubes or they may exhibit plate-like shapes. Printable ink has a wide range of choices such as conductive, semi-conductive, and dielectric inks. The conductive inks can be prepared from conductive metal nano-particles and micro-particles. The semi-conductive inks can be prepared from metal oxides, organic polymers, and inorganic semiconductors. The dielectric inks are organic polymers in solvents, organic polymer thermosets, or ceramic-filled organic polymers. The functional conductive inks, on the other hand, can be developed from metals, metal oxides, conductive polymers, organometallic inks, graphene, carbon nanotubes, and a mixture of the different inks. Some examples of the conductive inks employed for the development of conductive textiles are reactive silver [81], graphene ink [82], carbon nanotube [83], etc. For instance,

Liang et al. used a silver nanoparticle-based conductive ink that was configured with poly(styrene-block-ethylene-ran-butylene-block styrene) to develop a skin-inspired ultra-sensitive pressure sensor [21]. Kim et al. [84] also reported silver-based conductive ink in order to make mechanically and electrically robust stretchable-textile substrates.

2.3.2. Carbon-based Conductive Materials

As the need for conductive textiles gains importance, carbon-based materials such as graphene [85], CNT [86], carbon black [87], graphene oxide [88], and reduced graphene oxides [89], have been investigated to develop electrically conductive textiles. These carbon materials are preferable for producing conductive textiles as most of them are relatively inexpensive, and they are corrosion-resistant, and flexible [90]. In [91] graphene-based polyester conductive fabric was developed and used for bio-potential monitoring applications. Rahman and Mieno have also developed an electro-conductive cotton textile by multiple dip-coating of the cotton fabric in a multi-walled carbon nanotube solution. The surface resistance of the coated fabric decreased as the amount of carbon loading increased, which depends on the number of dipping [92]. The carbon-based conductive fabric and effect of loading Multi-walled CNT in the cotton textile on sheet resistance are shown in Figure 2.5. Therefore, these materials can be used to produce a conductive textile with different ranges of conductance, up to more than 0.20 S/m depending on the load content. Other integration techniques like plating, transfer printing, inkjet printing, and electrospinning of carbon-based conductive materials could also provide a textile material with better conductivity and bulk property. For instance, Zhu et al. used single-walled carbon nanotubes to fabricate machine-washable conductive textiles via dip-coating and spray coating [93]. The developed conductive textiles exhibit a high electrical conductivity of up to 7.4×10^2 S/m. CNT fibers integrate such properties as high mechanical strength, extraordinary structural flexibility, high thermal and electrical conductivities, novel corrosion and oxidation resistivity, and high surface area, which makes them a very promising candidate for next-generation smart textiles and wearable devices [94]. However, despite the advantages of working with CNT, its production is toxic, and exposure affects the various processes of lung toxicity, including inflammation, injury, fibrosis, and lung tumors [95].

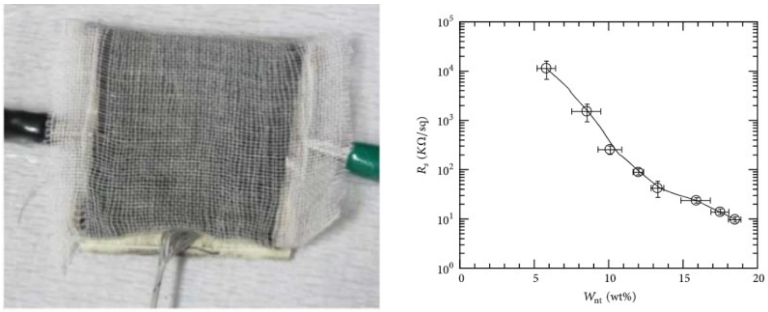

a) b)

Figure 2.5: a) Multi-walled carbon nanotube/cotton textile covered with one layer of -cotton sheet; **b**) the effect loading of Multi-walled carbon nanotube in the cotton textile on sheet resistance [92].

2.3.3. Intrinsically Conductive Polymers

At present, intrinsically conductive polymers are widely used in the development of electro-conductive textiles. Traditional organic polymers are electrical insulators or semiconductors, so the discovery of conductive polymers in the 1970s [96], opened a new opportunity to produce electro-conductive textiles. Conductive polymers are polymers that contain a conjugated molecular structure that is having alternative single and double bonds between carbon atoms. They can combine the electrical property of metals or semiconductors with the benefit of conventional polymers such as price, structural diversity, flexibility, and durability [97], which makes them an ideal choice for textile-based electrodes. Among the conductive polymers, polypyrrole (PPy), polyaniline (PANI), and polythiophene derivative poly(3,4-ethylene dioxythiophene):poly(styrene sulfonate) (PEDOT:PSS) are the most successful in the production of conductive textile [98]. The conductivity of the polymers can be enhanced by adding organic solvents called dopants, for instance, the conductivity of PEDOT:PSS can be enhanced from one to three orders of magnitude by adding polar organic solvents like ethylene glycol, dimethyl sulfoxide, glycerol [19], [99]–[101]. Therefore, these conductive polymers can be used to develop all building blocks of the smart textile system as a wide range of electrical properties could be achieved by playing with the polymer add-on, and the extent of dopant. The chemical structure of some conductive polymers is shown in Figure 2.6.

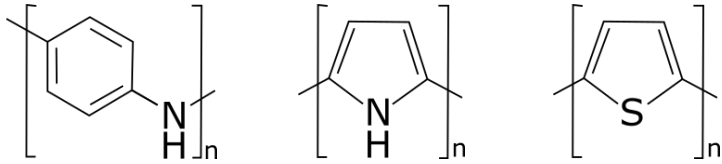

a) b) c)

Figure 2.6: The most successful conductive polymers: **a**) polyaniline; **b**) polypyrrole; **c**) polythiophene

Conductive polymers exhibit novel properties such as solution processability, high elasticity, toughness, and low-temperature synthetic routes. Some examples of conductive polymers and their properties are presented in Table 2.1. Due to these interesting properties, conductive polymers are used for several applications such as photovoltaic devices [102], organic light-emitting diodes [103], organic field-effect transistors [104], sensors [105], antennas [106], conductive textiles [107], supercapacitors [73] and many more.

Table 2.1: Non-exhaustive conductivity and properties of common conductive polymers.

Polymer	Conductivity (S/cm)	Type of Doping	Properties	Limitations	Ref.
PPy	2000	p-type	High electrical conductivity, ease of preparation, and ease of surface modification	Rigid, brittle, and insoluble	[108]
PANI	112	p-type	Diverse structural forms, environmentally stable, low cost	Hard to process, non-biodegradable, limited solubility	[109]
PTh	560	p-type	High electrical conductivity, ease of preparation, good optical property	Hard to process	[110]
PEDOT:PSS	4700	p-type	High electrical conductivity used as a transparent electrode	Needs additional steps to process	[111]

2.3.4. Conductive Polymer Composites

While the existing conductive polymers show promising conductivity, their mechanical properties need improvements. This has led to conductive polymeric composites with improved electrical conductivity and mechanical stability. As a result, a lot of conductive polymer composites have been introduced and used in developing conductive textiles. For instance, PEDOT:PSS-polydimethylsiloxane [112], PPy-silver nanocomposites [113], PANI-copper [114], graphene-PPy [115], PEDPT:PSS–CNT-Gr [116] have been reported as conductive polymer composites.

Metal-based conductive textiles have the highest conductivity but are often not flexible enough. While elastomeric interconnects are not conductive enough. Conventional conductive polymers such as PPy and PEDOT show promising conductivity for these applications; however, their mechanical properties, biocompatibility, and processability still need improvement [117]. This has led to more attention being directed towards conductive polymeric composites for improved electrical conductivity and mechanical stability. One way to increase the mechanical robustness of conductive polymers is by making a composite with commodity polymers. Electrically conductive polymer composites are polymers consisting of single or hybrid conductive fillers such as carbonaceous, metallic, and conducting polymeric particles dispersed in a polymer matrix. They can be produced based on a single polymer or a multi-phase blend depending upon the electrical and mechanical properties required. Composite materials based on conjugated conducting polymers and non-conducting polymers often show a low percolation threshold and improved environmental stability with respect to the conjugated polymer. For instance, compounding techniques used for the processing of conventional thermoplastics have been applied to prepare composites of PPy with certain thermoplastics which provided a drastic increase in oxidation stability [118]. In particular, a composite of conductive polymer with elastomers has been demonstrated for stretchable/elastic conductive materials/devices. Conductive polymer composites have been growing steadily and are being exploited for academic and industrial applications [119]–[121]. Conductive polymer nanocomposites also have promising applications for smart textiles. They are fabricated by embedding the metal and metal oxide nanoparticles, which give them sensing performance based on the electrical conductivity. Examples include a highly conductive, stretchable, and biocompatible Ag–Au core-sheath nanowire composite for smart wearable and implantable bioelectronics reported by Choi et al. [122]. Table 2.2 presents a non-exhaustive list of common conductive polymer composites with their suggested application areas.

Table 2.2: Properties of common conductive polymer composites.

Conductive Polymer Composite	Conductivity (S/cm)	Properties	Suggested Application	Ref.
Ag-Au/Hyaluronic Acid	4.1×10^{3}	Stretchable and biocompatible materials	Continuous electrophysiological recording, and electrical and thermal stimulation	[122]
PPy/Hyaluronic Acid	3.1×10^{-3}	Can support tissue growth and stimulate specific cell functions	Tissue engineering and wound-healing	[123]
PANI Nanofibers/Collagen	0.27	Well suited for cell culture	Scaffold Materials for biomedical	[124]
PPy/Chitosan	10^{-3}–10^{-7}	Radical scavenger	Food packaging and biomedical	[125]
PEDOT:Tos/Glycol	1486	Soft, flexible, and biocompatible	Implantable devices	[126]
PPy/Cellulose Acetate	6.9×10^{-4}–360	Soft and flexible and	Wearable electronics	[127]
PANI Nanoparticles/Polyacrylic Acid/Polyvinyl Alcohol	0.04–0.06	Hydrogel, biocompatible, good mechanical strength and good swelling properties	Strain sensor	[128]
Polythiophene derivative/PU	2.2×10^{-5}	Suitable for supporting electrically stimulated cell growth	Tissue engineering	[129]
PEDOT:PSS/PU/Ionic liquid	8.8×10^{-5}	Mechanically flexible and stretchable	Actuating devices	[42]
PPy/poly(D,L-Lactic Acid)	5.7×10^{-3}–15.7×10^{-3}	Nerve tissue regeneration, biocompatibility	Synthetic nerve conduits	[130]
PEDOT:PSS/PDMS	5 × 10−3	High sensitivity	Strain sensor	[131]

2.4. Responsive Materials for Smart Textiles

Various smart textiles made from conductive polymers are reported. Other smart textiles make use of adaptive polymers. Adaptive polymers are polymers designed to largely respond to known small external stimuli in a controlled and predictable manner. They are also known as stimuli-responsive or intelligent polymers. Scientists have made numerous attempts to create smart materials that can respond to various external stimuli such as temperature, pH, light, electric fields, chemicals, and ionic strength. Those responses are manifested as a dramatic transition in one or more methods of the subsequent: form, surface characteristics, solubility, color, and formation of intricate molecular self-assembly or a sol-to-gel transition.

Adaptive polymers, also called stimuli-sensitive polymers (SSPs), are a fascinating class of materials due to the fact they could undergo tremendous and speedy conformational changes in reaction to external stimuli. They are polymeric materials that can change their length, shape, or properties in response to stimuli whilst slight changes within the surrounding environment occur, these polymers can exchange their physical form or chemical arrangement. The adaptive polymers may additionally recognize a stimulus as a signal, and judge the strength of that signal, after which they directly alternate their conformation as a response. They acquire unique qualities as adaptable materials and offer the opportunity of controlling biocompatibility, wettability, permeability, swelling, transparency, and so forth. Due to their outstanding features, adaptive polymers have also drawn considerable interest in biotechnology. Sensing, intelligent fabrics, bio-separation, and medication delivery systems are all examples of successful uses.

There are several types of adaptive materials, including adaptive polymeric hydrogels [132], adaptive polymeric particles [133], shape memory polymers [134], smart film/fibers [135], and smart textiles [47]. Also included in the sphere of adaptive materials are some cyclodextrin and chitosan derivatives and copolymers, as well as some unique adaptive structures such as hyperbranched polymers, dendrimers, and supramolecular. There is a growing demand in society for materials that are better suited to present and future needs, such as better application response, versatile uses, and minimum environmental stress. In recent years, scientists all around the globe have concentrated on the synthesis and production of a wide range of smart polymers and textiles, which are based on a thorough understanding of smart material properties and structures. It is clear that new materials are looked for that are: (a) perfectly tailored to the

needs of the applications for which they are proposed, (b) fundamentally designed for essential intelligent devices, and (c) environmentally friendly.

In summary, textile materials that respond to external stimuli and have one or more properties are called responsive textile materials, also known as smart materials. These objects can change shape or behavior when exposed to heat, mechanical stress, chemicals, light, magnetic field, pH, moisture, and so on.

2.4.1. Piezoelectric Materials

Materials that produce a voltage upon mechanical stress are called piezoelectric materials. Examples include crystals and ceramics. Their application is basically for mechanical stress sensing, converting mechanical energy into electrical energy and vice versa. Examples include a textile piezoelectric generator demonstrated by Lund et al. [136] for energy harvesting, it was a shoulder strap of a laptop case, as shown in Figure 2.7a, that was able to produce a continuous output of 4 μW.

2.4.2. Chromic Materials

Materials that exhibit a distinct color change when exposed to an external stimulus are referred to as chromic materials. Based on the type of external stimuli that triggers the color change, there are various types of chromic materials. Examples include chromogenic material that changes its color in response to electrical, light intensity, or thermal changes known as electrochromic, photochromic, and thermochromic, respectively. Examples include a photochromic and florescent knitted cellulose fabric that changes its color with light reported by Khattab et al. [137], strontium aluminate pigment was used as a stimuli-responsive printing past, shown in Figure 2.7b.

2.4.3. Shape-Changing Materials

Shape-changing materials change their form, shape, or size when exposed to external stimuli. Shape-changing materials that remember their original form and return when the external stimulus is released are called shape-memory materials. This property makes such materials applicable for bio-engineering uses which would make them the future of 4D materials. Shape-changing materials can be used in the textile field to produce wrinkling releasing,

breathable, energy absorber damping, skin-care, wound dressing, deodorant realizing, and energy storage textiles. To make such smart textiles, various shape-changing polymers like shape memory polyurethane, poly-hydroxyproline, polysilane, and responsive hydrogels like poly(N-isopropyl acrylamide) (PNIPAAm) hydrogels are used. Another example is pH-sensitive materials that vary their dimensions in response to the changes in the pH of the surrounding medium. For instance, Yan et al. [138] developed a magnetic textile, shown in Figure 2.7c, able to switch its wettability when pH value varies for water/oil separation. Other smart materials also include magnetostrictive, halochromic, chromogenic, and self-healing materials.

2.4.4. Fiber Optics Materials

An optical fiber is a thin, flexible, transparent fiber made by drawing glass (silica) or plastic, that is commonly used to transmit light. For instance, Koncar reported an optical fiber fabric display that could potentially be used in fashion, information display, and communication [139]. Gauvreau et al. [140] also reported a woven color-changing and color-tunable photonic bandgap optical fiber into a textile structure, as shown in Figure 2.7d.

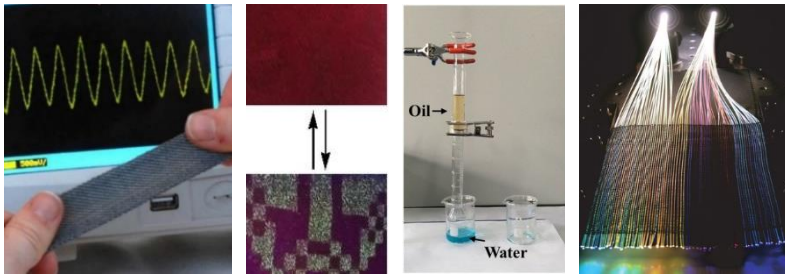

a) b) c) d)

Figure 2.7: a) Piezoelectric textiles band, when stretched by hand generating an output voltage shown on the oscilloscope screen [136], under CC by 4.0; **b**) screen-printed photochromic cotton fabric before and after UV (λ= 365 nm) irradiation for 1 min at room temperature [137], with permission; **c**) pH-responsive textile wetted with acidic water (pH = 2) before separation, water selectively permeated through the textile, while oil retained on the textile surface [138], with permission; **d**) an optical textile fabric lit in the dark [140].

2.5. Fabrication Methods of Smart Textiles

Several methods are used to integrate the different parts to get a smart textile structure. The components include the conductive and non-conductive parts. Conductive and/or chromic materials can be incorporated into the textile structure through embroidery [141], knitting [142], weaving [143], spinning [144], braiding [145], coating [146], printing [37], plating [147]. The techniques for integrating a conductive, shape-changing, and/or chromic material in/onto a textile structure can be classified according to the form of the starting conductive material used. Conductive and/or responsive compounds, fibers, yarns, or sheets can all be used as starting materials. As a result, the integrating techniques for these starting materials differ.

2.5.1. Integration of Conductive and/or Responsive Compounds: Finishing Touches

Once the textile has been fabricated, new functionality and smart capabilities can be added by applying condition compounds, shape-changing, and/or chromic material similarly. The conductive, chromic, and/or responsive compounds can be applied in the way dyestuff and pigments are added. In general, to produce required smart textiles, different approaches can be taken, such as adding the monomer, polymer, or ink into a polymer solution during fiber spinning, during the coating/dyeing of textile substrates (fibers, yarns, fabrics), and/or in a printing stage on textile fabrics and garments.

In electrospinning, smart textiles can be also produced by adding sensor materials to a polymer spinning solution at the nanotechnology level for use in microencapsulation and/or electrospinning technology. A process to encapsulate tiny particles or droplets into wall materials is quickly becoming a well-used technology for use in smart textiles [47]. Research is going into modifying fiber surfaces, such as grafting materials onto fibers to create multi-functional, responsive, and adaptive fibers, in order to tailor a hybrid nanolayer of polymer film that will afford several functions and properties through nanotechnology [148]. Printing is a common method to deposit a conductive layer on flexible fabrics and or garments fabric. Direct write printing is defined as an additive manufacturing method in which the deposited patterns directly follow a pre-designed layout without utilizing masks or subsequent etching processes. Direct write can deposit and pattern different thin film materials necessary for the fabrication of components and systems such as those found in electronic devices, sensors, and other systems. In the development of conductive textiles via

printing, the conductive compound can be deposited or transferred to the textile substrate such as in screen and transfer printing, respectively. Inkjet printing and 3D printing can be potentially used to inject conductive materials over the surface of the textile fabrics layer by layer using a nozzle.

Fiber Spinning: The integration of smart compounds into a smart textile structure is done by different techniques including fiber spinning, one of the promising methods to incorporate the conductive components, consisting of the techniques electrospinning, solution spinning, and melt spinning. Fiber spinning is used to produce conductive fibers.

In electrospinning, the conductive fiber is produced by employing electric force to draw charged threads of conductive polymer solutions up to fiber diameters of a few hundred nanometers. For example, Chronakis et al. [149] reported a conductive polypyrrole nanofiber with diameters in the range of about 70–300 nm through electrospinning processes. Electrospinning can also be applied to develop conductive mats.

Solution spinning (wet and dry-jet wet spinning) can be used to make continuous fibers from materials that cannot be melted, normally, the technique is, therefore, suitable in the manufacture of fibers from natural polymers and bio-based materials, such as cellulose, lignin, and proteins but a conductive fiber can also be produced from conductive polymer under a similar procedure. Conductive components can be integrated into the textile structure at the fiber spinning stage by adding a conductive component into the polymer solution which is then extruded together to produce conductive fibers or filament. For instance, Di et al. [94] used wet spinning, wherein a high-concentration (3 wt%) CNT solution dissolved in chlorosulfonic acid, was extruded through a spinneret into a coagulation bath, to produce carbon nanotube fiber. In [150], a conductive PANI fiber was also reported using modified carbon black materials as conductive fillers via the wet-spinning process. The conductivity and tensile strength of the fiber were improved after annealing. Liu et al. developed electrically conductive composite fiber from a blend of PEDOT:PSS and PANI using a conventional wet-spinning process having a diameter of 30–60 μm. They reported that the electrical conductivity of the composite fiber increased as the content of PEDOT:PSS increased, where the highest conductivity was 5.0 S/cm when the PEDOT–PSS content was 1.83 wt% [151]. The PEDOT:PSS content doesn't show any relation to fiber mechanical performance, but it did cause an increase in surface roughness. Zheng et al. used the wet-spinning method to fabricate hybrid microfibers composed of hyaluronic acid and multi-walled carbon nanotubes. The obtained hybrid microfibers presented excellent tensile properties with

Young's modulus of 9.04 ± 1.13 GPa and tensile strength of 130.25 ± 10.78 MPa, and excellent flexibility and stability [144].

Melt spinning is a common method of spinning thermoplastic synthetic fibers such as polyester, nylon, and polypropylene where the spinneret discharges melted polymer. In this method, the conductive polymers can be added alongside the thermoplastic synthetic polymers. For instance, Probst et al. [152] produced a highly stretchable conductive thermoplastic urethane/carbon nanotube filament yarn through melt spinning. Radzuan et al. also reported a PPy reinforced carbon fiber developed by the melt-spinning process [153]. The electrical conductivity of the fiber was 0.56 to 3.66 S/cm based on the die configurations. Åkerfeldt et al. also used the melt spinning technique to produce a fully textile piezoelectric strain sensor, consisting of bi-component fiber yarns of β-crystalline poly(vinylidene fluoride) sheath and conductive high-density polyethylene/carbon black core as insertions in a woven textile, with conductive PEDOT:PSS coatings developed for textile applications [154]. The absence of the binder leads to one order of magnitude less surface resistivity, 12.3 Ω/square. However, the surface resistivity increases more upon abrasion when compared to a fabric printed with a binder added to the solution. Schematic illustrations of the wet and melt spinning are shown in Figure 2.8.

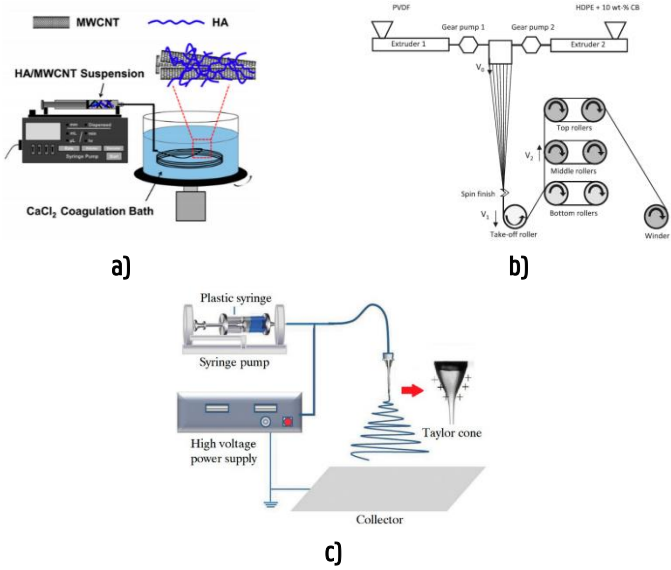

Figure 2.8: a) A schematic of the experimental design of the wet-spinning method [144] CC BY 4.0; **b**) schematic illustration of melt spinning [154] CC BY 4.0; **c**) schematic illustration of electrospinning [155] CC BY 4.0.

Coating: The coating of the textile substrate with smart compounds can be done through a dip-coating or spray-coating approach. Dip-coating is among the basic techniques to deposit the sol-gel coating and also conductive polymer on the surface of the textile substrate [156]. In this technique, textile materials such as fiber, yarn, or fabric are immersed for a certain duration of time in a bath containing conductive dispersion. The process can be discontinuous or continuous as the schematics shown in Figures 2.9a and 2.9b, respectively. In the discontinuous process, the fabric is batched for some time in a solution containing conductive components and other auxiliaries. This method can be used for any form of textile. Whereas in the continuous process, a batch fabric passes through a padding mangle containing a conductive solution and drying unit as a roll. This method is suitable for fabric processing but can be used for yarn too.

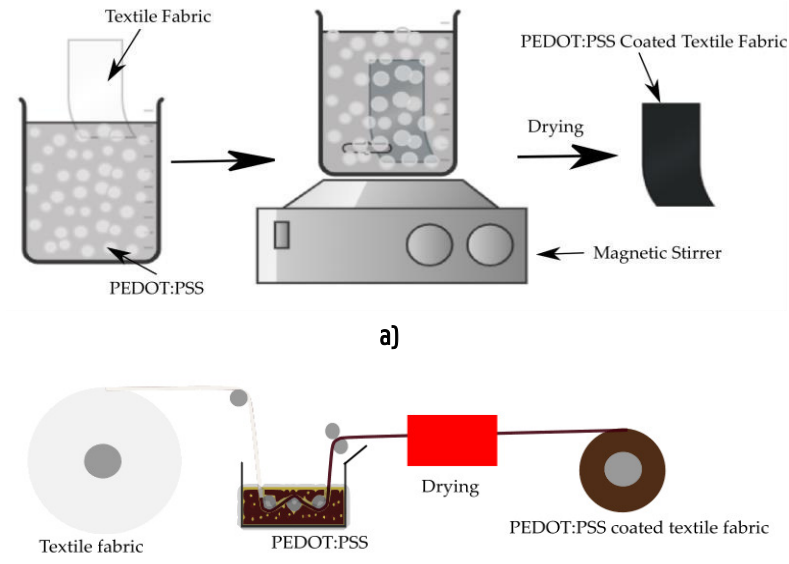

Figure 2.9: Schematic illustration of methods of dip-coating: **a**) discontinuous process; **b**) continuous process

Many conductive textiles made by coating have been reported. For instance, Liu et al. used the technique to fabricate a highly electrically conductive and excellent washing-resistant cotton fabric [157]. Kwon et al. [158] dip-coated a PEDOT:PSS solution several times on precleared polyester fibers to form a transparent conductive electrode used for high luminance fiber-based polymer light-emitting devices. Liu et al. also reported a polypyrrole dip-coated electro-

conductive cotton fabric developed by immersing the fabric in a solution containing polypyrrole at room temperature for 30 min [159]. The surface conductivity of the polypyrrole-coated cotton fabric depended on the concentration of pyrrole in the solution, and better conductivity was obtained at 0.5 mol/L. Ankhili et al. dip-coated cotton, polyester, and polyamide fabrics in a solution containing PEDOT:PSS dispersion. The cotton fabric gives better electrical conductivity because its good hydrophilic character caused a higher absorption of PEDOT:PSS than the other fabrics [160]. Tseghai et al. have also used the dip-coating technique to develop a textile-based strain sensor by in-situ polymerization of PPy on cotton fabric. The sheet resistance of the dip-coated fabric was 60 Ω/sq [25]. Furthermore, Mule et al. used this technique to fabricate conductive and robust PPy-coated cotton triboelectric nanogenerator (TENG) devices that were flexible and wearable [161]. The device efficiently converts mechanical energy into electricity while making a continuous touch-release with counter-friction objects like human skin i.e. tribo-friction layers. It showed strong characteristics even after long-term cyclic operations and conjointly produced an electrical yield under tender touching with the human hand. It can hence be utilized as a self-powered source to drive convenient electronic gadgets and light-emitting diodes The photographic image of the PPy-based wearable single-electrode-mode TENG is shown in Figure 2.10.

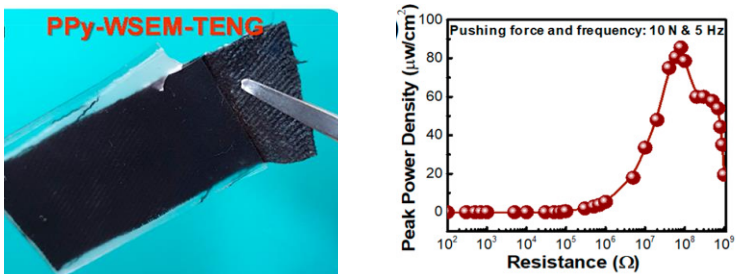

a) b)

Figure 2.10: a) Photographic image of a real polypyrrole-based wearable single-electrode-mode triboelectric nanogenerators (PPy- WSEM-TENG) device; **b**) estimated peak power density values of the PPy-WSEM-TENG device under the applied pressing force and frequency of 10 N and 5 Hz, respectively [161].

Spray coating is also widely used to integrate the conductive part into smart textiles. It is one of the promising techniques to overcome the limits of the uneven and coarse structures of textile fabrics' substrates. Piezoelectric transducers are used in the construction of ultrasonic spray nozzles to cause longitudinal high-frequency vibration. The power generator can adjust the

amplitude of standing waves produced by this longitudinal up-and-down motion in a thin film of applied liquid on the ultrasonic nozzle tip. With little to no kinetic energy, these standing liquid waves can be propagated upward from the ultrasonic nozzle tip until they divide into droplets of uniform size. In spray-coating, a spray of conductive particles or droplets is deposited on a textile substrate. A screen mesh or frame can be used to apply the conductive components at required locations. A schematic depiction of the ultrasonic spray coating is shown in Figure 2.11.

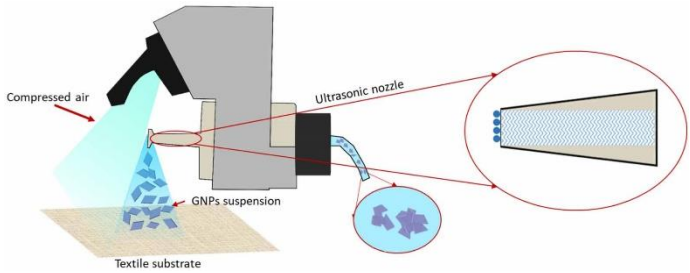

Figure 2.11: Schematic illustration of ultrasonic coating, [162], under CC by 3.0.

The spray coating has also been extensively investigated in textile applications. For instance, Sadanandan et al. [162] reported graphene-coated fabrics through ultrasonic spray coating. Li et al. also used spray-coating to develop a textile-based organic solar cell [146]. A 0.4 % power conversion efficiency was achieved. Arumugam et al. [163] also spray-coated silver single nanowire, zinc oxide nanoparticle, poly (3-hexylthiophene): indene-C60 bisadduct, and PEDOT:PSS layer-by-layer on a woven polyester/cotton substrate for solar cells as shown in Figure 2.12. A 0.1 % power conversion efficiency was achieved.

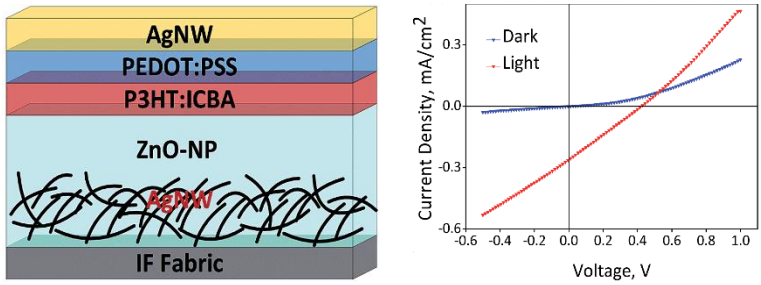

a) **b)**

Figure 2.12: **a**) layer-by-layer spray-coated conductive polyester/cotton; **b**) current density-voltage characteristics of the spray-coated conductive fabric [163], under CC by 4.0.

Plating: Plating is the process of adding a layer of metal components to the surface of textile materials. Before plating, the substrate must be cleaned to remove impurities, which offers assistance for the effective attachment of the metal particles to the surface of the substrate [147]. There are different ways of plating, mostly categorized as electroplating or electroless plating.

In electroplating, metals are plated on the surface of the conductive fabric by using an electric current. A clean substrate can be immersed in a solution of metal plating particles and an electric current is applied to deposit the metals on the surface. Hence, this way works only for conductive surfaces as otherwise, the current cannot flow. Conventional textiles are not electrically conductive, therefore, it is not possible to use electroplating, unless the material is prior conductive. However, this way can be used to improve the conductivity and stability of conductive textiles using metal particles. As an example of electroplated textiles, a carbon fiber electroplated with nickel for thermoelectric energy harvesting application was explored in [164]. A schematic representation of copper electroplating to a prior conductive cotton fabric is shown in Figure 2.13a.

Electroless plating is a chemical process to create metal coatings on various textile materials by an autocatalytic reaction, a chemical reduction of metal cations in a liquid bath. Electroless plating depends on a chemical reaction to coat the metals on the surface of a material rather than using an electric current.

In this way, the plating is first performed by cleaning unnecessary components and impurities with chemical cleaners that are able to remove oils and other corrosive elements from the textile, then dipping the substrate into an aqueous solution and adding anti-oxidation chemicals. The schematic representation of electroless plating is shown in Figure 2.13b.

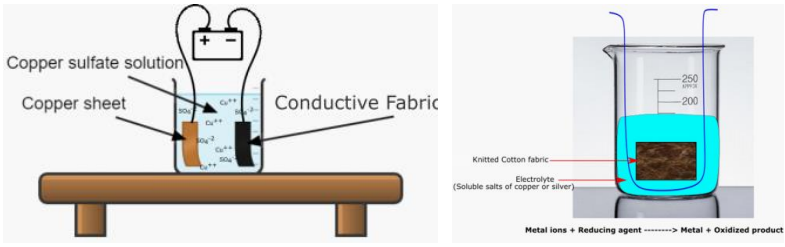

a) b)

Figure 2.13: Plating methods: **a**) Electroplating **b**) electroless plating

Among the ways of plating, electroless plating is more convenient for traditional textile fabrics as it gives a high friction and corrosion resistance to the resulting conductive textiles, and can be used for non-conductive textiles. Because of these, a lot of electroless-plated conductive textiles have been developed and reported. For instance, Kumar and Thilagavathi developed a copper-plated polyester fabric by using this technique. They reported that the plated polyester fabric's electrical conductivity was 300 kΩ/sq surface resistance [165]. Ma et al. used electroless silver plating to develop a conductive cotton/spandex blended fabric having robust electrical conductivity, 15.7 S/m [23]. The resultant fabric has high flexibility and stretchability due to the presence of spandex which could make it suitable as a strain sensor while obtaining an anti-bacterial property due to the presence of the silver. Therefore, this silver electroless plated textile could have a good potential prospect for wearable textiles. In addition, Root et al. reported copper electroless plated cellulose-based woven lyocell fabrics [24]. The resultant fabric was subjected to cyclic tensile tests; the resistance of the coated fabric (19 × 1.5 cm^2) dropped from 13.2 to 3.7 Ω at 2.2% elongation. This work could attribute to a better understanding of conductive copper coating on textiles and their applicability as strain sensors. The schematic representation of the copper deposition and the electrical response to the stretching of the fabric is shown in Figure 2.14.

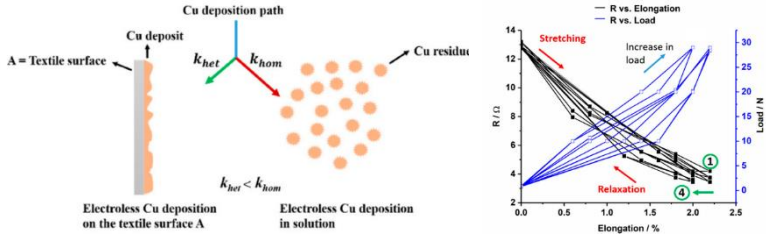

Figure 2.14: a) A schematic drawing of the electroless copper deposition during; **b**) the electrical response to stretching [24].

Screen Printing: As a feasible practical solution, screen printing is one of the most efficient and cost-effective methods of creating conductive patterns on different textile substrates. The screen-printing process consists of printing a viscous conductive paste through a patterned stencil followed by a curing process depending on the substrate and the property of the conductive compound used. It is among the highly recommended methods of printing since it can simplify fabrication [58]. Therefore, screen printing is a widely used printing technique [166] to realize textile electronics as one can easily deposit a pattern of conductive paste onto fabric to form a flexible strong, and suitably thick

functional layer after curing. The printing technique seems to be equal to dip-coating, but actually, it is different. Printing is a structured application of the conductive components on a selected or localized area whereas dip-coating is an unstructured application of conductive materials to the textile material similar to the conventional dyeing of textiles.

Screen printing has powerful potential for manufacturing wearable electronics [167]. This technique can be used to apply conductive polymers and metallic and electrolyte inks onto textile substrates. For instance, screen-printed silver ink on cotton and polyester for ECG electrodes [18] and dispersion of carbon nanotubes on cotton and polyester fabrics [168] have been reported.

A lot of research effort is put into obtaining textile electronic components with smaller dimensions and with improved performance. It has been reported that electronic textiles like antennas have been screen printed on a polyester fabric and also transmission lines for RF and microwave systems have been screen printed on cotton [169]. Roshni et al. used the technique to develop an E-shaped microstrip patch antenna designed on polyester fabric for WiMAX applications [58]. Since the fabricated antenna was thin, flexible, and water-resistant, it can be easily integrated into any textile structure, and garments like this are able to sense and communicate data in a non-intrusive way. Liu et al. reported screen-printed dye-sensitized solar cells (DSSCs) on woven polyester/cotton and Kapton fabrics for wearable energy harvesting applications. The screen-printed DSSCs on Kapton and polyester/cotton fabrics gave photovoltaic efficiency of 7.03% and 2.78%, respectively [71]. The schematic illustration of a typical flat screen printing of PEDOT:PSS on a textile fabric by Ankhili et al. [170] is shown in Figure 2.15.

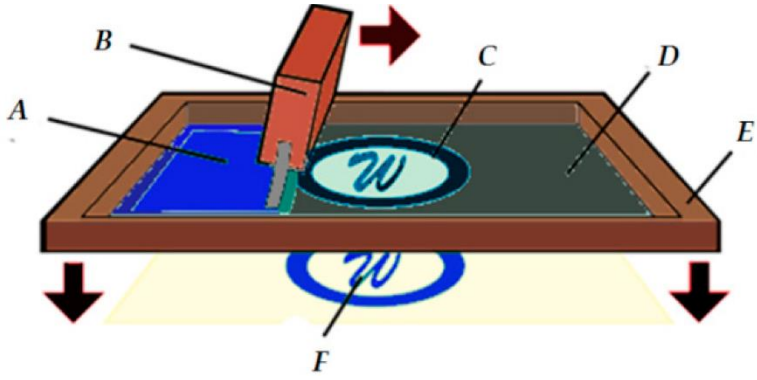

Figure 2.15: a) Screen printing process (A: PEDOT:PSS; B: squeegee; C: opening in screen; D: screen; E: screen frame, F: printed electrode) [170] CC by 4.0.

Transfer Printing: In transfer printing, the required design is first printed on a non-textile substrate called print master and then transferred by a separate process to a textile fabric or garment upon the application of heat and pressure. This route would be chosen if direct printing on the fabric is not suitable. In most cases, such difficulties may arise from the rough surface of the textile fabric or the migration of the conductive component with solvent to undesired parts of the fabric due to the wicking effect. The particles can be transferred from the pre-printed master to the textile by sublimation, melt, film release, and wet transfer.

The sublimation transfer is suitable for volatile compounds that can be preferentially adsorbed in a vapor phase by the textile material from a print master during heating. Though this method is commercially the most important of the transfer-printing methods, it is not well employed for the development of conductive textiles as volatile conductive compounds able to sublime during heating are not commercialized yet. The melt transfer can be used to print designs to a fabric with compounds that are able to melt onto the fabric in contact with the print master. This method is also not convenient for conductive polymers as they do not have a melting point. Metal conductive inks could be possible but commercial textiles could decompose before the melting point of the metal particles is reached. In the wet transfer, the design is transferred from a print master to a moistened textile under a carefully controlled contact pressure. The conductive particles could then transfer by diffusion through the aqueous medium. However, the method is not used to any significant extent at present. The film release transfer printing is a little bit similar to melt transfer except the design is held in an ink layer which is transferred to the textile from a release paper using heat and pressure. Adhesion forces stronger than between the conductive film and the paper in the print master are developed between the conductive particles and the textile substrate. Therefore, this method can be potentially used to develop conductive textiles as the heating weakens the adhesion between the conductive film and the paper but does not melt the conductive components in the film.

Film release transfer printing is already commonly used to develop conductive textiles. For instance, Maheshwari et al. used the film release transfer printing of silver nanowire conductive ink to textile fabric surface e-textile [171]. The resultant sheet resistance of the conductive fabric was small, i.e. 3 Ω/sq, and had a lightweight and more mechanical flexibility than other conductive fabrics. Shin et al. also used transfer printing to develop a textile-based flexible circuit for a wristwatch [172] which is shown in Figure 2.16. The transfer-printed textile circuit

showed no change of resistance after folding while its equivalent screen-printed circuit changed from 0.73Ω/cm to 12.85Ω/cm. Therefore, this is a promising integrating technique for any conductive particle in the form of a film to produce flexible and lightweight conductive textiles for different wearable applications.

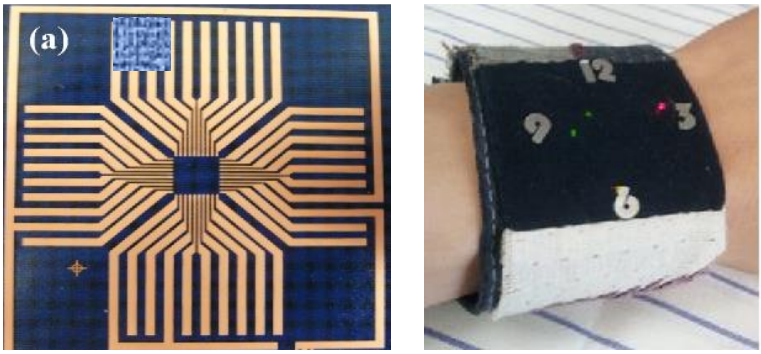

a) b)

Figure 2.16: a) Transfer-printed textile circuit; **b**) textile wristwatch [172].

Inkjet Printing: Inkjet printing is a widely used direct-write deposition tool that has rapidly migrated to electronics fabrication in recent years. It is a key printing technique that has not been widely applied to wearable textile fabrication. In inkjet printing, images and structures are built up in a droplet-by-droplet fashion. The user may make a change to the jetting parameters or the ink. The technique of inkjet printing structures can be an advantageous manufacturing technique as the functional component can be created within minutes of finalizing the design; the finish is aesthetic and has excellent resolution; it requires minimal material consumption and as no mask is required there is the flexibility to change the design regularly. The process is an additive process that does not require environmentally harmful etching chemicals while minimizing the amount of waste produced and has a high degree of reproducibility as droplet production allows a user to treat the droplets as building blocks. It is possible to print the ink directly on to the fabric but Chauraya et al., 2013 argued that the pattern would dissipate into the textile and cannot produce a continuous conducting track without many layers being printed due to the high solvent content (˜85%) of the inks required to ensure inkjet printability [169]. Ink-jet printing requires the use of a special liquid, usually referred to as ink, which contains the smallest possible electrically conductive particles (their dimensions are usually counted in tens of nanometers at the most). For the stability of such a suspension in time, each of the conductive particles (mostly silver or gold) is covered with a protective organic layer. Carbon nanotube and

graphene inks are also used but typically have lower conductivities than metallic inks [173].

Al-naiemy et al. used the inkjet printing technique to develop a microstrip antenna based on nano-silver inkjet material [174]. The developed antenna operated more efficiently than its identical antenna made by screen printing at 2.44 GHz. This indicates that the integration of microstrip antennas, electronic circuits, and sensors into the panels of photovoltaic cells using inkjet printing can be considered a successful and promising design approach for the future. Inkjet printing of sol-gel-derived tungsten inks on glass and transparent conductive tungsten oxide and the functionality of these transparent WO_3 layers were successfully demonstrated in an electrochromic device [175]. He et al. reported fully printed humidity sensors from graphene oxide and few-layered black phosphorus flakes dispersion printed silver nanoparticle electrodes via inkjet printing [176]. The sensor can give an electrical response from 11 to 97% relative humidity. In addition, the capacitance sensitivity was also high in both the graphene oxide (4.45 × 104 times) and the black phosphorus (5.08 × 103 times) sensor at a 10 Hz operation frequency. Weremczuk et al. also used this technique to produce a textile-based humidity sensor that has satisfying metrological parameters [177]. This work demonstrated a prospective opportunity for integration with smart wearable electronics used for making medical applications. The photographic image of the humidity sensor and some results are shown in Figure 2.17.

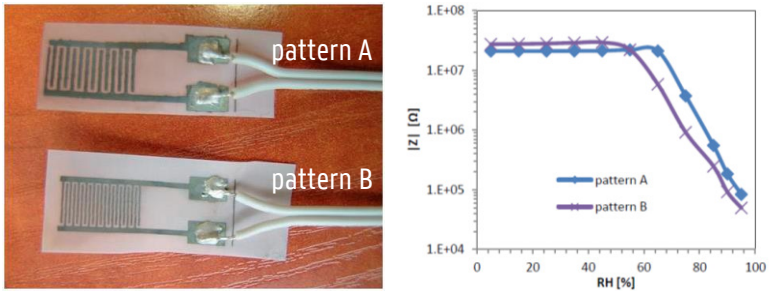

a) **b)**

Figure 2.17: **a**) A textile-based humidity sensor; **b**) impedance modulus dependence on the humidity for a pattern at 1kHz measurement frequency [177].

3D Printing: Recently, researchers are demanding that fabricating prototypes or producing complex structures can be done fast and at a low cost, but not many of the aforementioned fabrication techniques can offer this. However, as is well known, 3D printing can be a very cost-effective solution; as reported by [178], it

can reduce lead times, improve the design, and/or lower the weight of the structure. Today, people are coming up with new and exciting uses for 3D printers all the time. Here are just a few examples that show what these machines can do. The airplane company Airbus is trying to out a way to make a 3D printer that is as big as an airplane hangar [179]. 3D printers use designs made on computers to make three-dimensional objects right before your eyes. For instance, Bellacicca et al. produced all-printed monolithic functional devices with designed 3D geometry and embedding passive electrical components [180]. Chen et al. [181] also reported 3D printed stretchable smart fibers and textiles for self-powered e-skin which is shown in Figure 2.18a. Kuang et al. developed a 3D-printed shape memory elastomer that has potential application for biomedical devices, such as vascular repair devices, 3D printing of highly stretchable, shape-memory, and self-healing elastomer toward novel 4D printing [182]. Agarwalaa, et al. described the design, fabrication, and characterization of a microchannel-based strain sensor using flexible material [183]. The work explores the use of 3D printing to fabricate the sensor easily and cost-effectively. It is shown that 3D printing can print complex designs with ease and fabricate objects with embedded features. Microchannels with dimensions of 500-micrometer diameter are printed within the sensor structure and filled with conductive silver nanoparticle ink. The printed sensor can measure normal (orthogonal to channels) and in-plane (parallel to channels) tensile forces and is tested using a custom-built test rig. Muth et al. also used 3D printing to develop a three-layer strain and pressure sensor within highly stretchable elastomers [184]. A multi-component materials system composed of ink, reservoir, and filler fluid was used to enable an e-3D printed strain and pressure sensor. A carbon conductive grease, i.e. carbon black particles in silicone oil functional ink was used to pattern the sensing elements. The actual image of the three-layer strain and pressure sensor is shown in Figure 2.18c. The work revealed that 3D printing can easily print out objects with complex designs and embedded features. Thus, further evolution of 3D printing could highly impact bringing a novel approach to smart textiles.

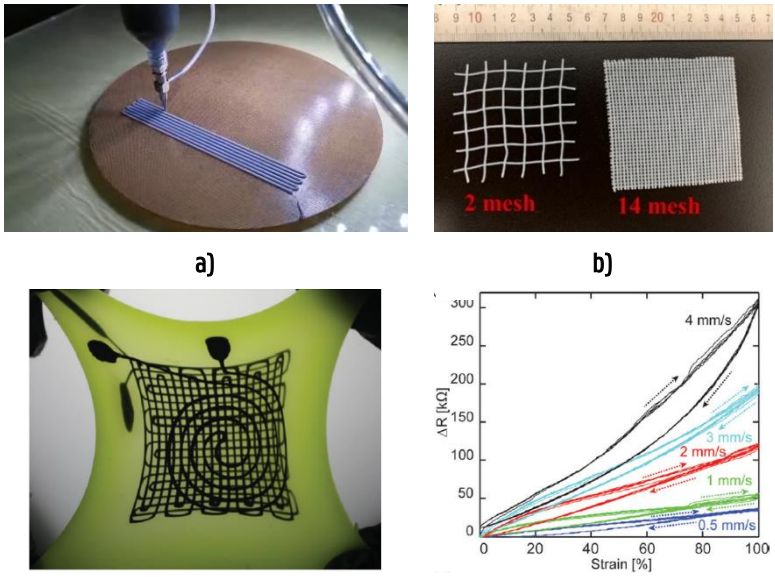

Figure 2.18: a) 3D Printing; **b**) 3D-printed of smart textiles with different meshes [181]; **c**) Photograph of a three-layer strain and pressure sensor in a stretched state. The top layer consists of a spiral pressure sensor, below which lies a two-layer biaxial strain sensor that consists of two square meander patterns (20 mm x 20 mm) oriented perpendicular to each other; **d**) electrical resistance change as a function of elongation for sensors subjected to cyclic deformation, in which each sensor is cycled 5 times to 100% strain at a crosshead speed of 2.96 mm/s [184], under CC by 4.0.

2.5.2. Integration of Conductive and/or Responsive Yarn/Filament Fiber

Conductive and/or responsive filament fibers, yarns, and metallic wires can be integrated into/onto a textile structure by weaving, knitting, embroidery, stitching laminating, and braiding techniques. Though a conductive and functional smart textile can be developed via these techniques, the electrical, functional, and mechanical properties of the textile substrate could significantly vary from the initial conductive material. This is because of the way the functional materials are placed, the structure of the textile substrate, the density of the conductive fabrics on the substrate, and other factors that could potentially determine the end-product properties.

Weaving: Weaving produces textiles that need work before they are usable in an end-product. The benefit is that there are more possibilities for integrating the active elements during the fabrication. As weaving typically utilizes a two-yarn system, i.e., it has a separate warp and weft, this naturally supports the use of different yarns. These can be varied, and even though looms require considerably more time and effort to set up, they seem to provide a reliable base for building electronic systems. As weaving is suitable for embedding electronic components into the textile during the weaving process, it also allows the encapsulation of the components between different layers. The woven textile forms a combination of thousands of threads in the warp and the weft. The warp has considerable tension, and warp threads move up and down during the weaving process, according to the harnesses they are connected to. The programmed pattern, which dictates how the threads connect within the weave, is realized with the weft. These yarns move orthogonally to the warp, and have typically low tension, with only the forces from the warp threads pressing against the weft.

For the case of developing an e-fabric, conductive yarn or filament can be integrated as warp and weft. It is also possible to insert conductive threads along with non-conductive warp and/or weft yarns. Therefore, the pattern designs possible to produce a convention textile fabric could be used to produce an entirely conductive fabric or a fabric with incorporated conductive threads or wires.

Mikkonen and Pouta developed a wire component suitable for direct integration into the textile during weaving like a normal yarn and successfully demonstrated the weaving [185]. Gidik et al. used weaving technology to develop a textile heat fluxmeter [186]. The textile fluxmeter was used as a base to produce a textile radiative heat fluxmeter i.e. to transform a textile heat fluxmeter into a textile radiative heat fluxmeter. Park et al. also used weaving as a simple fabrication procedure to develop a flexible single-strand fiber-based woven-structured triboelectric nano-generator for self-powered electronics [187]. This device converts mechanical energy from living/working environments into electrical energy. The schematic illustration of the fiber-based woven-structured triboelectric nano-generator and its dependence on the output power on external load resistances is shown in Figure 2.19a. Sun et al. also used a weaving method to construct a thermoelectric fabric woven out of thermoelectric fibers from alternately doped carbon nanotube fibers wrapped with acrylic fibers. The woven textile thermoelectric generator generated a peak power density of 70 mW/m^2 at a 44 K temperature difference and provided 80% strain without any

output degradation. The photographic image of the woven textile-based generator and its power output is shown in Figure 2.19b.

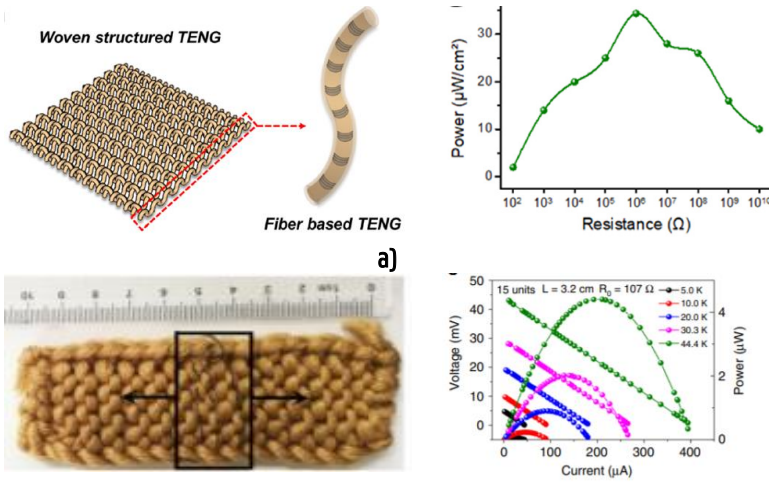

Figure 2.19: a) Schematic illustration of a fiber-based woven-structured triboelectric nano-generator (TENG) and its dependence of the output power on external load resistances [187]; **b**) a photograph of TEG composed of 15 units (3 × 5) with different length and identical resistivity and its power output at various steady temperature differences, under CC by 4.0.

Knitting: Knitting is a continuous and efficient fabric manufacturing process. Apart from creating the textile as a substrate, knitting allows the inclusion of active elements and conductive yarns during the fabrication process, making them integral to the textile structure. As knitting costs relatively less to fabricate than weaving for small samples, it is a good candidate for the rapid prototyping of smart clothing and wearable textiles. In addition, the existing industrial knitting machines are also already able to create entire and complete knitted ready-to-wear structures. Recent advancements in conductive yarns and fabrication technologies offer exciting opportunities to design and knit seamless garments equipped with sensors. For instance, Patron et al. used this technique to produce a wearable antenna for wearable applications [188]. This knit antenna works as a strain sensor taking advantage of the intensity variations of the backscattered power from an inductively-coupled RFID tag under physical stretching.

A computerized flatbed knitting method was also used to fabricate elliptical waveguides [189]. It is a conductive textile sleeve filled with knitted polyester

inside. A silver-coated polyamide conducting yarn was used. The same technique was also used to manufacture a microwave high impedance surface from a combination of both conducting and insulating yarns [190]. The entire structure of the high impedance surface; the conducting ground plane, spacer layer, conducting pattern top surface, and the vias are knitted. Such continuous development of an e-textile obviously has low cost and is highly efficient in terms of manufacturing time. Fan et al. also used the knitting technique to produce a machine washable textile-based triboelectric sensor array [142]. The sensor array exhibits a fast response time and wide working frequency bandwidth up to 20 Hz and stays functional for multiple machine washing. This textile-based sensor array was incorporated into a sweater as shown in Figure 2.20 to monitor the arterial pulse waves and respiratory signals simultaneously. The knitted triboelectric all-textile sensor array was also used to measure the cardiovascular pulse of different age groups.

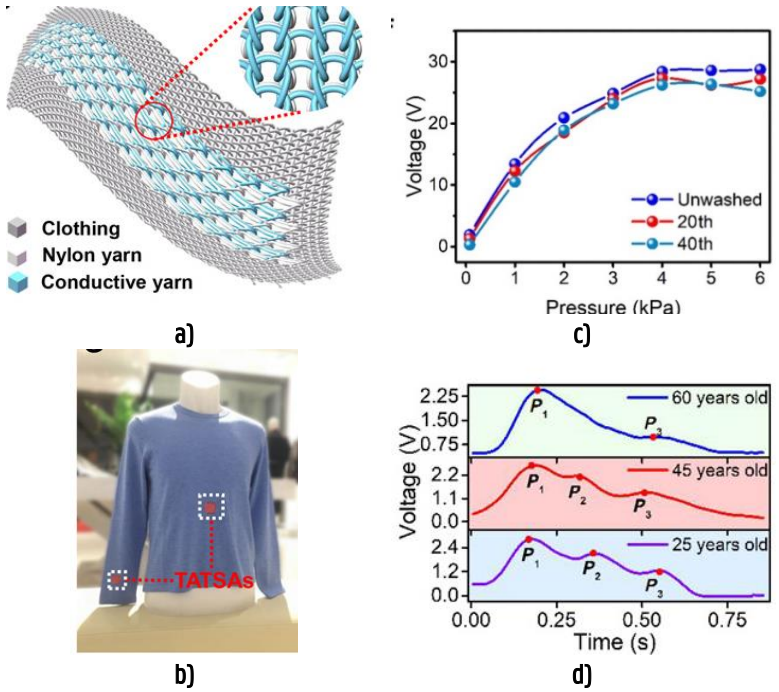

Figure 2.20: **a**) Schematic illustration of the combination of a triboelectric all-textile sensor array (TATSA): **b**) photograph of two TATSAs completely and seamlessly stitched into a sweater; **c**) output characteristics of the TATSA after washing; **d**) pulse waveforms of TATSAs for different ages [142].

Embroidery: Embroidery is applying conductive yarns or filament fibers on a textile fabric or other materials using a needle. It gives the flexibility to design and embroider traces of required shapes or contours on a plane. Compared to other textile production technologies, such as knitting or weaving, embroidery is a convenient alternative for complex and labor-intensive design and production processes. This technique enables one to integrate additional conductive threads into a finished fabric or readymade garment. Embroidery has been exploited to develop e-textiles. For instance, Moradi et al. embroidered an e-textile metamaterial transmission line for a signal propagation control for wearable applications [191]. It was a fully-embroidered conductive thread transmission line loaded with conductive yarn split-ring resonators on a felt fabric substrate.

Martinez-Estrada et al. also used the technique to embroider an interdigitated textile sensor over a cotton substrate with silver-plated nylon yarns [192]. The result showed the usefulness of the proposed sensors at the kHz range to develop a wearable application over textiles for moisture detection as shown in Figure 2.21. Besides, Alharbi et al. introduced and validated a novel class of origami dipole antennas fabricated via adaptive embroidery of conductive e-threads [193]. A shift in resonant frequency from 760 to 1015 MHz was observed while 84% of the original 10 dB bandwidth was retained, which shows an excellent agreement against a copper-based equivalent dipole.

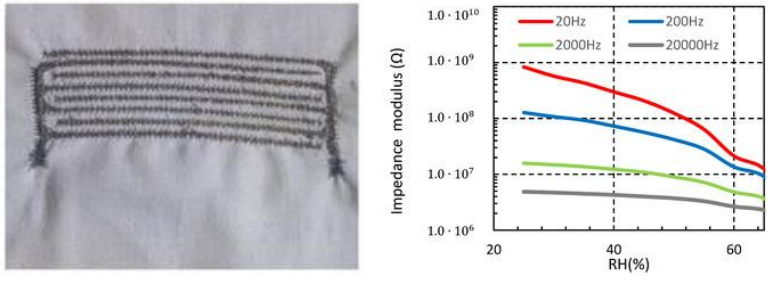

a) **b)**

Figure 2.21: a) Embroidered capacitive sensor; **b)** measured sensor impedance from 25% to 65% relative humidity (RH) at different frequencies (T = 20 °C) [192].

Embroidering has been also used to develop a textile-based sensor and antenna as shown in Figures 2.22a and 2.22b, respectively. The technique seems very promising to produce an entire set of smart textiles as the sensors, actuators, capacitors, energy harvesting devices, and interconnections can be embroidered step by step or one at a time.

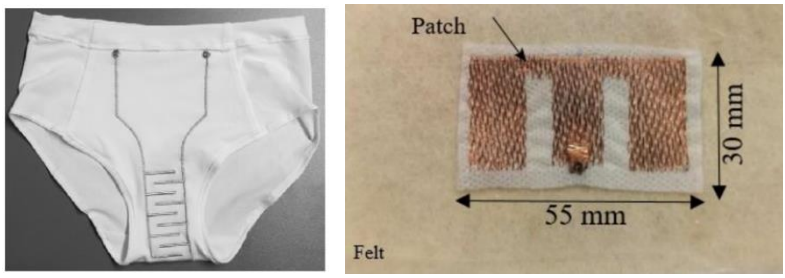

a) b)

Figure 2.22: a) Embroidered moisture sensor [62]; **b**) e-shape antenna fabricated based on embroidering technique [194].

Braiding: Braided conductive fabrics can be made by interlacing conductive yarns or strips of fabric. An entirely conductive braided fabric or partly conductive one can be made. This technique produces a wide range of structures. For example, Pragya et al. used the braiding technique to produce a conductive yarn by introducing conductive copper filament as the core and polyester multifilament yarn as the sheath. The resultant braided yarn was used to fabricate an e-heating fabric via interweaving. The electro-mechanical tests on the braided conductive yarn and e-heating fabric revealed superior tensile performance and heat-trapping with increasing the number of ends [195]. The braided conductive yarn and temperature variation around its immediate environment is shown in Figure 2.23. The braiding process is quite adaptable, however, there are certain inherent limitations related to the process itself, the input materials, the geometry of the part, and the specific needs and standards for material characteristics and uniformity [145].

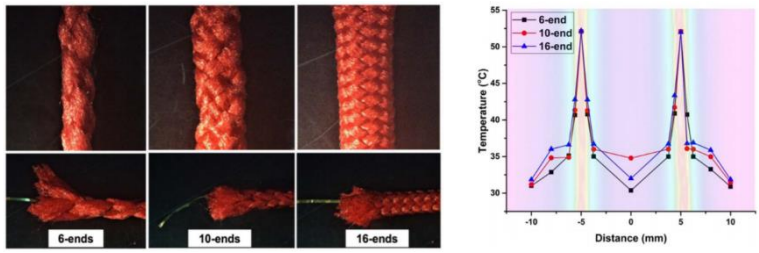

a) b)

Figure 2.23: a) Braided conductive yarns with single copper core covered with 6-, 10-, and 16-end polyester sheath and 76°, 96°, and 120° braiding angles, respectively; b) Temperature variation around BCYs immediate environment [195].

Stitching: Another approach could be stitching, the process of joining or fastening a fabric or an item of clothing with a continuous loop of thread or yarn. In this method, conductive filament fibers or yarns can be inserted into the textile structure in the way that a stitch is inserted during sewing. For instance, Tangsirinaruenart and Stylios [196] developed a strain sensor made up of a silver-plated nylon conductive thread with different stitch structures sewn directly onto a single jersey knit nylon fabric substrate as shown in Figure 2.24.

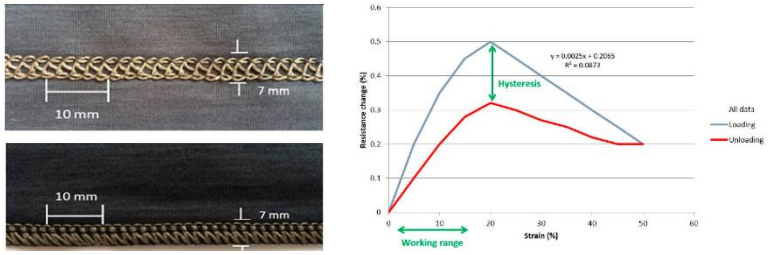

a) b)

Figure 2.24: **a**) a strain sensor from a silver-plated nylon conductive thread stitched onto a single jersey knit nylon fabric; **b**) graph of resistance change (%) vs. strain (%), for defining stitched sensor characteristics. [196], under CC by 4.0.

2.5.3. Integration of Conductive and/or responsive Fabric/Sheet

In this technique, a smart fabric, sheet, or stripe can be placed on textile fabrics by stacking and laminating via welding, an adhesive, or through the use of heat or pressure.

Lamination: Smart components can be laminated to a textile structure with adhesive materials or stitching. In sheet laminating, a conductive sheet, strip, or fabric, is combined with a substrate through heat and pressure in order to integrate it into a smart textile application. Therefore, this technique can be used to produce e-fabric quickly. For instance, Memon et al. [35] laminated a conductive copper sheet on a spacer fabric to develop a textile patch antenna. Vanveerdeghem et al. [197], Sorti and Company [198], and Choi et al. [199] have also reported e-textiles by conductive sheet lamination. As a specific example, Wagih et al. used the technique to develop a textile-based patch antenna based on a coplanar waveguide [200]. The efficiency of the coplanar waveguide monopole was independent of the thickness of the substrate and the type of

fabric. The fabricated antenna and the performance of the coplanar waveguide textile monopole are shown in Figure 2.25.

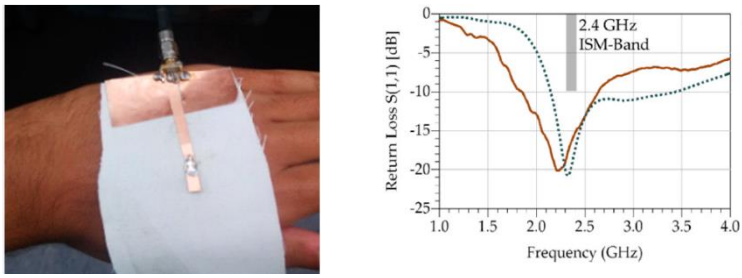

a) b)

Figure 2.25: Conductive sheet lamination: **a**) Fabricated antenna on-hand; **b**) simulated (dashed) and measured (solid)

Stitching: A normal sewing thread/stitch can also be used to attach the smart component with a textile substrate instead of using adhesives. A smart component can be simply sandwiched/encapsulated between two textile substrates. Polyurethane is commonly used to sandwich a smart component on a textile substrate. Photographic images of stitching methods are shown in Figure 2.26.

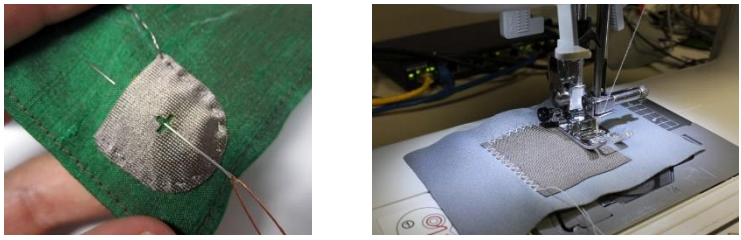

a) b)

Figure 2.26: a) Stitching of conductive fabric on a textile fabric: hand-stitching; **b**) machine stitching

2.6. Application of Smart Textiles

Commercial application of smart textiles is booming in civil, military, medical, and many high-risk areas and emergency services. Smart textiles can be utilized to assess light absorption intensity, and smart textiles can detect radiation zones, allowing environmental dangers to be identified. They can be also used for filtration and separation of matters in different states.

2.6.1. Medical and Health Care

Physiological activity monitoring smart textiles are used in healthcare and telemedicine [201]. Smart textiles that measure the pulse and immune systems [202], gloves with microphones [203], sensors in mattresses [12], cooling clothes [204], and warming clothes [205] are available. For instance, Lam et al. [82] developed a textile-based graphene-coated cotton electrode that can sense heart activity as shown in Figure 2.27.

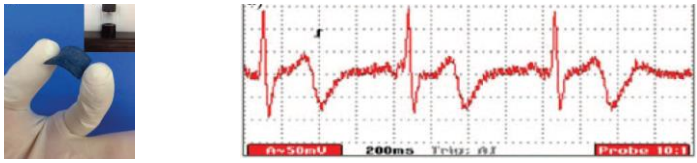

a) b)

Figure 2.27: a) Graphene-coated cotton fabric ECG electrode with great flexibility; **b**) ECG signal of a healthy subject recorded using graphene-coated cotton fabric electrode, [82].

2.6.2. Sport and Human Performance

Smart textile has promising applications in the field of sports for individual physiological monitoring and time-motion analysis during the race. For instance, Mao et al. reported self-powered piezoelectric bio-sensing textiles for physiological monitoring and time-motion analysis during sporting activity [206], shown in Figure 2.28.

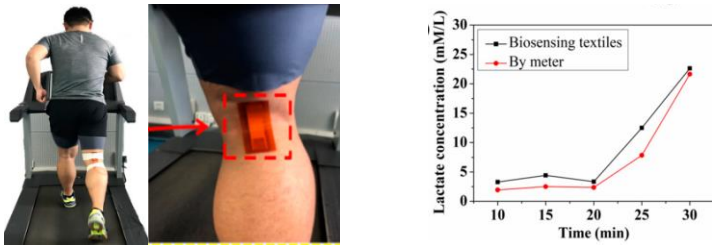

a) b)

Figure 2.28: a) piezoelectric textiles attached to an athlete on the treadmill for testing real-time motion analysis of individual sports; **b**) lactate concentration measured by the self-powered piezoelectric-biosensing textiles and commercial meter. [206], under CC BY 4.0.

2.6.3. Military and Security

Smart textiles can be also used in the military as color-changing camouflage providing advantages to the troops in war zones, making them less detectable. For example, Karpagam et al. reported a color-changing smart camouflage clothing for military applications using thermochromic colorants [30], shown in Figure 2.29. Smart textiles for military applications face a lot of challenges in terms of protection, durability, and comfort in different kinds of environments.

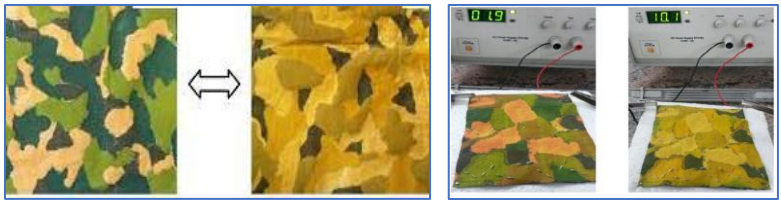

a) **b)**

Figure 2.29: A thermochromic camouflage military fabric clour change: **a**) heating to 60 °C; **b**) increasing voltage from 2V and 10V [30].

2.6.4. Detection and Protection

Smart textiles can also be used in detecting the intensity of light absorption. Environmental hazards can be identified by detecting radiation zones with smart textiles. The application of smart textiles for personnel protection is also numerous. For instance, Ghatak et al. designed a smart triboelectric-based self-powered smart mask for COVID-19 [207]. Kinnamon et al. reported on a screen-printed graphene oxide wearable textile biosensor for influenza detection for at-risk populations [37], shown in Figure 2.30.

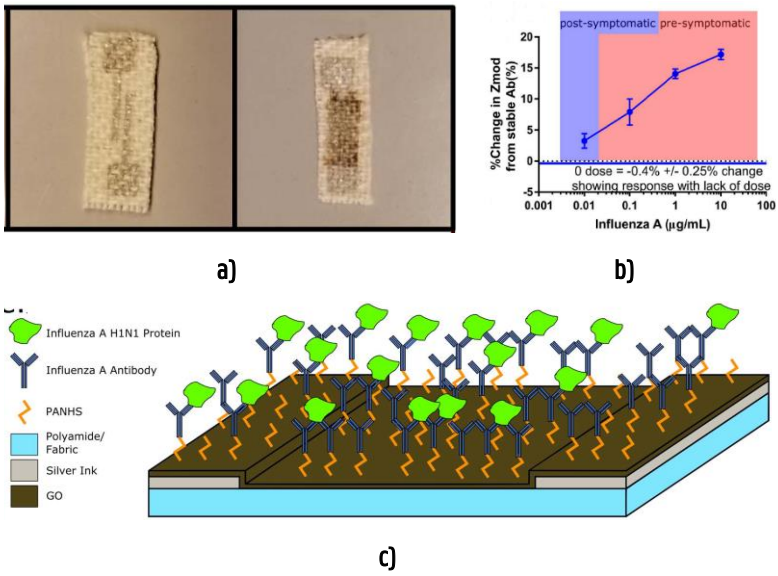

Figure 2.30: a) Screen-printed textile sheets electrodes with a ~100-micron thick pattern of conductive silver ink and a layer of graphene oxide; **b**) calibration dose-response for influenza A in buffer solution; **c**) cross-section schematic visually detailing the affinity assay for influenza. [37], under CC by 4.0.

2.6.5. Fashion and Entertainment

It is well known that the fashion industry is dependent on textiles and undoubtfully no textile means no fashion. The application of smart textiles in the fashion industry is growing very rapidly. Several smart wearable products with gorgeous and changing colors have been developed by applying the lateral light emission principle of optical fibers. Photo-chromic textiles that change their color under certain stimuli or with the preprogrammed system are also used in the fashion industry. Examples include a light-emitting e-textile developed by Wu et al. [208] which is shown in Figure 2.31. Other smart textiles applications also exist to make textiles more appealing, eye-catching, and gorgeous.

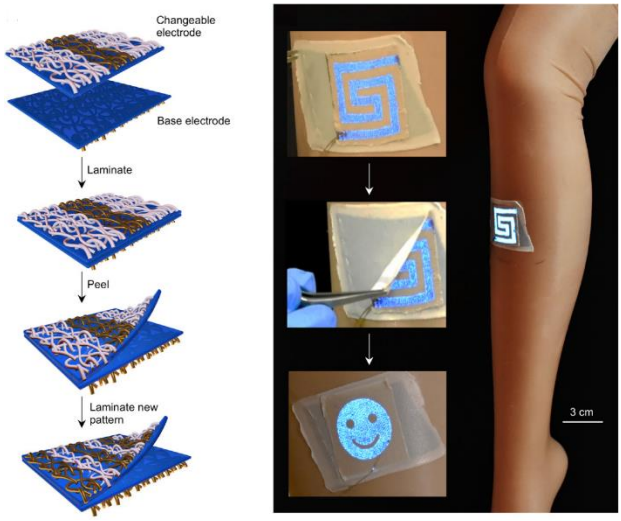

Figure 2.31: Photograph of changeable patterned e-textile worn on a mannequin leg [208].

2.7. Prospects and Sustainability

Humans interact with textiles across various aspects of their lives which make textiles useful as platforms in cloud computing systems, as user interfaces, and as health monitoring sensor arrays. Emerging novel technology platforms tackle the challenges of relying on textiles due to their structural topology complexity and variable mechanical stresses to the condition they are exposed to. Moreover, the rapid development in intelligent polymers and integration techniques like 4D printing could boost the performance, functionality, and state-of-the-art application of smart textiles in the future.

The evolution and development of smart textiles are ongoing. Smart textiles become less intrusive, more intelligent, and lower cost. Apart from this, there are also some groundbreaking developments. In this section, prospects of intelligent polymers, stealth invisible textiles, 4D printing, and visionary textiles are addressed.

2.7.1. Prospects on Intelligent Polymers

Numerous applications for adaptive materials exist or are envisaged, including associative thickeners in paints, personal care products, micelle systems for controlled drug release in medicine, and pollutant uptake in environmental

applications. Contemporary macromolecular materials may be spot-on to meet explicit needs that we have experience with and rely on. This is important for forthcoming generations of materials and products, mainly textiles. Smart textile products, such as those used in skincare, could be created by coalescing novel adaptive polymers with traditional textiles. As a result, smart textiles with temperature-controlled release and antibacterial activity will have colossal potential in the cosmetics and pharmaceutical industries.

Shape-memory adaptive polymers may be used in tissue engineering wherein self-growing and biocompatible inner organs, veins, and scaffolds can be created. For instance, Must et al. [209], demonstrated a self-powering mobile robot propelled by a single ionic electroactive polymer actuator that functions similarly to a supercapacitor. It was able to run on a dry surface while carrying all of its components, including electronics and power supplies, as well as an additional weight with the same mass as the robot. The ionic electroactive polymer robot is shown in Figure 2.32. Mingling adaptive polymers and 4D printing, the printing of 3D responsive objects that change form later by stimulants, ought to make self-growing cells and pulsing hearts. The responsive or adaptive polymers may additionally own biosensing features to internal diseases and actuate to limit and additionally adapt.

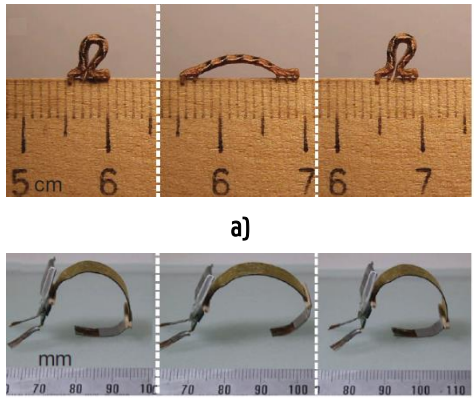

a)

b)

Figure 2.32: a) Locomotion of an inchworm inspires the design; **b**) a biomimetic ionic electroactive polymer robot [209].

Today's researchers in adaptive and functional polymers and textiles face several challenges. A thorough understanding of the structure-property relationship is essential for the rational design of new functional adaptive polymers, which will allow for the further development of novel technologies. Therefore,

professionals from the fields of chemical and material science, as well as electrical and textile engineering, computer science, and medicine, should work together to develop efficient, effective, biocompatible, and durable responsive forthcoming materials.

2.7.2. Stealth Invisible Textiles

The concept of stealth, to operate or hide in such a way that enemy forces are unaware of the presence of friendly forces, was first explored through camouflage to make an object's appearance blend into the visual background. Later, chameleonic camouflages with an improved degree of concealment function appeared. And now, Hyperstealth Biotechnology, a Canadian company, has patented paper fabrics that make objects invisible to the naked eye. Lee et al. demonstrated a soft, skin-like invisible device with a pixelized thermal operation that gives immediate cloaking ability in the visible and infrared regions [210], shown in Figure 2.33. The skin-like cloaking platform not only transmits key cephalopod camouflage qualities, but it also demonstrates excellent practicality for direct application to human skin. Coalescing the concept of quantum physics and stealth theory to color-changing adaptive materials could cause the emergence of state-of-the-art invisible cloak fabrics practical in the near future and amplify the scope of application of adaptive polymers. Application of refractive materials and metamaterials with negative refraction index into textile materials could be potentially used for this purpose.

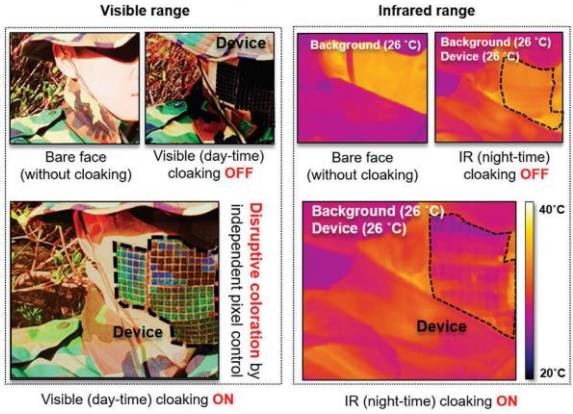

Figure 2.33: Actual demonstration of multispectral imperceptible artificial skin worn on half of the face for military stealth application [210]. The pixelization of the device allows an autonomous control of each pixel and thus is employed to exemplify disruptive coloration to blend into the environment.

2.7.3. Prospects on 4D-printed Smart Textiles

3D printing technology can be used to print objects through the use of a lot of materials. However, the objects have usually fixed geometrical structures, and are not helpful for multifunctional uses. For these reasons, there are also initiatives to materialize 4D items in which stimuli-responsive active smart materials can be used to produce a 3D static structure that can change over time [211]. 3D printed objects often have fixed geometrical structures, making them unsuitable for multifunctional usage. The concept of 4D printing refers to what happens after 3D printing is completed, i.e., a 3D static structure is first fabricated and then able to convert or reconfigure into a new structure in the presence of a stimulus such as light, heat, pH, water, a magnetic field, or other means, depending on the material used for 3D printing.

In its first 3D form, a smaller object is created, which can then expand, flex, or fold out into a larger object in its secondary form. This allows for the creation of enormous 3D items that would otherwise be too large to fit into a standard 3D printer. The concept of 4D printing may seem like something way beyond our time and factious, but many labs around the globe are already working on the futuristic prospects of this impressive approach. Most importantly, 4D printers do not exist as separate or special functioning machines. Instead, the 3D printer is used to create the initial static object and include all the necessary 4D coding prior to subjecting the object to the elements that encourage the shape to vary. For instance, Yang et al. developed originally a 3D structure that changed its shape with light like a sunflower [212] shown in Figure 2.34. Thus, 4D printing could be a viable option for creating dynamic structures for smart fabrics. To cope with 4D printing, a thorough understanding of the chemistry and physics of smart materials, as well as their behavior, is required.

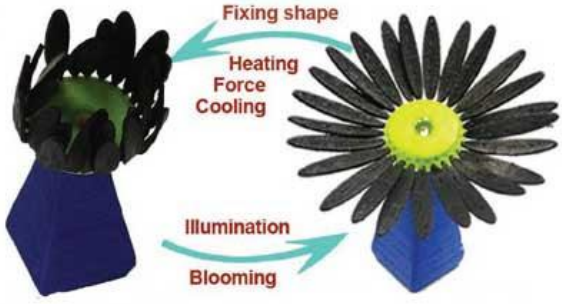

Figure 2.34: Photo-triggered shape memory behavior of 3D printed sunflower from closed to opened state like the blooming of flowers [212].

Generally, for integrated smart textiles, the fabrication of 2D and 3D textile structures will continue, and 4D printing technology will evolve in the near future. The emergence of new and advanced integration techniques will certainly speed up the reality of self-powered and computerized textiles leading to a new generation of smart textile applications.

2.7.4. Prospects on Visionary Textiles

Visionary textiles are fundamentally engineered biological functions that create their own textiles. The approach might involve the natural growth of genetically engineered conductive strands. For instance, boosting metallic mineral absorption in cotton and allowing them to accumulate in the seed. Cotton could also be treated with metallic nanoparticles throughout the flowering and boll opening stages. The emergence of self-healing which enables an autonomous repair response to damaged textiles would evolve. Gaddes et al. already reported a self-healing textile that retains enzyme activity even after repairing large defects. According to Collet [213], plants could be genetically engineered to produce textile lace among their roots, bio-lace, as shown in Figure 2.35, which is not a real product, but an art installation. These are purely conceptual ideas that are unlikely to reach commercial implementation at this time. They are now only hypothetical concepts, and they are unlikely to gain widespread acceptance. They do, however, expand the imagination in terms of the level of integration that smart textiles & clothing will very certainly achieve in the future.

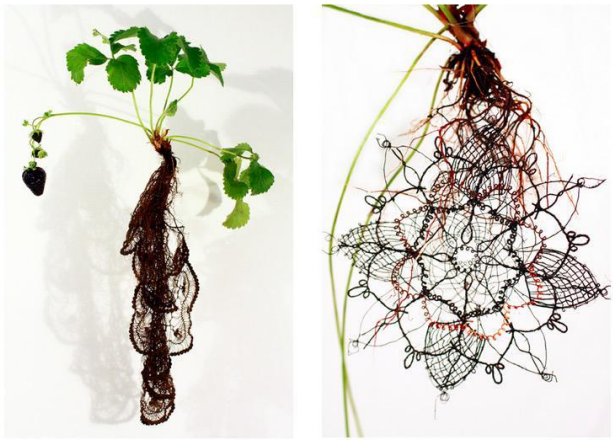

Figure 2. 35: Bio-lace growing on strawberry plant roots [213].

2.8. Conclusion

This review attempts to offer a concise and comprehensive introduction to the present-day large field of smart textiles, which has been driven by the release of many flexible electronics as well as growing demand from the electronics industry and society. Current advances in textile technology, new materials, nanotechnology, and miniaturized electronics make wearable systems more feasible, but fit comfort is the ultimate key factor for wearable device user acceptance. It is convincing that this objective can only be achieved by addressing mechanical robustness and material durability in what is recognized as a harsh electronic environment: the human body and society. Thus, the use of conductive polymer composites for smart textiles could possibly be the primal solution. Composites of conductive polymers have been explored to overcome their brittleness and processability while retaining their electrical conductivity and desirable biological properties such as cell adhesion. Enhanced mechanical properties of conductive composites usually come at the expense of the desired electrical conductivity of conductive polymers. On the other hand, a fundamental understanding of the interaction between the conductive polymer filler and the non-conductive commodity polymer matrix will lead to getting synergistic effect in the mechanical performance and electrical properties of the composites. There is a need to achieve reasonable electrical conductivity with the lowest possible amount of conductive filler while retaining the properties of the host polymer. The major challenges thus lie in the selection of conductive filler achieving a low percolation threshold and retaining biocompatibility for biomedical applications.

In addition, this comprehensive review revealed that there are no specific processes that have been designed for smart textiles, instead, existing processes are being modified. It is convincible that the goal of smart textile development can only be achieved by using appropriate and convenient e-textile integration techniques. For that matter, all production technologies require further progress in all aspects. Knitting, weaving, embroidery, braiding, and laminating are mostly used, but the flexibility of the final product is unsatisfactory. Printing, plating, fiber spinning, and coating methods are suitable if the starting conductive materials are a compound or ink. However, there is a technological challenge to print thin conductive compounds on textile fabrics that have rough, uneven, or porous surfaces. Printing the entire components of the smart textile layer-by-layer via 3D printing and realizing 4D structures would lead to an evolution of completely new smart textile materials.

From a textile perspective, the overall aim for smart textiles is to convert all required components, like sensors, actuators, transmission lines, etc. into 100% textile material. To achieve this aim, we must tackle a big challenge from a technological point of view, that is, concepts, materials, and integration techniques must be made appropriate for use in, on, or as textile materials. Hence, the focus should be directed to improving the existing techniques and introducing new approaches that are able to cope with the advancement of material science and electronics. Smart textiles will undoubtedly become an appealing solution for comfortable and unobtrusive monitoring of daily activity parameters as corresponding technologies evolve. The possibility for producing low-cost wearable solutions lies in achieving the requisite functionality and performance while using scalable production methodologies compatible with traditional textile technologies. To enable their usage in long-term monitoring and support systems, research is needed to improve the sensitivity, repeatability, durability, reproducibility, and level of integration of textile-based technologies. Materials, discrete sensor/device integration in textiles, production, regulatory compliance, and validation of end users' needs, are some of the research subjects that must be further investigated in order to improve the smart textiles available in the near future.

Bibliography

[1] M. Collard, L. Tarle, D. Sandgathe, and A. Allan, "Faunal evidence for a difference in clothing use between Neanderthals and early modern humans in Europe," *J. Anthropol. Archaeol.*, vol. 44, pp. 235–246, Dec. 2016, doi: 10.1016/j.jaa.2016.07.010.

[2] E. R. Post, M. Orth, E. Cooper, and R. S. Joshua, "Electrically Active Textiles and Articles Made Therefrom," US 6,210,771 B1, Apr. 03, 2001 [Online]. Available: https://patents.google.com/patent/US6210771B1/en

[3] C. M. Choi, S. N. Kwon, and S. I. Na, "Conductive PEDOT:PSS-coated poly-paraphenylene terephthalamide thread for highly durable electronic textiles," *J. Ind. Eng. Chem.*, vol. 50, pp. 155–161, 2017, doi: 10.1016/j.jiec.2017.02.009.

[4] K. Cherenack, C. Zysset, T. Kinkeldei, N. Münzenrieder, and G. Tröster, "Woven electronic fibers with sensing and display functions for smart textiles," *Adv. Mater.*, vol. 22, no. 45, pp. 5178–5182, 2010, doi: 10.1002/adma.201002159.

[5] V. Kaushik *et al.*, "Textile-Based Electronic Components for Energy Applications: Principles, Problems, and Perspective," *Nanomaterials*, vol. 5, no. 3, pp. 1493–1531, 2015, doi: 10.3390/nano5031493.

[6] A. Lymberis and R. Paradiso, "Smart fabrics and interactive textile enabling wearable personal applications: R&D state of the art and future challenges," in *2008 30th Annual International Conference of the IEEE Engineering in Medicine and Biology Society*, Vancouver, BC, Aug. 2008, pp. 5270–5273. doi: 10.1109/IEMBS.2008.4650403.

[7] L. Van Langenhove, "Smart Textiles: Past, Present, and Future," in *Handbook of Smart Textiles*, X. Tao, Ed. Singapore: Springer Singapore, 2014, pp. 1–20. doi: 10.1007/978-981-4451-68-0_15-1.

[8] CENTEXBEL VKC, "Smart Textiles," 2019. https://www.centexbel.be/en/lexicon/smart-textiles

[9] J. R. Steele *et al.*, "The Bionic Bra: Using electromaterials to sense and modify breast support to enhance active living," *J. Rehabil. Assist. Technol. Eng.*, vol. 5, p. 205566831877590, 2018, doi: 10.1177/2055668318775905.

[10] X. Tao, Y. Wang, H. Zhang, and G. Wang, "Method for manufacturing fabric strain sensors," US 2009/0282671 A1, Nov. 19, 2009 Accessed: Aug. 25, 2022. [Online]. Available: https://patents.google.com/patent/US20090282671A1/pt-PT

[11] Y. Koyama, M. Nishiyama, and K. Watanabe, "Smart Textile Using Hetero-Core Optical Fiber for Heartbeat and Respiration Monitoring," *IEEE Sens.*

J., vol. 18, no. 15, pp. 6175–6180, Aug. 2018, doi: 10.1109/JSEN.2018.2847333.

[12] Smartx-Europe, "Smart textiles in Europe: the next tech disruption – interview with Andreas," Feb. 25, 2021. https://www.smartx-europe.eu/smart-textiles-europe-next-tech-disruption-interview-lymberis-1/ (accessed Oct. 03, 2022).

[13] M. Stoppa and A. Chiolerio, "Wearable Electronics and Smart Textiles: A Critical Review," vol. 14, pp. 11957–11992, 2014, doi: 10.3390/s140711957.

[14] H. H. Dadi, "Literature over view of Smart textiles," Boras University, 2010.

[15] C. Gopalsamy, S. Park, R. Rajamanickam, and S. Jayaraman, "The Wearable Motherboard: The First Generation of Adaptive and Responsive Textile Structures (ARTS) for Medical Applications," *Virtual Real.*, vol. 4, pp. 152–168, 1999, doi: https://doi.org/10.1007/BF01418152.

[16] J. Xiaopei Wu and L. Li, "An Introduction to Wearable Technology and Smart Textiles and Apparel: Terminology, Statistics, Evolution, and Challenges," in *Smart and Functional Soft Materials*, X. Dong, Ed. IntechOpen, 2019. doi: 10.5772/intechopen.86560.

[17] M. Stoppa and A. Chiolerio, "Wearable Electronics and Smart Textiles: A Critical Review," *Sensors*, vol. 14, no. 7, pp. 11957–11992, Jul. 2014, doi: 10.3390/s140711957.

[18] A. B. Nigusse, B. Malengier, D. A. Mengistie, G. B. Tseghai, and L. Van Langenhove, "Development of Washable Silver Printed Textile Electrodes for Long-Term ECG Monitoring," *Sensors*, vol. 20, no. 21, p. 6233, Oct. 2020, doi: 10.3390/s20216233.

[19] R. Castrillón, J. J. Pérez, and H. Andrade-Caicedo, "Electrical performance of PEDOT:PSS-based textile electrodes for wearable ECG monitoring: a comparative study," *Biomed. Eng. OnLine*, vol. 17, no. 1, p. 38, Dec. 2018, doi: 10.1186/s12938-018-0469-5.

[20] J. Meyer, B. Arnrich, J. Schumm, and G. Troster, "Design and Modeling of a Textile Pressure Sensor for Sitting Posture Classification," *IEEE Sens. J.*, vol. 10, no. 8, pp. 1391–1398, Aug. 2010, doi: 10.1109/JSEN.2009.2037330.

[21] F.-C. Liang *et al.*, "An intrinsically stretchable and ultrasensitive nanofiber-based resistive pressure sensor for wearable electronics," *J. Mater. Chem. C*, vol. 8, no. 16, pp. 5361–5369, 2020, doi: 10.1039/D0TC00593B.

[22] G. B. Tseghai, B. Malengier, A. B. Nigusse, and L. V. Langenhove, "Development and evaluation of resistive pressure sensors from electro-conductive textile fabric," in *Proceeding of The Second*

International Forum on Textiles for Graduate Students (IFTGS) 2018, Tianjin, Sep. 2018, p. 9.

[23] Z. Ma, R. Xu, W. Wang, and D. Yu, "A wearable, anti-bacterial strain sensor prepared by silver plated cotton/spandex blended fabric for human motion monitoring," *Colloids Surf. Physicochem. Eng. Asp.*, vol. 582, p. 123918, Dec. 2019, doi: 10.1016/j.colsurfa.2019.123918.

[24] W. Root, T. Wright, B. Caven, T. Bechtold, and T. Pham, "Flexible Textile Strain Sensor Based on Copper-Coated Lyocell Type Cellulose Fabric," *Polymers*, vol. 11, no. 5, p. 784, May 2019, doi: 10.3390/polym11050784.

[25] G. B. Tseghai, B. Malengier, D. A. Mengistie, K. A. Fante, and L. Van Langenhove, "Knitted Cotton Fabric Strain Sensor by In-situ Polymerization of Pyrrole," *IOP Conf. Ser. Mater. Sci. Eng.*, vol. 827, p. 012041, Jun. 2020, doi: 10.1088/1757-899X/827/1/012041.

[26] M. Caldara, C. Colleoni, E. Guido, V. Re, G. Rosace, and A. Vitali, "Textile Based Colorimetric pH Sensing: A Platform for Future Wearable pH Monitoring," in *2012 Ninth International Conference on Wearable and Implantable Body Sensor Networks*, London, United Kingdom, May 2012, pp. 11–16. doi: 10.1109/BSN.2012.21.

[27] L. Manjakkal, W. Dang, N. Yogeswaran, and R. Dahiya, "Textile-Based Potentiometric Electrochemical pH Sensor for Wearable Applications," *Biosensors*, vol. 9, no. 1, p. 14, Jan. 2019, doi: 10.3390/bios9010014.

[28] X.-Z. Sun, C. Branford-White, Z.-W. Yu, and L.-M. Zhu, "Development of universal pH sensors based on textiles," *J. Sol-Gel Sci. Technol.*, vol. 74, no. 3, pp. 641–649, Jun. 2015, doi: 10.1007/s10971-015-3643-2.

[29] G. Bartkowiak, A. Dąbrowska, and A. Greszta, "Development of Smart Textile Materials with Shape Memory Alloys for Application in Protective Clothing," *Materials*, vol. 13, no. 3, p. 689, Feb. 2020, doi: 10.3390/ma13030689.

[30] K. R. Karpagam, K. S. Saranya, J. Gopinathan, and A. Bhattacharyya, "Development of smart clothing for military applications using thermochromic colorants," *J. Text. Inst.*, pp. 1–6, Aug. 2016, doi: 10.1080/00405000.2016.1220818.

[31] J. R. Steele *et al.*, "The Bionic Bra: Using electromaterials to sense and modify breast support to enhance active living," *J. Rehabil. Assist. Technol. Eng.*, vol. 5, p. 205566831877590, Jan. 2018, doi: 10.1177/2055668318775905.

[32] X. A. Zhang *et al.*, "Dynamic gating of infrared radiation in a textile," *Science*, vol. 363, no. 6427, pp. 619–623, Feb. 2019, doi: 10.1126/science.aau1217.

[33] G. Wallace, J. R. Steele, and K.-A. Bowles, "Smart bra heralds the age of intelligent fabrics," *Tech. Text. Int.*, vol. 9, no. 6, p. 32, 2000.

[34] T. Hughes-Riley, T. Dias, and C. Cork, "A Historical Review of the Development of Electronic Textiles," *Fibers*, vol. 6, no. 2, p. 34, May 2018, doi: 10.3390/fib6020034.

[35] A. W. Memon, I. L. de Paula, B. Malengier, S. Vasile, P. Van Torre, and L. Van Langenhove, "Breathable Textile Rectangular Ring Microstrip Patch Antenna at 2.45 GHz for Wearable Applications," *Sensors*, vol. 21, no. 5, p. 1635, Feb. 2021, doi: 10.3390/s21051635.

[36] R. Nolden, K. Zöll, and A. Schwarz-Pfeiffer, "Smart Glove with an Arduino-Controlled Textile Bending Sensor, Textile Data Conductors and Feedback Using LED-FSDsTM and Embroidery Technology," *Proceedings*, vol. 68, no. 1, p. 4, Jan. 2021, doi: 10.3390/proceedings2021068004.

[37] D. S. Kinnamon, S. Krishnan, S. Brosler, E. Sun, and S. Prasad, "Screen Printed Graphene Oxide Textile Biosensor for Applications in Inexpensive and Wearable Point-of-Exposure Detection of Influenza for At-Risk Populations," *J. Electrochem. Soc.*, vol. 165, no. 8, pp. B3084–B3090, 2018, doi: 10.1149/2.0131808jes.

[38] M. D. Husain, R. Kennon, and T. Dias, "Design and fabrication of Temperature Sensing Fabric," *J. Ind. Text.*, vol. 44, no. 3, pp. 398–417, Nov. 2014, doi: 10.1177/1528083713495249.

[39] S. Xu, Q. Ma, X.-F. Yang, and S.-D. Wang, "Design and fabrication of a flexible woven smart fabric based highly sensitive sensor for conductive liquid leakage detection," *RSC Adv.*, vol. 7, no. 65, pp. 41117–41126, 2017, doi: 10.1039/C7RA07273B.

[40] A. R. Salmon, S. Cormier, W. Wang, C. Abell, and J. J. Baumberg, "Motile Artificial Chromatophores: Light-Triggered Nanoparticles for Microdroplet Locomotion and Color Change," *Adv. Opt. Mater.*, vol. 7, no. 22, p. 1900951, Nov. 2019, doi: 10.1002/adom.201900951.

[41] J. Xiaopei Wu and L. Li, "An Introduction to Wearable Technology and Smart Textiles and Apparel: Terminology, Statistics, Evolution, and Challenges," in *Smart and Functional Soft Materials*, X. Dong, Ed. IntechOpen, 2019. doi: 10.5772/intechopen.86560.

[42] H. Okuzaki, S. Takagi, F. Hishiki, and R. Tanigawa, "Ionic liquid/polyurethane/PEDOT:PSS composites for electro-active polymer actuators," *Sens. Actuators B Chem.*, vol. 194, pp. 59–63, 2014, doi: 10.1016/j.snb.2013.12.059.

[43] R. Aigner, A. Pointner, T. Preindl, P. Parzer, and M. Haller, "Embroidered Resistive Pressure Sensors: A Novel Approach for Textile Interfaces," in *Proceedings of the 2020 CHI Conference on Human Factors in Computing*

Systems, Honolulu HI USA, Apr. 2020, pp. 1–13. doi: 10.1145/3313831.3376305.

[44] W. Mu *et al.*, "Double layer printed high performance OLED based on PEDOT : PSS/Ir (bt) 2acac : CDBP," *AIP Adv.*, vol. 115112, no. August 2018, 2019, doi: 10.1063/1.5053133.

[45] D. Shin, J. Lee, G. Kim, and J. Park, "Improved Intrapixel Thickness Uniformity of Slot-Coated PEDOT : PSS Films for OLEDs via Dilution and Predrying Treatments," *IEEE Trans. Electron Devices*, vol. 65, no. 10, pp. 4506–4512, 2018, doi: 10.1109/TED.2018.2866693.

[46] Y. Zheng *et al.*, "Highly efficient red fluorescent organic light-emitting diodes by sorbitol-doped PEDOT:PSS," *J. Phys. Appl. Phys.*, vol. 51, 2018.

[47] X. Tao, *Handbook of Smart Textiles*, 1st ed. Singapore: Springer Science+ Business Media Singapore, 2014. doi: 10.1007/978-981-4451-68-0_1-1.

[48] V. Koncar, *Smart Textiles and Their Applications*. Cambridge: Woodhead Publishing Series in Textiles, 2016.

[49] L. van Langenhove, *Advances in Smart Medical Textiles: Treatments and Health Monitoring*. Cambridge: Woodhead Publishing Series in Textiles, 2016.

[50] L. Dai, *Intelligent Macromolecules for Smart Devices: From Materials Synthesis to Device Applications*. London: Springer, 2004.

[51] T. Kirstein, *Multidisciplinary know-how for smart-textiles developers*, 1st ed. Cambridge: Woodhead Publishing Series in Textiles, 2013.

[52] S. Park *et al.*, "Textile Speaker Using Polyvinylidene Fluoride/ZnO Nanopillar on Au Textile for Enhancing the Sound Pressure Level," *Sci. Adv. Mater.*, vol. 10, no. 12, pp. 1788-1792(5), 2018, doi: https://doi.org/10.1166/sam.2018.3378.

[53] E. Grant *et al.*, "Developing portable acoustic arrays on a large-scale e-textile substrate," *Int. J. Cloth. Sci. Technol.*, vol. 16, no. 1/2, pp. 73–83, Feb. 2004, doi: 10.1108/09556220410520379.

[54] K. A. Luthy *et al.*, "Initial Development of a Portable Acoustic Array on a Large-Scale E-Textile Substrate," *MRS Proc.*, vol. 736, p. D3.7, 2002, doi: 10.1557/PROC-736-D3.7.

[55] T. L. Buckner, R. A. Bilodeau, S. Y. Kim, and R. Kramer-Bottiglio, "Roboticizing fabric by integrating functional fibers," *Proc. Natl. Acad. Sci.*, vol. 117, no. 41, pp. 25360–25369, Oct. 2020, doi: 10.1073/pnas.2006211117.

[56] C. Hertleer, H. Rogier, S. Member, L. Vallozzi, and L. Van Langenhove, "A Textile Antenna for Off-Body Communication Integrated Into Protective Clothing for Firefighters," *IEEE Trans. Propag.*, vol. 57, no. 4, pp. 919–925, 2009.

[57] S. Kannadhasan and A. C. Shagar, "Design and Analysis of U-Shaped Microstrip Patch Antenna," in *3rd International Conference on Advances in Electrical, Electronics, Information, Communication and Bio-Informatics (AEEICB17) Design*, 2017, pp. 3–6.

[58] S. B. Roshni, M. P. Jayakrishnan, P. Mohanan, and K. P. Surendran, "Design and fabrication of an E-shaped wearable textile antenna on PVB-coated hydrophobic polyester fabric," *Smart Mater. Struct.*, vol. 26, no. 105011, p. 8, 2017.

[59] S. J. Chen, C. Fumeaux, B. Chivers, and R. Shepherd, "A 5. 8-GHz Flexible Microstrip-Fed Slot Antenna Realized in PEDOT:PSS Conductive Polymer," *2016 IEEE Int. Symp. Antennas Propag. APSURSI*, vol. 2015, pp. 1317–1318, 2016, doi: 10.1109/APS.2016.7696366.

[60] B. Krykpayev, M. F. Farooqui, R. M. Bilal, and A. Shamim, "A WiFi tracking device printed directly on textile for wearable electronics applications," in *2016 IEEE MTT-S International Microwave Symposium (IMS)*, San Francisco, CA, May 2016, pp. 1–4. doi: 10.1109/MWSYM.2016.7540334.

[61] C. Luo, I. Gil, and R. Fernández-García, "Wearable Textile UHF-RFID Sensors: A Systematic Review," *Materials*, vol. 13, no. 15, p. 3292, Jul. 2020, doi: 10.3390/ma13153292.

[62] U. Briedis, A. Valisevskis, and M. Grecka, "Development of a Smart Garment Prototype with Enuresis Alarm Using an Embroidery-machine-based Technique for the Integration of Electronic Components," *Procedia Comput. Sci.*, vol. 104, pp. 369–374, 2017, doi: 10.1016/j.procs.2017.01.147.

[63] A. O. Komolafe, R. N. Torah, K. Yang, J. Tudor, and S. P. Beeby, "Durability of screen printed electrical interconnections on woven textiles," *Proc. - Electron. Compon. Technol. Conf.*, vol. 2015-July, pp. 1142–1147, 2015, doi: 10.1109/ECTC.2015.7159738.

[64] T. He, Q. Shi, H. Wang, F. Wen, and T. Chen, "Nano Energy Beyond energy harvesting - multi-functional triboelectric nanosensors on a textile," *Nano Energy*, vol. 57, no. November 2018, pp. 338–352, 2019, doi: 10.1016/j.nanoen.2018.12.032.

[65] A. Lund *et al.*, "Roll-to-Roll Dyed Conducting Silk Yarns: A Versatile Material for E-Textile Devices," *Adv. Mater. Technol.*, vol. 3, no. 12, pp. 1–6, 2018, doi: 10.1002/admt.201800251.

[66] A. Ankhili, X. Tao, V. Koncar, D. Coulon, and J. Tarlet, "Ambulatory Evaluation of ECG Signals Obtained Using Washable Textile-Based Electrodes Made with," *Sensors*, vol. 19, no. 416, p. 13, 2019, doi: 10.3390/s19020416.

[67] OpenBCI, "Ultracortex 'Mark IV' EEG Headset," 2019. https://openbci.com/

[68] H. Kim, Y. Kim, B. Kim, and H.-J. Yoo, "A Wearable Fabric Computer by Planar-Fashionable Circuit Board Technique," in *2009 Sixth International Workshop on Wearable and Implantable Body Sensor Networks*, Berkeley, CA, Jun. 2009, pp. 282–285. doi: 10.1109/BSN.2009.51.

[69] Y. Yang *et al.*, "A non-printed integrated-circuit textile for wireless theranostics," *Nat. Commun.*, vol. 12, no. 1, p. 4876, Dec. 2021, doi: 10.1038/s41467-021-25075-8.

[70] S. Jin *et al.*, "Synthesis of freestanding PEDOT:PSS/PVA@Ag NPs nanofiber film for high-performance flexible thermoelectric generator," *Polymer*, vol. 167, no. October 2018, pp. 102–108, 2019, doi: 10.1016/j.polymer.2019.01.065.

[71] J. Liu, Y. Li, S. Arumugam, J. Tudor, and S. Beeby, "Screen Printed Dye-Sensitized Solar Cells (DSSCs) on Woven Polyester Cotton Fabric for Wearable Energy Harvesting Applications," *Mater. Today Proc.*, vol. 5, no. 5, pp. 13753–13758, 2018, doi: 10.1016/j.matpr.2018.02.015.

[72] J. Ryu *et al.*, "Nano Energy Intrinsically stretchable multi-functional fiber with energy harvesting and strain sensing capability," *Nano Energy*, vol. 55, no. August 2018, pp. 348–353, 2019, doi: 10.1016/j.nanoen.2018.10.071.

[73] A. Giuri, S. Colella, A. Listorti, A. Rizzo, C. Mele, and C. Esposito, "GO/glucose/PEDOT : PSS ternary nanocomposites for fl exible supercapacitors," *Compos. Part B*, vol. 148, no. April, pp. 149–155, 2018, doi: 10.1016/j.compositesb.2018.04.053.

[74] C. Yin, H. Zhou, and J. Li, "Facile one-step hydrothermal synthesis of PEDOT:PSS/MnO2 nanorod hybrids for high-rate supercapacitor electrode materials," *Ionics*, vol. 25, pp. 685–695, 2019, doi: 10.1007/s11581-018-2680-6.

[75] K. D. Fong, S. K. Smoukov, and T. Wang, "Multidimensional performance optimization of conducting polymer-based supercapacitor electrodes," *Sustain. Energy Fuels*, vol. 1, no. 9, pp. 1857–1874, 2017, doi: 10.1039/C7SE00339K.

[76] I. Nuramdhani, B. Malengier, W. Deferme, G. De Mey, and L. Van Langenhove, "Charge-Discharge Characteristics of Textile Energy Storage Devices Having Different PEDOT:PSS Ratios and Conductive Yarns Configuration," *polymers*, vol. 11, no. 345, 2019, doi: 10.3390/polym11020345.

[77] T. Sun, B. Zhou, Q. Zheng, L. Wang, W. Jiang, and G. J. Snyder, "Stretchable fabric generates electric power from woven thermoelectric fibers," *Nat. Commun.*, vol. 11, no. 1, p. 572, Dec. 2020, doi: 10.1038/s41467-020-14399-6.

[78] X. Liu and P. B. Lillehoj, "A liquid-activated textile battery for wearable biosensors," *J. Phys. Conf. Ser.*, vol. 660, p. 012063, Dec. 2015, doi: 10.1088/1742-6596/660/1/012063.

[79] A. Schwarz-Pfeiffer, M. Obermann, M. O. Weber, and A. Ehrmann, "Smarten up garments through knitting," *IOP Conf. Ser. Mater. Sci. Eng.*, vol. 141, p. 012008, Jul. 2016, doi: 10.1088/1757-899X/141/1/012008.

[80] H. Qu and M. Skorobogatiy, "Conductive polymer yarns for electronic textiles," in *Electronic Textiles*, Elsevier, 2015, pp. 21–53. doi: 10.1016/B978-0-08-100201-8.00003-5.

[81] H. Shahariar, I. Kim, H. Soewardiman, and J. S. Jur, "Inkjet Printing of Reactive Silver Ink on Textiles," *ACS Appl. Mater. Interfaces*, vol. 11, no. 6, pp. 6208–6216, Feb. 2019, doi: 10.1021/acsami.8b18231.

[82] C. L. Lam *et al.*, "Graphene Ink-Coated Cotton Fabric-Based Flexible Electrode for Electrocardiography," in *2017 5th International Conference on Instrumentation, Communications, Information Technology, and Biomedical Engineering (ICICI-BME)*, Bandung, Nov. 2017, pp. 73–75. doi: 10.1109/ICICI-BME.2017.8537771.

[83] N. Thangakameshwaran and A. U. Santhoskumar, "Cotton Fabric Dipped in Carbon Nano Tube Ink for Smart Textile Applications," *Int. J. Polym. Mater. Polym. Biomater.*, vol. 63, no. 11, pp. 557–562, Jul. 2014, doi: 10.1080/00914037.2013.854227.

[84] S. H. Kim *et al.*, "Mechanically and electrically durable, stretchable electronic textiles for robust wearable electronics," *RSC Adv.*, vol. 11, no. 36, pp. 22327–22333, 2021, doi: 10.1039/D1RA03392A.

[85] X. Hu, M. Tian, L. Qu, S. Zhu, and G. Han, "Multifunctional cotton fabrics with graphene/polyurethane coatings with far-infrared emission, electrical conductivity, and ultraviolet-blocking properties," *Carbon*, vol. 95, pp. 625–633, Dec. 2015, doi: 10.1016/j.carbon.2015.08.099.

[86] B. S. Shim, W. Chen, C. Doty, C. Xu, and N. A. Kotov, "Smart Electronic Yarns and Wearable Fabrics for Human Biomonitoring made by Carbon Nanotube Coating with Polyelectrolytes," *Nano Lett*, vol. 8, no. 12, p. 7, 2008.

[87] R. Islam, N. Khair, D. M. Ahmed, and H. Shahariar, "Fabrication of low cost and scalable carbon-based conductive ink for E-textile applications," *Mater. Today Commun.*, vol. 19, pp. 32–38, Jun. 2019, doi: 10.1016/j.mtcomm.2018.12.009.

[88] B. Fugetsu, E. Sano, H. Yu, K. Mori, and T. Tanaka, "Graphene oxide as dyestuffs for the creation of electrically conductive fabrics," *Carbon*, vol. 48, no. 12, pp. 3340–3345, Oct. 2010, doi: 10.1016/j.carbon.2010.05.016.

[89] L. Zulan, L. Zhi, C. Lan, C. Sihao, W. Dayang, and D. Fangyin, "Reduced Graphene Oxide Coated Silk Fabrics with Conductive Property for Wearable Electronic Textiles Application," *Adv. Electron. Mater.*, vol. 5, no. 4, p. 1800648, Apr. 2019, doi: 10.1002/aelm.201800648.

[90] S. Pothupitiya Gamage *et al.*, "MWCNT Coated Free-Standing Carbon Fiber Fabric for Enhanced Performance in EMI Shielding with a Higher Absolute EMI SE," *Materials*, vol. 10, no. 12, p. 1350, Nov. 2017, doi: 10.3390/ma10121350.

[91] C. Lou *et al.*, "Flexible Graphene Electrodes for Prolonged Dynamic ECG Monitoring," *Sensors*, vol. 16, no. 11, p. 1833, Nov. 2016, doi: 10.3390/s16111833.

[92] M. J. Rahman and T. Mieno, "Conductive Cotton Textile from Safely Functionalized Carbon Nanotubes," *J. Nanomater.*, vol. 2015, pp. 1–10, 2015, doi: 10.1155/2015/978484.

[93] S. Zhu *et al.*, "Multi-functional and Highly Conductive Textiles with Ultra-high Durability through 'Green' Fabrication Process," p. 31.

[94] J. Di *et al.*, "Carbon-Nanotube Fibers for Wearable Devices and Smart Textiles," *Adv. Mater.*, vol. 28, no. 47, pp. 10529–10538, Dec. 2016, doi: 10.1002/adma.201601186.

[95] N. Kobayashi, H. Izumi, and Y. Morimoto, "Review of toxicity studies of carbon nanotubes," *J. Occup. Health*, vol. 59, no. 5, pp. 394–407, Sep. 2017, doi: 10.1539/joh.17-0089-RA.

[96] K. Chatterjee, J. Tabor, and T. K. Ghosh, "Electrically Conductive Coatings for Fiber-Based E-Textiles," *Fibers*, vol. 7, no. 6, p. 51, Jun. 2019, doi: 10.3390/fib7060051.

[97] S. Prakash, T. Chakrabarty, A. K. Singh, and V. K. Shahi, "Polymer thin films embedded with metal nanoparticles for electrochemical biosensors applications," *Biosens. Bioelectron.*, vol. 41, pp. 43–53, Mar. 2013, doi: 10.1016/j.bios.2012.09.031.

[98] S. Maity and A. Chatterjee, "Polypyrrole Based Electro-Conductive Cotton Yarn," *J. Text. Sci. Eng.*, vol. 04, no. 06, 2014, doi: 10.4172/2165-8064.1000171.

[99] A. Achilli, D. Pani, and A. Bonfiglio, "Characterization of Screen-Printed Textile Electrodes Based on Conductive Polymer for ECG Acquisition," presented at the 2017 Computing in Cardiology Conference, Sep. 2017. doi: 10.22489/CinC.2017.129-422.

[100] K. N. Amba Sankar and K. Mohanta, "Preparation of Highly Conductive Yarns by an Optimized Impregnation Process," *J. Electron. Mater.*, vol. 47, no. 3, pp. 1970–1978, Mar. 2018, doi: 10.1007/s11664-017-5998-3.

[101] T. Kellomäki, J. Virkki, S. Merilampi, and L. Ukkonen, "Towards Washable Wearable Antennas: A Comparison of Coating Materials for Screen-Printed Textile-Based UHF RFID Tags," *Int. J. Antennas Propag.*, vol. 2012, pp. 1–11, 2012, doi: 10.1155/2012/476570.

[102] P. Kopola *et al.*, "Gravure printed flexible organic photovoltaic modules," *Sol. Energy Mater. Sol. Cells*, vol. 95, no. 5, pp. 1344–1347, 2011, doi: 10.1016/j.solmat.2010.12.020.

[103] W. Mu *et al.*, "Double layer printed high performance OLED based on PEDOT:PSS/Ir(bt) $_2$ acac:CDBP," *AIP Adv.*, vol. 8, no. 11, p. 115112, Nov. 2018, doi: 10.1063/1.5053133.

[104] V. Venkatraman *et al.*, "Subthreshold Operation of Organic Electrochemical Transistors for Biosignal Amplification," *Adv. Sci.*, vol. 5, no. 8, p. 1800453, Aug. 2018, doi: 10.1002/advs.201800453.

[105] P. J. Taroni *et al.*, "Toward Stretchable Self-Powered Sensors Based on the Thermoelectric Response of PEDOT:PSS/Polyurethane Blends," *Adv Funct Mater*, vol. 1704285, pp. 1–7, 2018, doi: 10.1002/adfm.201704285.

[106] S. Alharbi *et al.*, "E-Textile Origami Dipole Antennas With Graded Embroidery for Adaptive RF Performance," *IEEE Antennas Wirel. Propag. Lett.*, vol. 17, no. 12, pp. 2218–2222, Dec. 2018, doi: 10.1109/LAWP.2018.2871643.

[107] S. D. A. S. Ramoa, G. M. O. Barra, C. Merlini, S. Livi, B. G. Soares, and A. Pegoretti, "Novel electrically conductive polyurethane/montmorillonite-polypyrrole nanocomposites," *EXPRESS Polym. Lett.*, vol. 9, no. 10, pp. 945–958, 2015, doi: 10.3144/expresspolymlett.2015.85.

[108] G. Qi, L. Huang, and H. Wang, "Highly conductive free standing polypyrrole films prepared by freezing interfacial polymerization," *Chem. Commun.*, vol. 48, no. 66, p. 8246, 2012, doi: 10.1039/c2cc33889k.

[109] A. Rahy and D. J. Yang, "Synthesis of highly conductive polyaniline nanofibers," *Mater. Lett.*, vol. 62, no. 28, pp. 4311–4314, Nov. 2008, doi: 10.1016/j.matlet.2008.06.057.

[110] C. K. Chiang *et al.*, "Electrical Conductivity in Doped Polyacetylene," *Phys. Rev. Lett.*, vol. 39, no. 17, pp. 1098–1101, Oct. 1977, doi: 10.1103/PhysRevLett.39.1098.

[111] B. J. Worfolk *et al.*, "Ultrahigh electrical conductivity in solution-sheared polymeric transparent films," *Proc. Natl. Acad. Sci.*, vol. 112, no. 46, pp. 14138–14143, Nov. 2015, doi: 10.1073/pnas.1509958112.

[112] R. Luo, X. Li, H. Li, B. Du, and S. Zhou, "A stretchable and printable PEDOT:PSS/PDMS composite conductors and its application to wearable strain sensor," *Prog. Org. Coat.*, vol. 162, p. 106593, Jan. 2022, doi: 10.1016/j.porgcoat.2021.106593.

[113] M. F. Ghadim, A. Imani, and G. Farzi, "Synthesis of PPy–silver nanocomposites via in situ oxidative polymerization," *J. Nanostructure Chem.*, vol. 4, no. 2, p. 101, Jun. 2014, doi: 10.1007/s40097-014-0101-6.

[114] A. Liu, L. H. Bac, J.-S. Kim, B.-K. Kim, and J.-C. Kim, "Synthesis and Characterization of Conducting Polyaniline-Copper Composites," *J. Nanosci. Nanotechnol.*, vol. 13, no. 11, pp. 7728–7733, Nov. 2013, doi: 10.1166/jnn.2013.7831.

[115] V. Loryuenyong, A. Khadthiphong, J. Phinkratok, J. Watwittayakul, W. Supawattanakul, and A. Buasri, "The fabrication of graphene-polypyrrole composite for application with dye-sensitized solar cells," *Mater. Today Proc.*, vol. 17, pp. 1675–1681, 2019, doi: 10.1016/j.matpr.2019.06.198.

[116] Y.-X. Liu, H.-H. Liu, J.-P. Wang, and X.-X. Zhang, "Thermoelectric behavior of PEDOT:PSS/CNT/graphene composites," *J. Polym. Eng.*, vol. 38, no. 4, pp. 381–389, Apr. 2018, doi: 10.1515/polyeng-2017-0179.

[117] G. Kaur, R. Adhikari, P. Cass, M. Bown, and P. Gunatillake, "Electrically conductive polymers and composites for biomedical applications," *RSC Adv.*, vol. 5, pp. 37553–37567, 2015, doi: 10.1039/C5RA01851J.

[118] B. Wessling and H. Volk, "Post-polymerization processing of conductive polymers: A way of converting conductive polymers to conductive materials?," *Synth. Met.*, vol. 15, no. 2–3, pp. 183–193, Jul. 1986, doi: 10.1016/0379-6779(86)90022-6.

[119] H. Pang, L. Xu, D.-X. Yan, and Z.-M. Li, "Conductive polymer composites with segregated structures," *Prog. Polym. Sci.*, vol. 39, no. 11, pp. 1908–1933, Nov. 2014, doi: 10.1016/j.progpolymsci.2014.07.007.

[120] S. Maity and A. Chatterjee, "Textile/Polypyrrole Composites for Sensory Applications," *J. Compos.*, vol. 2015, pp. 1–6, 2015, doi: 10.1155/2015/120516.

[121] J. F. Feller and Y. Grohens, "Electrical response of Poly(styrene)/carbon black conductive polymer composites (CPC) to methanol, toluene, chloroform and styrene vapors as a function of filler nature and matrix tacticity," *Synth. Met.*, vol. 154, no. 1–3, pp. 193–196, Sep. 2005, doi: 10.1016/j.synthmet.2005.07.050.

[122] S. Choi *et al.*, "Highly conductive, stretchable and biocompatible Ag–Au core–sheath nanowire composite for wearable and implantable bioelectronics," *Nat. Nanotechnol.*, vol. 13, no. 11, pp. 1048–1056, Nov. 2018, doi: 10.1038/s41565-018-0226-8.

[123] J. H. Collier, J. P. Camp, T. W. Hudson, and C. E. Schmidt, "Synthesis and characterization of polypyrrole-hyaluronic acid composite biomaterials for tissue engineering applications," *J. Biomed. Mater. Res.*, vol. 50, no. 4,

pp. 574–584, 2000, doi: 10.1002/(SICI)1097-4636(20000615)50:4<574::AID-JBM13>3.0.CO;2-I.

[124] H. S. Kim, H. L. Hobbs, L. Wang, M. J. Rutten, and C. C. Wamser, "Biocompatible composites of polyaniline nanofibers and collagen," *Synth. Met.*, vol. 159, no. 13, pp. 1313–1318, 2009, doi: 10.1016/j.synthmet.2009.02.036.

[125] R. J. Lee, R. Temmer, T. Tamm, A. Aabloo, and R. Kiefer, "Renewable antioxidant properties of suspensible chitosan-polypyrrole composites," *React. Funct. Polym.*, vol. 73, no. 8, pp. 1072–1077, 2013, doi: 10.1016/j.reactfunctpolym.2013.04.003.

[126] E. M. Stewart *et al.*, "Cell attachment and proliferation on high conductivity PEDOT-glycol composites produced by vapour phase polymerisation," *Biomater. Sci.*, vol. 1, no. 4, pp. 368–378, 2013, doi: 10.1039/c2bm00143h.

[127] L. Suo, X. Shang, R. Tang, and Y. Zhou, "The Preparation of Polypyrrole/Cellulose Acetate Composite Films and their Electrical Properties," in *ICECTT*, 2015, no. Icectt, pp. 566–569. doi: 10.2991/icectt-15.2015.108.

[128] A. K. Bajpai, J. Bajpai, and S. N. Soni, "Preparation and characterization of electrically conductive composites of poly(vinyl alcohol)-g-poly(acrylic acid) hydrogels impregnated with polyaniline (PANI)," *Express Polym. Lett.*, vol. 2, no. 1, pp. 26–39, 2008, doi: 10.3144/expresspolymlett.2008.5.

[129] M. M. Pérez-Madrigal *et al.*, "Thermoplastic polyurethane:polythiophene nanomembranes for biomedical and biotechnological applications," *ACS Appl. Mater. Interfaces*, vol. 6, no. 12, pp. 9719–9732, 2014, doi: 10.1021/am502150q.

[130] H. Xu *et al.*, "Conductive PPY/PDLLA conduit for peripheral nerve regeneration," *Biomaterials*, vol. 35, no. 1, pp. 225–235, 2014, doi: 10.1016/j.biomaterials.2013.10.002.

[131] M. Z. Ali, K. M. K. Ishak, M. A. M. Zawawi, M. Jaafar, and Z. Ahmad, "Tunneling Percolation Mechanism of Conductivity for PEDOT:PSS in Hydrophilic PDMS Composite for the Fabrication of Highly Sensitive Strain Sensors," *Macromol. Chem. Phys.*, vol. 223, no. 16, p. 2200077, Aug. 2022, doi: 10.1002/macp.202200077.

[132] K. Sano *et al.*, "A mechanically adaptive hydrogel with a reconfigurable network consisting entirely of inorganic nanosheets and water," *Nat. Commun.*, vol. 11, no. 1, p. 6026, Dec. 2020, doi: 10.1038/s41467-020-19905-4.

[133] S. Keller, B. J. Toebes, and D. A. Wilson, "Active, Autonomous, and Adaptive Polymeric Particles for Biomedical Applications," *Biomacromolecules*, vol. 20, no. 3, pp. 1135–1145, Mar. 2019, doi: 10.1021/acs.biomac.8b01673.

[134] M. Behl and A. Lendlein, "Shape-memory polymers," *Mater. Today*, vol. 10, no. 4, pp. 20–28, Apr. 2007, doi: 10.1016/S1369-7021(07)70047-0.

[135] S. Pirsa, T. Shamusi, and E. M. Kia, "Smart films based on bacterial cellulose nanofibers modified by conductive polypyrrole and zinc oxide nanoparticles," *J. Appl. Polym. Sci.*, vol. 135, no. 34, p. 46617, Sep. 2018, doi: 10.1002/app.46617.

[136] A. Lund, K. Rundqvist, E. Nilsson, L. Yu, B. Hagström, and C. Müller, "Energy harvesting textiles for a rainy day: woven piezoelectrics based on melt-spun PVDF microfibres with a conducting core," *Npj Flex. Electron.*, p. 9, 2018, doi: 10.1038/s41528-018-0022-4.

[137] T. A. Khattab, M. Rehan, and T. Hamouda, "Smart textile framework: Photochromic and fluorescent cellulosic fabric printed by strontium aluminate pigment," *Carbohydr. Polym.*, vol. 195, pp. 143–152, Sep. 2018, doi: 10.1016/j.carbpol.2018.04.084.

[138] T. Yan, T. Zhang, G. Zhao, C. Zhang, C. Li, and F. Jiao, "Magnetic textile with pH-responsive wettability for controllable oil/water separation," *Colloids Surf. Physicochem. Eng. Asp.*, vol. 575, pp. 155–165, Aug. 2019, doi: 10.1016/j.colsurfa.2019.04.083.

[139] V. Koncar, "Optical Fiber Fabric Displays," vol. 16, no. 4, pp. 40–44, 2005, doi: https://doi.org/10.1364/OPN.16.4.000040.

[140] B. Gauvreau *et al.*, "Color-changing and color-tunable photonic bandgap fiber textiles," *Opt. Express*, vol. 16, no. 20, p. 15677, Sep. 2008, doi: 10.1364/OE.16.015677.

[141] A. Shafti, R. B. Ribas Manero, A. M. Borg, K. Althoefer, and M. J. Howard, "Embroidered Electromyography: A Systematic Design Guide," *IEEE Trans. Neural Syst. Rehabil. Eng.*, vol. 25, no. 9, pp. 1472–1480, Sep. 2017, doi: 10.1109/TNSRE.2016.2633506.

[142] W. Fan *et al.*, "Machine-knitted washable sensor array textile for precise epidermal physiological signal monitoring," *Sci. Adv.*, vol. 6, no. 11, p. eaay2840, Mar. 2020, doi: 10.1126/sciadv.aay2840.

[143] J. Park, D. Kim, A. Y. Choi, and Y. T. Kim, "Flexible single-strand fiber-based woven-structured triboelectric nanogenerator for self-powered electronics," *APL Mater.*, vol. 6, no. 10, p. 101106, Oct. 2018, doi: 10.1063/1.5048553.

[144] T. Zheng *et al.*, "Wet-Spinning Assembly of Continuous, Highly Stable Hyaluronic/Multiwalled Carbon Nanotube Hybrid Microfibers," *Polymers*, vol. 11, no. 5, p. 867, May 2019, doi: 10.3390/polym11050867.

[145] "The mechanics of the braiding process," in *Braiding Technology for Textiles*, Elsevier, 2015, pp. 177–209. doi: 10.1533/9780857099211.2.177.

[146] Y. Li, S. Arumugam, C. Krishnan, M. D. B. Charlton, and S. P. Beeby, "Encapsulated Textile Organic Solar Cells Fabricated by Spray Coating," *ChemistrySelect*, vol. 4, pp. 407 –412, 2019, doi: 10.1002/slct.201803929.

[147] Z. Al-Maqdasi, A. Hajlane, A. Renbi, A. Ouarga, S. S. Chouhan, and R. Joffe, "Conductive Regenerated Cellulose Fibers by Electroless Plating," *Fibers*, vol. 7, no. 5, p. 38, May 2019, doi: 10.3390/fib7050038.

[148] S. Baurley, "Interactive and experiential design in smart textile products and applications," *Pres Ubiquit Comput*, vol. 8, pp. 274–281, 2004, doi: 10.1007/s00779-004-0288-5.

[149] I. S. Chronakis, S. Grapenson, and A. Jakob, "Conductive polypyrrole nanofibers via electrospinning: Electrical and morphological properties," *Polymer*, vol. 47, no. 5, pp. 1597–1603, Feb. 2006, doi: 10.1016/j.polymer.2006.01.032.

[150] D. Ahn, H.-J. Choi, H. Kim, and S. Y. Yeo, "Properties of Conductive Polyacrylonitrile Fibers Prepared by Using Benzoxazine Modified Carbon Black," *Polymers*, vol. 12, no. 1, p. 179, Jan. 2020, doi: 10.3390/polym12010179.

[151] Y. Liu, X. Li, and J. C. Lu, "Electrically Conductive Poly (3, 4-ethylenedioxythiophene)– Polystyrene Sulfonic Acid/Polyacrylonitrile Composite Fibers Prepared by Wet Spinning," *J. Appl. Polym. Sci.*, pp. 370–374, 2013, doi: 10.1002/app.39174.

[152] H. Probst, K. Katzer, A. Nocke, R. Hickmann, M. Zimmermann, and C. Cherif, "Melt Spinning of Highly Stretchable, Electrically Conductive Filament Yarns," *Polymers*, vol. 13, no. 4, p. 590, Feb. 2021, doi: 10.3390/polym13040590.

[153] N. A. M. Radzuan, A. B. Sulong, and M. R. Somalu, "Extrusion Process of Polypropylene Composites Reinforced Milled Carbon Fibre for Conductive Polymer Composite Application," *MATEC Web Conf.*, vol. 248, p. 01012, 2018, doi: 10.1051/matecconf/201824801012.

[154] M. Åkerfeldt, E. Nilsson, P. Gillgard, and P. Walkenström, "Textile piezoelectric sensors – melt spun bi-component poly(vinylidene fluoride) fibres with conductive cores and poly(3,4-ethylene dioxythiophene)-poly(styrene sulfonate) coating as the outer electrode," *Fash. Text.*, vol. 1, no. 1, p. 13, Dec. 2014, doi: 10.1186/s40691-014-0013-6.

[155] K. Chen, W. Chou, L. Liu, Y. Cui, P. Xue, and M. Jia, "Electrochemical Sensors Fabricated by Electrospinning Technology: An Overview," *Sensors*, vol. 19, no. 17, p. 3676, Aug. 2019, doi: 10.3390/s19173676.

[156] J. L. Hu, "Introduction to active coatings for smart textiles," in *Active Coatings for Smart Textiles*, Elsevier, 2016, pp. 1–7. doi: 10.1016/B978-0-08-100263-6.00001-0.

[157] H. Liu *et al.*, "A Novel Two-Step Method for Fabricating Silver Plating Cotton Fabrics," *J. Nanomater.*, vol. 2016, pp. 1–11, 2016, doi: 10.1155/2016/2375836.

[158] S. Kwon *et al.*, "High Luminance Fiber-Based Polymer Light-Emitting Devices by a Dip-Coating Method," *Adv. Electron. Mater.*, vol. 1, no. 9, p. 1500103, Sep. 2015, doi: 10.1002/aelm.201500103.

[159] Y. Liu, X. Zhao, and X. Tuo, "Preparation of polypyrrole coated cotton conductive fabrics," *J. Text. Inst.*, vol. 108, no. 5, pp. 829–834, May 2017, doi: 10.1080/00405000.2016.1193981.

[160] A. Ankhili, X. Tao, C. Cochrane, D. Coulon, and V. Koncar, "Washable and Reliable Textile Electrodes Embedded into Underwear Fabric for Electrocardiography (ECG) Monitoring," *Materials*, vol. 11, no. 2, p. 256, Feb. 2018, doi: 10.3390/ma11020256.

[161] A. R. Mule, B. Dudem, H. Patnam, S. A. Graham, and J. S. Yu, "Wearable Single-Electrode-Mode Triboelectric Nanogenerator via Conductive Polymer-Coated Textiles for Self-Power Electronics," *ACS Sustain. Chem. Eng.*, vol. 7, no. 19, pp. 16450–16458, Oct. 2019, doi: 10.1021/acssuschemeng.9b03629.

[162] K. Sreeja Sadanandan *et al.*, "Graphene coated fabrics by ultrasonic spray coating for wearable electronics and smart textiles," *J. Phys. Mater.*, vol. 4, no. 1, p. 014004, Jan. 2021, doi: 10.1088/2515-7639/abc632.

[163] S. Arumugam *et al.*, "Fully spray-coated organic solar cells on woven polyester cotton fabric for wearable energy harvesting applications," *Mater. Chem.*, vol. 4, p. 10, 2016, doi: 10.1039/C5TA03389F.

[164] H. Hardianto, G. D. Mey, B. Malengier, C. Hertleer, and V. Langenhove, "CHARACTERIZATION OF CARBON-NICKEL THERMOCOUPLES INTEGRATED IN TEXTILE FABRICS," p. 5, 2019.

[165] N. M. Kumar and G. Thilagavathi, "Design and Development of Textile Electrodes for EEG Measurement using Copper Plated Polyester Fabrics," vol. 8, no. 4, p. 8, 2014.

[166] A. Willfahrt, "Screen Printing Technology for Energy Devices," Ph.D., Linköping Univeristy, Linköping, Sweden, 2018. doi: 10.3384/diss.diva-152425.

[167] I. Kazani, "Study of Screen-Printed Electroconductive Textile Materials," Ghent University, 2012.

[168] E. Skrzetuska, M. Puchalski, and I. Krucińska, "Chemically Driven Printed Textile Sensors Based on Graphene and Carbon Nanotubes," *Sensors*, vol. 14, no. 9, pp. 16816–16828, Sep. 2014, doi: 10.3390/s140916816.

[169] J. Tudor *et al.*, "Inkjet printed dipole antennas on textiles for wearable communications," *IET Microw. Antennas Propag.*, vol. 7, no. 9, pp. 760–767, 2013, doi: 10.1049/iet-map.2013.0076.

[170] A. Ankhili, X. Tao, C. Cochrane, V. Koncar, D. Coulon, and J.-M. Tarlet, "Comparative Study on Conductive Knitted Fabric Electrodes for Long-Term Electrocardiography Monitoring: Silver-Plated and PEDOT:PSS Coated Fabrics," *Sensors*, vol. 18, no. 11, p. 3890, Nov. 2018, doi: 10.3390/s18113890.

[171] N. Maheshwari, M. Abd-Ellah, and I. A. Goldthorpe, "Transfer printing of silver nanowire conductive ink for e-textile applications," *Flex. Print. Electron.*, vol. 4, no. 2, p. 025005, Jun. 2019, doi: 10.1088/2058-8585/ab2543.

[172] Sungyong Shin, B. Kim, Y. K. Son, Ji Eun Kim, and Il-Yeon Cho, "A flexible textile wristwatch using Transfer Printed Textile Circuit technique," in *2012 IEEE International Conference on Consumer Electronics (ICCE)*, Las Vegas, NV, USA, Jan. 2012, pp. 21–22. doi: 10.1109/ICCE.2012.6161719.

[173] A. Chauraya, R. Seager, W. Whittow, S. Zhang, and Y. Vardaxoglou, "Embroidered Frequency Selective Surfaces on textiles for wearable applications," *2013 Loughb. Antennas Propag. Conf. LAPC 2013*, no. November, pp. 388–391, 2013, doi: 10.1109/LAPC.2013.6711926.

[174] Y. Al-naiemy, T. A. Elwi, H. R. Khaleel, and H. Al-rizzo, "A Systematic Approach for the Design, Fabrication, and Testing of Microstrip Antennas Using Inkjet Printing Technology A Systematic Approach for the Design, Fabrication, and Testing of Microstrip Antennas Using Inkjet Printing Technology," *ISRN Commun. Netw.*, no. June, p. 11, 2015, doi: 10.5402/2012/132465.

[175] T. Vidmar, M. Topič, P. Dzik, and U. Opara Krašovec, "Inkjet printing of sol-gel derived tungsten oxide inks," *Sol. Energy Mater. Sol. Cells*, vol. 125, pp. 87–95, 2014, doi: 10.1016/j.solmat.2014.02.023.

[176] P. He *et al.*, "Fully printed high performance humidity sensors based on two-dimensional materials," *Nanoscale*, vol. 10, no. 12, pp. 5599–5606, 2018, doi: 10.1039/C7NR08115D.

[177] J. Weremczuk, G. Tarapata, and R. Jachowicz, "Humidity sensor printed on textile with use of ink-jet Technology," *Procedia Eng.*, vol. 47, pp. 1366–1369, 2012, doi: 10.1016/j.proeng.2012.09.410.

[178] E. Köhler, S. Rahiminejad, and P. Enoksson, "Evaluation of 3D printed materials used to print WR10 horn antennas," *J. Phys. Conf. Ser.*, vol. 757, no. 1, 2016, doi: 10.1088/1742-6596/757/1/012026.

[179] T. O'Neill and J. Williams, *3D Printing*. Michigan: Chery Lake Publishing, 2013.

[180] A. Bellacicca, T. Santaniello, and P. Milani, "Embedding electronics in 3D printed structures by combining fused filament fabrication and supersonic cluster beam deposition," *Addit. Manuf.*, vol. 24, no. June, pp. 60–66, 2018, doi: 10.1016/j.addma.2018.09.010.

[181] Y. Chen *et al.*, "3D printed stretchable smart fibers and textiles for self-powered e-skin," *Nano Energy*, vol. 84, p. 105866, Jun. 2021, doi: 10.1016/j.nanoen.2021.105866.

[182] X. Kuang, K. Chen, C. K. Dunn, J. Wu, V. C. F. Li, and H. J. Qi, "3D Printing of Highly Stretchable, Shape-Memory, and Self-Healing Elastomer toward Novel 4D Printing," *ACS Appl. Mater. Interfaces*, vol. 10, no. 8, pp. 7381–7388, 2018, doi: 10.1021/acsami.7b18265.

[183] S. Agarwala *et al.*, "Development of bendable strain sensor with embedded microchannels using 3D printing," *Sens. Actuators Phys.*, vol. 263, pp. 593–599, 2017, doi: 10.1016/j.sna.2017.07.025.

[184] J. T. Muth *et al.*, "Embedded 3D Printing of Strain Sensors within Highly Stretchable Elastomers," *Adv. Mater.*, vol. 26, no. 36, pp. 6307–6312, Sep. 2014, doi: 10.1002/adma.201400334.

[185] J. Mikkonen and E. Pouta, "Flexible Wire-Component for Weaving Electronic Textiles," *Proc. - Electron. Compon. Technol. Conf.*, vol. 2016-Augus, pp. 1656–1663, 2016, doi: 10.1109/ECTC.2016.180.

[186] H. Gidik, D. Dupont, and G. Bedek, "Development of a radiative heat fluxmeter with a textile substrate," *Sens. Actuators Phys.*, vol. 271, pp. 162–167, 2018, doi: 10.1016/j.sna.2017.12.020.

[187] J. Park, D. Kim, A. Y. Choi, and Y. T. Kim, "Flexible single-strand fiber-based woven-structured triboelectric nanogenerator for self-powered electronics," *APL Mater.*, vol. 6, no. 10, 2018, doi: 10.1063/1.5048553.

[188] D. Patron *et al.*, "On the Use of Knitted Antennas and Inductively Coupled RFID Tags for Wearable Applications," *IEEE Trans. Biomed. Circuits Syst.*, vol. 10, no. 6, pp. 1047–1057, 2016, doi: 10.1109/TBCAS.2016.2518871.

[189] X. Jia, A. Tennant, R. J. Langley, W. Hurley, and T. Dias, "A knitted textile waveguide," *2014 Loughb. Antennas Propag. Conf. LAPC 2014*, vol. 1, no. November, pp. 679–682, 2014, doi: 10.1109/LAPC.2014.6996485.

[190] A. Tennant, W. Hurley, and T. Dias, "Knitted, textile, high impedance surface with integrated conducting vias," *Electron. Lett.*, vol. 49, no. 1, pp. 8–10, 2013, doi: 10.1049/el.2012.3896.

[191] B. Moradi, R. Fernández-García, and I. Gil, "E-textile embroidered metamaterial transmission line for signal propagation control," *Materials*, vol. 11, no. 6, 2018, doi: 10.3390/ma11060955.

[192] M. Martinez-Estrada, B. Moradi, R. Fernández-Garcia, and I. Gil, "Impact of manufacturing variability and washing on embroidery textile sensors," *Sens. Switz.*, vol. 18, no. 11, 2018, doi: 10.3390/s18113824.

[193] S. Alharbi *et al.*, "E-Textile Origami Dipole Antennas with Graded Embroidery for Adaptive RF Performance," *IEEE Antennas Wirel. Propag. Lett.*, vol. 17, no. 12, pp. 2218–2222, 2018, doi: 10.1109/LAWP.2018.2871643.

[194] B. Mohamadzade, R. M. Hashmi, R. B. V. B. Simorangkir, R. Gharaei, S. Ur Rehman, and Q. H. Abbasi, "Recent Advances in Fabrication Methods for Flexible Antennas in Wearable Devices: State of the Art," *Sensors*, vol. 19, no. 10, p. 2312, May 2019, doi: 10.3390/s19102312.

[195] A. Pragya, H. Singh, B. Kumar, H. Gupta, and P. Shankar, "Designing and investigation of braided-cum-woven structure for wearable heating textile," *Eng. Res. Express*, vol. 2, no. 1, p. 015003, Jan. 2020, doi: 10.1088/2631-8695/ab63f3.

[196] O. Tangsirinaruenart and G. Stylios, "A Novel Textile Stitch-Based Strain Sensor for Wearable End Users," *Materials*, vol. 12, no. 9, p. 1469, May 2019, doi: 10.3390/ma12091469.

[197] P. Vanveerdeghem, P. Van Torre, C. Stevens, J. Knockaert, and H. Rogier, "Synchronous Wearable Wireless Body Sensor Network Composed of Autonomous Textile Nodes," *Sensors*, vol. 14, no. 10, pp. 18583–18610, Oct. 2014, doi: 10.3390/s141018583.

[198] M. Storti and H. Company, "METHOD FOR PREPARING FABRIC LAMINATE," US3383263, May 14, 1968 [Online]. Available: https://patentimages.storage.googleapis.com/24/d9/63/d069fb2b392ea9/US3383263.pdf

[199] J. Choi and J. W. McCutcheon, "TAPES AND ARTICLES THEREFROM," US 2016/0333232 A1, Jul. 19, 2016 [Online]. Available: https://patentimages.storage.googleapis.com/f4/f0/a0/3543c58b9a3337/US20160333232A1.pdf

[200] M. Wagih, A. S. Weddell, and S. Beeby, "Overcoming the Efficiency Barrier of Textile Antennas: A Transmission Lines Approach," *Proceedings*, vol. 32, no. 1, p. 18, Dec. 2019, doi: 10.3390/proceedings2019032018.

[201] A. Angelucci *et al.*, "Smart Textiles and Sensorized Garments for Physiological Monitoring: A Review of Available Solutions and Techniques," *Sensors*, vol. 21, no. 3, p. 814, Jan. 2021, doi: 10.3390/s21030814.

[202] K. Meng *et al.*, "A Wireless Textile-Based Sensor System for Self-Powered Personalized Health Care," *Matter*, vol. 2, no. 4, pp. 896–907, Apr. 2020, doi: 10.1016/j.matt.2019.12.025.

[203] I. Cerro, I. Latasa, C. Guerra, P. Pagola, B. Bujanda, and J. J. Astrain, "Smart System with Artificial Intelligence for Sensory Gloves," *Sensors*, vol. 21, no. 5, p. 1849, Mar. 2021, doi: 10.3390/s21051849.

[204] Y. Peng *et al.*, "Integrated cooling (i-Cool) textile of heat conduction and sweat transportation for personal perspiration management," *Nat. Commun.*, vol. 12, no. 1, p. 6122, Dec. 2021, doi: 10.1038/s41467-021-26384-8.

[205] C. Xi, Z. Zhou, D. Youbo, Y. Xuan, and W. Xing, "Self-Heating Composite Fabric and Its Application in Sports Injury Protection of Athletes," *Integr. Ferroelectr.*, vol. 210, no. 1, pp. 41–48, Sep. 2020.

[206] Y. Mao, M. Shen, B. Liu, L. Xing, S. Chen, and X. Xue, "Self-Powered Piezoelectric-Biosensing Textiles for the Physiological Monitoring and Time-Motion Analysis of Individual Sports," *Sensors*, vol. 19, no. 15, p. 3310, Jul. 2019, doi: 10.3390/s19153310.

[207] B. Ghatak *et al.*, "Design of a Self-powered Smart Mask for COVID-19," p. 21.

[208] Y. Wu, S. S. Mechael, C. Lerma, R. S. Carmichael, and T. B. Carmichael, "Stretchable Ultrasheer Fabrics as Semitransparent Electrodes for Wearable Light-Emitting e-Textiles with Changeable Display Patterns," *Matter*, vol. 2, no. 4, pp. 882–895, Apr. 2020, doi: 10.1016/j.matt.2020.01.017.

[209] I. Must *et al.*, "Ionic and Capacitive Artificial Muscle for Biomimetic Soft Robotics: Ionic and Capacitive Artificial Muscle for Biomimetic Soft Robotics," *Adv. Eng. Mater.*, vol. 17, no. 1, pp. 84–94, Jan. 2015, doi: 10.1002/adem.201400246.

[210] J. Lee *et al.*, "Thermally Controlled, Active Imperceptible Artificial Skin in Visible-to-Infrared Range," *Adv. Funct. Mater.*, vol. 30, no. 36, p. 2003328, Sep. 2020, doi: 10.1002/adfm.202003328.

[211] A. Rayate and P. K. Jain, "A Review on 4D Printing Material Composites and Their Applications," *Mater. Today Proc.*, vol. 5, no. 9, pp. 20474–20484, 2018, doi: 10.1016/j.matpr.2018.06.424.

[212] H. Yang *et al.*, "3D Printed Photoresponsive Devices Based on Shape Memory Composites," *Adv. Mater.*, vol. 29, no. 33, p. 1701627, Sep. 2017, doi: 10.1002/adma.201701627.

[213] C. Collet, "Biolace: vegetable lace from Carole Collet," Nov. 28, 2014. https://www.paperblog.fr/7267888/biolace-la-dentelle-vegetale-de-carole-collet/ (accessed Oct. 05, 2021).

3. Textile-based EEG Electrodes

This chapter presents a brief review of textile-based EEG electrodes. The current status of textile-based dry EEG electrodes and prospects have been addressed.

This chapter is redrafted from published journal papers:

G.B. Tseghai, B. Malengier, K.A. Fante, and L. Van Langenhove, "Validating Poly(3,4-ethylene dioxythiophene) Polystyrene Sulfonate-Based Textile Electroencephalography Electrodes by a Textile-Based Head Phantom", *Polymers*, 13 (21): 3629, 2021. doi.org/10.3390/polym13213629

G.B. Tseghai, B. Malengier, K.A. Fante, and L. Van Langenhove, "The Status of Textile-Based Dry EEG Electrodes", *ARJ*, 21 (1): 63-70, 2021. doi.org/10.2478/aut-2019-0071.

Table of Contents

3.1. Introduction

The brain is the largest and most complex organ in the human body, consisting of more than 100 billion nerves [1]; it is considered the central organ of the human nervous system and, together with the spinal cord, forms the central nervous system [2]. The condition of the brain can be diagnosed through an electroencephalogram (EEG) measurement, where the current flow within its regions (Figure 3.1) is determined and displayed as a wave. Each person's brain wave patterns are unique, which makes it possible to distinguish between people only based on their typical brain activity [3].

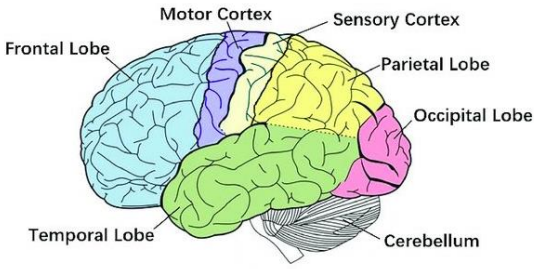

Figure 3.1: The human brain [4], under CC by 4.0.

The human brain is always a frequency wave of electrical activity. The brain cells send and receive electrical signals even when we are sleeping. Functional Magnetic Resonance Imaging (fMRI), magnetoencephalography (MEG), and electroencephalography (EEG) are the three most prevalent and widely used techniques used to measure brain activity. The techniques are pictorially indicated in Figure 3.2.

Among all, EEG is the most adaptable and cost-effective approach. The direct recording of brain electrical activity of neuronal interactions by placing electrodes on the scalp surface is known as electroencephalography (EEG). It is one of the most widely used brain imaging techniques because it provides an excellent time resolution of brain activity. It also has cost and space advantages over other technologies such as magnetoencephalography, functional magnetic resonance imaging, and positron emission tomography.

During brain condition diagnosis through an EEG measurement, the current flow within its regions is determined and displayed as a wave. Each person's brain wave patterns are unique, which makes it possible to distinguish and biometrically identify between people only based on their typical brain activity

[5]. EEG is used to diagnose brain-related seizures and inflammation including epilepsy [6]. The application of EEG in brain-computer interfaces [7], sleep disorder diagnosis [8], and cognitive neurosciences [9] are also booming.

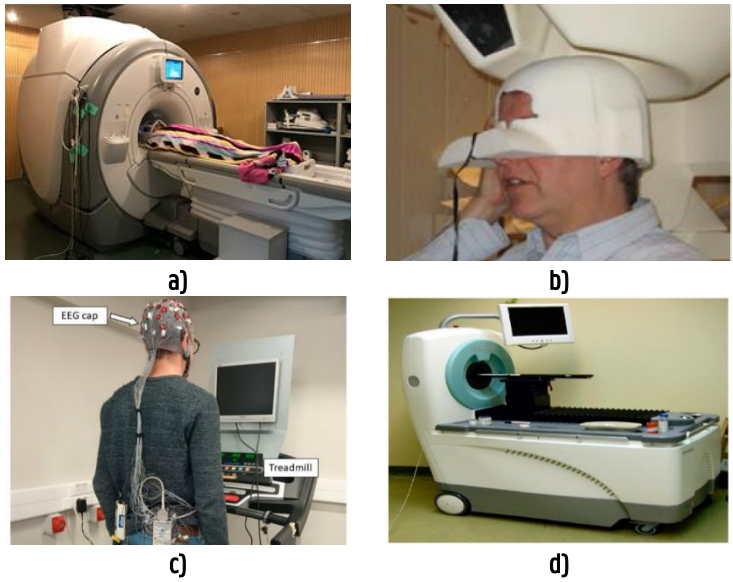

Figure 3.2: Brain activity measurement approaches; **a**) Functional Magnetic Resonance Imaging (fMRI) [10], under CC by 4.0; **b**) Magnetoencephalography (MEG) [11], under CC by 3.0; **c**) Electroencephalography (EEG) [12], under CC by 4.0; **d**) Positron Emission Tomography (PET) [13], under CC by 4.0.

The first human EEG was reported in 1929 by Hans Berger [14]. This measurement technique is often employed in the diagnosis of neurological disorders [15], the intensity of anesthesia [16], encephalopathies [17], brain death [18], and so on. Novel applications such as brain-computer interface [19], robotic rehabilitation of patients [20], and the investigation of brain development [21] increased the interest in EEG measurements.

EEG waveforms are classified based on their frequency and denoted with Greek numerals based on their spectrum as delta (0.5 to 4 Hz), theta (4 to 7 Hz), alpha (8 to 12Hz), sigma (12 to 16 Hz), beta (13 to 30 Hz), and gamma (30 to 100 Hz) [22]. Delta waves, which have the lowest frequency and highest amplitude, reflect the activity of the gray matter in the brain. They occur in all stages of sleep but are uncommon in awake adults. Theta waves usually occur in the parietal and temporal regions in children, and some adults, during times of frustration. Alpha waves originate on both sides of the head and can collect in the occipital and parietal regions. They usually occur in an awake and relaxed

state with closed eyes and disappear completely during sleep. These waves represent the gray matter of the brain and connect conscious and subconscious states. Sigma waves appear predominantly in the frontal-central head regions during sleep and are called sleep spindles. They quickly occur, similar to the shape of an “eye” in that they rapidly increase in amplitude and then quickly decay. Beta waves can be detected on both sides of the frontal and parietal lobes during active brain states such as speech, problem-solving, judgment, and decision-making. Gamma waves are waves that occur during hyperactive wakefulness with the integration of sensory inputs and indicate the connection of feelings with memory activity.

3.2. Overview of EEG Electrodes

Electroencephalogram (EEG) is a classic example of a bio-potential recording of the electrical signals produced by the activity of the brain [23]–[25]. It is the direct recording of the electrical activity in the brain of neuronal interactions by placing electrodes on the scalp surface. The EEG electrodes are placed on the scalp to see the activities in the brain as shown in Figure 3.3. It is one of the most widely used brain imaging techniques because it provides an excellent time resolution of brain activity. It also has cost and space advantages over other technologies, such as magnetoencephalography, functional magnetic resonance imaging, and positron emission tomography. It is useful for monitoring the quality and alertness of sleep, for clinical applications such as epilepsy and other neurological disorders diagnosis, and for continuous monitoring of fatigue/alertness of staff deployed in the field or under strain [26]. EEG carries a large amount of complex information valuable for the detection of ongoing seizures [27]. As a result, EEG sensors have long been considered the gold standard for seizure diagnosis.

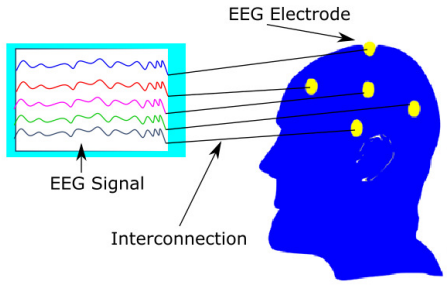

Figure 3.3: Brain activity measurement using EEG electrodes

Many groups developed automatic seizure detection algorithms based on EEG [28]–[30]. Most of them used data from the Freiburg seizure prediction and the European epilepsy database to test their algorithms using data from 2 to 6 electrodes to recreate conditions for outpatient performance. The database in Freiburg uses six electrodes; three electrodes near the focal area and three electrodes at a distance [28], [31]. Nevertheless, seizure detection is still difficult in the field and therefore not easy or fully validated. Furthermore, various types of novel EEG sensor electrodes have been introduced by many researchers. Chen et al. designed and developed an EEG recording frontend circuitry headband for epileptic seizure detection, a textile headband with printed-circuit-board (PCB) inside, and textile electrodes on it yielding a compact and low-power design for EEG recording that makes it convenient for a wearable purposes [32]. Wang et al. proposed a novel porous ceramic 'semi-dry' electrode with a key feature that electrode tips can slowly and continuously release a small amount of electrolyte liquid into the scalp, providing an ionic conducting path for detecting neural signals that can effectively capture electrophysiological responses and is a viable alternative to conventional electrodes in brain-computer interface applications [33]. Radhakrishnan et al. developed a needle array dry electrode microstrip from stainless steel (SS) having an impedance of about 6.8 kΩ at 20 Hz in a 0.9% NaCl solution, which is sufficiently low to fulfill the requirements of biopotential measurement and suitable for penetrating the stratum corneum of the skin and acquire the EEG signal directly from the interstitial fluidic layer underneath which could make it a promising dry electrode for long-duration EEG Monitoring [26]. In 2017, Kannan et al. developed a wearable and less visible Ear-EEG recording device [34]. It records Ear-EEG raw data in real-time and allows displaying the brain signals obtained, which then can be analyzed for further investigation of any particular neural disorder. Kappel et al. developed a dry-contact ear-EEG platform [35], comprising actively shielded and nano-structured electrodes embedded in an individualized soft-earpiece. This electrode eliminates the gel application at the electrode-skin interface which shows its user-friendliness and technological feasibility. Xing et al. demonstrated a high performance high-speed Steady-State Visual Evoked Potentials (SSVEP)-based BCI system using claw-like structure dry EEG electrodes created from thermoplastic polyurethanes (TPU) coated with conductive ink of Ag/AgCl mixture[36]. This device can be worn comfortably over a hair-covered head area and the pins of the electrode can go easily through the hair and contact the scalp providing a stable impedance of the electrode. Therefore, the electrode is capable to record reliable and high-quality signals for subsequent signal processing.

3.3. Types of EEG Electrodes

Electrodes can be categorized as polarizable or non-polarizable. In perfectly non-polarizable, the electrodes require electrically-conductive skin interfacing materials to improve their performance [37]. Whereas in perfectly polarizable, the electrodes work based on the capacitive coupling technique between a conductive material and the skin [38].

Existing EEG measurements are done in hospitals and clinics using non-polarizable wet electrodes (e.g., Ag/AgCl and gold cup electrodes) that performs based on galvanic coupling [39]. Wet electrodes are standard EEG electrodes because of their signal quality, reproducibility, and biocompatibility. Despite this, EEG measurement requires skin preparation and the use of a conductive paste to lower the scalp-electrode contact impedance. The skin preparation method takes time, invites the presence of a trained physician, and leaves a neurotic excoriation lesion with skin scratching. That is why highly skilled professionals are required and the patients need to stay for a long time at the diagnosis location. In addition, for example for seizure detection many numbers of electrodes are used making them very labor-intensive, especially to perform long-term EEG recording. Dehydration of the gel over time, unless properly maintained, also causes an increase in skin-to-electrode impedance which in turn deteriorates the quality of EEG signals. This is why patients need to be admitted to the hospital to do long-term EEG monitoring as the conventional clinical wet electrodes need to be kept wet all the time. Continuous use of conductive pastes can cause hair damage and allergic reactions [40]. Wet electrodes are single-use and thrown away, thus increasing the cost per diagnosis and producing a large amount of waste. Some examples of standard wet electrodes are shown in Figure 3.4.

a) **b)**

Figure 3.4: EEG cup wet electrodes: **a**) Ag/AgCl; **b**) Au plated.

The aforementioned problems associated with wet electrodes caused a demand for more comfortable and user-friendly electrodes that has, in turn, led to the

development of an increasing number of dry electrodes made of a conductive substance that mechanically interfaces with the skin, avoiding the skin preparation procedure and the use of conductive paste. They can work without any physical contact on pure capacitive coupling or with dry sensor-skin contact. Capacitive EEG electrodes [41]–[45] are unlikely to be appropriate for recording spontaneous EEG signals as the amplitude levels are so low, moreover, the high impedance of these electrodes, on the other hand, necessitates the use of an ultra-high impedance on-site amplifier [46]. In addition, the "floating" fixation on the scalp causes motion artifacts. Skin-contact dry EEG electrodes that work on galvanic coupling were also introduced [47]–[50]. Flat skin contact dry electrodes cannot be used in the hairy regions. Although needle-based dry electrodes can be used on the hairy region, they are still heavy in weight and stiff in structure. Datwayler [51] reported a so-called flexible conductive polymer and customizable design of dry electrodes, however from the data sheet, the impedance is more than 25 kΩ, which is much higher than the required impedance for EEG measurement which is less than 10 kΩ. Thus, all the aforementioned EEG electrodes are inappropriate for long-term monitoring and wearable applications. Some examples of commercial dry electrodes are shown in Figure 3.4.

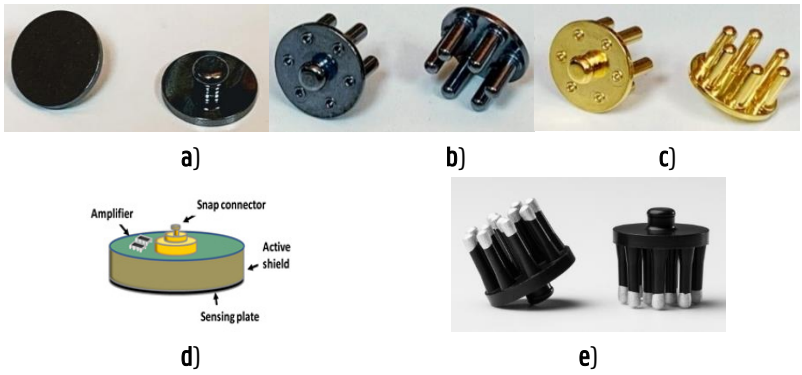

Figure 3.5: Reusable dry EEG electrodes: **a**) flat dry Ag/AgCl electrode; **b**) spike dry Ag/AgCl electrode; **c**) spike dry gold plated electrode; **d**) capacitive EEG electrode [46]; **e**) SoftPulse™ – Soft dry electrodes [51]

The emergence of dry electrodes led to the development of portable EEG devices that would be used at home even for long-term monitoring. In Table 3.1, we provided a few examples of commercially available EEG devices based on dry electrodes such as X series-EEG [52], Neuro:On Smart Sleep Mask [53], Ultracortex “Mark IV” EEG Headset [54] TGAM EEG Biosensor [55], XWave EEG [56], EEG SENSOR - T9305M [57] and SENS-EEG-UCE6 [58].

Table 3.1: Examples of Commercial EEG Device

Company	Brand Name	Device Type	Website
Advanced Brain Monitoring	X series – EEG wireless monitoring	EEG wireless headset for interpretation of physiological signals	Adva.BrainMon.com
Neuro:On	Neuro:On Smart Sleep Mask	Measures brain waves (EEG), muscle tension (EMG), eye movement (EOG), pulse (pulse oximetry), body temp, and body movement during sleep (actigraphy)	neurooon.com
OpenBCI	Ultracortex "Mark IV" EEG Headset	EEG Monitoring	openbci.com
Neurosky	ThinkGear™ AM (TGAM EEG Biosensor)	Understand the mind.	neurosky.com
PLX Devices	XWave EEG	EEG Brain-computer Interface for iPhone/iPad	plxdevices.com
Science Division	EEG SENSOR - T9305M	Provide EEG from 2-1000 Hz with less than 0.3 µV noise	thoughttech.com
Plux	SENS-EEG-UCE6	Purpose-built sensor for brain activity measurement.	store.plux.info

3.4. Textile-based EEG Electrodes

The combination of textile material with electronics led to a new class of large-area, flexible, conformable, and interactive smart textiles. New value-added textile products led to significant results in wearable multifunctional smart textiles, enabling several applications in healthcare, protection, fashion, military, and so on. Similarly, the use of textile electrodes for biopotential sensing applications has been booming and demands the attention of textile, electronic, and medical expertise owing to their flexibility and low weight, which are advantages over existing commercial electrodes. Many dry electrodes for bio-potential measurement have been researched. For instance, a textile-based electrocardiography (ECG) [59]–[66], electromyography (EMG) [67]–[72] and electrooculography (EOG) [70], [73], [74] are among the recently reported textile-based electrodes for bio-potential measurement. Some typical examples of textile electrodes reported for biopotential sensing are shown in Figure 3.6.

However, there is limited information on which devices for sensor detection are optimal for each type of application. The ideal monitoring device for patients, families, and medical staff should be safe and easy to use. For patients, especially during sleep, it must be comfortable and therefore preferably wireless, miniaturized, and light. If electrodes are used, they must be as small and as few as possible as a significant percentage of patients are unwilling to wear long-term electrodes [27]. The device should be discrete and unobtrusive. It is important to avoid uncomfortable cables, electrodes, lights, buttons, and sounds as this disturbs the patient and family, even more so in the long run. This was confirmed by a recent survey evaluating the desires of patients, which revealed a strong preference for a seizure detection device with little interference with daily activities [75]. Using textile electrodes, therefore, overcomes the related issues and would fill the gap of existing metal electrodes. Textile electrodes are fabric-made electrodes. Textile materials are usually insulators, but the conductive yarns are attached to, or incorporated in, the fabric forming the textile electrodes during their production process. These electrodes need no gel to connect to the skin. Weaving, knitting, or embroidering conductive yarn to the structure can make the textile electrodes. The textile electrodes are good for long-term measurement, as they do not irritate the skin. They are also light, ductile, and washable [76]. This review chapter focuses further on these textile-based EEG electrodes.

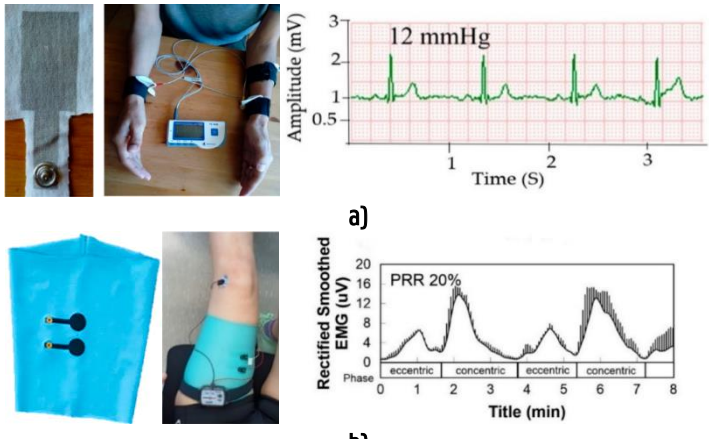

Figure 3.6: Textile-based bio-potential sensors: **a**) silver-printed cotton electrocardiography under CC by 4.0; **b**) silver and carbon paste conductive sheet

electromyography electrodes laminated polyester/spandex sleeve [72], under CC by 4.0

The demand for more comfortable and user-friendly electrodes has led to a growing number of dry electrodes being developed that can overcome the limitations of wet electrodes. Dry electrodes have the disadvantage of a higher impedance of the electrode-skin boundary, additional circuitry, and sensitivity to artifacts of movement. However, it is reported in the literature that the impedance decreases considerably after a settling time due to the accumulation of sweat under the electrodes, and the noise of artifacts is lower than for wet electrodes [77]. Other studies have also reported that dry electrodes have several advantages over wet ones, such as the impedance of the electrode-skin interface, signal intensity, and electrode size [78].

Promising textile-based dry electrode research that provides better user comfort and stable EEG recordings has been consistently reported since 2010 in the fields of electrical, textile, material, and biomedical disciplines. In 2010, Löfuede et al. tested the EEG signals obtained with knitted soft textile EEG electrodes made of nylon, conductive fibers, spandex, and thinner yarn polypropylene [79]. It showed a larger total surface area and was very good for absorbing liquids, which could be very useful in long-term monitoring applications, particularly in neonates. In 2011, Linet et al. developed a novel dry foam-based electrode EEG electrode from conductive fabric [80]. It provided partly polarizable electric characteristics and they found better performance for long-term EEG measurement, so it could possibly be practical for daily life applications. Later in 2012, Salvo et al. fabricated 3D printed dry medical electrodes by sputtering titanium as an adhesion promotion layer, evaporation of gold to lower the impedance and prevent oxidation of the electrode, and finally insulating it with an acrylic-based photopolymer [81]. They found qualitative results comparable to wet electrodes. In the same year, Löfhede et al. developed a long-term EEG electrode for newborns based on several electrodes distributed over the head of the baby [82], shown in Figure 3.7. A test on five healthy adults was performed and was found comparable to standard quality electrodes. Researchers working in the field have consistently been looking for an EEG electrode with better flexibility and stable signals. In 2014, Kumar & Thilagavathi created a copper-plated polyester fabric for EEG measurement and found similar signals as with commercially available electrodes hinting at their feasible long-term EEG monitoring candidacy [83]. In 2015, Sahi et al. worked on the development of a textile-based nano-structure sensor electrode array for EEG measurement in the motor cortex and the occipital lobe for autism disorder. A mu-wave attenuation was detected [84]. In 2016, a number of research outputs came out on the development of EEG

electrodes from different conductive textile materials. Muthukumar et al. developed a polyaniline (PANI) polymer-coated polyurethane (PU) foam textile electrode with surface resistance and impedance values of 7 kΩ/sqr and 1.45 MΩ/sqr, resulting in similar results to commercial Ag/AgCl electrodes, making it feasible for EEG measurements, especially for continuous monitoring purposes [85]. However, for good EEG measurements, the impedance should preferably be less than 5 kΩ [86]. Peng et al. presented a skin-electrode with relatively low contact impedance based on porous titanium (Ti) for EEG recording that does not cause skin irritations or allergic reactions [87]. In 2018, Gao et al. introduced a novel soft pin-shaped dry electrode fabricated from carbon fiber bristles for EEG reading [88]. The carbon fibers were processed to reduce the contact impedance between skin and dry electrodes and realize a larger contact area and better comfort with a smaller pressure.

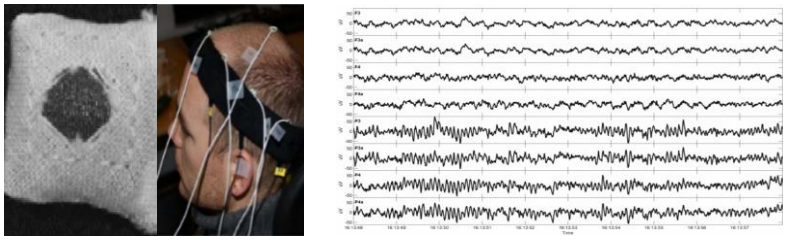

a) b)

Figure 3.7: Textile-based EEG electrode: **a**) silver-plated nylon/spandex fabric EEG electrode; **b**) EEG signal collected from silver-plate polyamide/elastomer fabric electrode [82], under CC by 4.0.

Apart from the development of textile-based electrodes, researchers have also been working on reviewing, testing, and characterizing existing electrodes and searching for better EEG monitoring software. Renz et al. reported a review on the recent progress in interfacing both the central and peripheral nervous systems for long-term functional devices [89]. The review could serve as a guide for long-term functional electrodes interfacing neural tissue.

There is also interest to deal with the challenges in signal processing and protocol. For instance, a deep review work by Zerafa et al. highlighted the strengths and weaknesses of the three categories of steady-state visually evoked potential training methods [90]. Feature extraction techniques incorporating certain training data address and have outperformed training-free methods: subject-specific Brain-Computer Interfaces (BCIs) are tailored to the individual, delivering the best performance at the cost of long, tiring training sessions. These do make these methods unsuitable for one-time or sporadic use,

creating a remaining need for subject-independent BCIs. Senn et al. suggested a Single-Source Multipolar Stimulation (SSMPS), a novel form of stimulation based on a single current supply and a passive present-day divider [91]. This demonstrates that the SSMPS efficiently limits the broadening of the excitatory field along with the electrode array and hence a subsequent reduction in neural excitation. Craik et al. summarized the present-day practices and performance effects of the use of EEG [92]. This EEG classification provides sensible guidelines on the selection of many hyper-parameters in the hope that they would promote or inform the deployment of deep learning to EEG datasets in future lookups. Sadatnejad et al. studied the EEG representation using a multi-instance framework on the manifold of symmetric effective precise matrices by using computerized attenuation of the extra-physiologic noise contribution and exploiting the discriminative statistics of physiological artifacts [93].

3.5. Outlook on Textile-based EEG Electrodes

The conclusions drawn in the published works showed that the developed textile-based dry EEG electrodes gave similar and comparable EEG signals when compared with the commercially available Ag/AgCl wet electrodes. Although promising comparisons were presented, the findings in each research work were not compared in quantitative and figurative terms with standard electrodes, but merely referred to in qualitative terms. Therefore, to bring such electrodes into practical real-world applications, scientific research that could show the actual values of textile EEG electrodes versus standard electrodes must be conducted. Otherwise, ongoing EEG research would likely continue to lead to a publication but will not allow other researchers to determine what is really important, as any conductive material can be used to create an electrode. In Table 3.2, we presented the method of comparison used for the textile-based EEG electrode signal in several references. Only the 3D printed electrode [75] and the pin-shaped carbon fiber EEG electrodes [88] were tested on a hairy part of the head surface, whereas all the others mentioned in Table 3.2 were placed on the forehead.

Table 3.2 shows that not all the textile-based EEG electrodes were quantitatively compared with standard electrodes. Moreover, there is no information on flexibility, tensile strength, thickness, and other physical characteristics of the electrode in order to determine if using textiles had a benefit over standard electrodes. We suggest such properties of the textile should also be characterized as long as we are dealing with textile-based electrodes.

Table 3.2: Device Comparison of Textile-based EEG Electrodes with Standard Electrode

EEG Electrode	Conductive materials used	Integration approach	Comparison with standard wet electrode and conclusion drawn	Type of Comparison	Ref.
Nylon, conductive fibers, spandex, and polypropylene	Silver plated fibers	Knitting	Visual inspection of EEG data in time and frequency domains and an EEG signal was found	Not compared	[79]
Conductive polymer foam-conductive fabric	Ni/Cu	Coating	Not compared with standard electrodes but an EEG signal was found	Qualitative	[80]
3D Conductive Acrylic Photopolymer	Titanium and Gold	3D Printing	Visual observation of EEG signal with wet electrodes and a comparable result was found	Qualitative	[81]
Knitted conductive fabric	Silver plated conductive fibers	Knitting	Visual inspection of EEG data in time and frequency domains with standard electrodes found comparable results	Qualitative	[82]
Copper Plated Polyester Fabrics	Copper	Electroless copper plating	Compared with commercially available electrodes and a similar signal was found	Qualitative	[83]
Nano-structures sensor electrode array	Not disclosed	Seamlessly integration	Not compared with standard electrode but a mu-wave attenuation was detected	Not compared	[84]
PANI-coated polyurethane foam	Polyaniline	Coating	Visual comparison of EEG data with standard electrodes	Qualitative	[94]
Ti and PDMS foam	Porous Titanium	Leaching	Not compared with standard electrodes but an EEG signal was found	Not compared	[87]
Pin-shaped carbon fiber	Carbon fiber	Coating	Not compared with standard electrodes but an EEG signal was found	Not compared	[88]

3.6. Conclusion

Existing EEG devices rely on wet electrodes (e.g. Ag/AgCl electrodes) with three major drawbacks: abrasive lesions during skin preparation, allergic reaction due to the use of the conductive gel or paste, and artifacts due to moisture change. Moreover, the gel must be cleaned off afterward. In addition, when a large number of electrodes are required, skin preparation and gel application are time-consuming. The demand for more comfortable and user-friendly electrodes has led to the development of an increasing number of dry electrodes capable of overcoming the limitations of wet electrodes, but dry electrodes have the disadvantages of higher electrode-skin impedance, additional circuitry, and movement artifact susceptibility. However, it is reported in the literature that the impedance decreases considerably after a settling time due to the accumulation of perspiration under the electrodes, and the noise of artifacts is reported to be lower than that of wet electrodes.

The ideal monitoring device for users must be comfortable, safe, and simple to use. It is important to avoid uncomfortable cables, electrodes, lights, buttons, and sounds as this disturbs the patient and family, even more so in the long run. Textile electrodes are a logical next step in the development of electrodes. These electrodes need no gel to connect to the skin. It is possible to make the textile electrodes by weaving, knitting, or embroidering conductive yarn to the structure or coating and printing conductive pastes on the surface of the substrate. In addition, different material types can be deposited on the textile fabric layer by layer at different paste viscosity allowing the possibility of covering electronic components vulnerable to top layer washing using water-insoluble hydrophobic polymers. Most of the so far developed and published textile-based EEGs are kept on shelves only due to limited flexibility, skin adhesiveness, and washability. Therefore, new approaches to integration and new conductive polymer composites should be evolved to overcome the associated limitations and to make the application of textile-based EEG for bio-potential monitoring a reality. At the same time, reporting on textile-based dry-electrodes should always include a discussion of the textile properties of the electrodes, and a quantitative comparison of the EEG signal with standard wet electrodes.

Bibliography

[1] C. S. von Bartheld, J. Bahney, and S. Herculano-Houzel, "The search for true numbers of neurons and glial cells in the human brain: A review of 150 years of cell counting: Quantifying neurons and glia in human brain," *J. Comp. Neurol.*, vol. 524, no. 18, pp. 3865–3895, Dec. 2016, doi: 10.1002/cne.24040.

[2] C. R. Noback, Ed., *The human nervous system: structure and function*, 6. ed. Totowa, NJ: Humana Press, 2005.

[3] D. Van De Ville, R. Liégeois, Y. Farouj, M. G. Preti, and E. Amico, "When makes you unique: Temporality of the human brain fingerprint," *Sci. Adv.*, vol. 7, no. 42, p. 10, 2021, doi: 10.1126/sciadv.abj0751.

[4] J. Liu, Y. Sheng, and H. Liu, "Corticomuscular Coherence and Its Applications: A Review," *Front. Hum. Neurosci.*, vol. 13, p. 100, Mar. 2019, doi: 10.3389/fnhum.2019.00100.

[5] I. Nakanishi, S. Baba, and C. Miyamoto, "EEG based biometric authentication using new spectral features," in *2009 International Symposium on Intelligent Signal Processing and Communication Systems (ISPACS)*, Kanazawa, Japan, Dec. 2009, pp. 651–654. doi: 10.1109/ISPACS.2009.5383756.

[6] S. J. M. Smith, "EEG in the diagnosis, classification, and management of patients with epilepsy," *J. Neurol. Neurosurg. Psychiatry*, vol. 76, no. suppl_2, pp. ii2–ii7, Jun. 2005, doi: 10.1136/jnnp.2005.069245.

[7] K. Douibi, S. Le Bars, A. Lemontey, L. Nag, R. Balp, and G. Breda, "Toward EEG-Based BCI Applications for Industry 4.0: Challenges and Possible Applications," *Front. Hum. Neurosci.*, vol. 15, p. 705064, Aug. 2021, doi: 10.3389/fnhum.2021.705064.

[8] D. E. B. Tan, R. S. Tung, W. Y. Leong, and J. C. M. Than, "Sleep Disorder Detection and Identification," *Procedia Eng.*, vol. 41, pp. 289–295, 2012, doi: 10.1016/j.proeng.2012.07.175.

[9] Y. Höller, "Quantitative EEG in Cognitive Neuroscience," *Brain Sci.*, vol. 11, no. 4, p. 517, Apr. 2021, doi: 10.3390/brainsci11040517.

[10] C. Li, X. Li, M. Lv, F. Chen, X. Ma, and L. Zhang, "How Does Approaching a Lead Vehicle and Monitoring Request Affect Drivers' Takeover Performance? A Simulated Driving Study with Functional MRI," *Int. J. Environ. Res. Public. Health*, vol. 19, no. 1, p. 412, Dec. 2021, doi: 10.3390/ijerph19010412.

[11] M. Elvira, E. Iáñez, V. Quiles, M. Ortiz, and J. M. Azorín, "Pseudo-Online BMI Based on EEG to Detect the Appearance of Sudden Obstacles during

Walking," *Sensors*, vol. 19, no. 24, p. 5444, Dec. 2019, doi: 10.3390/s19245444.

[12] L. Troebinger, P. Anninos, and G. Barnes, "Neuromagnetic effects of pico-Tesla stimulation," *Physiol. Meas.*, vol. 36, no. 9, pp. 1901–1912, Sep. 2015, doi: 10.1088/0967-3334/36/9/1901.

[13] J. Bruggemann, A. Gross, and S. Pate, "Non-Intrusive Visualization of Optically Inaccessible Flow Fields Utilizing Positron Emission Tomography," *Aerospace*, vol. 7, no. 5, p. 52, Apr. 2020, doi: 10.3390/aerospace7050052.

[14] H. Berger, "Uber das Elektrenkephalogramm des Menschen," *Archiv f. Psychiatrie*, vol. 87, pp. 527–570, 1929, doi: https://doi.org/10.1007/BF01797193.

[15] F. A. Alturki, K. AlSharabi, A. M. Abdurraqeeb, and M. Aljalal, "EEG Signal Analysis for Diagnosing Neurological Disorders Using Discrete Wavelet Transform and Intelligent Techniques," *Sensors*, vol. 20, no. 9, p. 2505, Apr. 2020, doi: 10.3390/s20092505.

[16] P. L. Purdon, A. Sampson, K. J. Pavone, and E. N. Brown, "Clinical Electroencephalography for Anesthesiologists," *Anesthesiology*, vol. 123, no. 4, pp. 937–960, Oct. 2015, doi: 10.1097/ALN.0000000000000841.

[17] J. E. Jacob, G. K. Nair, T. Iype, and A. Cherian, "Diagnosis of Encephalopathy Based on Energies of EEG Subbands Using Discrete Wavelet Transform and Support Vector Machine," *Neurol. Res. Int.*, vol. 2018, pp. 1–9, Jul. 2018, doi: 10.1155/2018/1613456.

[18] Z. Chen *et al.*, "An empirical EEG analysis in brain death diagnosis for adults," *Cogn. Neurodyn.*, vol. 2, no. 3, pp. 257–271, Sep. 2008, doi: 10.1007/s11571-008-9047-z.

[19] I. Lazarou, S. Nikolopoulos, P. C. Petrantonakis, I. Kompatsiaris, and M. Tsolaki, "EEG-Based Brain–Computer Interfaces for Communication and Rehabilitation of People with Motor Impairment: A Novel Approach of the 21st Century," *Front. Hum. Neurosci.*, vol. 12, p. 14, Jan. 2018, doi: 10.3389/fnhum.2018.00014.

[20] B. Xu, S. Peng, A. Song, R. Yang, and L. Pan, "Robot-Aided Upper-Limb Rehabilitation Based on Motor Imagery EEG," *Int. J. Adv. Robot. Syst.*, vol. 8, no. 4, p. 40, Sep. 2011, doi: 10.5772/45703.

[21] H. Namazi, "Investigating the Brain Development in Newborns by Information-Based Analysis of Electroencephalography (EEG) Signal," *Fluct. Noise Lett.*, vol. 19, no. 04, p. 2050043, Dec. 2020, doi: 10.1142/S0219477520500431.

[22] A. Brancaccio, D. Tabarelli, M. Bigica, and D. Baldauf, "Cortical source localization of sleep-stage specific oscillatory activity," *Sci. Rep.*, vol. 10, no. 1, p. 6976, Dec. 2020, doi: 10.1038/s41598-020-63933-5.

[23] Y. Sun, F. P. W. Lo, and B. Lo, "EEG-based user identification system using 1D-convolutional long short-term memory neural networks," *Expert Syst. Appl.*, vol. 125, pp. 259–267, 2019, doi: 10.1016/j.eswa.2019.01.080.

[24] A. Khalaf, E. Sejdic, and M. Akcakaya, "EEG-fTCD Hybrid brain-computer interface using template matching and wavelet decomposition," *J. Neural Eng.*, 2019, doi: 10.1088/1741-2552/ab0b7f.

[25] X. Zhang, R. D'Arcy, and C. Menon, "Scoring upper-extremity motor function from EEG with artificial neural networks: a preliminary study," *J. Neural Eng.*, 2019, doi: 10.1088/1741-2552/ab0b82.

[26] J. K. Radhakrishnan, S. Nithila, S. N. Kartik, T. Bhuvana, G. U. Kulkarni, and U. K. Singh, "A Novel, Needle-Array Dry-Electrode With Stainless Steel Micro-Tips, for Electroencephalography Monitoring," *J. Med. Devices*, vol. 12, no. 4, pp. 1–7, 2018, doi: 10.1115/1.4041227.

[27] S. Wunder, A. Hunold, P. Fiedler, F. Schlegelmilch, K. Schellhorn, and J. Haueisen, "Novel bifunctional cap for simultaneous electroencephalography and transcranial electrical stimulation," *Sci. Rep.*, vol. 8, no. 1, pp. 1–11, 2018, doi: 10.1038/s41598-018-25562-x.

[28] H. Alawieh, H. Hammoud, M. Haidar, M. H. Nassralla, A. M. El-Hajj, and Z. Dawy, "Patient-aware adaptive ngram-based algorithm for epileptic seizure prediction using EEG signals," *2016 IEEE 18th Int. Conf. E-Health Netw. Appl. Serv. Heal. 2016*, pp. 1–6, 2016, doi: 10.1109/HealthCom.2016.7749471.

[29] R. Spies and R. Gassert, "A penalized time-frequency band feature selection and classification procedure for improved motor intention decoding in multichannel EEG," 2019, doi: 10.1088/1741-2552/aaf046.

[30] H. R. Al Ghayab, Y. Li, S. Siuly, and S. Abdulla, "Epileptic seizures detection in EEGs blending frequency domain with information gain technique," *Soft Comput.*, vol. 23, no. 1, pp. 227–239, 2018, doi: 10.1007/s00500-018-3487-0.

[31] G. Higgins *et al.*, "The effects of lossy compression on diagnostically relevant seizure information in EEG signals," *IEEE J. Biomed. Health Inform.*, vol. 17, no. 1, pp. 121–127, 2013, doi: 10.1109/TITB.2012.2222426.

[32] Y. J. Chen, Y. S. Lin, and H. Chiueh, "EEG recording frontend circuitry for epileptic seizure detection headband," *2016 IEEE Healthc. Innov. Point--Care Technol. Conf. HI-POCT 2016*, pp. 42–45, 2016, doi: 10.1109/HIC.2016.7797692.

[33] F. Wang, G. Li, J. Chen, and Y. Duan, "Novel semi-dry electrodes for brain – computer interface applications," 2016.

[34] R. Kannan, S. S. A. Ali, A. Farah, S. H. Adil, and A. Khan, "Smart Wearable EEG Sensor," *Procedia Comput. Sci.*, vol. 105, no. December 2016, pp. 138–143, 2017, doi: 10.1016/j.procs.2017.01.193.

[35] S. L. Kappel, M. L. Rank, H. O. Toft, M. Andersen, and P. Kidmose, "Dry-Contact Electrode Ear-EEG," *IEEE Trans. Biomed. Eng.*, vol. 66, no. 1, pp. 150–158, 2018, doi: 10.1109/TBME.2018.2835778.

[36] X. Xing *et al.*, "A High-Speed SSVEP-Based BCI Using Dry EEG Electrodes," *Sci. Rep.*, vol. 8, no. 1, pp. 1–10, 2018, doi: 10.1038/s41598-018-32283-8.

[37] G. Ruffini *et al.*, "A dry electrophysiology electrode using CNT arrays," *Sens. Actuators Phys.*, vol. 132, no. 1, pp. 34–41, Nov. 2006, doi: 10.1016/j.sna.2006.06.013.

[38] R. J. Ilmoniemi and D. Kičić, "Methodology for Combined TMS and EEG," *Brain Topogr.*, vol. 22, no. 4, pp. 233–248, Jan. 2010, doi: 10.1007/s10548-009-0123-4.

[39] S. Grimnes and Ø. G. Martinsen, *Bioimpedance and bioelectricity basics*, 2nd ed. Amsterdam Boston: Elsevier Academic Press, 2008.

[40] C. Drees *et al.*, "Skin Irritation during Video-EEG Monitoring," *Neurodiagnostic J.*, vol. 56, no. 3, pp. 139–150, Jul. 2016, doi: 10.1080/21646821.2016.1202032.

[41] T. J. Sullivan, S. R. Deiss, and G. Cauwenberghs, "A Low-Noise, Non-Contact EEG/ECG Sensor," in *2007 IEEE Biomedical Circuits and Systems Conference*, Montreal, QC, Canada, Nov. 2007, pp. 154–157. doi: 10.1109/BIOCAS.2007.4463332.

[42] H. J. Baek, H. J. Lee, Y. G. Lim, and K. S. Park, "Conductive Polymer Foam Surface Improves the Performance of a Capacitive EEG Electrode," *IEEE Trans. Biomed. Eng.*, vol. 59, no. 12, pp. 3422–3431, Dec. 2012, doi: 10.1109/TBME.2012.2215032.

[43] Y. M. Chi, Y.-T. Wang, Y. Wang, C. Maier, T.-P. Jung, and G. Cauwenberghs, "Dry and Noncontact EEG Sensors for Mobile Brain–Computer Interfaces," *IEEE Trans. Neural Syst. Rehabil. Eng.*, vol. 20, no. 2, pp. 228–235, Mar. 2012, doi: 10.1109/TNSRE.2011.2174652.

[44] S. Gonzalez, "Non-Contact EEG Active Multielectrode Hardware Design," Flinders University, Adelaide, South Australia, 2017. Accessed: Jul. 21, 2022. [Online]. Available: https://flex.flinders.edu.au/file/08b2128d-31c2-4765-862c-8c3e2b2439a2/1/Scheina%20Thesis%20Edited%2002_01_2018.pdf

[45] Y. M. Chi and G. Cauwenberghs, "Wireless Non-contact EEG/ECG Electrodes for Body Sensor Networks," in *2010 International Conference on Body*

Sensor Networks, Singapore, Singapore, Jun. 2010, pp. 297–301. doi: 10.1109/BSN.2010.52.

[46] M. Lopez-Gordo, D. Sanchez-Morillo, and F. Valle, "Dry EEG Electrodes," *Sensors*, vol. 14, no. 7, pp. 12847–12870, Jul. 2014, doi: 10.3390/s140712847.

[47] P. Salvo, R. Raedt, E. Carrette, D. Schaubroeck, J. Vanfleteren, and L. Cardon, "A 3D printed dry electrode for ECG/EEG recording," *Sens. Actuators Phys.*, vol. 174, pp. 96–102, Feb. 2012, doi: 10.1016/j.sna.2011.12.017.

[48] J. Lofhede, F. Seoane, and M. Thordstein, "Soft textile electrodes for EEG monitoring," in *Proceedings of the 10th IEEE International Conference on Information Technology and Applications in Biomedicine*, Corfu, Greece, Nov. 2010, pp. 1–4. doi: 10.1109/ITAB.2010.5687755.

[49] W. E. Audette, J. Bieszczad, L. V. Allen, S. G. Diamond, and D. B. Kynor, "Design and Demonstration of a Head Phantom for Testing of Electroencephalography (EEG) Equipment," 2020, doi: 10.13140/RG.2.2.12078.25920.

[50] T. J. Sullivan, S. R. Deiss, Tzyy-Ping Jung, and G. Cauwenberghs, "A brain-machine interface using dry-contact, low-noise EEG sensors," in *2008 IEEE International Symposium on Circuits and Systems*, Seattle, WA, USA, May 2008, pp. 1986–1989. doi: 10.1109/ISCAS.2008.4541835.

[51] Datwyler, "SoftPulse™ – Soft dry electrodes for bio-monitoring." Datwyler, Dec. 07, 2022. Accessed: Aug. 25, 2022. [Online]. Available: https://datwyler.com/media/news/softpulse-soft-dry-electrodes-for-bio-monitoring

[52] Advanced Brain Monitoring, "X series – EEG wireless monitoring," 2019. https://www.advancedbrainmonitoring.com/

[53] Neuro:On, "Neuro: On Smart Sleep Mask," 2019. https://neuroonopen.com/

[54] OpenBCI, "Ultracortex 'Mark IV' EEG Headset," 2019. https://openbci.com/

[55] Neurosky, "ThinkGear™ AM (TGAM EEG Biosensor)," 2019. http://neurosky.com/biosensors/eeg-sensor/

[56] PLX Devices, "XWave EEG," 2019. https://www.plxdevices.com/

[57] Science Division, "EEG SENSOR - T9305M," 2019. http://www.thoughttechnology.com/sciencedivision/pages/products/eegflex.html

[58] Plux, "SENS-EEG-UCE6," 2019. https://plux.info/

[59] A. B. Nigusse, B. Malengier, D. A. Mengistie, G. B. Tseghai, and L. Van Langenhove, "Development of Washable Silver Printed Textile Electrodes for Long-Term ECG Monitoring," *Sensors*, vol. 20, no. 21, p. 6233, Oct. 2020, doi: 10.3390/s20216233.

[60] E. Lee and G. Cho, "PU nanoweb-based textile electrode treated with single-walled carbon nanotube/silver nanowire and its application to ECG

monitoring," *Smart Mater. Struct.*, vol. 28, no. 4, p. 045004, 2019, doi: 10.1088/1361-665x/ab06e0.

[61] A. Ankhili, X. Tao, V. Koncar, D. Coulon, and J. Tarlet, "Ambulatory Evaluation of ECG Signals Obtained Using Washable Textile-Based Electrodes Made with," *Sensors*, vol. 19, no. 416, p. 13, 2019, doi: 10.3390/s19020416.

[62] T. Kang, J. Park, G. Yun, H. Hee, and H. Lee, "A real-time humidity sensor based on a microwave oscillator with conducting polymer PEDOT : PSS film," *Sens. Actuators B Chem.*, vol. 282, pp. 145–151, 2019, doi: 10.1016/j.snb.2018.09.080.

[63] A. Achilli, A. Bonfiglio, and D. Pani, "Design and characterization of screen-printed textile electrodes for ECG monitoring," *IEEE Sens. J.*, vol. 18, no. 10, pp. 4097–4107, 2018, doi: 10.1109/JSEN.2018.2819202.

[64] X. An and G. K. Stylios, "A hybrid textile electrode for electrocardiogram (ECG) measurement and motion tracking," *Materials*, vol. 11, no. 10, 2018, doi: 10.3390/ma11101887.

[65] W. Wu, S. Pirbhulal, A. K. Sangaiah, S. C. Mukhopadhyay, and G. Li, "Optimization of signal quality over comfortability of textile electrodes for ECG monitoring in fog computing based medical applications," *Future Gener. Comput. Syst.*, vol. 86, pp. 515–526, 2018, doi: 10.1016/j.future.2018.04.024.

[66] P. S. Das and J. Y. Park, "A flexible touch sensor based on conductive elastomer for biopotential monitoring applications," *Biomed. Signal Process. Control*, vol. 33, pp. 72–82, 2017, doi: 10.1016/j.bspc.2016.11.008.

[67] S. Lee, M. O. Kim, T. Kang, J. Park, and Y. Choi, "Knit Band Sensor for Myoelectric Control of Surface EMG-Based Prosthetic Hand," *IEEE Sens. J.*, vol. 18, no. 20, pp. 8578–8586, 2018, doi: 10.1109/JSEN.2018.2865623.

[68] A. Shafti, R. B. Ribas Manero, A. M. Borg, K. Althoefer, and M. J. Howard, "Embroidered Electromyography: A Systematic Design Guide," *IEEE Trans. Neural Syst. Rehabil. Eng.*, vol. 25, no. 9, pp. 1472–1480, 2017, doi: 10.1109/TNSRE.2016.2633506.

[69] Y. G. *et al.*, "An IoT-Enabled Stroke Rehabilitation System Based on Smart Wearable Armband and Machine Learning," *IEEE J. Transl. Eng. Health Med.*, vol. 6, no. March, 2018.

[70] G. M. Paul, F. Cao, R. Torah, K. Yang, S. Beeby, and J. Tudor, "A smart textile based facial EMG and EOG computer interface," *IEEE Sens. J.*, vol. 14, no. 2, pp. 393–400, 2014, doi: 10.1109/JSEN.2013.2283424.

[71] A. Niijima, T. Isezaki, R. Aoki, and T. Watanabe, "hitoeCap: Wearable EMG Sensor for Monitoring Masticatory Muscles with PEDOT-PSS Textile Electrodes," in *ISWC '17*, 2017, pp. 215–220.

[72] S. Kim, S. Lee, and W. Jeong, "EMG Measurement with Textile-Based Electrodes in Different Electrode Sizes and Clothing Pressures for Smart Clothing Design Optimization," *Polymers*, vol. 12, no. 10, p. 2406, Oct. 2020, doi: 10.3390/polym12102406.

[73] T. H. Kang *et al.*, "Sensors on textile substrates for home-based healthcare monitoring," *Conf. Proc. - 1st Transdiscipl. Conf. Distrib. Diagn. Home Healthc. D2H2 2006*, vol. 2006, pp. 5–7, 2006, doi: 10.1109/DDHH.2006.1624783.

[74] A. J. Golparvar and M. K. Yapici, "Electrooculography by Wearable Graphene Textiles," *IEEE Sens. J.*, vol. 18, no. 21, pp. 8971–8978, 2018, doi: 10.1109/JSEN.2018.2868879.

[75] J. Wu, W. Jia, C. Xu, D. Gao, and M. Sun, "Impedance analysis of ZnO nanowire coated dry EEG electrodes," *J. Biomed. Eng. Inform.*, vol. 3, no. 1, p. 44, 2017, doi: 10.5430/jbei.v3n1p44.

[76] H. Li *et al.*, "Textile-based ECG acquisition system with capacitively coupled electrodes," *Trans. Inst. Meas. Control*, vol. 39, no. 2, pp. 141–148, 2017, doi: 10.1177/0142331215600254.

[77] L. Kirkup and A. Searle, "A direct comparison of wet, dry and insulating bioelectric recording electrodes," *Physiol. Meas.*, 2000.

[78] M. A. Lopez-Gordo, D. Sanchez Morillo, and F. Pelayo Valle, "Dry EEG electrodes," *Sens. Switz.*, vol. 14, no. 7, pp. 12847–12870, 2014, doi: 10.3390/s140712847.

[79] J. Löfuede, F. Seoane, and M. Thordstein, "Soft textile electrodes for EEG monitoring," in *Proceedings of the IEEE/EMBS Region 8 International Conference on Information Technology Applications in Biomedicine, ITAB*, 2010, pp. 4–7. doi: 10.1109/ITAB.2010.5687755.

[80] Chin-Teng Lin, Lun-De Liao, Yu-Hang Liu, I-Jan Wang, Bor-Shyh Lin, and Jyh-Yeong Chang, "Novel Dry Polymer Foam Electrodes for Long-Term EEG Measurement," *IEEE Trans. Biomed. Eng.*, vol. 58, no. 5, pp. 1200–1207, 2011, doi: 10.1109/tbme.2010.2102353.

[81] P. Salvo, R. Raedt, E. Carrette, D. Schaubroeck, J. Vanfleteren, and L. Cardon, "A 3D printed dry electrode for ECG/EEG recording," *Sens. Actuators Phys.*, vol. 174, no. 1, pp. 96–102, 2012, doi: 10.1016/j.sna.2011.12.017.

[82] J. Löfhede, F. Seoane, and M. Thordstein, "Textile electrodes for EEG recording - a pilot study," *Sens. Switz.*, vol. 12, no. 12, pp. 16907–16919, 2012, doi: 10.3390/s121216907.

[83] N. M. Kumar and G. Thilagavathi, "Design and Development of Textile Electrodes for EEG Measurement using Copper Plated Polyester Fabrics," *Jtatm*, vol. 8, no. 4, 2014.

[84] A. Sahi, P. Rai, S. Oh, M. Ramasamy, R. E. Harbaugh, and V. K. Varadan, "Neural activity based biofeedback therapy for Autism spectrum disorder through wearable wireless textile EEG monitoring system," *Nanosensors Biosens. Info-Tech Sens. Syst. 2014*, vol. 9060, pp. 1–9, 2014, doi: 10.1117/12.2045530.

[85] N. Muthukumar, G. Thilagavathi, and T. Kannaian, "Polyaniline-coated foam electrodes for electroencephalography (EEG) measurement," *J. Text. Inst.*, vol. 107, no. 3, pp. 283–290, 2016, doi: 10.1080/00405000.2015.1028248.

[86] J. Górecka and P. Makiewicz, "The Dependence of Electrode Impedance on the Number of Performed EEG Examinations," *Sensors*, vol. 19, no. 11, p. 2608, Jun. 2019, doi: 10.3390/s19112608.

[87] H. L. Peng *et al.*, "A novel passive electrode based on porous Ti for EEG recording," *Sens. Actuators B Chem.*, vol. 226, pp. 349–356, 2016, doi: 10.1016/j.snb.2015.11.141.

[88] K. P. Gao, H. J. Yang, X. L. Wang, B. Yang, and J. Q. Liu, "Soft pin-shaped dry electrode with bristles for EEG signal measurements," *Sens. Actuators Phys.*, vol. 283, pp. 348–361, 2018, doi: 10.1016/j.sna.2018.09.045.

[89] A. F. Renz, A. M. Reichmuth, F. Stauffer, G. Thompson-steckel, and V. Janos, "A guide towards long-term functional electrodes interfacing neuronal tissue," *J. Neural Eng.*, vol. 15, 2018, doi: https://doi.org/10.1088/1741-2552/aae0c2.

[90] R. Zerafa, T. Camilleri, O. Falzon, and K. P. Camilleri, "To train or not to train? A survey on training of feature extraction methods for SSVEP-based BCIs," *J. Neural Eng.*, vol. 15, 2018, doi: https://doi.org/10.1088/1741-2552/aaca6e.

[91] P. Senn, R. K. Shepherd, and J. B. Fallon, "Focused electrical stimulation using a single current source".

[92] A. Craik, Y. He, and J. L. Contreras-Vidal, "Deep learning for electroencephalogram (EEG) classification tasks: a review," *J. Neural Eng.*, vol. 16, no. 3, p. 031001, 2019, doi: 10.1088/1741-2552/ab0ab5.

[93] K. Sadatnejad, M. Rahmati, and R. Rostami, "EEG representation using multi-instance framework on the manifold of symmetric positive definite matrices," 2019.

[94] N. Muthukumar, G. Thilagavathi, and T. Kannaian, "Polyaniline-coated foam electrodes for electroencephalography (EEG) measurement," *J. Text. Inst.*, vol. 107, no. 3, pp. 283–290, 2016, doi: 10.1080/00405000.2015.1028248.

4. Development of PEDOT:PSS/PDMS-Printed Conductive Textile Fabric

This chapter presents a successful development of a conductive and stretchable knitted cotton fabric by screen printing of poly(3,4-ethylene dioxythiophene) polystyrene sulfonate (PEDOT:PSS) and poly(dimethylsiloxane-b-ethylene oxide) (PDMS) conductive polymer composite. Mechanical and electrical analysis of the conductive fabric has been addressed. A proof of concept as textile-based strain, moisture, and bio-potential sensors depending upon their respective surface resistance has been also provided.

This chapter is redrafted from published journal and proceeding papers:
G.B. Tseghai, B. Malengier, K.A. Fante, A.B. Nigusse and L. Van Langenhove, "Development of a Flex and Stretchy Conductive Cotton Fabric Via Flat Screen Printing of PEDOT:PSS/PDMS Conductive Polymer Composite", *Sensors*, 20(6): 1742, 2020. doi.org/10.3390/s20061742.

G.B. Tseghai, D.A. Mengistie, B. Malengier, K.A. Fante, and L. Van Langenhove, "PEDOT:PSS-Based Conductive Textiles and Their Applications", *Sensors*, 20 (7): 1881, 2020. doi.org/10.3390/s20071881.

G.B. Tseghai, B. Malengier, K.A. Fante, A.B. Nigusse, B.B. Etana, and L. Van Langenhove, "PEDOT:PSS/PDMS-printed cotton fabric for ECG electrode", *IEEE*, 2020 IEEE International Conference on Flexible and Printable Sensors and Systems (FLEPS), Manchester, UK, 20116374, 2020. doi.org/10.1109/FLEPS49123.2020.9239526.

G.B. Tseghai, B. Malengier, K.A. Fante, and L. Van Langenhove, "PEDOT:PSS/PDMS-printed Cotton Fabric for Strain and Moisture Sensors", *Proceedings*, International Conference on the Challenges, Opportunities, Innovations, and Applications in Electronic Textiles (E-Textiles 2020), Virtual venue, UK, 68 (1): 1, 2021. doi.org/10.3390/proceedings2021068001.

Table of Contents

4.1. Introduction

Poly(3,4-ethylene dioxythiophene) polystyrene sulfonate (PEDOT:PSS) conductive polymer is well-known for its high conductivity and applications in conductive synthetic textiles. It has been used with encouraging results as an electrode material for flexible electronics. Unfortunately the use of PEDOT:PSS is currently constrained by its brittleness and limited processability. As a result, many researchers have been trying to prepare PEDOT:PSS-based conductive polymer composites. For instance, PEDOT:PSS and graphene oxide (GO) as an efficient alternative structure for indium tin oxide (ITO) in organic photovoltaics, ITO-PEDOT:PSS/poly(3-hexylthiophene):phenyl-C61-butyric acid methyl ester/Al [1], poly (vinyl alcohol) (PVA)–PEDOT:PSS blend filled with synthesized GO and reduced GO by the solvent casting technique [2], PEDOT:PSS@polyurethane nonwovens by electrospinning and dip-coating [3], superparamagnetic PEDOT/magnetite nanoparticles [4], GO/glucose/PEDOT:PSS supercapacitor [5], graphene, and poly(3,4-methylenedioxy thiophene)–poly(styrene sulfonate) (G-PEDOT:PSS) electroactive bacterium [6], Shewanellaoneidensis MR-1, inside a conductive three-dimensional PEDOT:PSS matrix [7], thermoelectric PEDOT:PSS with polyurethane [8], UV-ozone treated GO/PEDOT:PSS [9], graphene nano-platelets with PEDOT:PSS solutions to produce conductive, breathable, and light-weight mercerized cotton fabrics by spray coating [10]. PVA, phosphoric acid, PEDOT:PSS, and silver flakes [11], 3D graphene–PEDOT:PSS skeleton with poly(dimethylsiloxane) (PDMS) [12], and single-walled carbon nanotubes/PEDOT:PSS coated Tenano-rod composite films [13] have all been successfully developed. Though promising results have been found, a truly textile-based conductive device with adequate flexibility and stretchability without intensive impact on the bulk property of the textile fabric is still required.

On the other hand, highly flexible and biocompatible conductive polymer composites are required. Because it is biocompatible, transparent, gas permeable, and economical, PDMS is widely used in medical research and technology [14], and there are a wide array of manufacturing techniques used for forming PDMS including soft-lithography and its derivatives [15], molding [16], dip coating [17], spin coating [18], and many others. Besides, PDMS has a good dielectric constant and a tunable elasticity which makes it suitable for flexible electronic sensors [19]. As a result, PDMS-based flexible composites have been studied by many researchers. For example, high strain biocompatible PDMS-based conductive graphene and multi-walled carbon nanotube as nano-composite strain sensors [20], electrically conductive PDMS-grafted carbon nanotubes-reinforced silicone elastomer [21], enhanced conductivity behavior of

PDMS hybrid composites containing exfoliated graphite nano-platelets and carbon nanotubes [22], high electro-conductive PDMS/short carbon fiber binary composites with electrical conductivity of 1.67 x 10^2 S/m [23], conductive elastomers based on multi-walled carbon nanotubes in PDMS with up to 0.01 S/cm conductivity [24], silver nano-wire network embedded in PDMS as a stretchable, transparent, and conductive substrate with 15 Ω/sq [24], and stretchable electronics based on Ag-PDMS PCB (Printed circuit board) with a typical resistance of 2 Ω/cm [25], have been reported.

It was noticed that the common limitations of the conductive polymer composite-based conductive textiles reported in many works of literature are that they possess inadequate flexibility, stretchability, and biocompatibility. Moreover, technical and scientific experimental evidence about the effect the conductive polymer composite has on the textile bulk properties like flexural rigidity, tensile strength, and extension at the break, were not reported, which does not allow to determine if the fabrics still remain true textiles or if they lost their texture.

Therefore, another approach is introduced in this work to produce a PEDOT:PSS Clevios PH 1000 (Figure 4.1a) and PDMS (Figure 4.1b) conductive polymer composite-based fabric. As a fabric, we selected knitted cotton, as cotton fabric is available everywhere, and making cotton conductive will make access to conductive fabric easier. In addition, this work contains an in-depth study on the properties of the conductive textile, not only from an electronic point of view but also as a textile material. The effect of the conductive polymer composite on bending length, flexural rigidity, tensile strength, and extension at the break, thickness, add-on, and weight has been studied.

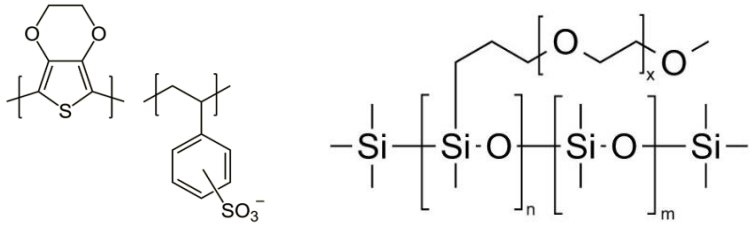

a) b)

Figure 4.1: Chemical structure: **a**) polystyrene sulfonate (PEDOT:PSS); **b**) poly(dimethylsiloxane-b-ethylene oxide) (PDMS).

4.2. PEDOT:PSS-Based e-Textiles

4.2.1. PEDOT:PSS

Among conductive polymers, PEDOT is the most extensively explored, successful, and widely used for many applications due to its high conductivity, stability in the air up to high temperatures, resistance to humidity including moist air, and because it is also processable in water. PEDOT can be polymerized from 3,4-ethylene dioxythiophene (EDOT) chemically or electrochemically. However, PEDOT synthesized this way and doped with small-molecule counter ions is insoluble in any solvent and large-size sample preparations are a challenge [26]. When polymerization is carried out in the presence of aqueous polyelectrolyte poly(styrene sulfonate) (PSS), it becomes water dispersible which is stable, easy to process, and with good film-forming properties, and with high visible light transmittance. PSS acts as a template during polymerization and charge balancing counter ion, hence keeping the cationic PEDOT segments dispersed in an aqueous medium. The molecular weight of PEDOT and PSS is about 1000–2500 g/mol (around 10 to 20 monomer units) and 400,000 g/mol, respectively. PEDOT:PSS in the aqueous media (and the as-prepared film too) has a core-shell structure as shown in Figure 4.2 where the core is conductive PEDOT-rich and the shell is insulator PSS-rich. The hydrophobic PEDOT and hydrophilic PSS nature led to the core-shell structure [27]. PEDOT:PSS films prepared from aqueous dispersions have lower conductivity (<1 S/cm) than PEDOT films prepared by oxidative and vapor phase polymerization and stabilized with small-molecule counter ions. The main reason for the low conductivity is the core-shell structure which leads to an increase in the energy barrier for charge transport across PEDOT chains by the insulator PSS-rich shell and charge localization due to the coiled PEDOT-rich core [28].

The conductivity can be enhanced up to four orders of magnitude by treatment with polar solvents like dimethyl sulfoxide, ethylene glycol, acids, and alcohols called “secondary dopants”. Secondary dopants are different from primary dopants in that they are apparently “inert” and the newly enhanced property persists even upon complete removal of the secondary dopants. Generally, the treatment methods can be grouped into three types: mixing secondary dopant into the aqueous PEDOT:PSS dispersion, film treatment after drying with a secondary dopant, or a combination of both methods. The exact mechanism of conductivity enhancement is still a topic of intense investigation. Shi et al. have nicely reviewed treatment methods for conductivity enhancement and the mechanism of conductivity enhancement [29]. The additives bring about charge

screening between PEDOT and PSS due to their high dielectric constant leading to phase separation. The PEDOT chains will be free to be linearly oriented (from the coiled structure), and hence, have a more compact structure (smaller $\pi-\pi$ stacking distance), leading to stronger interchain coupling and better crystallinity with larger crystal size [30]. In the case of post-treatment, the excess PSS will also be removed [31]. All these combined effects will lead to increases in carrier concentration and mobility [51, 52].

There are different grades of PEDOT:PSS commercially available with different conductivities which may be due to the molecular weight difference of PEDOT. Recently, the most extensively used high conductivity grade is Clevios PH1000. Rigorous work has shown very high conductivities of 4700 S/cm for PEDOT:PSS [34] and 7619 S/cm for single crystal PEDOT nanowires [35]. With such improved conductivities, further advancements in different applications are expected.

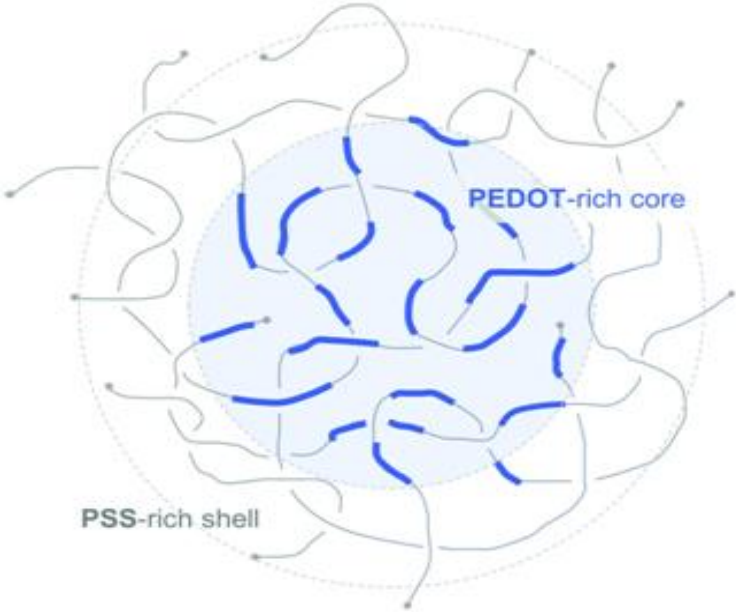

Figure 4.2: Core-shell structure of PEDOT:PSS, adapted from [36].

4.2.2. PEDOT:PSS-Based Conductive Polymer Composites

As mentioned above, PEDOT:PSS is well known for its high conductivity and applications in conductive textiles and has been used with encouraging results for different applications. Unfortunately, the use of pure PEDOT:PSS is currently constrained by its brittleness. As outlined earlier, one way to improve its mechanical flexibility is to make a composite with traditional commodity polymers. Giuri et al. reported GGO-PEDOT composites with thermal stability up to 270°C for supercapacitors [5], Hilal and Han developed graphene and PEDOT:PSS composites with improved electrical conductivity by 63% of a pristine PEDOT:PSS for solar cells [6]. Taroni et al. reported a thermoelectric PEDOT:PSS/PU blend [8] with improved ductility while maintaining reasonable conductivity. Polyvinyl alcohol (PVA) combined with phosphoric acid and PEDOT:PSS and silver flakes that withstand about 230% strain before fracture was reported by Houghton et al. [11]. Furthermore, a PEDOT:PSS-based multi-layer bacterial composite was developed by embedding an electro-active bacterium inside a conductive three-dimensional PEDOT:PSS matrix to increase the electron transfer through the PEDOT:PSS [37]. Table 4.1 presents non-exhaustive lists of PEDOT:PSS composites with their preparation technique, properties, and proposed applications.

Table 4.1: Properties of common PEDOT:PSS- based conductive polymer composites.

Conductive Polymer Composite	Resistivity, Ω cm (Resistance, Ω/sq)	Properties	Manufacturing Technique	Proposed Application	Ref.
GO/rGO filled PVA/PEDO:: PSS	10^7	Highly flexible free-standing	Solvent casting	Strain sensor	[2]
PEDOT:PSS/ PU	(35–240)	Highly flexible, stretchable	Electrospinning	Strain sensor	[38]
PEDOT:PSS/ Bacteria	103[1]	20 times more steady-state current than native biofilms baseline with signal level of 6.31 μA/cm^3	Embedding bacteria into electro-polymerized PEDOT:PSS on carbon felt anodes	Bioelectronics	[37]
PEDOT:PSS/ PU	1.26×10^{-2}	Sensitivity to different stimuli including strain, ambient temperature and/or air flow high electrical conductivity	Dispersion mixing	Stretchable self-powered sensors	[8]
PEDOT:PSS/ graphene	(25)	Strong resistance against fatigue upon repeated folding-unfolding	Spray coating	Data storage and transmission, biosensors and actuators	[10]
3D Graphene/ PEDOT:PSS	4.1×10^{-2}	Good resistance retention capability under deformations	Graphene networks coated by PEDOT:PSS	Next-generation stretchable electronics	[12]
CNT/PEDOT :PSS	3×10^{-3}	Good thermoelectric performance	Vacuum-assisted filtration method and H_2SO_4 treatment	Flexible thermoelectric generator	[13]

[1] The unit for the value of Ref. [37] is Ω.

4.2.3. Methods of Treating Textiles with PEDOT:PSS

PEDOT:PSS can be applied to textile materials by carrying out an in-situ polymerization of 3,4-ethylenedioxythiophene (EDOT) on the textile substrate in the presence of PPS or by applying the polymer PEDOT:PSS dispersion onto a textile substrate. In general, adding the polymer into a polymer solution during fiber spinning, coating/dyeing textile substrates (fibers, yarns, fabrics), and/or printing textile fabrics, can be used to produce PEDOT-based conductive textiles.

A. Conductive Fiber Spinning

In this technique, PEDOT:PSS is added to a conventional polymer solution during fiber wet spinning or electrospinning (Figure 4.3a) in order to produce a conductive fiber or filament, or the PEDOT:PSS alone can be spun into a fiber. In 2003, Okuzaki and Ishihara presented their first study on the manufacture of 4.6 to 16 μm PEDOT:PSS microfibers using a wet-spinning technique with an electrical conductivity of 0.1 S/cm [39]. The Young's modulus, tensile strength, and elongation at break for the resulting microfibers were 1.1 GPa, 17.2 MPa, and 4.3%, respectively. Jalili et al. reported a simplified wet-spinning process for continuous PEDOT:PSS fibers which showed a conductivity up to 223 S/cm by post-treatment of the fibers with ethylene glycol [40]. In another approach, they used an aqueous blend of PEDOT:PSS and poly(ethlylene glycol) and the conductivity of the fibers increased 30-fold (from 9 to 264 S/cm) without the need for a post-treatment. Okuzaki et al. developed PEDOT:PSS microfibers with a diameter of ca. 5 μm by wet-spinning [41]. They improved the electrical conductivity of the fibers from 74 S/cm to 467 S/cm by subsequent dip-treatment of the fibers in ethylene glycol. The mechanical properties of the microfibers were also improved by the dip-treatment; Young's modulus and tensile strength increased from 3.2 GPa and 94 MPa to 4.0 GPa and 130 MPa, respectively. Zhou et al. further enhanced the electrical conductivity of wet spun PEDOT:PSS microfibers to 2804 S/cm via wet-spinning followed by post-treatment with ethylene glycol and hot-drawing [42]. This high conductivity is due to the combined effects of the vertical hot-drawing process and doping/de-doping of the microfibers with ethylene glycol. Moreover, they had a semiconductor metal transition at 313 K with superior mechanical properties with Young's modulus up to 8.3 GPa, a tensile strength reaching 409.8 MPa, and a large elongation before failure (21%). J. Zhang et al. also carried out a wet spinning of PEDOT:PSS fiber and obtained better conductivity of PEDOT:PSS fiber, 3828 S/cm, by decreasing the fiber diameter using a fine gauge needle [43]. The wet-spinning set-up was modified as shown in Figure 4.3a. Liu et al. also reported composite conductive fibers based on PEDOT:PSS blended with polyacrylonitrile [44] by wet spinning.

Fibers with 1.83 wt% of PEDOT:PSS showed a conductivity of 5.0 S/cm. Seyedin et al. demonstrated a scaled-up fiber wet-spinning production of electrically conductive and highly stretchable PU/PEDOT:PSS fibers which were then used in knitting for a knee sleeve prototype with application in personal training and rehabilitation following injury [45]. The fiber showed a conductivity of 166 S/cm, very close to pristine PEDOT:PSS film with a wide strain sensing capability up to 260 % strain.

Jin et al. employed an electrospinning and in-situ synthesis process to fabricate silver nanoparticles coated PEDOT:PSS/PVA flexible self-supporting nanofibers with greatly improved electrical conductivity [46]. Q. Zhang et al. also used electrospinning to fabricate a PVA/PEDOT:PSS nanofiber with an average diameter of 68 nm for a gas sensor, shown in Figure 4.3b, [47].

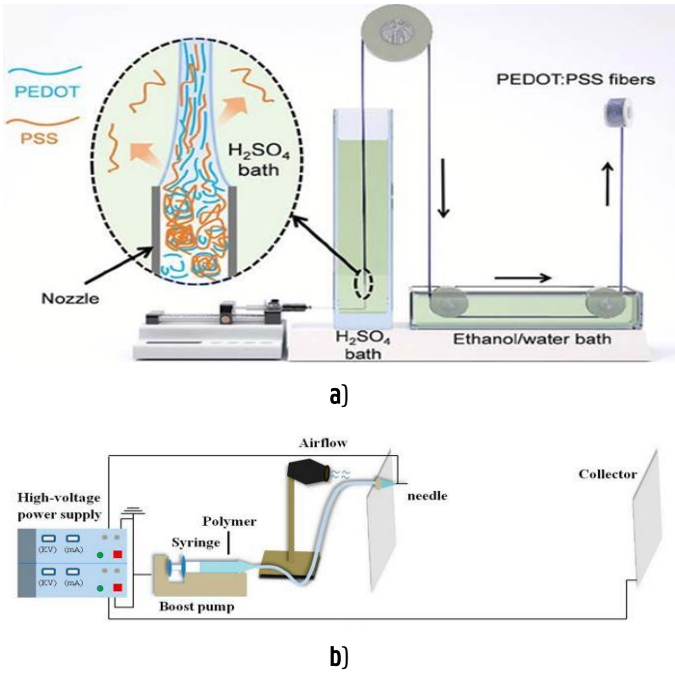

Figure 4.3: Fiber spinning process: **a**) schematic illustration of a modified set-up used in wet-spinning PEDOT:PSS fibers. Inset shows the schematic illustration of the alignment of PEDOT:PSS chains during fiber formation and the outward diffusion of excess PSS to H_2SO_4 coagulation bath. Adapted from[43]; **b**) schematic diagram of electrospinning setup; the distance between the needle and collector was 120 cm. Adapted from [47].

B. Polymerization of PEDOT on the Textile Substrate

The PEDOT monomer can be polymerized on the textile substrate (fiber, yarn, fabric, or garment form) in situ, by vapor phase or electrochemical polymerization by using EDOT and appropriate chemicals like oxidants [48]. This method combines polymerization of the PEDOT and coating of the textile.

The attachment of PEDOT on the fabric surface depends on the chemistry of the fiber as well as the surface roughness of the fiber. Though direct polymerization of PEDOT on the textile seems straightforward, it is difficult to control the parameters. Moreover, it is used only for a small sample size and is a challenge for industrial requirements. Hong et al. carried out five cycles of in-situ polymerization of PEDOT on poly(trimethylene terephthalate) fabrics in the presence of ferric p-toluenesulfonic acid and ferric chloride as oxidants followed by butane treatment and obtained an electrical conductivity of 3.6 S/cm [49]. Bashir et al. reported an electrically conductive polyester fabric with an electrical resistance of ˜2000 Ω, coated by PEDOT through oxidative vapor phase polymerization (VPP) in the presence of Fe (III) chloride hexahydrate oxidant [50]. They also obtained electro-conductive aramid, viscose, and nylon fabrics by the same approach. In another work, they produced a conductive viscose yarn with an electrical resistance of 6 kΩ by oxidative chemical vapor deposition, by removing the impurities like acetone and ethyl acetate, prior to the oxidant enrichment and polymerization steps [51]. Trindade et al. also coated a polyester fabric by PEDOT through VPP and obtained a lower sheet resistance of ˜20 Ω/sq by increasing the concentration of the oxidant, Fe (III) chloride hexahydrate [52]. L. Zhang et al. coated textile fabrics (silk, linen, wool, pineapple, bamboo rayon) by PEDOT through VPP and obtained a sheet resistance from 200 to 9.46 kΩ depending on the porosity of the fabric; porous fabric gives higher sheet resistance than tight-fabric [53]. Overall, the electrical and mechanical properties of conductive textiles are determined by the concentration of oxidants, pretreatment of the original pristine fabric and post-treatments of the conductive fabric, type and form of a textile substrate, and the polymerization conditions. An illustration of the vapor deposition system is shown in Figure 4.4.

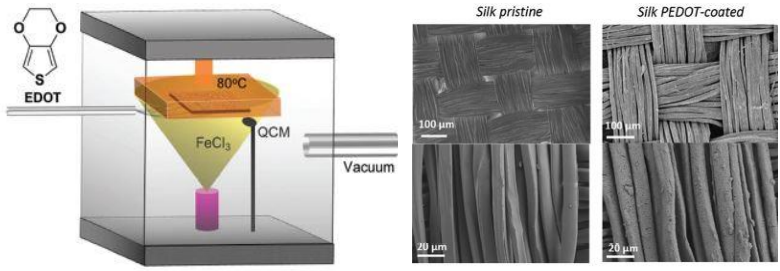

a) b)

Figure 4. 4: a) Schematic illustration of a vapor deposition system for PEDOT; **b**) SEM images of pristine silk textile and PEDOT-coated silk textile. Adapted from [53].

C. Dip-Coating/Dyeing of Textile with PEDOT:PSS

In the coating/dyeing method, the appropriate form of textile is treated by immersing/dipping it in PEDOT:PSS dispersion with appropriate auxiliary chemicals. This method mimics either the exhaust or continuous dyeing method of commercial textile processing. It is the most popular method practiced for making conductive textiles with PEDOT:PSS. The uniformity, as well as depth of dyeing/coating, depends on the functional group of the textile. Ding et al. treated cotton, cotton/polyester, polyester, and nylon/spandex fabrics by impregnating them with PEDOT:PSS and showed that conductivity is higher for fabrics that swell well in water [54]. Ryan et al. dyed up to 40 m long silk yarn with PEDOT:PSS with a conductivity of ~14 S/cm which was durable for machine washing [55]. The reason for the wash durability of PEDOT:PSS on silk is due to the dyeing effect and the use of a fluorosurfactant Zonyl FS-300 during dyeing. When cotton was dyed by the same method, it was too fragile due to hydrolysis of the cellulose by the strong acidic PEDOT:PSS. The same group further demonstrated a continuous dyeing process to produce more than 100 m of silk thread dyed with PEDOT:PSS for a wash and wear-resistant functional thread with a conductivity of about 70 S/cm [56]. Ding et al. produced PU fibrous nonwoven and treated it with PEDOT:PSS by dip-coating [38]. The PEDOT:PSS@PU nonwovens showed sheet resistance of 35–240 Ω/sq (electrical conductivity of 30–200 S/m) by varying the number of dip-coating times. This conductive nonwoven maintained its surface resistance up to 50% strain, promising for wearable application. Tadesse et al. also treated polyamide/lycra elastic fabric with PEDOT:PSS by dipping only once and showed a sheet resistance of ~ 1.7 Ω/sq [57]. The fabric was stretchable up to ~650% and maintained reasonable conductivity up to several washing cycles. The durability of washing, in this case, is also due to the dyeing effect where there is

some kind of chemical interaction between the fiber and PEDOT:PSS. A schematic representation of discontinuous and continuous PEDOT:PSS dip-coating/dyeing on a textile fabric is shown in Figure 4.5.

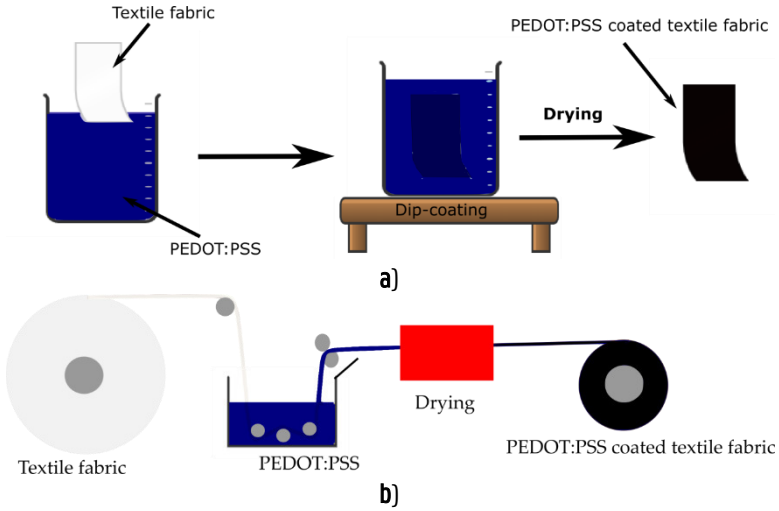

Figure 4.5: Schematic representation of the setup for dyeing: **a**) discontinuous process; **b**) continuous process.

D. Printing of PEDOT:PSS on Textile

Printing is a well-developed industrial textile processing method used to apply PEDOT:PSS to the textile structure in the presence of thickening agents to obtain an adequate paste or ink viscosity. Guo et al. demonstrated the fabrication of all-organic conductive wires by utilizing patterning techniques such as inkjet printing and sponge stencil to apply PEDOT:PSS onto a nonwoven polyethylene terephthalate (PET) providing a wide range of resistance, i.e., tens of kΩ/sq to less than 2 Ω/sq that allows the resistance to be tailored to a specific application [58]. Sinha et al. demonstrated the integration of screen-printed PEDOT:PSS electrocardiography (ECG) circuitry on finished textiles and recorded an ECG signal comparable to Ag/AgCl connected to copper wires [59]. Zhao et al. also used screen-printing to produce a PEDOT:PSS and a carbon-based disposable electrochemical sensor for sensitive and selective determination of carmine. The conductive textile fabric stays conductive until its infliction point of stretching. The schematic illustration of screen printing is shown in Figure 4.6.

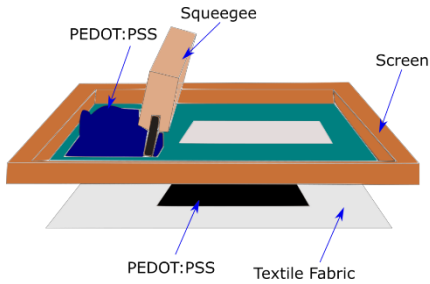

Figure 4.6: Schematic illustration of PEDOT:PSS screen printing on a textile fabric.

4.2.4. Applications of PEDOT:PSS-based Conductive Textiles

As outlined earlier, PEDOT:PSS has high electrical conductivity, thermal stability, decent biocompatibility, and is solution processable. These interesting properties make it attractive for different textile-based applications including sensors, energy harvesting, and storage devices.

A. Sensors

The demand for textile-based sensors is increasing because of their low weight, flexibility, and the possibility of washing. PEDOT:PSS-based textiles have been widely used as sensing components for strain, pH, humidity, biopotential, and temperature. Zahid et al. applied graphene nanoplatelets dispersed in PEDOT:PSS solutions for producing conductive, breathable, and lightweight mercerized cotton fabrics by spray coating which showed a highly repeatable and stable response to cyclic deformation tests at 5% and 10% strain rates for up to 1000 cycles with ˜90% viscoelastic recovery levels after cessation [10]. Kang reported a resistive memory graphene-PEDOT:PSS coated nylon thread with a strain response for wearable applications as an example of bio-potential sensors, shown in Figure 4.7, [60]. Seyedin et al. developed a strain sensor from PU/PEDOT:PSS fibers with a conductivity of 9.4 S/cm [45]. The resistance of this textile sensor stays stable up to 160% strain and up to 500 cycles. The high conductive textile-based hybrid showed high stability during stretching. Pani et al. developed a new textile ECG electrode based on woven fabrics treated with PEDOT:PSS for bio-potential recordings tested on humans, both in terms of skin contact impedance and quality of ECG signals recorded at rest and during physical activity [61]. The electrode was found to be capable of operating under both wet and dry conditions, which could be an important milestone in wearable monitoring of the heart. Ankhili et al. developed an ECG sensor electrode from a

PEDOT:PSS screen-printed cotton fabric and obtained clear ECG wave amplitudes up to 50 washing cycles [62]. The same group also produced washable screen-printed cotton textile electrodes with and without lycra of different PEDOT:PSS concentrations, providing a medical quality ECG signal to be used for long-term ECG measurements with a similar result to the silver-plated cotton fabric at 12.8 wt% of PEDOT:PSS to pure cotton [63]. Niijima et al. produced "hitoeCap" from PEDOT:PSS textile electrodes for securing electromyography of the masticating muscles [64].

Furthermore, Abbasi et al. worked on the use of PEDOT:PSS material for the implementation of high-sensitivity moisture sensor devices, which showed significant frequency shifts [65]. They demonstrated sensing capacity even for small moisture variations. Smith et al. developed a wearable pH sensor cotton yarn in PEDOT:PSS and multi-walled carbon nanotubes followed by PANI deposition that produced electrodes with significant biocompatibility and antibacterial properties that could be manufactured (alongside quasi-reference electrodes) into wearable solid-state pH sensors and achieved wearable pH sensors [66].

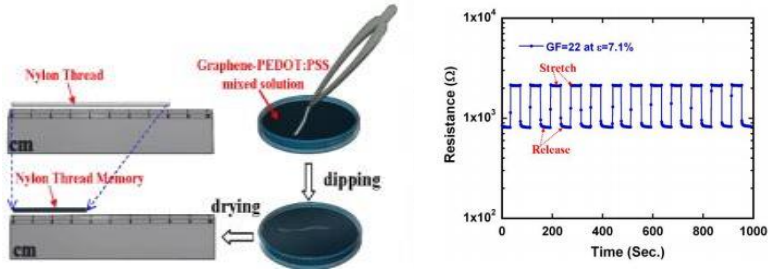

a) b)

Figure 4.7: A graphene-PEDOT:PSS coated nylon thread: **a**) schematic of the simple two-step dip-and-dry solution process for the fabrication (right) and the actual picture of the sample with the length reduction from 80 to 29.48 mm after dip-and-dry; **b**)resistive memory strain sensor thread at many stretch and release cycle under applied a fixed ε = 7.1%. Adopted from [60].

B. Energy Harvesting and Storage

Textiles coated with PEDOT:PSS have been used to manufacture flexible and lightweight energy harvesting and storage devices. This is quite an interesting way to provide power from wearable electronics to medical implantable devices. PEDOT:PSS is a promising organic thermoelectric material, a material that changes temperature difference into electricity or vice versa [36]. PEDOT:PSS-printed textiles have been studied for wearable thermoelectric applications to

harvest the temperature difference between the body and outer surroundings. Du et al. coated polyester fabric strips with PEDOT:PSS where the flexibility and air permeability were not affected [67]. The treated fabric showed electrical conductivity of ~1.5 S/cm and generated a thermoelectric voltage of 4.3 mV at a temperature difference of 75.2 K. Ryan et al. dyed silk yarn with PEDOT:PSS and made 26 thermoelectric legs by embroidering on felted wool fabric which showed a thermoelectric voltage output of ~351 μV/K [55]. This PEDOT:PSS-dyed silk yarns were stable to machine washing and up to a thousand bending cycles. Recently, Jia et al. coated textile with PEDOT via VPP which combined thermoelectric generation and strain sensing application [68]. Allison et al. used a vapor printing method on commercial cotton fabric to make all textile wearable bands that generated thermovoltages as high as 20 mV when worn on the hand, shown in Figure 4.8, [69].

Supercapacitors are alternative energy storage devices for fast charge-discharge applications. Textile-based supercapacitors have attracted attention due to their inherent flexibility and their potential use in wearable electronics. Nuramdhani et al. demonstrated that PEDOT:PSS sandwiched between two stainless steel conductive yarns showed capacitive behavior as an energy storage device [70]. Ma et al. reported flexible stainless steel/cotton blend yarn coated with PEDOT:PSS and PPy which can be up to 5000 cycles [71]. Yuan et al. reported fiber-shaped yarn supercapacitors by twisting wet spun PEDOT:PSS which showed a high areal capacitance of 119 mF/cm^2 [72]. Li et al. prepared flexible textile supercapacitors by spray coating graphene nanosheets and PEDOT:PSS which exhibited an enhanced specific areal capacitance of 245.5 mF/cm^2 [73]. Yuksel et al. reported cotton fabric coated with MnO_2/SWNT/PEDOT:PSS ternary nanocomposite supercapacitors that gave a specific capacitance up to 246 F/g and areal capacitance of 64.5 mF/cm^2 [74].

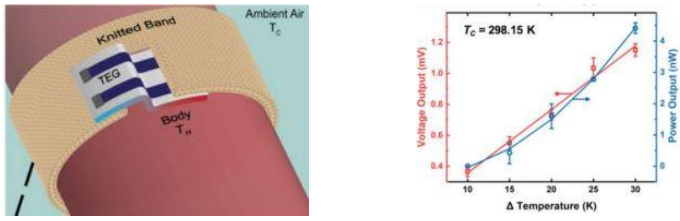

a) b)

Figure 4.8: a) Design schematic of a wearable thermoelectric generator; **b)** thermoelectric power and voltage outputs for a tobacco cotton thermopile at 25 °C. Adapted from [69].

C. Other Applications

There is a strong need for flexible and wearable actuators, organic light-emitting diodes (OLED), and antennas. The inherent properties of PEDOT:PSS makes it ideal to fabricate these devices on textiles. For instance, Li et al. developed a screen-printed textile patch antenna capable of operating at 2.4 GHz by using PEDOT:PSS as a patch and ground on polyester fabric [75]. The antenna is flexible and breathable which makes it well-fit for wearable applications.

Actuation is another application area of smart textiles. Miura et al. developed a foldable PEDOT:PSS/PVA fiber by wet spinning that exhibits a table contraction motion in the air by applying alternating square-wave voltages between 0 and 8 V [76]. Verboven et al. reported an OLED with maintained textile properties by screen printing of silver as a bottom electrode, barium titanate as a dielectric, copper-dopped zinc-oxide as an active layer, and PEDOT:PSS as a top electrode on polyester fabric that requires 3–5 V power supply [77]. The thickness of the OLED on the textile fabric was only 0.5 µm which is a good platform for wearable applications; the schematic illustration and actual OLED are shown in Figure 4.9.

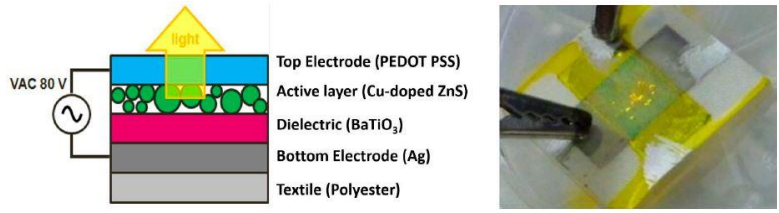

a) **b**)

Figure 4.9: a) Build-up of the alternating current powder electroluminescence technology; **b**) OLED stack printed on textile. Adapted from [77].

4.3. Experiment

The purpose of this experiment was to develop a PEDOT:PSS/PDMS conductive polymer composite and print it on knitted cotton fabric. The conductive fabric was then used to demonstrate a proof of concept for strain, moisture, and ECG sensing.

4.3.1. Materials

The conductive textile fabric produced consists of two parts: a water-repellent textile substrate and an electro-conductive polymer composite. A weft knitted

cotton fabric (S0) with 140 GSM and 0.5 mm thickness obtained from UGent, MaTCh laboratory was used as the textile fabric. Nano Spray water repellent (WR) for textiles obtained from Lab@Home, Netherlands was utilized. PEDOT:PSS PH1000 Clevious conductive polymer obtained from Ossila Ltd.(Sheffield, UK) and poly(dimethylsiloxane-b-ethylene oxide) methyl terminated (PDMS-b-EO) obtained from Polyscience, Inc. (Warrington, UK) were used to produce the conductive polymer composite. The sheet resistance of each conductive polymer composite (PEDOT:PSS/PDMS) screen-printed fabric with different dimensions (sample sizes) was measured by the two point-method.

4.3.2. Fabric Water Repellency Pre-Treatment

Before applying the PEDOT:PSS/PDMS conductive polymer composite (CPC), the fabric was pre-treated with WR to impart a hydrophobic effect on the fabric surface, and therefore prevent absorption of CPC into the fabric structure giving a confined CPC distribution within the required area. 3% owf (own weight of fabric) WR was gently sprayed on the fabric surface and then dried at 80°C for 3 min. A drop test with water and PEDOT:PSS performed on the fabric showed an effective hydrophobicity as shown in Figure 4.10.

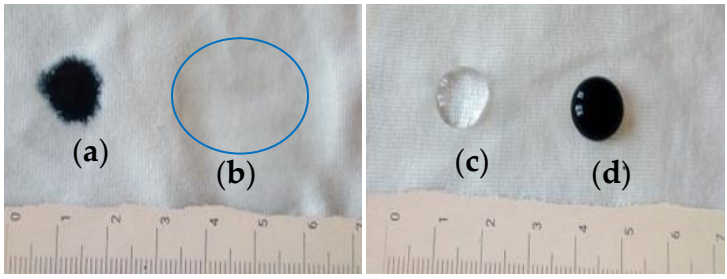

Figure 4.10: Effect of WR treatment on knitted cotton fabric: **a**) PEDOT:PSS polymer dispersion on untreated fabric (S0); **b**) drops of water on untreated fabric (S0); **c**) drops of water on water repellent (WR)-treated fabric (S1); **d**) PEDOT:PSS polymer dispersion on water repellent (WR)-treated fabric.

4.3.3. Flat Screen Printing

Flat-screen printing was preferred for this work because attaining the required conductive polymer composite paste viscosity and transferring it to the substrate by this technique is straightforward. Another possible technique that could be explored is transfer printing [78], while also designs mechanics via

transfer printing may provide another effective route toward stretchable conductive fabric [79].

Different amounts of PDMS (0.1 to 0.9 of PDMS to PEDOT:PSS ratio) were manually mixed with a fixed amount of PEDOT:PSS (4 mL) for 3 minutes at room temperature. A mixing rod was used to prepare a homogenous blend of the two polymers. It was observed that stirring of the polymers showed a shearing property, the mixture solution was converted into a thicker paste which is convenient for screen printing. As a result, the thickening agent present in conventional screen printing was not employed. Then the paste was applied to the surface of WR-treated cotton fabric (S1) via flat screen printing. Gentle agitation of the PEDOT:PSS and PDMS mix formed a thick paste and then the paste was simply swept over the flat screen mesh by a mini squeegee to improve the distribution. The overall printing process for this work is schematically represented in Figure 4.11.

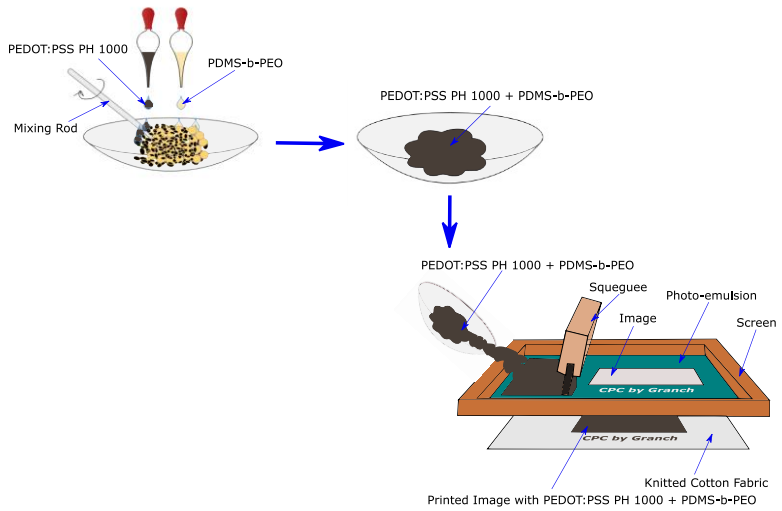

Figure 4.11: Screen printing of conductive polymer composite on knitted cotton fabric.

After the printing process, drying was performed in an oven at 70°C for 5 min and cured at 150°C for 5 min. The printed samples were thoroughly washed with distilled water. An example of the actual conductive knitted fabric produced is shown in Figure 4.12.

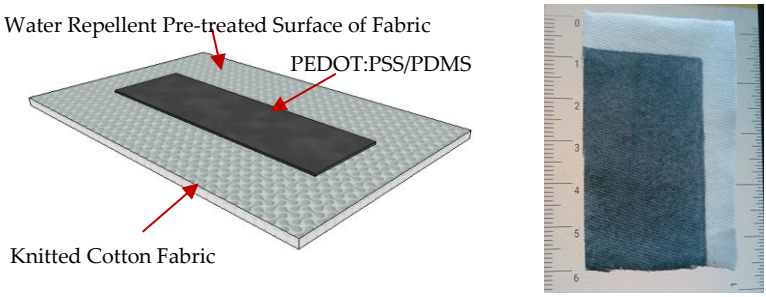

a) **b)**

Figure 4.12: a) Schematic design of the conductive textile fabric; **b**)actual conductive textile fabric.

To study the effect of PDMS on surface resistance, ten different ratios of PDMS to PEDOT:PSS as shown in Table 4.2 were prepared and applied on the previously WR-treated knitted fabric via screen printing over an area of 62.5 cm^2 (12.5 cm × 5 cm). The solid add-ons of the PEDOT:PSS/PDMS conductive polymer composite on the textile fabric were calculated using Equation (4.1).

$$w = (W_a - W_b)/A, \quad (4.1)$$

where, W_a = weight of fabric after printing in g and W_b = weight of fabric before printing in g, A = coated surface area in cm^2, and w = solid add-on per coated surface area (A) in g/cm^2.

The respective solid add-ons (w) for each percentage volume mix ratio of PDMS to PEDOT:PSS are provided in Table 4.3. The percentage volume mix ratio was calculated using Equation (4.2).

$$r = (V_e/V_c) \times 100, \quad (4.2)$$

where, V_e = volume of PDMS in mL, V_c = volume of PEDOT:PSS in mL, and r = percentage volume mix ratio of PDMS to PEDOT:PSS in %.

Table 4.2: Mix ratios of the conductive polymer composite and weight before printing.

Sample	The ratio of PDMS to PEDOT:PSS (V_e/V_c) [%]	Volume of PEDOT:PSS (V_c) [mL]	Volume of PDMS (V_e) [mL]	Weight of fabric before printing (W_b) [g]	Area (A) [cm^2]
r00	0	4	0	1.655	5×12.5
r10	10	4	0.4	1.653	5×12.5
r20	20	4	0.8	1.629	5×12.5
r30	30	4	1.2	1.608	5×12.5
r40	40	4	1.6	1.578	5×12.5
r50	50	4	2	1.645	5×12.5
r60	60	4	2.4	1.678	5×12.5
r70	70	4	2.8	1.661	5×12.5
r80	80	4	3.2	1.622	5×12.5
r90	90	4	3.6	1.628	5×12.5

4.3.4. Mechanical Characterization

Thickness: The thickness was determined using ISO 5084:1996(E) (determination of the thickness of textile and textile products) using "Mitutoyo Digimatic Indicator".

Bending Analysis: The bending length was measured according to the test method BS 3356:1990 using a bending meter. Using the appropriate mean value, we calculated the flexural rigidity G, in mg cm, separately for the warp and weft directions by Equation (4.3).

$$G = 0.1\ M\ C^3, \qquad (4.3)$$

where, G = flexural rigidity (mg cm), C = bending length (cm), M= mass/area of the specimen (g/m^2).

Tensile Strength and Elongation at Break: The strength and elongation at break were tested using INSTRON universal strength tester. A tensile test according to ISO 13934-1 was used.

SEM analysis of CPC: The surface topology, cracks, holes, and appearance of yarns within the fabric before and after coatings were studied using FEI Quanta 200

FFE-SEM. Images were taken with an accelerating voltage of 20 kV. The non-conductive samples were prepared prior to analysis by applying a gold coating using Balzers Union SKD 030 sputter coater.

4.3.5. Electrical Characterization

The sheet resistance of all samples was measured by using the two-point method. The samples were placed in a 3-7/8" MaxSteel Light Duty Drill Vise 83070 Stanley Hand Tool on both ends to make them stable for measurement as presented in Figure 4.5. The effect of stretching on sheet resistance has been studied from 0 to 35% elongation. The effect of repeated stretching on the sheet resistance has been studied by stretching the samples to their infliction point within five seconds, releasing them from a stretch, and measuring the sheet resistance after 5 seconds. The stretching and releasing have been continued until the sheet resistance reached an infinite value. The surface electrical resistances for all measurements were calculated using equation (4.4).

$$R = R_M \times L/D \qquad (4.4)$$

Where R is the surface resistance (Ω/sq), R_M is the measured resistance (Ω). L is the length of the voltage electrodes (cm) and D is the distance between voltage electrodes (cm) as shown in Figure 4.13 (a).

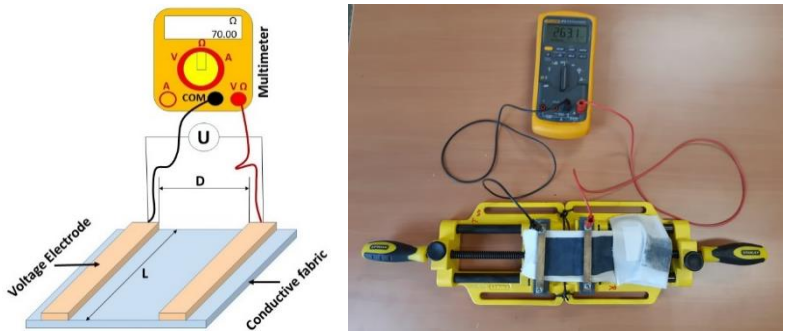

a) b)

Figure 4.13: Two-point method resistance measurements set up: **a**) Schematic illustration; **b**) actual measurement

In addition, we constructed a 2.5 cm × 5 cm strain and moisture electrode from sample r60 as a demonstrator. We also developed a PEDOT:PSS/PDMS (4:1) coated cotton fabric with a 332.5 Ω/sq sheet resistance by increasing the add-on to 0.013

g/cm^2 and tested the performance of the fabric as an electrode for use in electrocardiography (ECG) and electroencephalography (EEG).

To study the sensing stability of the conductive polymer composite-treated fabric an Arduino Nano set-up for this particular purpose with the circuitry as shown in Figure 4.14 was used. One end of the PEDOT:PSS/PDMS CPC-treated fabric was connected to 5V of Arduino Nano input and the other was connected to a 1 MΩ pull-down resistor and analog-to-digital converter (ADC) input. An IDE program suitable for reading out dynamically the resistance of the CPC was written. Then, the percentage change in resistance at its respective change in elongation from 0 to 35% was calculated using Equation (4.5).

$$\Delta R = 100 \times (R_f - R_i)/R_i, \qquad (4.5)$$

where, ΔR = percentage change in linear resistance (%), R_i = initial linear resistance (kΩ), R_f = final linear resistance (kΩ).

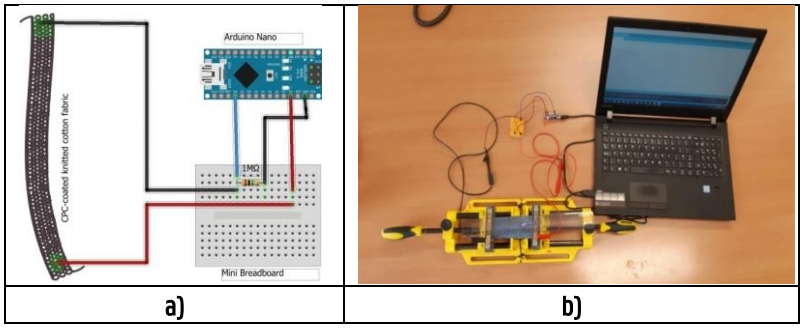

Figure 4.14: a) Arduino Nano electronic circuitry design; **b**) resistance measurements set-up.

In addition, the effect of washing on the surface resistance was measured. PEDOT:PSS/PDMS-printed knitted cotton fabric specimens of 4×4cm were sandwiched between the cotton fabric and polyester fabric and then sewn along all four sides to form a composite specimen. This was done to protect the sample, and because it could be a practical way of using the sample as a sensor. The washing solution containing 5 g/l soap was taken into the launder-o-meter with a liquor ratio of 1:40. The specimen was treated for 30 min at 30°C at a speed of 40 revolutions per minute. The specimen was removed and rinsed in cold water. The stitch was opened on three sides and dried in shadow. The surface resistance after washing was measured using a multi-meter and the two-point method. Finally, the percentage change in surface resistance was calculated using Equation (4.5).

4.4. Result and Discussion

4.4.1. Solid Add-on

The solid add-on (w) of the conductive polymer composite on the knitted cotton fabric obviously increased with the increase in the amount of PDMS percentage mix ratio as presented in Table 4.3. This increase in add-on due to the increase in the amount of PDMS may raise the sheet resistance as the conductive component could probably be trapped inside the PDMS elastomer.

Table 4.3: The solid add-on (w) of printed samples.

Sample	Volume of PEDOT:PSS [mL]	Volume of PDMS [mL]	Weight of fabric [g]		Area [cm2]	Weight add-on [g/cm2]
			before printing	after printing		
r00	4	0	1.655	1.913	5×12.5	0.0041
r10	4	0.4	1.653	2.142	5×12.5	0.0078
r20	4	0.8	1.629	2.344	5×12.5	0.0114
r30	4	1.2	1.608	2.401	5×12.5	0.0127
r40	4	1.6	1.578	2.462	5×12.5	0.0141
r50	4	2	1.645	2.44	5×12.5	0.0144
r60	4	2.4	1.678	2.646	5×12.5	0.0155
r70	4	2.8	1.661	2.671	5×12.5	0.0162
r80	4	3.2	1.622	2.688	5×12.5	0.0171
r90	4	3.6	1.628	2.733	5×12.5	0.0177

4.4.2. Thickness Analysis

From Figure 4.15, the thickness of the fabric increased by 0.03 mm when water repellent was applied. After the conductive polymer composite has been applied, the thickness has moreover increased by ≤ 0.14 mm until a percentage mix ratio of 60% and continues with a thickness equal to the sample r60 until the mix ratio is 90% (sample r90). This shows that the presence of PDMS has less effect on the thickness than when PEDOT:PSS alone (sample r00) was utilized. This could have a positive contribution to the flexibility of the fabric.

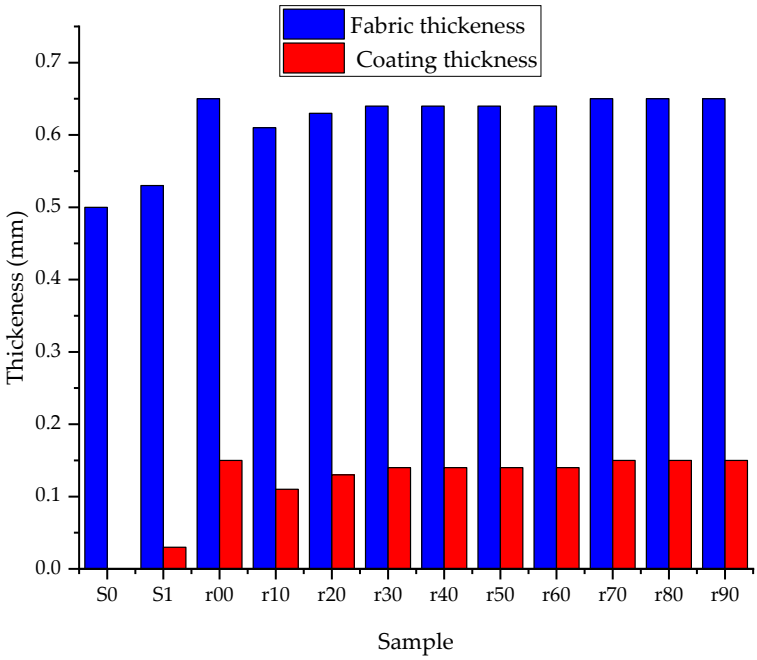

Figure 4. 15: Effect of PEDOT:PSS/PDMS on thickness. S0 the base fabric, S1 with WR coating, and r00 to r90 the different add-ons

4.4.3. Bending Length Analysis

In Table 4.4, we presented the measured values of bending length and respective calculated flexural rigidity according to Equation (3). The fabric became stiffer when treated with a water-repelling agent, as evidenced by an increase in bending length of 29%. The fabric became again stiffer when the CPC was applied, with double the bending length of the r00 sample over the S0 sample (base cotton fabric). Moreover, this increase in bending length was more intensive when PEDOT: PSS alone was used, reducing again as the PDMS content became more pronounced. For instance, the bending length of the PEDOT:PSS-printed fabric decreased on average by 11% when r was 50% (sample r50) and the flexural rigidity reduced by 13%.

Table 4.4: Bending length and flexural rigidity results.

Fabric	Weight (g/m²)	Bending Length (cm)					Flexural Rigidity (mg cm)				
		Wale direction		Course direction		Avg	Wale direction		Course direction		Avg
		[2]F	[3]B	F	B		F	B	F	B	
S0	140.0	1.3	1.2	1.3	1.7	1.4	27	24	27	71	35
S1	146.0	1.8	1.7	1.7	1.9	1.8	78	66	72	100	78
r00	176.0	3.0	2.9	2.9	2.5	2.8	475	407	407	26	382
r10	191.0	2.9	2.8	2.8	2.4	2.7	456	397	428	248	376
r20	199.0	2.9	2.7	2.7	2.3	2.7	461	396	409	245	371
r30	205.0	2.8	2.7	2.7	2.2	2.6	455	395	408	230	365
r40	209.0	2.8	2.7	2.6	2.2	2.6	454	389	372	220	351
r50	213.0	2.7	2.6	2.6	2.1	2.5	433	383	353	200	334
r60	216.0	2.7	2.6	2.5	2.1	2.5	416	371	342	192	322
r70	221.0	2.6	2.5	2.5	2.0	2.4	393	344	341	180	307
r80	224.0	2.5	2.5	2.5	1.9	2.3	363	338	334	154	287
r90	228.0	2.5	2.5	2.4	1.9	2.3	356	335	315	149	279
[2]Face [3]Back											

4.4.4. Tensile Strength

From the load-elongation curve in Figure 4.16, we obtained that both the tensile strength and strain at the break of the fabric reduced from 72.2 to 68.1 N and 115.3 to 112.3% because of the water repellent treatment. This could be due to the effect of the water repellent that might cause a very slight degradation during drying and curing but is overall a minor influence on the textile properties.

The application of only PEDOT:PSS (r00) increased the tensile strength in line with a stiffer fabric as found in the bending testing, but the strain was greatly decreased. This indicates that the PEDOT:PSS on the surface adds to the strength of the fabric making it stiffer, but reduces the stretch. The addition of PDMS to the fabric gives again higher tensile strength and allows again higher strain. Further increase of PDMS ratio has little influence on the strength but does further increase the strain. For instance, a shift of tensile strength from 78.2 to 115.8 N and a strain of 69.7 to 77 % at break was observed when r shifts from 0% to 50%. In general, the tensile strength becomes constant at around 118 N. Therefore, it is rational to say the new conductive polymer composite gives a smaller Young's modulus which is important for e-textile applications.

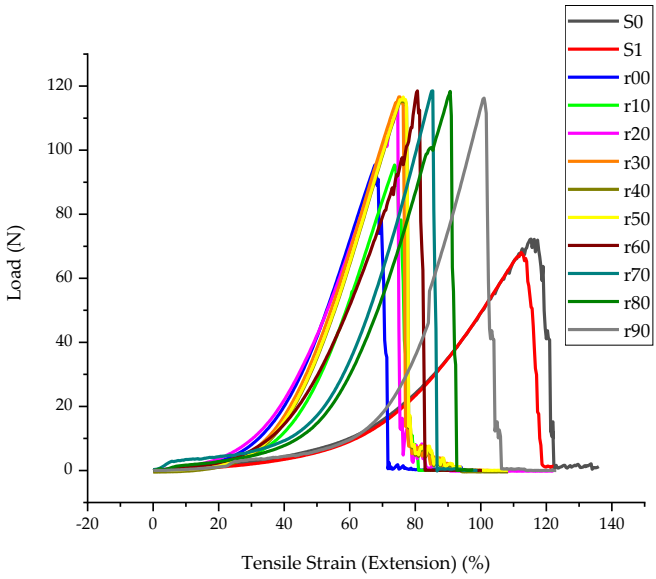

Figure 4.16: Load-elongation curve.

4.4.5. SEM Characteristics of the Conductive Polymer Composite

The SEM results (Figure 4.17) showed that the yarn loop interstices in the fabric were covered by the addition of PEDOT:PSS/PDMS conductive polymer composite. Protruding loops were also observed in the base fabric but not after the screen printing. As a result, printed fabrics are smoother than uncoated fabrics. The presence of PDMS further improved the smoothness and the coverage of the yarn loop interstices. The surface of the PEDOT:PSS-printed fabric looks more glassy when PDMS was added.

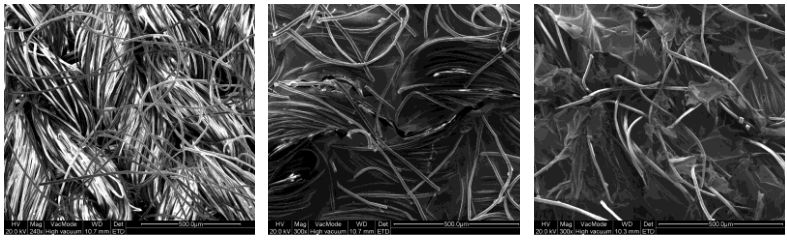

a) **b)** **c)**

Figure 4.17: SEM: **a**) WR treated; **b**) PEDOT:PSS-printed r00; **c**) PEDOT:PSS-PDMS-printed r60.

4.4.6. Effect of PDMS to PEDOT:PSS Ratio on Resistance

For all the samples, the resistance increases with an increase in the surface area when the length was increased by keeping the width constant. Therefore, it is obvious that resistance linearly increases with the increasing concentration of the non-conductive polymer and the surface area as shown in Figure 4.18.

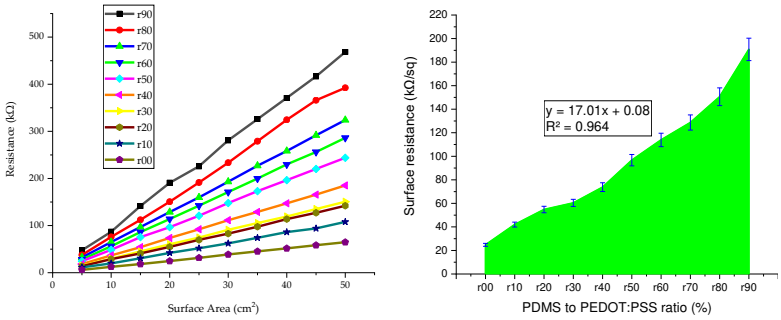

a) b)

Figure 4.18: Effect of PDMS concentration on resistance: **a**) effect of PEDOT:PSS to PDMS ratio on the resistance at the different surface areas, width kept constant; **b**)effect of PDMS on surface resistance.

In all the samples with five replicas, it was observed that the reproducibility was fairly good but still needs improvement. This could arise from the homogeneity of the polymer blend, uneven distribution of the conductive polymer composite during screen printing, and the uneven property of the textile fabric at its different portions.

The surface resistance increased from 24.8 kΩ/sq to 196.7 kΩ/sq as the PDMS to PEDOT:PSS ratio increased from 0 to 90% (Figure 4.18b). Thus, the ratio determines the application area, as each requires a specific surface resistance value. When high resistance is required, one can select a higher concentration of PDMS, and when lower resistance is required a lower ratio. Instead of the high resistance values obtained in this paper, one can also obtain lower resistance as mentioned in the case of an add-on of 0.013 g/cm^2, where we obtained 300 Ω/sq on the same fabric. Further increasing the add-on (71.4%) and optimizing the ratio of PDMS to PEDOT:PSS (1:4, so r=25%) dropped the surface resistance to 67.03 Ω/sq. The thickness of the conductive component over the fabric surface would also lower the resistivity. Therefore, layer-by-layer printing could also be followed when much lower resistivity is required.

4.4.7. Effect of Stretching on Sensing Stability

Figure 4.19 (a) shows that the stretching of the PEDOT:PSS/PDMS has a complex effect on the surface resistance in all samples for up to 35% elongation. In all cases, the resistance increased over 0% elongation. This could be due to a decrease in the density of conductive components during the stretch. It was observed that the change in resistance due to stretching increases at the beginning of stretching and then decreases with an increasing amount of PDMS, with the inflection point depending on the ratio r. Whereas, when r is zero (sample r00), the percentage change in resistance increases with stretching. Moreover, the change in resistance is smaller when PDMS was employed. For instance, the change in resistance of sample r00 was 0.74% which is smaller than sample r60 i.e., 16% when the change in elongation was 5%. But, when the change in elongation reached 35%, the change in resistance of r60 i.e., 4%, was smaller than that of r00 i.e., 131%. In addition, increasing the ratio of PDMS to PEDOT:PSS showed a better surface resistance recovery after stretching and better stability when re-stretched up to eight cycles. The surface resistance of sample r00 reached an infinite value at three cycles. Whereas, the most stable sample, sample r90, stayed conductive up to eight stretching cycles to its infliction point. The surface resistance of the samples after recovering from each stretch and 5 s rest is shown in Figure 4.19b. Though the sensing stability is not bad, it needs further improvement. A specific sample with PDMS can only be used to sense stretch up to the infliction point of that sample, as afterward the strain to resistivity change is unstable. Further refinement in the way of making the composite or coating technique may solve this problem.

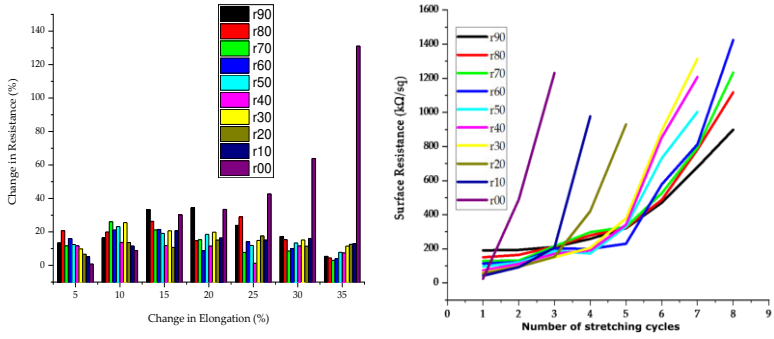

a) b)

Figure 4.19: Effect of stretching on surface resistance and sensing stability: a) Change in resistance due to stretching; **b**) surface resistance at different stretching cycles after recovering 5s from the stretch op to the infliction point.

4.4.8. Effect of Washing on Surface Resistance

Figure 4.20 shows that the resistance increased after a single wash. But, the increase in surface resistance due to washing decreased from ~ 470% to ~ 30% with an increasing r ratio from 0 to 90. Thus, the washing fastness improved with the increase in the amount of PDMS. This property of the fabric with CPC should be improved further if it is going to be used for frequently washed products.

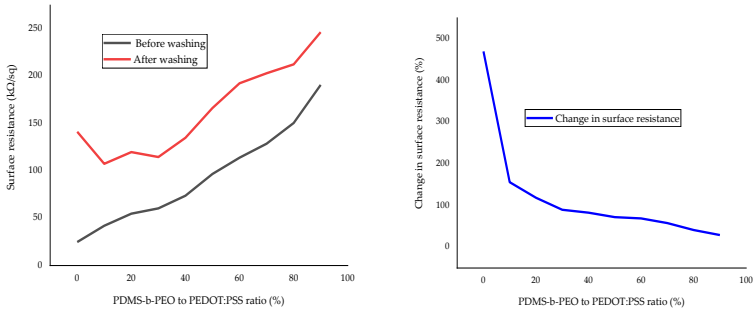

a) b)

Figure 4.20: Effect of washing on the surface resistance at different PDMS to PEDOT:PSS ratios: **a**) surface resistance before and after washing; **b**) percentage change in surface resistance due to washing.

4.5. Proof of Concept

As the obtained resistance covers a big range from 67.03 Ω/sq to 96.7 kΩ/sq depending on the concentration of PDMS and the surface area of the treated fabric, it can be used as a textile-based electrode for different sensors such as strain, moisture, biopotential (EEG, ECG), interconnection, energy storage, and other applications. For instance, the strain sensor demonstration of sample r60 showed a linear increase in resistance during the stretch to its infliction point and detected moisture change. Moreover, the ECG and EEG electrodes constructed from the PEDOT:PSS/PDMS (4:1) coated cotton fabric (332.5 Ω) at an add-on of 0.013g/cm^2, showed good qualities of collected ECG and EEG waveforms. The strain, moisture, and ECG, responses from a PEDOT:PSS/PDMS-printed cotton fabric electrodes are discussed below. An EEG response from a PEDOT:PSS/PDMS-printed cotton fabric (67.03 Ω/sq) is also covered in-depth in Chapter 5.

4.5.1. Strain and Moisture Sensors

Textile articles have attained all-embracing demand to construct flex, stretchy, and washable hardware in different domains. However, how a conductive polymer can be applied to conventional textiles without or with limited effect on their bulk properties to be utilized for a sensing function is still under investigation. For example, a textile-based strain sensor based on poly(3,4-ethylene dioxythiophene) polystyrene sulfonate (PEDOT:PSS) was reported by Zein et al. [80]. A dispersion solution of PEDOT:PSS was applied to low-density polyethylene (LDPE) to produce a conductive LDPE that showed an electromechanical response during the stretch. However, LDPE is highly hydrophobic and is not recommended for wearable applications. In addition, in that work, silicon was used as an agent, which has bio-compatibility issues. Here, we used a biocompatible elastomer instead of silicon, as well as a soft knitted cotton fabric, which makes it suitable for wearable applications.

A PEDOT: PSS-based humidity sensor was also reported at the IEEE International Symposium on Antennas and Propagation and USNC/URSI National Radio Science Meeting [81]. The humidity sensor was incorporated in a patch antenna, which means that the substrate was thick and heavy in weight. Furthermore, only PEDOT:PSS was used; therefore, the flexibility was compromised as seen also by the results given in the previous sections. Being lightweight and flexible are among the prime interests of e-textiles. By using a conventional knitted fabric with good extensibility and moisture absorption, the application area of the sensor is wider, even though the technique should also work on other textile substrates.

This type of sensor could have a typical use as humidity, sweat, stretch, swell, relaxation, and contraction detection in biomedical and sports applications. The dependence of the electrical resistance on strain and moisture allows the PEDOT:PSS/PDMS-printed cotton fabric to be used as a strain sensor. This was the case, and surface resistance of the conductive fabric r60, randomly selected, increased from 60.2 kΩ/sq to 400 kΩ/sq at 40% elongation and dropped to 29.98 kΩ/sq at 100% moisture regain.

A 2 × 5 cm^2 PEDOT:PSS/PDMS-printed textile-based electrode was constructed to test the dynamic response during stretching and moisture spreading. A stainless steel yarn and metal snap button were used as an interconnection between the textile-based electrode and an Arduino micro-controller, as it has neglectable resistance change with moisture regain and stretch. A resistance detection setup

with the circuitry was established to test the strain and moisture detection separately. One end of the PEDOT:PSS/PDMS coated fabric was connected to 5V of Arduino input and the other was connected in series to a 220 kΩ pull-down resistor, with the midpoint connected to the analog-to-digital converter of the Arduino. A schematic view of the established electrical circuitry setup is shown in Figure 4.3a. For the dynamic tests, the electrode was subjected to a continuous stretching from 0 to 40% elongation at 0.67 cm/s using a 3-7/8" MaxSteel Light Duty Drill Vise 83070 Stanley Hand Tool to study the stretch sense, while water was spread over the electrode surface at 1 mL/s using the bottle of Nano sprayer to study the moisture sensing. The data was transferred from the controller to data storage using the HC05 Bluetooth Module to make the setup portable. A 6V battery was used to power the portable setup. The photographic pictures of the actual stretch and moisture sensing dynamic test using Arduino Nano are shown in Figures 4.21b and c, respectively.

a) b) c)

Figure 4.21: Dynamic tests: **a**) electrical circuitry establishment setup; **b**) stretch; **c**) moisture.

The strain sensitivity of the coated fabric was found to be reasonably stable with an increase from 0.61 kΩ to 8.26 kΩ towards 40% elongation at 0.67 cm/s constant rates of stretching dynamic response. A graph of the effect of the dynamic stretching on surface resistance is shown in Figure 4.22a. The moisture regaining sensitivity of the coated fabric was also reasonably stable showing a drop in the resistance from 0.62 kΩ to 0.46 kΩ when the moisture regains reached 150% at 1 mL/s rate of water spray. A graph of the effect of dynamic moisture regaining on-resistance is shown in Figure 4.22b. In both the testing, the difference in percentage change of resistance response to strain (Figure 4.22c, 0.0488 *f*-ratio, and 0.828 *p*-values) and moisture (Figure 4.22d, 0.0583 *f*-ratio, and 0.456 *p*-values) before and after washing was statistically insignificant based on one-way ANOVA at a 95% confidence level.

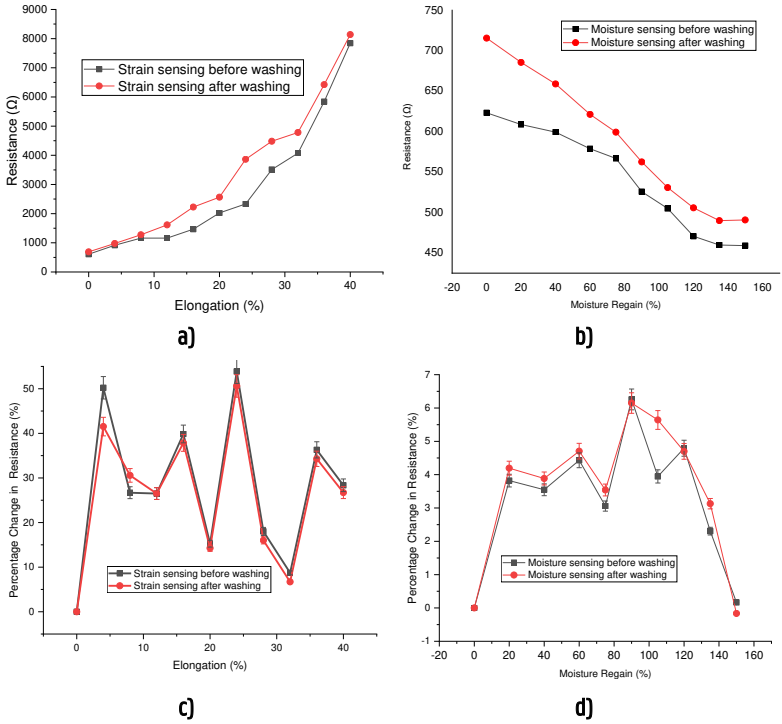

Figure 4.22: Dynamic responses in sheet resistance: **a**) Stretching; **b**) moisture regaining; **c**) percentage change of sheet resistance response to strain; **d**) percentage change of sheet resistance response to moisture

These principles could be applied in medical applications, for instance, to determine the status of peripheral edema, where the increase in resistance indicates that edema is becoming severe, in sports applications, to detect the extent of sweat and positional movement of bicyclists, and at home, to sense urination of babies and elders, etc. Furthermore, the conductive fabric can be used for other wearable applications which need to be lightweight and flexible, and where washing is unavoidable.

4.5.2. ECG Electrode

ECG is one of the most widely used health diagnostic techniques that provide useful information on the activity of the heart. Conventional ECG electrodes are developed from Ag/AgCl. However, Ag/AgCl standard electrodes need a gel to reduce the skin-to-electrode impedance mismatch [82]. The gels could cause skin irritation [83] and get dried out over time [84]. On the other hand, though

metallic discs and dry ECG electrodes have been recently introduced [85], they have a rigid structure and are heavyweight. Thus, gel-dependent and metallic disc dry electrodes are not suitable for wearable systems especially when long-term monitoring is required.

A. Achilli et al. 2017 developed a textile-based ECG electrode from PEDOT:PSS via screen printing [86]. They reported that signals collected with a saline solution and a solid hydrogel were comparable to Ag/AgCl electrodes. However, they did not study the effect of bending and reusing cycles on ECG signal acquisition. R. Castrillón et al. 2018 constructed ECG electrodes from cotton, cotton-polyester, lycra, and polyester woven fabric coated with PEDOT:PSS [87]. They reported that the PEDOT:PSS treated materials did not show a significant difference in acquiring ECG signals even though lycra-based and cotton-polyester electrodes exhibit better conductivity. Moreover, the findings in both A. Achilli et al. 2017 and R. Castrillón et al. 2018 revealed only the signal quality against the standard electrode. But no evidence was reported indicating if the textile materials retained their textile texture. The solid add-on, coating thickness flexibility, and weight of the PEDOT:PSS-printed textile materials have not been evaluated. Moreover, they have not used PDMS along PEDOT:PSS which could impart necessary flexibility.

This proof of concept aimed to explore a homemade textile-based ECG electrode comparable to standard electrodes from a PEDOT:PSS/PDMS conductive polymer composite coated knitted cotton fabric. Conductive fabric with 25% PDMS to PEDOT:PSS ratio and higher add-on, 0.008 g/cm^2, was produced as the previously produced conductive fabrics possess high electrical resistance which is not suitable for ECG electrodes.

The average surface resistance and resistivity of five PEDOT:PSS/PDMS-printed knitted cotton fabrics used in this proof of concept were measured using a four-probe method MR-1 Surface Measurement Instrument. The results were 332.5 ± 1.386 (±0.42%) Ω/sq and 6.6 ± 0.334 (±5.06%) Ω cm, respectively at 95% confidence interval. Three 2.5x4.5 cm^2 each PEDOT:PSS/PDMS-printed textile-based ECG electrodes were constructed. The schematic view and actual image of the electrode are shown in Figures 4.23a and 4.23b, respectively.

The active electrodes were placed one on the right wrist and the other on the left wrist. The third reference electrode was placed on the left arm 10 cm away from the active electrode. A schematic view and an actual image of the electrode

placement are shown in Figures 4.23c and 4.23d, respectively. An elastic bandage was used to keep the electrodes from sliding and to get better tight-fitting.

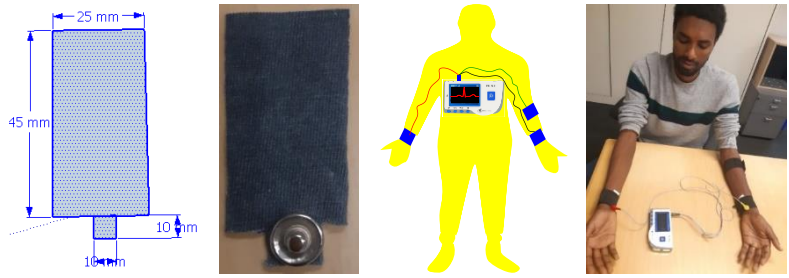

a) b) c) d)

Figure 4.23: a) schematic illustration PEDOT:PSS/PDMS-printed cotton; **b**) actual ECG electrode; **c**) ECG electrode placement; **d**) the actual ECG measurement on human

In a 3-minute static ECG measurement using PC-80B Easy ECG Monitor, 0.14, 0.96, and 0.36 mV average peak amplitudes for P, QRS, and T ECG complex were found, respectively. All have been collected with the PEDOT:PSS/PDMS-printed cotton electrode (Figure 24a). These are comparable with the peaks collected from a standard electrode which were 0.15, 0.98 and 0.48 mV for P, QRS, and T, respectively (Figure 24b). Based on a One-way ANOVA test of QRS at a 95% confidence level, the *f*-ratio value was 3.38 and the *p*-value was 0.07 which shows the difference is not significant at a 95% confidence level. The signal quality of the waveform was also comparable with the standard. The ECG waveforms of PEDOT:PSS/PDMS-based and standard electrodes are shown in Figure 4.24.

The ECG electrodes also gave reliable ECG signals for up to 120 hours while staying in an open-air environment without a significant difference, giving an *f*-ratio value of 1.312 and *p*-value of 0.26 based on a One-way ANOVA at a 95% confidence level. Therefore, the electrode could be continuously used for up to 120 hours which makes it better than the electrodes reported by R. Castrillón et al. 2018, which presented a PEDOT:PSS-printed textile electrode functional after 36 hours of continued use [87]. The improvement could be due to the presence of PDMS in this work. Thus, this type of ECG electrode could have a potential application to monitor heart-related activities and detect cardiovascular-related diseases.

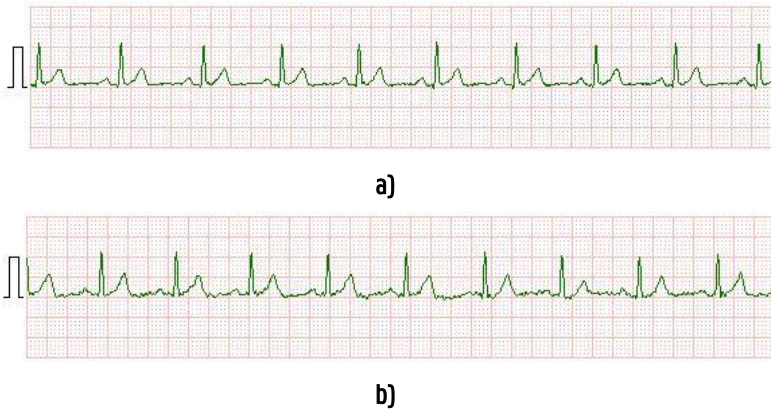

a)

b)

Figure 4.24: ECG waveforms **a**) PEDOT:PSS/PDMS-printed cotton electrode; **b**) Standard Ag/AgCl electrode

4.6. Conclusion

PEDOT:PSS-based conductive polymer composites are promising for the manufacturing of smart textiles with better biocompatibility, flexibility, conductivity, printability, miscibility, and weight, and as such much better suited for wearable applications compared to the common electrodes such as metallic coatings and others. As a result, many PEDOT:PSS-based conductive textiles have been developed by different approaches as a sensor, energy harvesting devices, antennas, OLEDs, etc. However, the conductivity stability of PEDOT:PSS conductive polymer composites after being applied on textile substrates still needs improvement. This improvement could be in the synthesis of PEDOT:PSS itself, on the combination and proportion of the polymers in the composite, or by seeking new approaches to integration.

In the experimental work, we have successfully developed a flexible conductive textile fabric with improved sensing stability of stretch and better washing fastness via screen printing of PEDOT:PSS and PDMS polymers. It was observed that the increase in the proportion of PDMS increases the tensile strength at break. The bending length analysis proved that the flexural rigidity drops at a higher PDMS to PEDOT:PSS ratio which shows as the PDMS imparts flexibility over the pure PEDOT:PSS sample. SEM results showed that the presence of the conductive polymer composite brought smoothness and better coverage of yarn loop interstices. Samples with PEDOT:PSS/PDMS conductive polymer composite showed fewer protruding yarn loops than PEDOT:PSS alone. We found different electrical characteristics that range from 67.72 to 190.8 kΩ/sq before washing

when the ratio of PDMS to PEDOT:PSS varies from 0 to 90%. The conductive character remained after washing but was decreased, though much less so if PDMS is present. This indicates that the developed material is not stable under washing, which for many applications would be a drawback.

The presence of PDMS improved the surface resistance recovery after release from stretching and PDMS-containing samples remained conductive for more stretching cycles than sample r00. We have also realized that the surface resistance can be dropped further by increasing the add-on of the conductive polymer composite. These different electrical resistance characteristics could be chosen based on the application required to use them for sensors, interconnections, antenna, storage, and others. For instance, a conductive fabric has been used to develop a strain and moisture sensor allowing washing, which provided fairly stable sensing stability up to 40% elongation and 150% moisture regain. The work has explored the use of conductive polymer composites to attain adequate flexibility and conductivity simultaneously. The developed sensor could have a potential application in detecting stretching for bicyclists, sweat, and urine for babies and elders, and the extent of swelling in peripheral edema, etc. In addition, an ECG signal comparable to Ag/AgCl standard electrode that can be used in a wearable application for long-term monitoring has been explored.

Some further work on this developed approach is needed, however. After long storage, it was found that the printed fabric easily ruptures, probably because of the acidic nature of PEDOT:PSS which degraded the cotton over longer time periods. For full wearable applications, full wash resistance would also be needed, though this might be possible with for example a PU coating applied locally.

Bibliography

[1] H. Y. Güney, Z. Avdan, and H. Yetkin, "Optimization of annealing temperature and the annealing effect on life time and stability of P3HT:PCBM-based organic solar cells," *Mater. Res. Express*, vol. 6, no. 4, p. 045103, Jan. 2019, doi: 10.1088/2053-1591/aafdee.

[2] V. Hebbar, R. F. Bhajantri, H. B. Ravikumar, and S. Ningaraju, "Journal of Physics and Chemistry of Solids Role of free volumes in conducting properties of GO and rGO filled PVA- PEDOT : PSS composite free standing films : A positron annihilation lifetime study," *J. Phys. Chem. Solids*, vol. 126, no. November 2018, pp. 242–256, 2019, doi: 10.1016/j.jpcs.2018.11.014.

[3] Y. Ding, W. Xu, W. Wang, H. Fong, and Z. Zhu, "Scalable and Facile Preparation of Highly Stretchable Electrospun PEDOT:PSS@PU Fibrous Nonwovens toward Wearable Conductive Textile Applications," *ACS Appl. Mater. Interfaces*, vol. 9, no. 35, pp. 30014–30023, 2017, doi: 10.1021/acsami.7b06726.

[4] A. Sedighi, M. Montazer, and S. Mazinani, "Fabrication of electrically conductive superparamagnetic fabric with microwave attenuation, antibacterial properties and UV protection using PEDOT/magnetite nanoparticles," *Mater. Des.*, vol. 160, pp. 34–47, 2018, doi: 10.1016/j.matdes.2018.08.046.

[5] A. Giuri, S. Colella, A. Listorti, A. Rizzo, C. Mele, and C. Esposito, "GO/glucose/PEDOT : PSS ternary nanocomposites for fl exible supercapacitors," *Compos. Part B*, vol. 148, no. April, pp. 149–155, 2018, doi: 10.1016/j.compositesb.2018.04.053.

[6] M. Hilal and J. I. Han, "Interface engineering of G-PEDOT:PSS hole transport layer via interlayer chemical functionalization for enhanced efficiency of large-area hybrid solar cells and their charge transport investigation," *Sol. Energy*, vol. 174, pp. 743–756, 2018, doi: 10.1016/j.solener.2018.09.031.

[7] T. J. Zajdel *et al.*, "OPEN PEDOT:PSS-based Multilayer Bacterial-Composite Films for Bioelectronics," *Sci. Rep.*, vol. 8, no. 15293, pp. 1–12, 2018, doi: 10.1038/s41598-018-33521-9.

[8] P. J. Taroni *et al.*, "Toward Stretchable Self-Powered Sensors Based on the Thermoelectric Response of PEDOT:PSS/Polyurethane Blends," *Adv Funct Mater*, vol. 1704285, pp. 1–7, 2018, doi: 10.1002/adfm.201704285.

[9] S. Ra, N. Adilah, S. Mah, L. Li, and A. Supangat, "UV- ozone treated graphene oxide/PEDOT : PSS bilayer as a novel hole transport layer in

highly efficient and stable organic solar cells," *Org. Electrons*, vol. 66, no. 2018, pp. 32–42, 2019, doi: 10.1016/j.orgel.2018.12.005.

[10] M. Zahid, E. L. Papadopoulou, A. Athanassiou, and I. S. Bayer, "Strain-responsive mercerized conductive cotton fabrics based on PEDOT:PSS/graphene," *Mater. Des.*, vol. 135, pp. 213–222, 2017, doi: 10.1016/j.matdes.2017.09.026.

[11] T. Houghton, J. Vanjaria, and H. Yu, "Conductive and Stretchable Silver-Polymer Blend for Electronic Applications," *2016 IEEE 66th Electron. Compon. Technol. Conf. ECTC*, pp. 812–816, 2016, doi: 10.1109/ECTC.2016.218.

[12] M. Chen, S. Duan, L. Zhang, Z. Wang, and C. Li, "conductive polymer composites based on graphene networks grown by chemical vapour deposition and PEDOT:PSS coating," *Chem Commun*, pp. 3169–3172, 2015, doi: 10.1039/c4cc09367d.

[13] Q. Meng, K. Cai, Y. Du, and L. Chen, "Preparation and thermoelectric properties of SWCNT/PEDOT : PSS coated tellurium nanorod composite fi lms," *J. Alloys Compd.*, vol. 778, pp. 163–169, 2019, doi: 10.1016/j.jallcom.2018.10.381.

[14] I. Miranda *et al.*, "Properties and Applications of PDMS for Biomedical Engineering: A Review," *J. Funct. Biomater.*, vol. 13, no. 1, p. 2, Dec. 2021, doi: 10.3390/jfb13010002.

[15] B. Prabhakarpandian, M.-C. Shen, K. Pant, and M. F. Kiani, "Microfluidic devices for modeling cell–cell and particle–cell interactions in the microvasculature," *Microvasc. Res.*, vol. 82, no. 3, pp. 210–220, Nov. 2011, doi: 10.1016/j.mvr.2011.06.013.

[16] T.-K. Shih, C.-F. Chen, J.-R. Ho, and F.-T. Chuang, "Fabrication of PDMS (polydimethylsiloxane) microlens and diffuser using replica molding," *Microelectron. Eng.*, vol. 83, no. 11–12, pp. 2499–2503, Nov. 2006, doi: 10.1016/j.mee.2006.05.006.

[17] X. Liu, Y. Gu, T. Mi, X. Wang, and X. Zhang, "Dip-Coating Approach to Fabricate Durable PDMS/STA/SiO2 Superhydrophobic Polyester Fabrics," *Coatings*, vol. 11, no. 3, p. 326, Mar. 2021, doi: 10.3390/coatings11030326.

[18] M.-T. Lee, I.-C. Lee, S.-W. Tsai, C.-H. Chen, M.-H. Wu, and Y.-J. Juang, "Spin coating of polymer solution on polydimethylsiloxane mold for fabrication of microneedle patch," *J. Taiwan Inst. Chem. Eng.*, vol. 70, pp. 42–48, Jan. 2017, doi: 10.1016/j.jtice.2016.10.032.

[19] K. F. Lei, K.-F. Lee, and M.-Y. Lee, "Development of a flexible PDMS capacitive pressure sensor for plantar pressure measurment," *Microelectron. Eng.*, vol. 99, pp. 1–5, 2012, doi: 10.1016/j.mee.2012.06.005.

[20] C. Lee, L. Jug, and E. Meng, "High strain biocompatible polydimethylsiloxane-based conductive graphene and multiwalled carbon nanotube nanocomposite strain sensors," *Appl. Phys. Lett.*, vol. 102, no. 18, p. 183511, May 2013, doi: 10.1063/1.4804580.

[21] J. Kong, Y. Tong, J. Sun, Y. Wei, and W. Thitsartarn, "Electrically conductive PDMS-grafted CNTs-reinforced silicone elastomer," *Compos. Sci. Technol.*, vol. 159, pp. 208–215, 2018, doi: 10.1016/j.compscitech.2018.02.018.

[22] K. T. S. Kong, M. Mariatti, A. A. Rashid, and J. J. C. Busfield, "Composites : Part B Enhanced conductivity behavior of polydimethylsiloxane (PDMS) hybrid composites containing exfoliated graphite nanoplatelets and carbon nanotubes," *Compos. PART B*, vol. 58, pp. 457–462, 2014, doi: 10.1016/j.compositesb.2013.10.039.

[23] X. Gao, Y. Huang, Y. Liu, S. Kormakov, and X. Zheng, "Improved electrical conductivity of PDMS/SCF composite sheets with bolting cloth prepared by a spatial con fi ning forced network assembly," *RSC Adv.*, vol. 7, pp. 14761–14768, 2017, doi: 10.1039/C7RA02061A.

[24] J. Kim, J. Park, U. Jeong, and J.-W. Park, "Silver nanowire network embedded in polydimethylsiloxane as stretchable, transparent, and conductive substrates," *J. Appl. Polym. Sci.*, vol. 133, no. 33, Sep. 2016, doi: 10.1002/app.43830.

[25] A. Larmagnac, S. Eggenberger, H. Janossy, and J. Vo, "Ag-PDMS composites," *Sci. Rep.*, vol. 4, no. 7254, pp. 1–7, 2014, doi: 10.1038/srep07254.

[26] A. J. Heeger, "Semiconducting and Metallic Polymers: The Fourth Generation of Polymeric Materials (Nobel Lecture)*," *Angew Chem Int Ed*, p. 21, 2001.

[27] S. Kirchmeyer and K. Reuter, "Scientific importance, properties and growing applications of poly(3,4-ethylenedioxythiophene)," *J. Mater. Chem.*, vol. 15, no. 21, p. 2077, 2005, doi: 10.1039/b417803n.

[28] J. Ouyang, "'Secondary doping' methods to significantly enhance the conductivity of PEDOT:PSS for its application as transparent electrode of optoelectronic devices," *Displays*, vol. 34, no. 5, pp. 423–436, Dec. 2013, doi: 10.1016/j.displa.2013.08.007.

[29] H. Shi, C. Liu, Q. Jiang, and J. Xu, "Effective Approaches to Improve the Electrical Conductivity of PEDOT:PSS: A Review," *Adv. Electron. Mater.*, vol. 1, no. 4, p. 1500017, Apr. 2015, doi: 10.1002/aelm.201500017.

[30] C. M. Palumbiny, F. Liu, T. P. Russell, A. Hexemer, C. Wang, and P. Müller-Buschbaum, "The Crystallization of PEDOT:PSS Polymeric Electrodes

Probed In Situ during Printing," *Adv. Mater.*, vol. 27, no. 22, pp. 3391–3397, Jun. 2015, doi: 10.1002/adma.201500315.

[31] D. Alemu, H.-Y. Wei, K.-C. Ho, and C.-W. Chu, "Highly conductive PEDOT:PSS electrode by simple film treatment with methanol for ITO-free polymer solar cells," *Energy Environ. Sci.*, vol. 5, no. 11, p. 9662, 2012, doi: 10.1039/c2ee22595f.

[32] Q. Wei, M. Mukaida, Y. Naitoh, and T. Ishida, "Morphological Change and Mobility Enhancement in PEDOT:PSS by Adding Co-solvents," *Adv. Mater.*, vol. 25, no. 20, pp. 2831–2836, May 2013, doi: 10.1002/adma.201205158.

[33] D. A. Mengistie, M. A. Ibrahem, P.-C. Wang, and C.-W. Chu, "Highly Conductive PEDOT:PSS Treated with Formic Acid for ITO-Free Polymer Solar Cells," *ACS Appl. Mater. Interfaces*, vol. 6, no. 4, pp. 2292–2299, Feb. 2014, doi: 10.1021/am405024d.

[34] B. J. Worfolk *et al.*, "Ultrahigh electrical conductivity in solution-sheared polymeric transparent films," *Proc. Natl. Acad. Sci.*, vol. 112, no. 46, pp. 14138–14143, Nov. 2015, doi: 10.1073/pnas.1509958112.

[35] B. Cho, K. S. Park, J. Baek, H. S. Oh, Y.-E. Koo Lee, and M. M. Sung, "Single-Crystal Poly(3,4-ethylenedioxythiophene) Nanowires with Ultrahigh Conductivity," *Nano Lett.*, vol. 14, no. 6, pp. 3321–3327, Jun. 2014, doi: 10.1021/nl500748y.

[36] R. Kroon *et al.*, "Thermoelectric plastics: from design to synthesis, processing and structure–property relationships," *Chem. Soc. Rev.*, vol. 45, no. 22, pp. 6147–6164, 2016, doi: 10.1039/C6CS00149A.

[37] T. J. Zajdel *et al.*, "PEDOT:PSS-based Multilayer Bacterial-Composite Films for Bioelectronics," *Sci. Rep.*, vol. 8, no. 1, p. 15293, Dec. 2018, doi: 10.1038/s41598-018-33521-9.

[38] Y. Ding, W. Xu, W. Wang, H. Fong, and Z. Zhu, "Scalable and Facile Preparation of Highly Stretchable Electrospun PEDOT:PSS @ PU Fibrous Nonwovens toward Wearable Conductive Textile Applications," *ACS Appl Mater Interfaces*, 2017, doi: 10.1021/acsami.7b06726.

[39] H. Okuzaki and M. Ishihara, "Spinning and Characterization of Conducting Microfibers," *Macromol. Rapid Commun.*, vol. 24, no. 3, pp. 261–264, Mar. 2003, doi: 10.1002/marc.200390038.

[40] R. Jalili, J. M. Razal, P. C. Innis, and G. G. Wallace, "One-Step Wet-Spinning Process of Poly (3, 4-ethylenedioxy- thiophene): Poly (styrenesulfonate) Fibers and the Origin of Higher Electrical Conductivity," pp. 3363–3370, 2011, doi: 10.1002/adfm.201100785.

[41] H. Okuzaki, Y. Harashina, and H. Yan, "Highly conductive PEDOT/PSS microfibers fabricated by wet-spinning and dip-treatment in ethylene

glycol," *Eur. Polym. J.*, vol. 45, no. 1, pp. 256–261, 2009, doi: 10.1016/j.eurpolymj.2008.10.027.

[42] J. Zhou *et al.*, "Semi-metallic, strong and stretchable wet-spun conjugated polymer microfibers," *J. Mater. Chem. C*, vol. 3, no. 11, pp. 2528–2538, 2015, doi: 10.1039/c4tc02354d.

[43] J. Zhang *et al.*, "Fast and scalable wet-spinning of highly conductive PEDOT:PSS fibers enables versatile applications," *J. Mater. Chem. A*, no. 7, pp. 6401–6410, 2019, doi: 10.1039/Chttps://doi.org/10.1039/C9TA00022D5TA06869J.

[44] Y. Liu, X. Li, and J. C. Lu, "Electrically Conductive Poly (3, 4-ethylenedioxythiophene)– Polystyrene Sulfonic Acid/Polyacrylonitrile Composite Fibers Prepared by Wet Spinning," *J. Appl. Polym. Sci.*, pp. 370–374, 2013, doi: 10.1002/app.39174.

[45] S. Seyedin, J. M. Razal, P. C. Innis, A. Jeiranikhameneh, S. Beirne, and G. G. Wallace, "Knitted Strain Sensor Textiles of Highly Conductive All-Polymeric Fibers," *ACS Appl. Mater. Interfaces*, vol. 7, no. 38, pp. 21150–21158, 2015, doi: 10.1021/acsami.5b04892.

[46] S. Jin *et al.*, "Synthesis of freestanding PEDOT:PSS/PVA@Ag NPs nanofiber film for high-performance flexible thermoelectric generator," *Polymer*, vol. 167, no. October 2018, pp. 102–108, 2019, doi: 10.1016/j.polymer.2019.01.065.

[47] Q. Zhang *et al.*, "Electrospinning of Ultrafine Conducting Polymer Composite Nanofibers with Diameter Less than 70 nm as High Sensitive Gas Sensor," *Materials*, vol. 11, no. 9, p. 1744, Sep. 2018, doi: 10.3390/ma11091744.

[48] L. Allison, S. Hoxie, and T. L. Andrew, "Towards Seamlessly-Integrated Textile Electronics: Methods to Coat Fabrics and Fibers with Conducting Polymers for Electronic Applications," *Chem. Commun.*, no. 53, 2017, doi: DOI: 10.1039/C7CC02592K.

[49] K. H. Hong, K. W. Oh, and T. J. Kang, "Preparation and properties of electrically conducting textiles byin situ polymerization of poly(3,4-ethylenedioxythiophene)," *J. Appl. Polym. Sci.*, vol. 97, no. 3, pp. 1326–1332, Aug. 2005, doi: 10.1002/app.21835.

[50] T. Bashir, M. Skrifvars, and N.-K. Persson, "High-strength electrically conductive fibers: Functionalization of polyamide, aramid, and polyester fibers with PEDOT polymer," *Polym. Adv. Technol.*, vol. 29, no. 1, pp. 310–318, Jan. 2018, doi: 10.1002/pat.4116.

[51] T. Bashir, M. Ali, S.-W. Cho, N.-K. Persson, and M. Skrifvars, "OCVD polymerization of PEDOT: effect of pre-treatment steps on PEDOT-coated conductive fibers and a morphological study of PEDOT

distribution on textile yarns: OPTIMIZATION OF CVD PROCESS AND SURFACE MORPHOLOGY," *Polym. Adv. Technol.*, vol. 24, no. 2, pp. 210–219, Feb. 2013, doi: 10.1002/pat.3073.

[52] I. G. Trindade, F. Martins, and P. Baptista, "High electrical conductance poly(3,4-ethylenedioxythiophene) coatings on textile for electrocardiogram monitoring," *Synth. Met.*, vol. 210, pp. 179–185, Dec. 2015, doi: 10.1016/j.synthmet.2015.09.024.

[53] L. Zhang, M. Fairbanks, and T. L. Andrew, "Rugged Textile Electrodes for Wearable Devices Obtained by Vapor Coating Off-the-Shelf, Plain-Woven Fabrics," *Adv. Funct. Mater.*, vol. 27, no. 24, p. 1700415, Jun. 2017, doi: 10.1002/adfm.201700415.

[54] Y. Ding, M. A. Invernale, and G. A. Sotzing, "Conductivity trends of pedot-pss impregnated fabric and the effect of conductivity on electrochromic textile," *ACS Appl. Mater. Interfaces*, vol. 2, no. 6, pp. 1588–1593, 2010, doi: 10.1021/am100036n.

[55] J. D. Ryan, D. A. Mengistie, R. Gabrielsson, A. Lund, and C. Müller, "Machine-Washable PEDOT:PSS Dyed Silk Yarns for Electronic Textiles," *ACS Appl. Mater. Interfaces*, vol. 9, no. 10, pp. 9045–9050, Mar. 2017, doi: 10.1021/acsami.7b00530.

[56] A. Lund *et al.*, "Roll-to-Roll Dyed Conducting Silk Yarns: A Versatile Material for E-Textile Devices," *Adv. Mater. Technol.*, vol. 3, no. 12, p. 1800251, Dec. 2018, doi: 10.1002/admt.201800251.

[57] M. G. Tadesse, D. A. Mengistie, Y. Chen, L. Wang, C. Loghin, and V. Nierstrasz, "Electrically conductive highly elastic polyamide/lycra fabric treated with PEDOT:PSS and polyurethane," *J. Mater. Sci.*, vol. 54, no. 13, pp. 9591–9602, Jul. 2019, doi: 10.1007/s10853-019-03519-3.

[58] Y. Guo *et al.*, "PEDOT:PSS 'wires' Printed on Textile for Wearable Electronics," *ACS Appl. Mater. Interfaces*, vol. 8, no. 40, pp. 26998–27005, 2016, doi: 10.1021/acsami.6b08036.

[59] S. K. Sinha *et al.*, "Screen-Printed PEDOT:PSS Electrodes on Commercial Finished Textiles for Electrocardiography," *ACS Appl. Mater. Interfaces*, vol. 9, pp. 37524–37528, 2017, doi: 10.1021/acsami.7b09954.

[60] T.-K. Kang, "Piezoresistive Characteristics of Nylon Thread Resistive Memories for Wearable Strain Sensors," *Coatings*, vol. 9, no. 10, p. 623, Sep. 2019, doi: 10.3390/coatings9100623.

[61] D. Pani, A. Dess, J. F. Saenz-cogollo, G. Barabino, B. Fraboni, and A. Bonfiglio, "Fully Textile, PEDOT:PSS Based Electrodes for Wearable ECG Monitoring Systems," vol. 63, no. 3, pp. 540–549, 2016, doi: 10.1109/TBME.2015.2465936.

[62] A. Ankhili, X. Tao, V. Koncar, D. Coulon, and J. Tarlet, "Ambulatory Evaluation of ECG Signals Obtained Using Washable Textile-Based Electrodes Made with," *Sensors*, vol. 19, no. 416, p. 13, 2019, doi: 10.3390/s19020416.

[63] A. Ankhili, X. Tao, C. Cochrane, V. Koncar, D. Coulon, and J.-M. Tarlet, "Comparative Study on Conductive Knitted Fabric Electrodes for Long-Term Electrocardiography Monitoring: Silver-Plated and PEDOT:PSS Coated Fabrics," *Sensors*, vol. 18, no. 11, p. 3890, Nov. 2018, doi: 10.3390/s18113890.

[64] A. Niijima, T. Isezaki, R. Aoki, and T. Watanabe, "hitoeCap: Wearable EMG Sensor for Monitoring Masticatory Muscles with PEDOT-PSS Textile Electrodes," in *ISWC '17*, 2017, pp. 215–220.

[65] M. A. B. Abbasi, P. Vryonides, and S. Nikolaou, "Humidity Sensor Devices using PEDOT : PSS," in *2015 IEEE International Symposium on Antennas and Propagation & USNC/URSI National Radio Science Meeting*, 2015, pp. 1366–1367. doi: 10.1109/APS.2015.7305072.

[66] R. E. Smith *et al.*, "Development of a novel highly conductive and flexible cotton yarn for wearable pH sensor technology," *Sens. Actuators B Chem.*, vol. 287, pp. 338–345, May 2019, doi: 10.1016/j.snb.2019.01.088.

[67] Y. Du *et al.*, "Thermoelectric Fabrics: Toward Power Generating Clothing," *Sci. Rep.*, vol. 5, no. 1, p. 6411, Mar. 2015, doi: 10.1038/srep06411.

[68] X. Jia, A. Tennant, R. J. Langley, W. Hurley, and T. Dias, "A knitted textile waveguide," in *2014 Loughborough Antennas and Propagation Conference (LAPC)*, Loughborough, Leicestershire, United Kingdom, Nov. 2014, pp. 679–682. doi: 10.1109/LAPC.2014.6996485.

[69] L. K. Allison and T. L. Andrew, "A Wearable All-Fabric Thermoelectric Generator," *Adv. Mater. Technol.*, vol. 4, no. 5, p. 1800615, May 2019, doi: 10.1002/admt.201800615.

[70] I. Nuramdhani *et al.*, "Charge-Discharge Characteristics of Textile Energy Storage Devices Having Different PEDOT:PSS Ratios and Conductive Yarns Configuration," *Polymers*, vol. 11, no. 2, p. 345, Feb. 2019, doi: 10.3390/polym11020345.

[71] Y. Ma, Q. Wang, X. Liang, D. Zhang, and M. Miao, "Wearable supercapacitors based on conductive cotton yarns," *J. Mater. Sci.*, vol. 53, no. 20, pp. 14586–14597, Oct. 2018, doi: 10.1007/s10853-018-2655-z.

[72] D. Yuan *et al.*, "Twisted yarns for fiber-shaped supercapacitors based on wetspun PEDOT:PSS fibers from aqueous coagulation," *J. Mater. Chem. A*, vol. 4, no. 30, pp. 11616–11624, 2016, doi: 10.1039/C6TA04081K.

[73] Z. Li *et al.*, "Multidimensional Hierarchical Fabric-Based Supercapacitor with Bionic Fiber Microarrays for Smart Wearable Electronic Textiles,"

ACS Appl. Mater. Interfaces, vol. 11, no. 49, pp. 46278–46285, Dec. 2019, doi: 10.1021/acsami.9b19078.

[74] R. Yuksel and H. E. Unalan, "Textile supercapacitors-based on MnO_2/SWNT/conducting polymer ternary composites: Textile-based supercapacitors," *Int. J. Energy Res.*, vol. 39, no. 15, pp. 2042–2052, Dec. 2015, doi: 10.1002/er.3439.

[75] Z. Li *et al.*, "All-organic flexible fabric antenna for wearable electronics," 2020, doi: https://doi.org/10.1039/D0TC00691B.

[76] H. Miura *et al.*, "Foldable Textile Electronic Devices Using All-Organic Conductive Fibers: Foldable Textile Electronic Devices Using ...," *Adv. Eng. Mater.*, vol. 16, no. 5, pp. 550–555, May 2014, doi: 10.1002/adem.201300461.

[77] I. Verboven, J. Stryckers, V. Mecnika, G. Vandevenne, M. Jose, and W. Deferme, "Printing Smart Designs of Light Emitting Devices with Maintained Textile Properties," *Materials*, vol. 11, no. 2, p. 290, Feb. 2018, doi: 10.3390/ma11020290.

[78] J. Bian, L. Zhou, X. Wan, C. Zhu, B. Yang, and Y. Huang, "Laser Transfer, Printing, and Assembly Techniques for Flexible Electronics," *Adv. Electron. Mater.*, vol. 5, no. 7, p. 1800900, Jul. 2019, doi: 10.1002/aelm.201800900.

[79] M. Cai, S. Nie, Y. Du, C. Wang, and J. Song, "Soft Elastomers with Programmable Stiffness as Strain-Isolating Substrates for Stretchable Electronics," *ACS Appl. Mater. Interfaces*, vol. 11, no. 15, pp. 14340–14346, Apr. 2019, doi: 10.1021/acsami.9b01551.

[80] A. El Zein, C. Huppé, and C. Cochrane, "Development of a Flexible Strain Sensor Based on PEDOT:PSS for Thin Film Structures," *Sensors*, vol. 17, no. 6, p. 1337, Jun. 2017, doi: 10.3390/s17061337.

[81] M. A. B. Abbasi, P. Vryonides, and S. Nikolaou, "Humidity sensor devices using PEDOT:PSS," in *2015 IEEE International Symposium on Antennas and Propagation & USNC/URSI National Radio Science Meeting*, Vancouver, BC, Canada, Jul. 2015, pp. 1366–1367. doi: 10.1109/APS.2015.7305072.

[82] Jin-Woo Lee and Kwang-Seok Yun, "ECG Monitoring Garment Using Conductive Carbon Paste for Reduced Motion Artifacts," *Polymers*, vol. 9, no. 12, p. 439, Sep. 2017, doi: 10.3390/polym9090439.

[83] T. Kannaian, R. Neelaveni, and G. Thilagavathi, "Design and development of embroidered textile electrodes for continuous measurement of electrocardiogram signals," *J. Ind. Text.*, vol. 42, no. 3, pp. 303–318, Jan. 2013, doi: 10.1177/1528083712438069.

[84] P. S. Das, J. W. Kim, and J. Y. Park, "Fashionable wrist band using highly conductive fabric for electrocardiogram signal monitoring," *J. Ind. Text.*, vol. 49, no. 2, pp. 243–261, Aug. 2019, doi: 10.1177/1528083718779427.

[85] N. Meziane, J. G. Webster, M. Attari, and A. J. Nimunkar, "Dry electrodes for electrocardiography," *Physiol. Meas.*, vol. 34, no. 9, pp. R47–R69, Sep. 2013, doi: 10.1088/0967-3334/34/9/R47.

[86] A. Achilli, D. Pani, and A. Bonfiglio, "Characterization of Screen-Printed Textile Electrodes Based on Conductive Polymer for ECG Acquisition," presented at the 2017 Computing in Cardiology Conference, Sep. 2017. doi: 10.22489/CinC.2017.129-422.

[87] R. Castrillón, J. J. Pérez, and H. Andrade-Caicedo, "Electrical performance of PEDOT:PSS-based textile electrodes for wearable ECG monitoring: a comparative study," *Biomed. Eng. OnLine*, vol. 17, no. 1, p. 38, Dec. 2018, doi: 10.1186/s12938-018-0469-5.

5. Dry PEDOT:PSS/PDMS-Printed Cotton Fabric EEG Textrode for Brain Activity Monitoring

This chapter presents a textile-based dry EEG electrode that can detect the activities in the brain. The EEG electrodes were constructed from an electrically conductive cotton fabric with 67.23 Ω/sq produced by PEDOT:PSS/PDMS conductive polymer composite coating on cotton fabric via screen printing. The signal quality was compared with commercial dry electrodes. This chapter also addresses the robustness and reliability of the EEG textrode to washing, bending, and multiple and continuous uses. It also addresses the effect of the shape and size of the electrode on signal quality.

This chapter is redrafted from published journal papers:

G.B. Tseghai, B. Malengier, K.A. Fante and L. Van Langenhove, "Dry Electroencephalography Textrode for Brain Activity Monitoring", *IEEE Sensors Journal*, 21(19): 22077 - 22085, 2021. doi.org/10.1109/JSEN.2021.3103411.

G.B. Tseghai, B. Malengier, K.A. Fante and L. Van Langenhove, "Validating Poly(3,4-ethylene dioxythiophene) Polystyrene Sulfonate-Based Textile Electroencephalography Electrodes by a Textile-Based Head Phantom", *Polymers*, 13(21): 3629, 2021. doi.org/10.3390/polym13213629.

G.B. Tseghai, B. Malengier, K.A. Fante and L. Van Langenhove, "A Dry EEG Textrode from a PEDOT:PSS/PDMS-coated Cotton Fabric for Brain Activity Monitoring", *IEEE*, 2021 IEEE International Conference on Flexible and Printable Sensors and Systems (FLEPS), Manchester, UK, 20-23 June 2021. doi.org/10.1109/FLEPS51544.2021.9469840.

Table of Contents

5.1. Introduction

The use of smart textiles for health monitoring is a booming business. To make it more user-friendly, it is important to develop e-textile-based bio-potential sensors for active control of your health without compromising the comfort and bulk property of the textile. In the case of brain-related health issues, medical treatment might eventually decrease mortality and increase the quality of life, but to do so, both the consequences of the diseases and responses to treatments need to be objectively quantified. Moreover, most brain disorder patients do not recognize the commencement and also do not understand what is happening during the occurrence. Therefore, disorder detection devices that allow a rapid objective assessment and recognition of the illness frequency and treatment through closed-loop systems could potentially lessen morbidity and mortality. With this in mind, the ideal monitoring device should be safe and easy to use for patients, families, and medical staff. It must be comfortable for the users, especially during sleep, and thus preferably wireless and lightweight. If electrodes are used, they must be as small and few as possible since a significant percentage of patients are not willing to wear electrodes on a long-term basis [1]. On top of that, the device should be unobtrusive and discrete. Uncomfortable cables, electrodes, lights, buttons, and sounds should be avoided as this disturbs the patient and family, even more so in the long term. This was confirmed by a recent survey evaluating patients' desires that revealed a strong preference for a seizure detection device that had little interference with daily activities [2]. The use of textile electrodes could overcome the problems associated with metal-based dry electrodes like structural rigidity and weight and would fill the gap. Textile electrodes are electrode types that are made from conductive textile fabric. These electrodes do not need a gel to achieve connection to the skin. Moreover, they are good for long-time measurements as they do not irritate the skin. In addition, they are lightweight and ductile, and it is possible to make them reusable and washable [3].

Modern applications of brain-computer interface (BCI) based EEG rely heavily on the so-called wet electrodes (e.g. Ag/AgCl electrodes) which require gel application and skin preparation to operate properly. However, these electrodes can cause skin irritation as a conductive gel is necessary to reduce electrode-to-skin impedance mismatch. Besides, it may also lead to artifact generation due to drying out of the gel over time and humidity changes. Furthermore, skin preparation and gel application are time-consuming when a high number of electrodes are required.

The demand for more comfortable and user-friendly electrodes led to the emergence of metal-based dry EEG electrodes, primarily dry Ag/AgCl EEG electrodes, that can overcome the aforementioned limitations associated with wet electrodes. However, metal-based dry electrodes have the disadvantages of higher electrode-to-skin impedance and susceptibility to movement artifacts. In literature, it is reported that because of the accumulation of perspiration sweat under the electrodes, after a settling time, the impedance greatly decreases, and artifact noise becomes lower than for wet electrodes [4]. Other studies reported that dry electrodes have several advantages in comparison with wet ones, such as signal intensity and smaller size [5]. However, metal-based dry electrodes, are heavier and have a rigid structure which makes them unsuitable for wearable applications, especially when long-term monitoring is needed. This led to the emergence of textile-based dry EEG electrodes.

Recently, some research on textile-based dry electrodes has been reported: a passive electrode based on porous titanium (Ti) and PDMS for long term EEG recording [6]; a porous ceramic-based 'semi-dry' electrode that has tips that can slowly and continuously release a tiny amount of electrolyte liquid to the scalp, which provides an ionic conducting path for detecting neural signals [7]; wearable, less visible ear-EEG recording [8]; copper plate fabric textile EEG electrode that can give similar signals as commercially available EEG [9]; knitted soft textile electrodes for EEG Monitoring made from nylon, conductive fibers, spandex and polypropylene [10]; a textile electrode using electrically conductive polyurethane (PU) foam developed through a coating of inherently conductive polyaniline (PANI) polymer on PU foam [11] and a 3D printed dry electrode made by an insulating acrylic-based photopolymer [12]. All these works reported that the signals acquired were comparable to the standard wet EEG electrodes. However, there is no scientific information or experimental evaluation on the property of the electrodes as a textile material such as the tensile strength, flexural rigidity, coating thickness, and weight. Therefore, it is not known if the textile substrates own the characteristics of normal textile materials and the important factors for wearable long-monitoring like flexibility and light weightiness could be compromised. The use of PEDOT:PSS for EEG electrodes has been successfully explored. For instance, Leleux et al. reported PEDOT:PSS-based electrode cups that give better performance than gold cup electrodes [13]. Ferrari et al. also reported a PEDOT:PSS-based EEG tattoo that collects signal qualities comparable to standard Ag/AgCl electrodes [14].

As mentioned in Chapter 2, from a textile perspective, the aim is to produce the entire component, like sensors, actuators, transmission lines, and so on, from

100% textile material. However, the use of metallic particles like silver, copper, and gold does not support this target as the texture of the textile is often compromised. Metallic particles impart stiffness to the fabric and cause them to lose part of their textile characteristics. In addition, the formulation of metallic inks is a complex process requiring a lot of additives and specialized processes and is thus expensive. Hence, the use of conductive polymers for biopotential sensing electrodes like EEG could be a problem-solving alternative owing to their highly effective contact areas with human skin, biocompatibility, high electrical conductivity, and inherent mechanical flexibility [15]. Among the conductive polymers, poly(3,4-ethylene dioxythiophene) polystyrene sulfonate (PEDOT:PSS) has gained attention and has been already reported in different formats. For instance, Ferrari et al. [14] have developed a PEDOT:PSS tattoo EEG electrode, as shown in Figure 5.1.

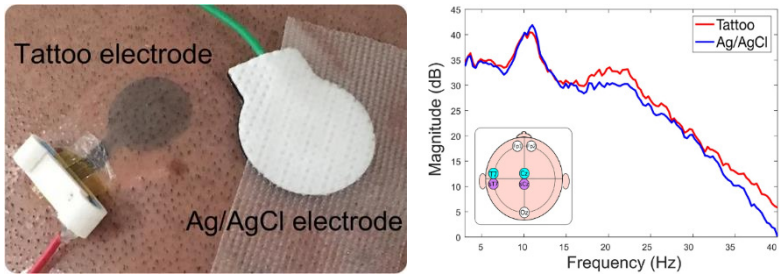

a) b)

Figure 5. 1: a) picture of two electrodes in Cz position on the head of the participant; **b**) superimposed power spectral density (dB) during alpha wave recordings from the textile tattoo electrodes (TTEs)—in red, and Ag/AgCl electrodes—in blue. The insert at the bottom left shows the placement of the electrodes with the used derivation (Tz–Cz, in light blue for the TTEs, and sT7-sCz for the Ag/AgCl electrodes in light violet); [14]. Under CC by 4.0.

Though the EEG tattoo approach is novel and seemingly promising, it only remains until washed and is not reusable in the case of temporary tattoos and fades in the case of permanent tattoos owing to skin development. Moreover, tattoos may cause an allergic reaction in humans, resulting in a rash that is typically red, bumpy, or itchy. These symptoms may appear in the days following the initial tattooing or months or years later. Thus, reusable textile-based electrodes are still a primal choice as long as the concern is long-term monitoring, as well as from an economic point of view.

Applications, where a polymer is applied to conventional textiles to make them conductive and use for an appropriate type of sensing function, are of course under investigation. One of the series of challenges for the development and widespread adoption of conductive polymer-based e-textile is longevity. For instance, electrodes that come in contact with skin will inevitably get stained. Like traditional clothing, e-textiles, therefore, must be able to be washed, however, this could cause performance deterioration over time. Here, both mechanical and electrical properties of the electrodes have been assessed as textile and electronic materials. Moreover, the effect of electrode size and shape and its performance under multiple and continuous uses, as well as bending and washing, have been studied.

5.2. Experimental Design

The purpose of this experiment is to develop a PEDOT:PSS/PDMS-printed cotton EEG textrode and study the effect of washing, bending, and multiple uses on signal qualities.

5.2.1. Materials and Chemicals

Knitted cotton fabric was used as a textile substrate owing to its wearing comfort and is adequately available. A high-conductivity grade PEDOT/PSS PH1000 Clevious conductive polymer obtained from (Ossila Ltd., Belfast, UK) and a biocompatible PDMS-b-EO elastomer obtained from (Polyscience, Inc., Hirschberg, Germany) were used to produce a conductive polymer composite as in Chapter 4. PEDOT/PSS was selected because of its acceptable electrical conductivity and flexibility [16] and its biocompatibility [17]. PDMS was chosen because of its biocompatibility and extensibility [18]. In addition, PDMS has several properties making it favorable such as low cost [19] and transparent (240 nm–1100 nm range) [20] products. 1,2,3,4-Butanetetracarboxylic acid (BTCA) obtained from (Sigma-Aldrich, Inc, Darmstadt, Germany) was also used as a fixing agent to improve wash fastness, a problem encountered before, see Chapter 4. The chemical structures of PEDOT/PSS, PDMS, and cellulose, the polymeric units of cotton, are shown in Figure 5.2.

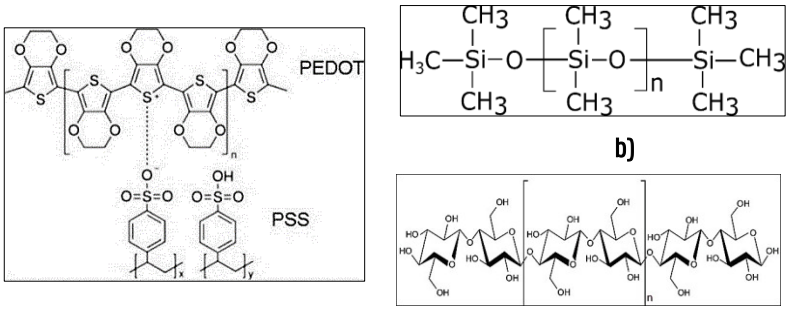

Figure 5.2: a) The chemical formula of PEDOT/PSS [21], under CC by 4.0; **b**) the chemical structure of PDMS; **c**) the chemical structure of a polymeric unit of cotton, cellulose, which is a linear polymer made up of β-D-glucopyranose units covalently linked with (1–4) glycosidic bonds [22], under CC by 3.0.

5.2.2. Conductive Fabric Development

The development of the conductive fabric followed previous work, Chapter 4. A 1:4 proportion of PDMS to PEDOT:PSS was mixed at room temperature using a 2 mm diameter circular rod until a homogenous PEDOT:PSS-PDMS paste was obtained. Then, BTCA, 10% of the weight of the paste, was added to the recipe. The PEDOT:PSS/PDMS paste was next screen-printed onto knitted cotton fabric and, finally, the printed fabric was dried at 70°C for 10 min and cured at 150°C for 3 min. The schematic illustration of the screen printing and the actual conductive fabric are shown in Figures 5.3a and 5.3b, respectively.

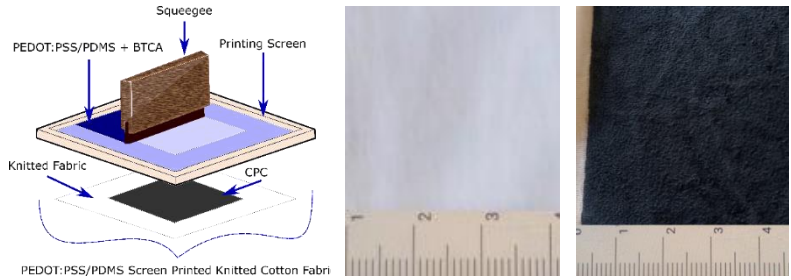

Figure 5.3: a) Schematic illustration of flat screen printing; **b**) unprinted bare fabric; **c**) PEDOT:PSS/PDMS-printed knitted cotton fabric

5.2.3. Conductive Fabric Characterization

The increase in weight which could be also considered as the increase in GSM was mathematically determined as a difference in the conditioned weight before and after printing. The thickness was determined according to ISO 5084:1996(E) and printing thickness was determined from the difference in thickness before and after printing. Bending length was measured according to BS 3356:1990 and its respective flexural rigidity was calculated using (4.3), Chapter 4.

The strength and elongation at break were tested according to ISO 13934-1. The surface topology and appearance of yarns within the fabric before and after printing were also tested using FEI Quanta 200 FFE-SEM at an accelerating voltage of 20 kV. The non-conductive sample was printed with gold using Balzers Union SKD 030 sputter printer prior to analysis. FTIR test was also conducted to verify the presence of PEDOT:PSS/PDMS conductive polymer composite on the knitted cotton fabric after printing.

Next, the electrical characteristics, specifically the sheet resistance and resistivity of the conductive fabric used to construct EEG electrodes were measured using a four-probe method according to FprEN 16812 and using a portable MR-1 Surface Resistance Meter as shown in Figure 5.4. The MR-1 directly reads the surface resistance (Ω/sq). Whereas for the measurement according to FprEN 16812, the surface resistance was calculated using Equation 4.4. The measurement was carried out at five different positions of a 5 cm x 5 cm conductive fabric and recorded the average. The electrical analysis was also done after washing the fabric, washing was carried out according to ISO6330:2012(E) Type A (mild).

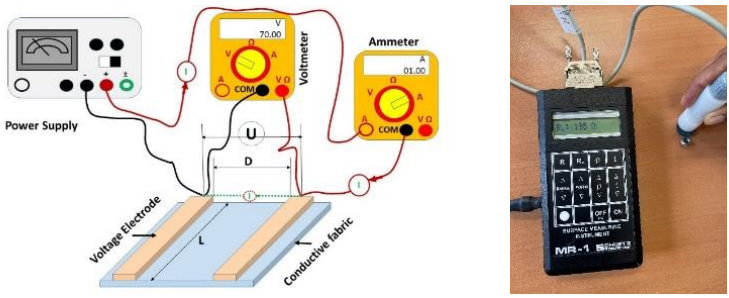

a) b)

Figure 5.4: Electrical resistance measurement: **a**) four-point method according to FprEN 16812; **b**) Using MR1-Surface Resistance Instrument

In addition, the textile-based EEG electrodes were subjected to 25 washing cycles according to the ISO6330:2012(E) Type A (mild) test method and were bent to a 5 mm bending radius. The impact of this on the EEG signal quality has been studied. Also, the effect on the signal quality of multiple and continued use of the electrodes has been studied.

5.2.4. Textile-Based Electrode (Textrode) Design

Circular electrodes with 1 cm, 2 cm, and 4 cm diameters were constructed from the printed fabric to examine the effect of electrode size on signal quality. In addition, the effect of electrode shape on signal quality was studied. For this purpose, circular, square, and equilateral triangular electrodes of each approx. π cm^2 surface area was constructed and compared with each other, the textile electrodes with different shapes are shown in Figure 5.5a. The electrodes were placed on a non-conductive foam (Figure 5.5b) to ensure the conductive fabric is sufficiently pressed against the skin on the active sides of the electrode.

Figure 5.5: EEG textrode design: **a**) square, triangular, and circular active component of the textrode; **b**) schematic illustration of the EEG textrode on a foam

5.2.5. Impedance Measurement

The electrical impedance at the skin-electrode interface influences the EEG signal quality [23], [24], thus designing a dry electrode with a low skin-contact impedance improves EEG performance. The skin-to-electrode impedance test was performed in the EEG alpha band power using a Cyton Biosensing (OpenBCI) board and an IVIUM potentiostat. In both instruments, three-electrode configurations (reference electrode, counter electrode, and active electrode) were used. A 2 cm diameter (π cm^2) PEDOT:PSS/PDMS-printed cotton textrode was

used. A dry Ag/AgCl electrode, most commercialized, was used for comparison under the same testing conditions.

The skin-to-electrode impedance measurement using an OpenBCI board was according to the illustrated setup shown in Figure 5.6a [25], [26]. The Cyton Biosensing OpenBCI board is an ADS1299 integrated circuit from Texas Instruments. The ADS1299 has a "Lead Off Detection" feature that allows it to measure impedance by injecting a known current into each electrode.

The ADS1299 [27] forces a 6 nA current into the electrode line regardless of the resistance or impedance between the current source and the ground. As a result, a 6 nA current was flown through the electrode to the ground during this test. A 5 kΩ resistor is built into the OpenBCI board in series with each electrode, as shown in Figure 5.6. The average voltage measured during the test was expressed as root mean square voltage (Vrms). The impedance directly found from the voltage is a raw impedance. The actual impedance is found by subtracting the load resistance from the raw impedance. Therefore, the skin-to-electrode impedance was calculated using Equation (5.1).

$$\begin{aligned}&\text{Actual Average Impedance } (\Omega)\\&= \frac{\text{Vrms} \times 2\sqrt{2}\ (\text{V})}{\pi \times \text{Current } (\text{A})} \text{-Load Resistance } (\Omega)\end{aligned} \tag{5.1}$$

where the current and the load resistance are 6 nA and 5 kΩ, respectively.

On the other hand, the measurement using IVIUM potentiostat was according to the setup illustrated by Chen et al. [28]. The potentiostat controlled a 25 mV AC signal between the working and reference electrodes, with the signal frequency ranging from 0.1 Hz to 60 Hz. The corresponding impedances are labeled as ZWE (impedance of skin-to-working electrode), ZRE (impedance of skin-to-reference electrode), and ZCE (impedance of skin-to-counter electrode) in the schematic shown in Figure 5.6b, where Z1 represents the impedance of the tissue between the working electrode (WE) and reference electrode (RE), Z2 represents the impedance of the tissue between RE and counter electrode (CE), and Z3 represents the impedance of the tissue between WE and CE.

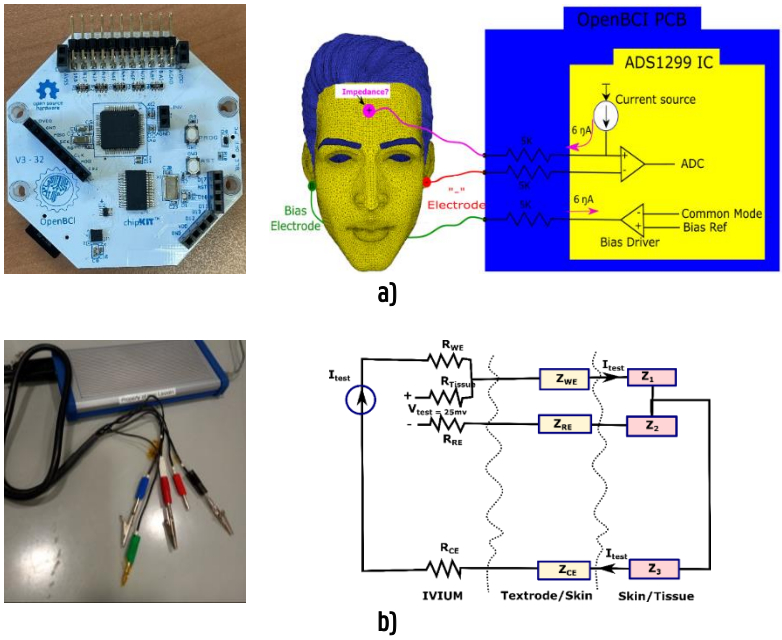

Figure 5.6: Impedance measurement: **a**) an OpenBCI board and schematic circuitry of skin-to-electrode impedance measurement using an OpenBCI board that is built around an ADS1299; **b**) IVIUM potentiostat and schematic of the three-electrode circuitry set up for impedance measurement by the IVIUM potentiostat [28], adopted under CC by 4.0.

5.2.6. EEG Measurement and Analysis

In this chapter, on-body EEG measurement was conducted using a Cyton Biosensing OpenBCI board. In addition, as a proof of concept, an EEG measurement was conducted at a clinical level using Brain Quick Clinical EEG Line. In both instruments, the international federation's 10–20 EEG placement (Figure 5.7a), i.e., the most commonly used system for mounting electrodes for clinical EEG monitoring, was used to place five electrodes, three active (Fp1, Fz, and Fp2) on the head and two references (A1 and A2) on the earlobe. The 10–20 system of electrode placement is a method for describing where scalp electrodes should be placed [29]. The 10 and 20 in the system indicate the distance of the electrodes from each other in proportion to the size of the head. The numbers in the indicated positions represent the corresponding position of the forehead. These scalp electrodes are used to record the EEG with an electroencephalograph machine. To hold the textile electrode in the required positions, a tight-fitting headband made of elastic bandage was used. A non-conductive foam was placed

between the elastic bandage and the electrode to ensure the electrode is sufficiently pressed against the skin. An on-body EEG measurement was also performed with a Florida Research Instrument Inc product reusable Ag/AgCl standard dry Electrode (TDE-20-15 reusable EEG electrode) obtained from OpenBCI for comparison.

In the first instrument, the EEG waveforms were recorded with eight channels at a sampling frequency of 250 Hz for 300 s via an OpenBCI board at a 1–50 Hz bandpass filter. Each channel measures the difference between one electrode and a reference electrode as the referential electrode installation was followed. In this type of installation, the reduction in disturbances and noise is common for all the electrodes. The schematic illustration of the EEG measurement setup used in this work is shown in Figure 5.7b.

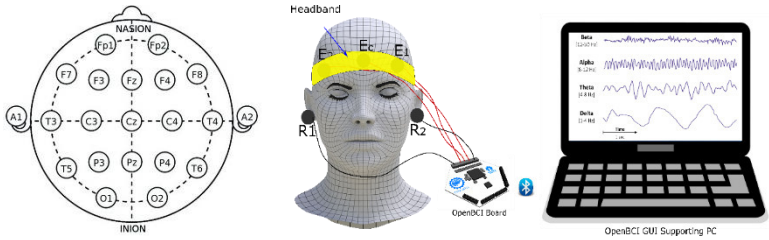

a) b)

Figure 5.7: a) The 10–20 international system of EEG electrode placement [29], under CC by 4.0; **b**) EEG measurement setup using a Cyton Biosensing OpenBCI board

In the second instrument, as a proof of concept, on-body EEG measurement was performed with a volunteer subject at Ghent University Hospital, Neurology Department. All the studies were approved by the Ethical Clearance Committee of EiTEX (04-11-2020). Brain Quick Clinical EEG Line (Figure 5.8a) was used to conduct the EEG measurement using three active electrodes and two more reference electrodes. The active electrodes were placed on Fp1, Fpz, and Fp2 head positions, and the reference electrodes were placed in the earlobe, as shown in Figure 5.8b.

a) b)

Figure 5.8: Clinical Electroencephalography (EEG) measurement: **a**) Brain Quick Clinical EEG Line; **b**) photographic image of EEG measurement with the clinical system.

Finally, the EEGLAB software [41] was used to perform data treatment and statistics offline. A 250 Hz low pass filter, 512 Hz resampling, and a 0.5 Hz high pass filter were used in the beginning. The event-related spectral perturbation (ERSP) was obtained for the time domain analysis by averaging baseline-corrected epochs taken from 0.5 to 2.5 s after the target apparition event. From the initial 1960 epochs (5% discarded), a total of 1862 epochs remained after artifact rejection. Meanwhile, intertrial coherence (ITC) was obtained for wave cycles from 3 to 0.5, epoch time limit from 0 to 1960, and frequency limit from 0.5 to 250 Hz. ITC and ERSP were analyzed via EEGLAB software that is treated as in Equations (5.2) and (5.3) according to spectral and coherence estimates on EEG recordings. We have

$$\mathrm{ITC}\,(f,t) = \frac{1}{n}\sum_{k=1}^{n}\frac{F_k\,(f,t)}{|F_k\,(f,t)|} \tag{5.2}$$

$$\mathrm{ERSP}\,(f,t) = \frac{1}{n}\sum_{k=1}^{n}|F_k(f,t)|^2 \tag{5.3}$$

where, $F_k(f,t)$, f, t, and n denote the spectral estimate of k trials, frequency, time, and numbers of data, respectively.

5.3. Result and Discussion

5.3.1. Mechanical Property Analysis

The gram per square meter (GSM) of the fabric increased by 100 GSM (71.4%) after screen printing. The increase in weight can also be considered as a solid add-on from conductive polymer composite to the fabric. The thickness measurement based on ISO 5084:1996 (E) showed an increase from 0.5 mm to 0.65 mm (+30%) which means the thickness of the printed layer was 0.15 mm. The significant change in weight and thickness might lead us to believe that the textile aspect of the fabric was greatly changed. This was not the case, however, as the bending length test according to the BS 3356:1990 test method revealed a very small increase from 2.45 cm to 2.61 cm (+7%), though its respective flexural rigidity (1) increased from 205.88 to 426.71 mg cm (+107%), which is a consequence of the added weight. This new value indicates the knitted fabric now behaves as a twill ¼ cotton fabric or a twill 2/1 kermel/viscose of the same approximate GSM [30]. The effect of the presence of PDMS on flexural rigidity was studied in the previous chapter. In that study, the flexural rigidity of a PEDOT:PSS/PDMS conductive polymer composite printed fabric was lower than the same fabric printed with pristine PEDOT:PSS. Therefore, the flexibility of the conductive fabric used for the construction of the EEG electrodes is also better than a pristine PEDOT:PSS printed fabric. Most importantly, the current conductive polymer composite printing caused an improvement in tensile strength i.e. from 68.1 to 116.4 N, and a drop in the tensile strain at break i.e. from 113 to 86.5%.

The surface morphology analysis using SEM showed an evenly smooth fabric surface with fewer protruding yarn loops after printing and the yarn loop interstices were filled up by the conductive polymer composite. SEM images of the fabric before and after printing are shown in Figures 5.9a and 5.9b, respectively. Therefore, from the mechanical analysis, we can say that the conductive cotton fabric retains its textile texture.

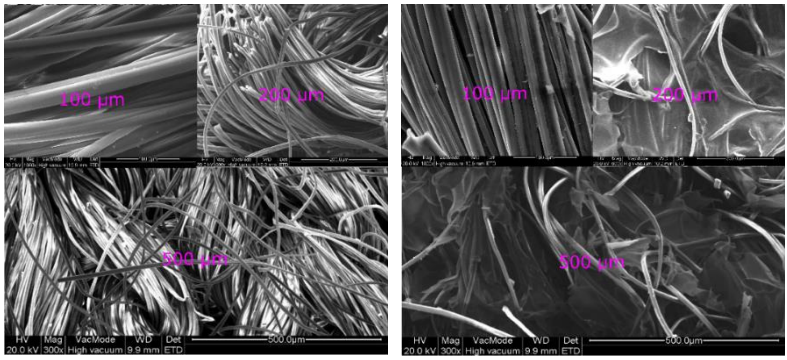

a) b)

Figure 5.9: SEM images: **a**) unprinted bare fabric; **b**) PEDOT:PSS/PDMS-printed knitted cotton fabric

The FT-IR absorption spectra, Figure 5.10, of the bare cotton fabric and PEDOT:PSS/PDMS-printed cotton fabric showed cellulose characteristic FT-IR peaks, i.e. O–H (3331.86 and 3331.85 cm^{-1}) [31], C-H (2889.82 and 2867.77 cm^{-1}) [32] and C–O (1052.58 and 1049.59 cm^{-1}) [33] stretching vibrations, respectively, as does the knitted cotton substrate used. In the presence of BTCA, the O-H stretching is disappeared and the C-H and C-O stretching vibrations are shifted to 2879.28 and 1054.27 cm^{-1}, respectively, which could be due to the esterification of cellulose with BTCA. The peaks in the spectrum at 830.98 and 882.89 cm^{-1} are attributed to the C-S stretching vibrations [34] of the thiophene ring of the PEDOT. The peaks at 1313.44 and 1401.71 cm^{-1} attributed to the S=O symmetric stretching [35] of the sulfonate of the PSS. The peak at, 1162.98 cm^{-1} attributed to the Si-O-Si stretching [36] confirms the presence of the PDMS. At 1707.04 cm^{-1} attributed to C=O [37] appeared which confirms the presence of conjugated ester bonds BTCA. This bond did not appear in raw cotton, while for the PEDOT:PSS sample only a small 1723.58 cm^{-1} peak attributed to C=O [38] is present. Finally, the FT-IR test confirms the presence of PEDOT:PSS/PDMS and BTCA on cotton fabric. Thus, the FT-IR test confirms the presence of PEDOT:PSS/PDMS and BTCA on cotton.

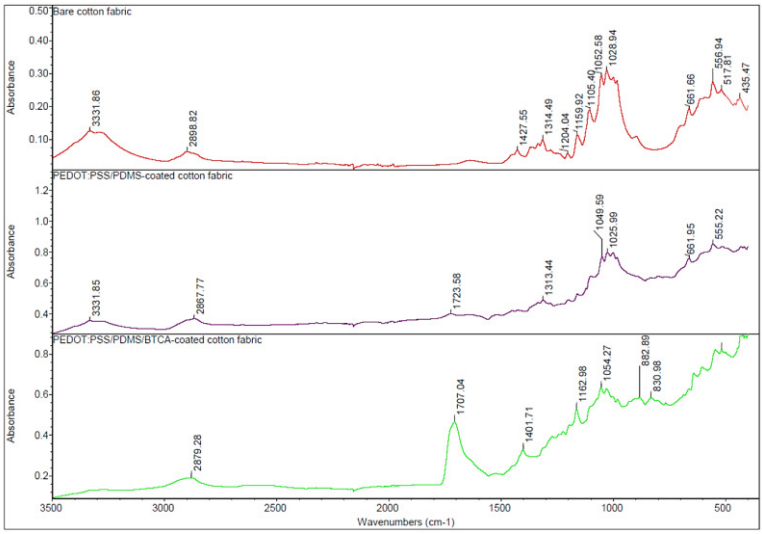

Figure 5.10: Fourier transform infrared spectroscopy absorption spectra of bare cotton fabric and PEDOT:PSS/PDMS-printed cotton fabric

5.3.2. Electrical Property Analysis

The surface resistance and resistivity of the PEDOT:PSS/PDMS-printed knitted cotton fabrics were measured at five different positions of the fabric (top-left, bottom-left, top-right, bottom-right, and center of a 25 cm^2 printed fabric) via a four-probe MR-1 Surface Measurement Instrument was 67.08, 67.19, 67.09, 67.78 and 67.03 Ω/sq and 1.34, 1.33, 1.33, 1.34, and 1.32 Ω cm, respectively. Therefore, the average sheet resistance and resistivity with their standard deviation and margin of error are 67.23 ±0.27 (±0.41%) Ω/sq and 1.33 ±0.007 (±0.55%) Ω cm, respectively, at a 95% confidence interval (CI). This indicates that printing uniformity and distribution of the conductive component over the fabric surface were good.

Moreover, the conductive fabric stayed conductive for up to 20 washing cycles. The sheet resistance of 20 times washed conductive fabric at five different positions was 68.13, 67.81, 67.25, 67.47, and 67.96 Ω/sq and the average with its standard deviation and margin of error is thus 67.72 ±0.32 (±0.47%) Ω/sq. Though a very small increase in sheet resistance was observed (+0.73%), the difference was found to be not significant providing 5.32 *f*-ratio and 0.05 *p*-values at a 95% CI based on One-way ANOVA. This good washing fastness is due to the use of BTCA as a fixing agent.

5.3.3. Skin-to-Electrode Contact Impedance

At the beginning of the measurement, the skin-to-electrode contact impedance of the circular textrode (π cm^2) at alpha frequency was higher than the Ag/AgCl dry electrode. But, it becomes lower after 3 minutes as shown in Figure 5.11a, the average numerical results of five replicas are provided in Table 5.1. These results could be because perspiration can wick to the textrode but not to the Ag/AgCl dry electrode i.e. metal. The one-way ANOVA at a 95% CI showed the skin-to-electrode contact impedance of the textrode and Ag/AgCl dry electrode is significantly different after three minutes providing an *f*-ratio value of 20.97 and *p*-value of <0.05. Moreover, the skin-to-electrode contact impedance of the textrode also significantly dropped at a 95% CI after three minutes. The One-way ANOVA test before and after three minutes resulted in an *f*-ratio value of 165.59 and a *p*-value of < 0.05. Most importantly, the skin-to-electrode contact impedance after three minutes stayed strongly uniform in the textrode as shown in Figure 5.11a. Thus, the textrode could have a potential advantage over the Ag/AgCl dry electrode for long-term monitoring, especially for wearable applications. Moreover, the impedance is less than 5 kΩ [39], so it fulfills the requirement to be used as an EEG electrode. Besides, the coefficient of determination (R^2) indicated that more than 90% of the response data are around the mean as shown in Figure 5.11a.

From the IVIUM potentiostat, it was observed that the PEDOT:PSS/PDMS-printed textrode gives similar skin-to-electrode impedance to Ag/AgCl dry electrode in the frequency range of 10 Hz to 60 Hz as shown in Figure 5.11b. However, the results are significantly different according to One-way ANOVA with a *p*-value of 0.06 for the frequency less than 10 Hz, PEDOT:PSS/PDMS-printed textrode gives higher skin-to-electrode impedance than Ag/AgCl dry electrode.

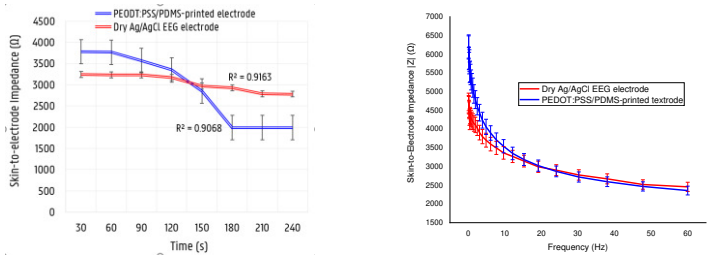

a) b)

Figure 5.11: Skin-to-electrode impedance condition of the PEDOT:PSS/PDMS-printed textrode and dry Ag/AgCl electrode: a) from an OpenBCI board that possesses an ADS1299; b) from IVIUM potentiostat.

Table 5.1: Comparison of the skin-to-electrode impedance

	Commercial dry electrode						Textile-based electrode					
Time (s)	Z_{act}	Z_{raw}	V_{avg}	V_{pp}	V_{fil}	V_{raw}	Z_{act}	Z_{raw}	V_{avg}	V_{pp}	V_{fil}	V_{raw}
30	3239.55	8239.55	49.44	77.67	19.5	54.91	3779.75	8779.75	52.68	82.76	20.77	58.51
60	3235.05	8235.05	49.41	77.62	19.48	54.88	3767.74	8767.74	52.61	82.64	20.75	58.43
90	3233.55	8233.55	49.4	77.61	19.48	54.87	3568.17	8568.17	51.41	80.76	20.27	57.1
120	3169.02	8169.02	49.01	77	19.33	54.44	3350.59	8350.59	50.1	78.71	19.76	55.65
150	2970.95	7970.95	47.83	75.13	18.86	53.12	2852.41	7852.41	47.11	74.02	19.11	52.33
180	2924.43	7924.43	47.55	74.7	17.33	52.81	1991.09	6991.09	41.95	65.9	14.67	46.59
210	2790.88	7790.88	46.75	73.44	16.35	51.92	1989.59	6989.59	41.94	65.88	14.66	46.58
240	2781.88	7781.88	46.69	73.35	16.33	51.86	1991.09	6991.09	41.95	65.9	14.66	46.59

Key

- V_{raw} = Raw RMS Voltage [μV], V_{fil} = Filtered RMS Voltage [uV], V_p = Raw Pick Voltage [μV], V_{avg} = Raw Average Voltage [μV]
- Z_{avg} = Raw Average Impedance [Ω], Z_{act} = Actual Average Impedance [Ω]

5.3.4. EEG Signal Analysis against Standard Electrodes

The EEG signals recorded by the textrode were comparable to Ag/AgCl dry electrode. The textrode gave a similar range of bandwidth. The EEG signals from both the textrode and Ag/AgCl dry electrode are shown in Figures 5.12a and 5.12b respectively. Moreover, the amplitude of the signal was as high as the Ag/AgCl dry electrode. The five-second-average amplitudes of the textrode and Ag/AgCl dry electrode for a 3-minute EEG measurement is shown in Figure 5.12c.

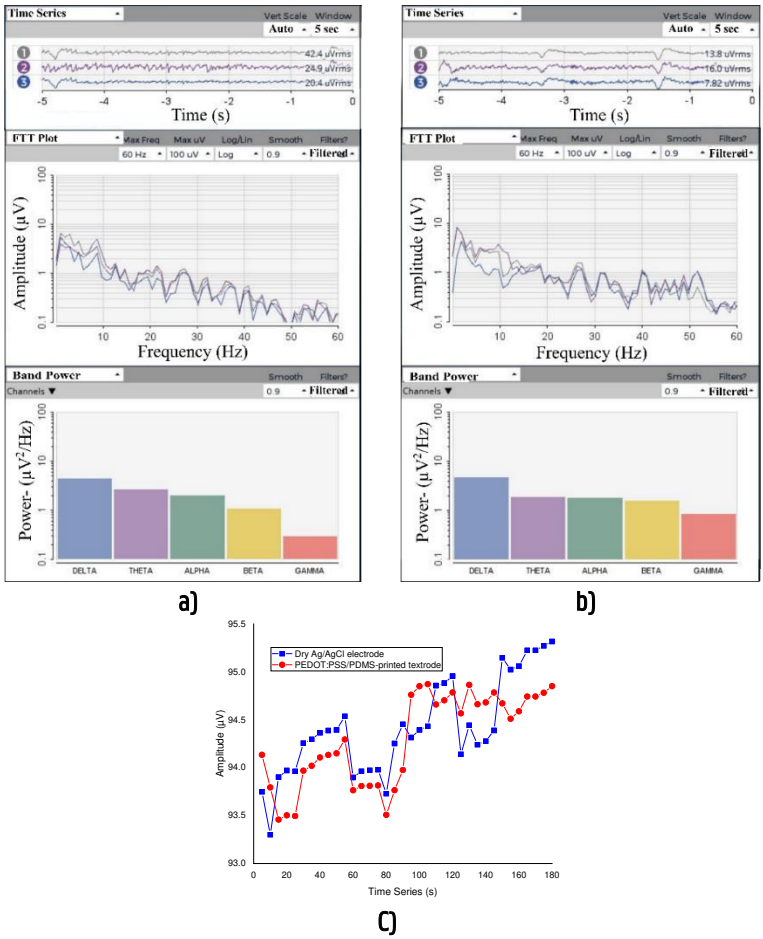

Figure 5.12: a) EEG signal from silver-silver chloride commercial dry electrode tested at 1–50 Hz bandpass filter; **b**) EEG signal from textile-based electrode tested at 1–50 Hz bandpass; **c**) five-second-average EEG amplitudes of dry Ag/AgCl and PEDOT:PSS/PDMS-printed cotton electrodes.

5.3.5. ITC, ERSP and PSD

The output graph of inter-trial coherence (ITC) from the textrode and the dry Ag/AgCl electrodes was compared using EEGLAB software. ITC shows the degree of a tendency for the data phase at each frequency to be in the same phase in each trial. It is a measure of phase consistency over trials. In each plot, the frequency range and the time range are placed on the y-axis and x-axis, respectively, and a color scale is used where green is for non-significant, and red represents significant ITC at a 99% confidence interval (CI). Beneath each ITC plot is the averaged ERSP response for that individual (in blue), in microvolts.

The amplitude scale for the ITC response is fairly similar for both the textrode and Ag/AgCl dry electrodes from 1 to 50 Hz frequency. To the left of each ITC plot, the average power is shown for that electrode at each frequency, while a black dotted line shows the significance threshold at each frequency relative to the baseline period at a 99% confidence level. The ITC and ERSP phases of the Ag/AgCl dry electrode and textrode are shown in Figures 5.13a and 5.13b, respectively. From EEGLAB software analysis, the maximum log power spectral density (PSD) for both the textrode and Ag/AgCl dry electrode was ~95 $\mu V^2/Hz$. The PSD graph is also shown in Figure 5.13c.

5.3.6. Clinical EEG Result

From the EEG clinical line measurement, it was observed that the PEDOT:PSS/PDMS-printed textile can collect EEG signals, as shown in Figure 5.14a. The ITC and ERSP were also found to be identical with Ag/AgCl dry electrodes. The EEG signals, ITC, and ERSP graphs for the textile-based electrode and Ag/AgCl dry electrodes are shown in Figures 5.14b and 5.14c. This indicates that the PEDOT/PSS/PDMS-printed textile electrodes are promising for EEG measurement in brain activity monitoring, especially for wearable applications.

5.3.7. Effect of Bending on EEG Signal Quality

The EEG signals for three active electrodes at a 1–50 Hz bandpass filter before and after bending are shown in Figure 5.15. The numbers (1, 2, and 3) in the vertical axis in Figure 5.15-19 represent the active electrodes E1, E2, and E3, respectively. The five-second-average amplitudes of the textrodes at different bending cycles for a 3-minute EEG measurement are shown in Figure 5.15c. The electrodes showed good EEG signals up to 60 cycles of bending to a 5mm radius.

Based on the one-way ANOVA Tukey HSD Test at a 95% CI, the difference of the means of the maximum voltage amplitude up to the 60 bending cycles was insignificant giving Tukey HSD *p*-values of 2.34. This robustness to bending could be due to the presence of PDMS elastomer that contributes much to the flexibility of the conductive fabric and so to the electrode.

5.3.8. Effect of Multiple and Continuous Use on EEG Signal Quality

The washed textrode has been used five times and collected clear signals and similar amplitudes as the unwashed electrode used for the first time. Moreover, the electrodes were also tried for 8 hours of continuous use and no variation in the quality of signal acquisition was observed. In this test, the result was not collected for 8 hours but electrodes were simply placed on the forehead for 8 hours, and then the actual measurement was done after that. The one-way ANOVA Tukey HSD Test at a 95% CI on the multiple and continuous tests proved that there were no significant differences in the mean of the voltage amplitude. The HSD Tukey *p*-values were 0.80 and 0.43 for the multiple and continuous use test, respectively. Their respective EEG signals at 1–50 Hz bandpass filter are shown in Figures 5.16a and 5.16b, respectively. The five-second-average amplitudes of the textrodes at different multiple and continuous uses for a 3-minute EEG measurement are shown in Figure 5.15c.

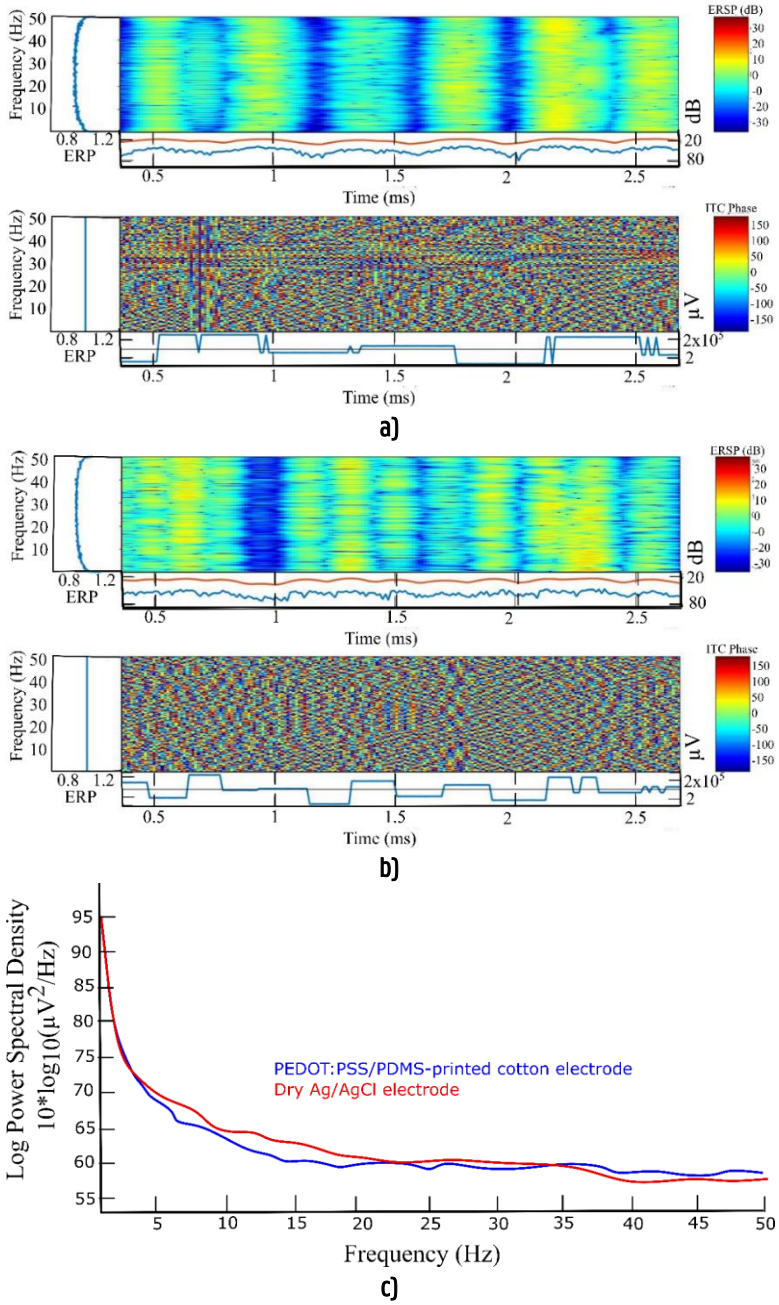

Figure 5.13: ITC and ERSP responses (**a** and **b**): **a**) Ag/AgCl dry electrode CDEs; **b**) textile-based electrode; **c**) PSD plots of the dry Ag/AgCl electrode and textile-based electrode.

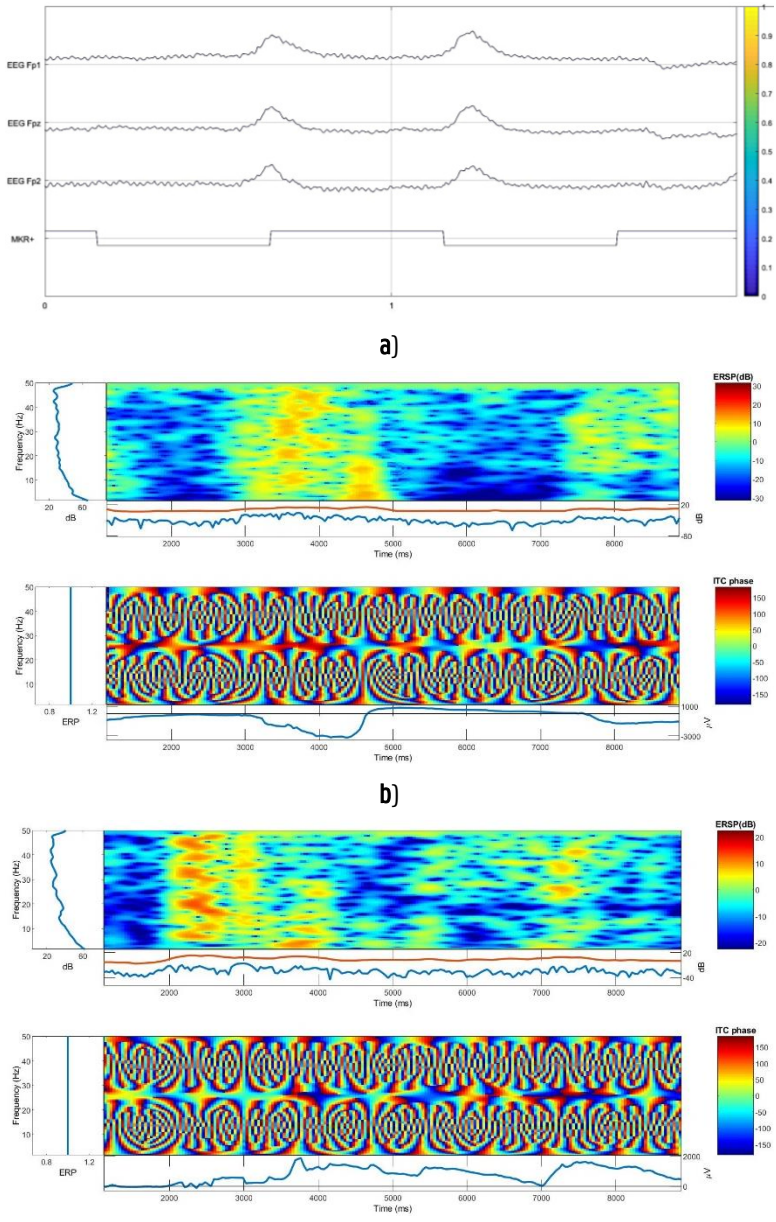

Figure 5.14: a) Electroencephalography (EEG) signals from the textile electrode with the clinical system; (**b**,**c**) event-related spectral perturbation (ERSP) and intertrial coherence (ITC) plots: **b**) textile electrode and **c**) dry Ag/AgCl electrode.

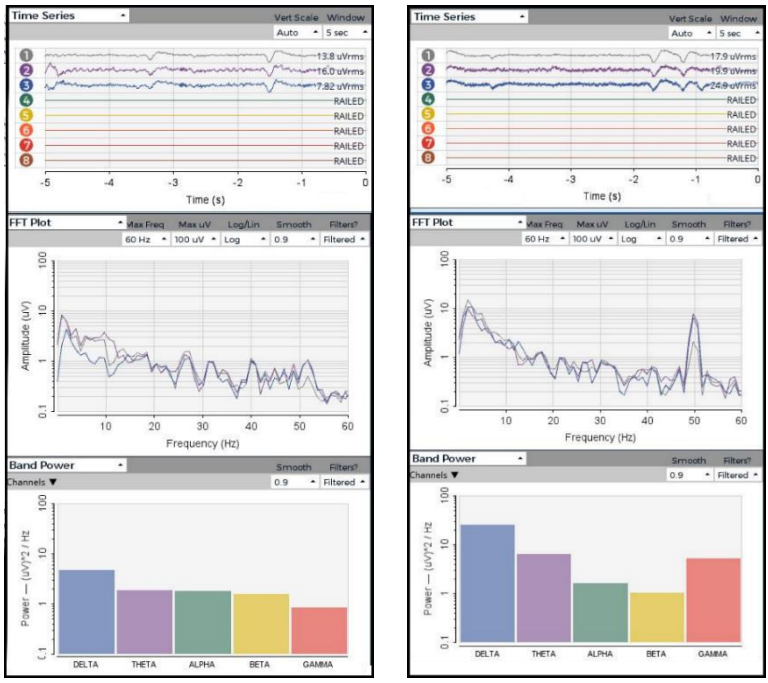

a) b)

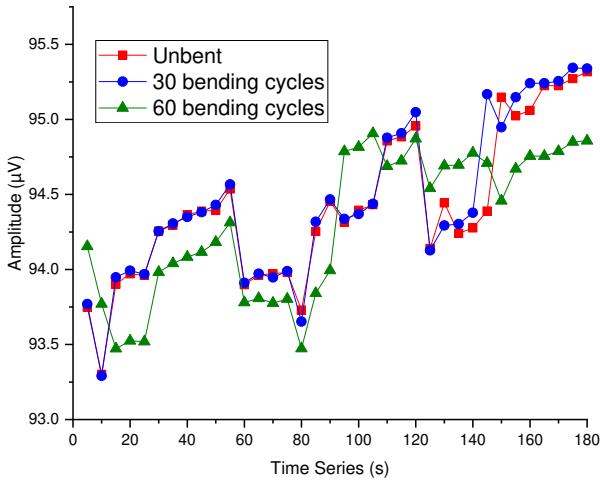

c)

Figure 5.15: Effect of bending on signal stability tested at 1–50 Hz bandpass filter: a) unbent; **b**) 60 bending cycles; **c**) five-second-average EEG amplitudes at different bending cycles.

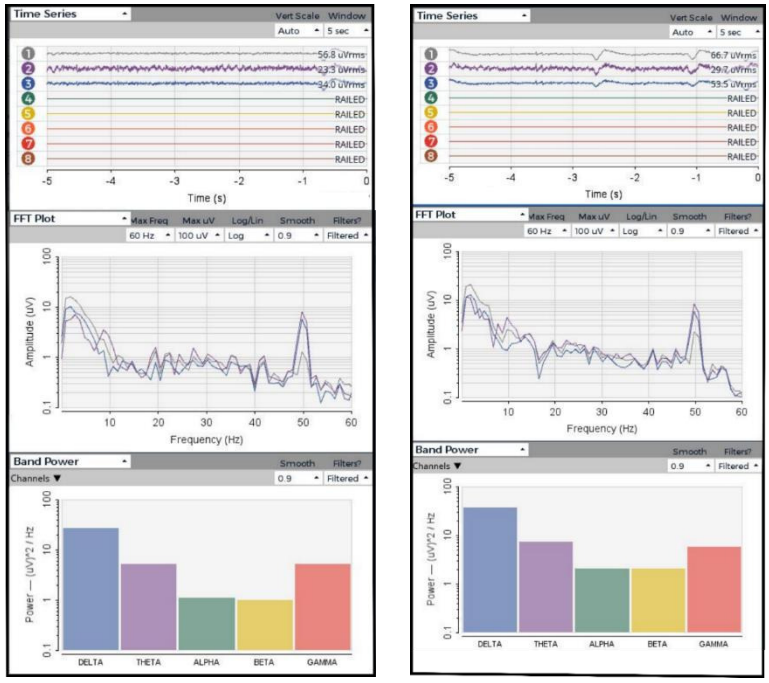

Figure 5.16: Effect of multiple and continuous uses on signal stability tested at 1–50 Hz bandpass filter: **a**) 5 multiple uses; **b**) 8 hours continued use; **c**) five-second-average EEG amplitudes of multiple and continuous uses.

5.3.9. Effect of Washing on EEG Signal Quality

The textrode constructed from 15 cycles of washed conductive fabric gave almost similar signals to unwashed ones. The EEG signal at 1–50 Hz bandpass filter before and after 15 washing cycles are shown in Figures 5.17 and 5.17b, respectively. The five-second-average amplitudes of the textrodes at different washing cycles for a 3-minute EEG measurement are shown in Figure 5.17c. Based on a one-way ANOVA Tukey HSD Test at a 95% CI, the Tukey HSD p-value was 0.09 for 15 washing cycles. The improvement in the washing fastness is because of BTCA which was intentionally incorporated during the printing for this purpose. The PEDOT:PSS/PDMS could become fixed to cotton using the polycarboxylic acid crosslinker BTCA, a group of widely used durable press crosslinkers in the textile industry in the presence of sodium hypophosphite (SHPI) catalyst. SHPI is a widely used catalyst with BTCA. According to a US patent, the catalyst can be effective in the range of 0.3% (3 g/l) to 11% of the crosslinker [40]. For this work the median ratio i.e. 5.5% has been used.

BTCA possesses four carboxylic acid groups and one to three of the carboxylic acid groups are involved in an esterification reaction with cotton by the formation of a five-membered cyclic anhydride through the dehydration of the adjacent carboxyl groups followed by the formation of ester links between the anhydride intermediate and the cellulose of the cotton [41].

5.3.10. Effect of Electrode Size on EEG Signal Quality

The dry Ag/AgCl EEG electrode is 1 cm in diameter. However, at this size, the signal qualities of the textrode are not satisfactory, resulting for example during blinking in artifacts such as very wavy signals. Hence, the size was doubled. The effect of electrode size on EEG signal acquisition is shown in Figure 5.18a-c. As shown in Figure 5.18d, the voltage amplitude was also significantly affected by the size of the electrode, the larger the electrode the bigger the amplitude. Based on the one-way ANOVA Tukey HSD test at a 95% confidence level, reducing the 2 cm electrode by half or doubling the size caused a significant difference in the voltage amplitude of the EEG signals, providing a Tukey HSD p-value of less than 0.01. But, there is no bandwidth shift, though there is an intensity difference, during decreasing by half and doubling the size of the electrode and collected clear signals even to visual observation. However, for EEG electrodes, smaller electrodes are preferable. Therefore, a 2cm diameter textrode that gave similar amplitude to dry Ag/AgCl electrodes were chosen for further comparisons.

5.3.11. Effect of Shape on EEG Signal Quality

With the shape, as shown in Figure 5.19a-c, the signal did not show any influence on the quality when observed visually. However, the voltage amplitude was highly affected as shown in Figure 5.19d, within decreasing order of the circular electrode, rectangular square, and lowest value for the equilateral triangle, with Tukey HSD *p*-values of less than 0.01, based on a one-way ANOVA Tukey HSD Test at a 95% CI. Besides, rectangular and triangular electrodes need bigger space to place on the skin as they have pointed tips. Thus, the circular electrode is preferable.

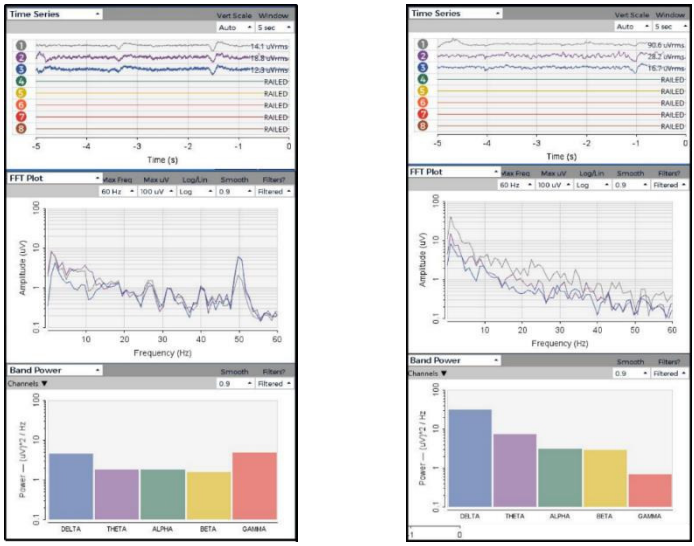

Figure 5.17: Stability of signal quality to washing tested at 1–50 Hz bandpass filter: **a**) unwashed textile electrode (TE); **b**) TE after 15 washing cycles; **c**) five-second-average EEG amplitudes at different washing cycles.

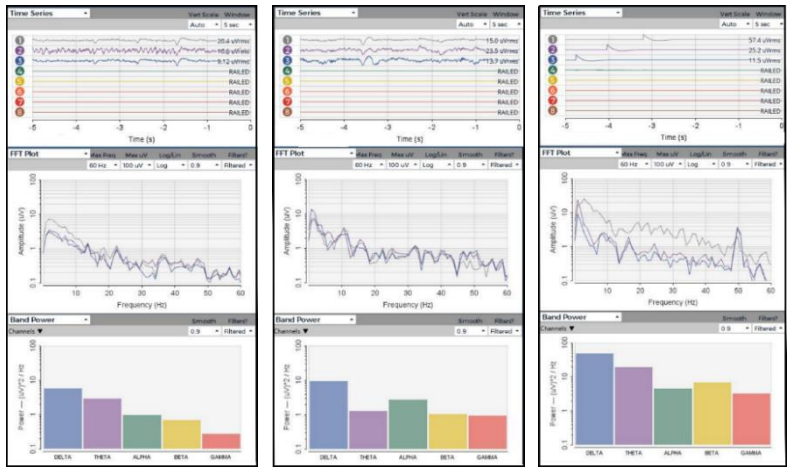

a) b) c)

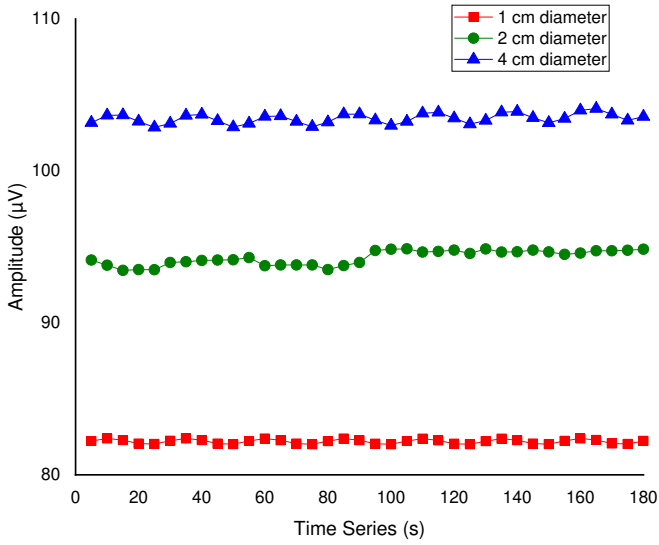

d)

Figure 5.18: Effect of electrode size on signal stability tested at 1–50 Hz bandpass filter: **a**) 1 cm diameter circular electrode; **b**) 2 cm diameter circular electrode; **c**) 4 cm diameter circular electrode; **d**) five-second-average EEG amplitudes of the different size textrodes.

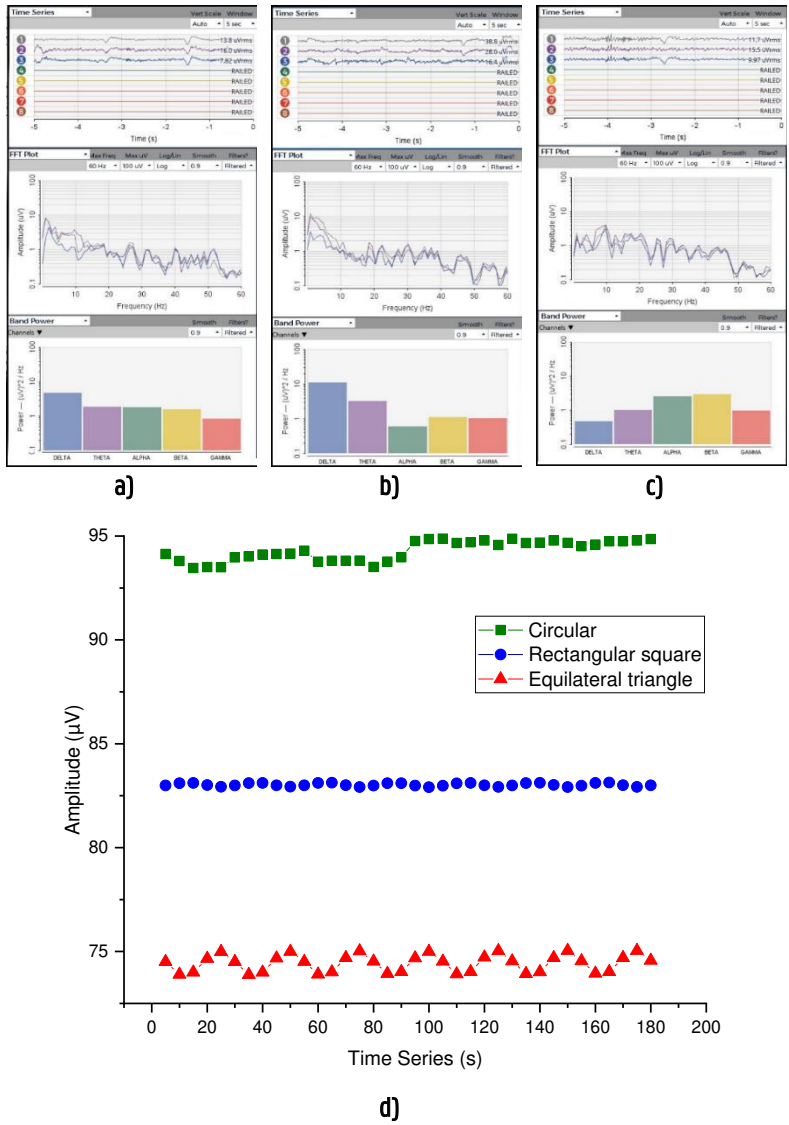

Figure 5. 19: Effect of electrode shape on signal stability tested at 1–50 Hz bandpass filter: **a**) π cm^2 circular electrode **b**) π cm^2 rectangular square electrode; **c**) π cm^2 equilateral triangle electrode; **d)** five-second-average EEG amplitudes of the different shape textrodes.

5.4. Conclusion

The demand for more comfortable and user-friendly electrodes has led to the development of an increasing number of dry EEG electrodes that can overcome the limitations of wet electrodes, however, the commercial electrodes are metal-based and still lack flexibility, while they are also relativity heavy, which makes them unsuitable for wearable applications. Therefore, the use of textile electrodes would overcome these associated problems. This work explored textrodes suitable for long-term brain activity monitoring, especially for wearable applications.

In this work, we have successfully developed a machine-washable, flexible and lightweight textile-based dry electrode from PEDOT:PSS/PDMS-printed cotton fabric that collects good quality EEG signals comparable to the commercially available metal-based dry electrodes. Moreover, the impedance of the textrode is lower than that of the Ag/AgCl dry electrode after 3 minutes and gives a higher signal-to-noise ratio.

The performance and durability of textile-based electrodes are crucial factors to consider for biomedical applications. Moreover, conductive polymer-based electrodes are demanded various flexible electronic industrial products, however, their performance after washing is unconventional, yet important to be considered. This experiment explores the robustness and reliability of conductive PEDOT:PSS/PDMS-printed cotton fabric EEG textrode. Various factors such as washing, bending, continuous, and multiple uses were considered. The effect of electrode size and shape on EEG signal quality has also been studied. This EEG textrode showed good stability up to 15 machine-washing cycles, 60 bending cycles, 5 multiple reuses, and 8 hours of continuous use. Circular electrodes with a 2 cm diameter achieved better results in collecting clear EEG signals. Most importantly, the electrode does not need a gel to achieve a connection to the skin, unlike common clinical practice.

Bibliography

[1] S. Wunder, A. Hunold, P. Fiedler, F. Schlegelmilch, K. Schellhorn, and J. Haueisen, "Novel bifunctional cap for simultaneous electroencephalography and transcranial electrical stimulation," *Sci. Rep.*, vol. 8, no. 1, pp. 1–11, 2018, doi: 10.1038/s41598-018-25562-x.

[2] J. Wu, W. Jia, C. Xu, D. Gao, and M. Sun, "Impedance analysis of ZnO nanowire coated dry EEG electrodes," *J. Biomed. Eng. Inform.*, vol. 3, no. 1, p. 44, 2017, doi: 10.5430/jbei.v3n1p44.

[3] H. Li *et al.*, "Textile-based ECG acquisition system with capacitively coupled electrodes," *Trans. Inst. Meas. Control*, vol. 39, no. 2, pp. 141–148, 2017, doi: 10.1177/0142331215600254.

[4] L. Kirkup and A. Searle, "A direct comparison of wet, dry and insulating bioelectric recording electrodes," *Physiol. Meas.*, 2000.

[5] M. A. Lopez-Gordo, D. Sanchez Morillo, and F. Pelayo Valle, "Dry EEG electrodes," *Sens. Switz.*, vol. 14, no. 7, pp. 12847–12870, 2014, doi: 10.3390/s140712847.

[6] H. L. Peng *et al.*, "A novel passive electrode based on porous Ti for EEG recording," *Sens. Actuators B Chem.*, vol. 226, pp. 349–356, 2016, doi: 10.1016/j.snb.2015.11.141.

[7] F. Wang, G. Li, J. Chen, Y. Duan, and D. Zhang, "Novel semi-dry electrodes for brain–computer interface applications," *J. Neural Eng.*, vol. 13, no. 4, p. 046021, Aug. 2016, doi: 10.1088/1741-2560/13/4/046021.

[8] R. Kannan, S. S. A. Ali, A. Farah, S. H. Adil, and A. Khan, "Smart Wearable EEG Sensor," *Procedia Comput. Sci.*, vol. 105, no. December 2016, pp. 138–143, 2017, doi: 10.1016/j.procs.2017.01.193.

[9] N. M. Kumar and G. Thilagavathi, "Design and Development of Textile Electrodes for EEG Measurement using Copper Plated Polyester Fabrics," *Jtatm*, vol. 8, no. 4, 2014.

[10] J. Löfuede, F. Seoane, and M. Thordstein, "Soft textile electrodes for EEG monitoring," *Proc. IEEEEMBS Reg. 8 Int. Conf. Inf. Technol. Appl. Biomed. ITAB*, no. Figure 1, pp. 4–7, 2010, doi: 10.1109/ITAB.2010.5687755.

[11] N. Muthukumar, G. Thilagavathi, and T. Kannaian, "Polyaniline-coated foam electrodes for electroencephalography (EEG) measurement," *J. Text. Inst.*, vol. 107, no. 3, pp. 283–290, 2016, doi: 10.1080/00405000.2015.1028248.

[12] P. Salvo, R. Raedt, E. Carrette, D. Schaubroeck, J. Vanfleteren, and L. Cardon, "A 3D printed dry electrode for ECG/EEG recording," *Sens.*

Actuators Phys., vol. 174, pp. 96–102, Feb. 2012, doi: 10.1016/j.sna.2011.12.017.

[13] P. Leleux *et al.*, "Conducting Polymer Electrodes for Electroencephalography," *Adv. Healthc. Mater.*, vol. 3, no. 4, pp. 490–493, Apr. 2014, doi: 10.1002/adhm.201300311.

[14] L. M. Ferrari, U. Ismailov, J.-M. Badier, F. Greco, and E. Ismailova, "Conducting polymer tattoo electrodes in clinical electro- and magneto-encephalography," *Npj Flex. Electron.*, vol. 4, no. 1, p. 4, Dec. 2020, doi: 10.1038/s41528-020-0067-z.

[15] B. J. Worfolk *et al.*, "Ultrahigh electrical conductivity in solution-sheared polymeric transparent films," *Proc. Natl. Acad. Sci.*, vol. 112, no. 46, pp. 14138–14143, Nov. 2015, doi: 10.1073/pnas.1509958112.

[16] E. Zeglio, A. L. Rutz, T. E. Winkler, G. G. Malliaras, and A. Herland, "Conjugated Polymers for Assessing and Controlling Biological Functions," *Adv Mater*, p. 66, 2019.

[17] L. Bießmann, N. Saxena, N. Hohn, M. A. Hossain, J. G. C. Veinot, and P. Müller-Buschbaum, "Highly Conducting, Transparent PEDOT:PSS Polymer Electrodes from Post-Treatment with Weak and Strong Acids," *Adv. Electron. Mater.*, vol. 5, no. 2, p. 1800654, Feb. 2019, doi: 10.1002/aelm.201800654.

[18] M. Bełanger and Y. Marois, "Hemocompatibility, biocompatibility, inflammatory and in vivo studies of primary reference materials low-density polyethylene and polydimethylsiloxane: A review," *J Biomed Mater Res*, p. 11, 2001, doi: https://doi.org/10.1002/jbm.1043.

[19] M. De Ville, P. Coquet, P. Brunet, and R. Boukherroub, "Simple and low-cost fabrication of PDMS microfluidic round channels by surface-wetting parameters optimization," *Microfluid. Nanofluidics*, vol. 12, no. 6, pp. 953–961, May 2012, doi: 10.1007/s10404-011-0929-8.

[20] F. Akther, S. B. Yakob, N.-T. Nguyen, and H. T. Ta, "Surface Modification Techniques for Endothelial Cell Seeding in PDMS Microfluidic Devices," *Biosensors*, vol. 10, no. 11, p. 182, Nov. 2020, doi: 10.3390/bios10110182.

[21] I. Karbovnyk *et al.*, "Effect of Radiation on the Electrical Properties of PEDOT-Based Nanocomposites," *Nanoscale Res. Lett.*, vol. 11, no. 1, p. 84, Dec. 2016, doi: 10.1186/s11671-016-1293-0.

[22] J. George and S. Sabapathi, "Cellulose nanocrystals: synthesis, functional properties, and applications," *Nanotechnol. Sci. Appl.*, p. 45, Nov. 2015, doi: 10.2147/NSA.S64386.

[23] W. Jia, J. Wu, D. Gao, M. Sun, and R. J. Sclabassi, "Characteristics of skin-electrode impedance for a novel screw electrode," in *2014 40th Annual*

Northeast Bioengineering Conference (NEBEC), Boston, MA, USA, Apr. 2014, pp. 1–2. doi: 10.1109/NEBEC.2014.6972825.

[24] J. L. Vargas Luna, M. Krenn, J. A. Cortés Ramírez, and W. Mayr, "Dynamic Impedance Model of the Skin-Electrode Interface for Transcutaneous Electrical Stimulation," *PLOS ONE*, vol. 10, no. 5, p. e0125609, May 2015, doi: 10.1371/journal.pone.0125609.

[25] OpenBCI, "Impedance of Electrodes on my Head." https://openbci.com/community/impedance-of-electrodes-on-my-head/ (accessed Jun. 14, 2020).

[26] "OpenBCI: Measuring Electrode Impedance." https://eeghacker.blogspot.com/2014/04/openbci-measuring-electrode-impedance.html (accessed Jun. 14, 2020).

[27] TEXAS INSTRUMENTS, "ADS1299-x Low-Noise, 4-, 6-, 8-Channel, 24-Bit, Analog-to-Digital Converter for EEG and Biopotential Measurements." 2017. [Online]. Available: https://www.ti.com/lit/ds/symlink/ads1299.pdf

[28] Y.-H. Chen *et al.*, "Soft, Comfortable Polymer Dry Electrodes for High Quality ECG and EEG Recording," *Sensors*, vol. 14, no. 12, pp. 23758–23780, Dec. 2014, doi: 10.3390/s141223758.

[29] G. H. Klem, H. O. LuÈders, H. H. Jasper, and C. Elger, "The ten±twenty electrode system of the International Federation," *Int. Fed. Clin. Neurophysiol. Electroencephalogr Clin Neurophysiol Suppl*, vol. 52, pp. 3–6, 1999.

[30] A. B. H. Musa, B. Malengier, S. Vasile, L. Van Langenhove, and A. De Raeve, "Analysis and Comparison of Thickness and Bending Measurements from Fabric Touch Tester (FTT) and Standard Methods," *Autex Res. J.*, vol. 18, no. 1, pp. 51–60, Mar. 2018, doi: 10.1515/aut-2017-0011.

[31] M. F. Rosa *et al.*, "Cellulose nanowhiskers from coconut husk fibers: Effect of preparation conditions on their thermal and morphological behavior," *Carbohydr. Polym.*, vol. 81, no. 1, pp. 83–92, May 2010, doi: 10.1016/j.carbpol.2010.01.059.

[32] M. Poletto, V. Pistor, M. Zeni, and A. J. Zattera, "Crystalline properties and decomposition kinetics of cellulose fibers in wood pulp obtained by two pulping processes," *Polym. Degrad. Stab.*, vol. 96, no. 4, pp. 679–685, Apr. 2011, doi: 10.1016/j.polymdegradstab.2010.12.007.

[33] V. Tserki, P. Matzinos, S. Kokkou, and C. Panayiotou, "Novel biodegradable composites based on treated lignocellulosic waste flour as filler. Part I. Surface chemical modification and characterization of waste flour," *Compos. Part Appl. Sci. Manuf.*, vol. 36, no. 7, pp. 965–974, Jul. 2005, doi: 10.1016/j.compositesa.2004.11.010.

[34] Y.-H. Cheng, C.-W. Kung, L.-Y. Chou, R. Vittal, and K.-C. Ho, "Poly(3,4-ethylenedioxythiophene) (PEDOT) hollow microflowers and their application for nitrite sensing," *Sens. Actuators B Chem.*, vol. 192, pp. 762–768, Mar. 2014, doi: 10.1016/j.snb.2013.10.126.

[35] E. Susanti, P. Wulandari, and Herman, "Effect of localized surface plasmon resonance from incorporated gold nanoparticles in PEDOT:PSS hole transport layer for hybrid solar cell applications," *J. Phys. Conf. Ser.*, vol. 1080, p. 012010, Aug. 2018, doi: 10.1088/1742-6596/1080/1/012010.

[36] G. Anbalagan, A. R. Prabakaran, and S. Gunasekaran, "Spectroscopic characterization of indian standard sand," *J. Appl. Spectrosc.*, vol. 77, no. 1, pp. 86–94, Mar. 2010, doi: 10.1007/s10812-010-9297-5.

[37] J. Chungprempree, S. Charoenpongpool, J. Preechawong, N. Atthi, and M. Nithitanakul, "Simple Preparation of Polydimethylsiloxane and Polyurethane Blend Film for Marine Antibiofouling Application," *Polymers*, vol. 13, no. 14, p. 2242, Jul. 2021, doi: 10.3390/polym13142242.

[38] K. M. George *et al.*, "FT-IR quantification of the carbonyl functional group in aqueous-phase secondary organic aerosol from phenols," *Atmos. Environ.*, vol. 100, pp. 230–237, Jan. 2015, doi: 10.1016/j.atmosenv.2014.11.011.

[39] T. C. Ferree, P. Luu, G. S. Russell, and D. M. Tucker, "Scalp electrode impedance, infection risk, and EEG data quality," *Clin. Neurophysiol.*, vol. 112, no. 3, pp. 536–544, Mar. 2001, doi: 10.1016/S1388-2457(00)00533-2.

[40] C. M. Welch, "Formaldehyde-free durable-press finishes," *Rev. Prog. Color. Relat. Top.*, vol. 22, no. 1, pp. 32–41, Oct. 2008, doi: 10.1111/j.1478-4408.1992.tb00087.x.

[41] C. Q. Yang, "Infrared spectroscopy studies of the cyclic anhydride as the intermediate for the ester crosslinking of cotton cellulose by polycarboxylic acids. I. Identification of the cyclic anhydride intermediate," *J. Polym. Sci. Part Polym. Chem.*, vol. 31, no. 5, pp. 1187–1193, Apr. 1993, doi: 10.1002/pola.1993.080310514.

6. Validating EEG Textrodes with a Textile-Based Head Phantom

In Chapter 5, the EEG signals were collected directly from a human. Though EEG waves have been found, it was observed that maintaining the human mind at a constant state was hardly possible. Besides, it was also difficult to identify noise and signals. Therefore, a head phantom was developed. Thus, this chapter presents the validation of EEG textrodes on a novel long-lasting textile-based anatomically realistic head phantom. The performance of the durable textile-based head phantom has been compared with a gelatin-based head phantom. Then, the PEDOT:PSS/PDMS-printed cotton fabric EEG electrode of Chapter 5 has been validated using this textile-based head phantom. The performance of the textile-based electrode has also been compared to a commercial dry Ag/AgCl electrode.

This chapter is redrafted from published journal papers:

G.B. Tseghai, B. Malengier, K.A. Fante, and L. Van Langenhove, "A Long-Lasting Textile-Based Anatomically Realistic Head Phantom for Validation of EEG Electrodes", *Sensors*, 21 (14): 922, 2021. doi.org/10.3390/s21144658.

G.B. Tseghai, B. Malengier, K.A. Fante and L. Van Langenhove, "Validating Poly(3,4-ethylene dioxythiophene) Polystyrene Sulfonate-Based Textile Electroencephalography Electrodes by a Textile-Based Head Phantom", Polymers, 13 (21): 3629, 2021. doi.org/10.3390/polym13213629.

Table of Contents

6.1. Introduction

Measuring the electrical activity in the brain, heart, muscles, etc., using electrodes to know the health condition of humans and/or animals is a common clinical practice. Whatever the nature of the electrodes, it has to be validated before being employed in clinical practices. Thus, in this work, we focused on the validation of PEDOT:PSS/PDMS-based EEG electrodes.

During the validation of EEG electrodes, the brain waves should be collected directly from a human and the validation should be performed in the same state of mind. State of mind, for instance, frustration, concentration, meditation, anxiety, etc. influence brain waves. However, maintaining the human mind stable is not practically possible. It is also difficult to exactly identify the extent of noise and signals as the original currents flowing in the brain are unknown. EEG measurements to monitor brain activity are variable with changes over seconds.

For the validation of EEG electrodes, it is, therefore, required to develop head phantoms that can be used to inject or model a known stable signal. It is required to conduct a test in an environment as realistic as possible with a known ground truth of source location and brain activity. One way to perform this is via digital phantoms which is software that models the propagation of the signal originating within the brain to the electrodes [1]. However, the studies via these digital head phantom are hardly suited to mimic motion artifacts of a realistic EEG or electromagnetic interference noise generated by the power lines and high-power electronic equipment [2]. For that reason, many researchers have developed tangible head phantoms predominantly from ballistic gelatin [3]–[7]. Gelatin-based materials are a good material to be used in phantom applications of human body parts, but unfortunately, this type of phantom has a short life span [8] and is too heavyweight. Examples of gelatin-based head phantoms are shown in Figure 6. 1.

a) b)

Figure 6.1: Examples of gelatin-based phantoms: **a**) from [6]; **b**) from [7].

Recently, Tsizin et al. developed a realistic head phantom mimicking the electromagnetic properties of the head where the internal volume of a human skull was filled with a conductive gel [9]. However, the lifetime of the phantom was only about a month. Other EEG head phantoms [10], [11] prepared by casting were also introduced but still, the casting process is complicated, and the phantoms are heavy and expensive. Therefore, developing a simple lightweight and long-lasting textile-based head phantom would be an important improvement.

The emergence of electrically conductive textiles led textile materials to be used for versatile applications in the electronic and medical industries [12]. Electrically conductive textiles can be developed by different techniques and in different forms [13]. Moreover, the electrical and physical properties of the textile substrate can be easily controlled and the required extent of stretchability, flexibility, and conductivity can be imparted by regulating the substrate, textile construction, and application of the conductive component. Therefore, this work explores the use of e-textiles for a head phantom and then uses the textile head phantom in turn to validate PEDOT:PSS/PDMS-based EEG textrodes.

6.2. Methodology

6.2.1. Head Phantom Construction

A textile-based head phantom was constructed by placing a bi-directional stretchy nylon/spandex (18:7) EeonTex conductive stretchable fabric (obtained from MANDU, Finland) over an anatomically realistic 3D-print polylactic acid (PLA) skull. The conductive fabric has a surface resistivity that can be custom-tuned for specific requirements in the range of 10^4 to 10^7 Ω/sq. To mimic the neurons, twenty (20) 3.5 mm stereo male-male dipole wires were installed underneath the conductive fabric per the 10–20 EEG placement system as shown in Figure 2a. Side to side, a gelatin-based head phantom was also constructed from 900 g gelatin, 40.5 g table salt, and 4.5 L demineralized water according to [14]. Thirty-seven (37) dipole wires were installed inside the ballistic gelatin as shown in Figure 2b. The skull, base-ring, inner-post, and guiding wires have been constructed from PLA using an FDM 3D printer at Ingegno Maker Space (Drongen, Belgium). The photographic images of the constructed textile and gelatin-based head phantoms and their components are shown in Figures 6.2a, and b, respectively.

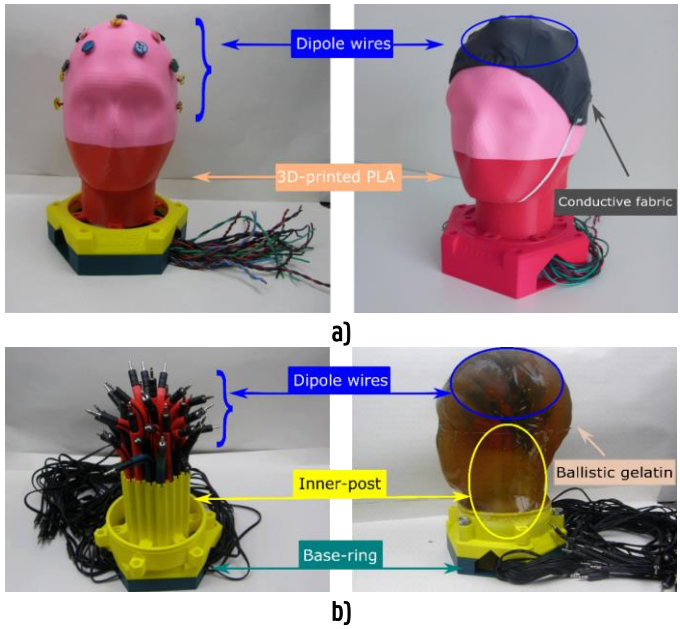

Figure 6.2: Head Phantom: **a**) textile-based; **b**) ballistic gelatin-based.

6.2.2. Textile Electrode Design and Construction

Textile electrodes will be placed on the head phantoms. The textile electrode design and construction were according to Chapter 5, where a 67.23 Ω/sq electrically resistive conductive fabric was employed. As studied in Chapter 4 and Chapter 5, the fabric behaves as a twill 1/4 cotton fabric or a twill 2/1 kermel/viscose of the same approximate gram per square reported by Musa et al. [15]. Five replicas of electrodes with a 2 cm diameter, as shown in Figure 5.5b in Chapter 5, were constructed to examine the repeatability and reproducibility of signal quality. In addition, the signal qualities were compared against a dry Ag/AgCl electrode.

6.2.3. Synthetic Sine Wave Generation

A synthetic sine wave was generated using a portable DDS function signal generator and digital oscilloscope Micsig T01104 (peak to peak voltage 360 mV, maximum voltage 168 mV, minimum voltage −192 mV, frequency 9.925 Hz, duration 50 ms), and then injected into the textile phantom as shown in Figure 6.3. To mimic events, the parameters of the EEG signal were set in the alpha wavelength range and the amplitude was changed to simulate a neural event.

The synthetic sine wave was used for both the phantom-to-electrode impedance and EEG measurements through an active textile electrode connected to an OpenBCI board.

a)

b)

c)

Figure 6.3: Synthetic sine wave generation: **a**) DDS Function Signal Generator; **b**) Micsig TO1104 Digital Oscilloscope; **c**) synthetic sine wave generated by the function generator on a digital oscilloscope

6.2.4. Head Phantom and Textrode Validation

The head phantom replaces a real human head, and EEG electrodes can be attached as one would do to a human. To validate the head phantom and the textrodes, the synthetic sine wave generated in 6.2.3 was injected into the head phantoms and the EEG wave was measured on both types of head phantoms using an active electrode connected to a Cyton biosensing Board (8-channels) of OpenBCI according to the setup in Figure 6.4.

Firstly, the textile-based head phantom was validated with a standard Ag/AgCl dry electrode and then the textrode has been validated with the already validated textile-based head phantom. For the validation, phantom-to-electrode impedance and EEG signal quality parameters such as impedance, FFT, band power, SNR, ITC, and ERSP were used.

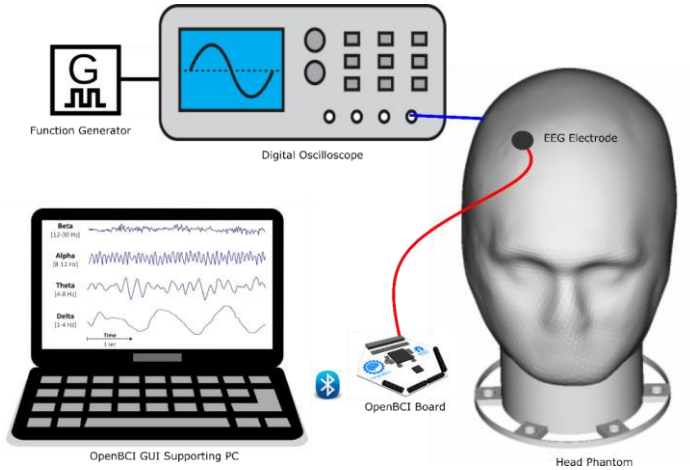

Figure 6.4: Schematic illustration of the EEG measurement-setup

6.2.5. Phantom-to-Electrode Impedance Measurement

The electrical impedance at the skin–to-electrode interface influences the EEG signal quality [16], [17], thus designing a dry electrode with a low skin-contact impedance improves EEG performance. In this work, the term phantom-to-electrode impedance is used as the testing was performed with a head phantom in the EEG alpha band power, not with a human. The textrode used for this experiment was circular (π cm^2) made from a PEDOT:PSS/PDMS-printed cotton fabric that is available in Chapter 5.

The phantom-to-electrode impedance was measured using a three-electrode configuration (reference, counter, and active/working electrodes) with the Cyton Biosensing (OpenBCI) board and reusable snap Ag/AgCl dry EEG electrodes to study the difference between the ballistic gelatin and textile-based head phantoms. Then, to validate the EEG textrode, the textile-based head phantom was used. As mentioned in Chapter 5, the system was adopted from OpenBCI and was suggested to measure skin-to-electrode impedance as the OpenBCI Cython board has an installed ADS1299 to measure impedance. A 5 kΩ resistor is built into the OpenBCI board in series to each electrode and has to be taken into account. The ADS1299 has a feature called "Lead Off Detection" that can do the impedance measurement by injecting a known current into each electrode. A 6 nA current is forced into the electrode line by a current source built into the ADS1299 [18], regardless of how much resistance or impedance there is between the current source and the ground (within reason). Hence, a 6 nA current is

present through the electrode to the ground during this test. For this work, only the head phantoms were used, no humans. Therefore, the impedance was analytically calculated using Equation (5.2) in Chapter 5, where the current is 6 × 10^{-9} A.

6.2.6. EEG Measurement

Five electrodes, three active (Fp1, Fp2, and Fz) and two references (A1 and A2), were placed on the head phantom between the bumps according to the International Federation's 10–20 EEG placement as shown in Figure 5.6a in Chapter 5. The other EEG channel positions where no electrodes were placed were kept railed. A tight-fitting headband made of elastic bandage was employed to keep the electrode in the necessary places. The EEG waveforms were recorded with eight channels at a sampling frequency of 250 Hz for 300 seconds using an OpenBCI board with a 1–50 Hz bandpass filter. As the referential electrode placement was followed, each channel monitors the difference between one electrode and a reference electrode. The reduction in disturbances and noise is common across all electrodes in this type of arrangement. The photographic image of the EEG measurement is shown in Figure 6.5.

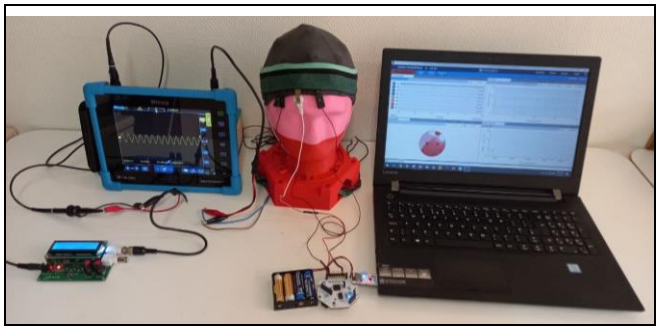

Figure 6.5: The photographic image of the EEG measurement setup

6.2.7. Signal Analysis

I. ITC and ERSP

The event-related spectral perturbation (ERSP) and inter-trial coherence (ITC) time-frequency measurements were then processed and analyzed via EEGLAB software that was treated as in Equations (5.3) and (5.4) in Chapter 5 according to spectral and coherence estimates on EEG recordings [17]. ITC is computed from

single-trial EEG to reflect the temporal and spectral synchronization within EEG, explaining the extent to which underlying phase-locking occurs, whereas ERSP plots mean event-related spectral power fluctuations at each frequency and time during the epoch.

II. SNR

The initial peak-to-peak voltage signal is the synthetic peak-to-peak voltage injected from the digital oscilloscope to the head phantom. Then, undenoised EEG waves were collected using an OpenBCI board supported with OpenBCI GUI and then denoised. Thus, the actual peak-to-peak voltage signals are the denoised peak-to-peak voltage waves collected from the head phantom, whereas the peak-to-peak voltage noises are the difference between the undenoised and denoised peak-to-peak voltage waves. The quality of signals collected was mathematically determined in terms of Signal-to-Noise Ratio (SNR) using (6.1).

$$\mathrm{SNR(dB)} = 20\log\left(\frac{\text{Peak to Peak Voltage Signal}}{\text{Peak to Peak Voltage Noise}}\right) \quad (6.1)$$

6.3. Results and Discussions

6.3.1. Validity of the Textile-Based Head Phantom

The new textile-based head phantom has a much lighter weight than the gelatin-based i.e., 0.5 and 6 kg, respectively. Therefore, the weight reduction is 91.67% which makes it more suitable for handling and moving from place to place. In addition, it is not delicate as ballistic gelatin-based, where the shape of ballistic gelatin could distort and decay fast even when kept in a refrigerator. In our case, the gelatin-based head phantom began decaying after a week of its construction which may also depend on the weather where it is placed during testing. In contrast, the textile-based head phantom does not decay at all.

For validation of the head phantom, during phantom-to-electrode impedance and EEG measurements, dry Ag/AgCl electrodes were used.

I. Phantom-to-Electrode Impedance

The results in Table 6.1 indicate that the impedance of the textile-based head phantom is significantly lower with an f-ratio value of 14.47 and a p-value of

0.002 at a 95% confidence interval according to one-way ANOVA. It is 1384.38 Ω for the textile-based head phantom and 1575.08 Ω for the gelatin-based one, so they are in the same operating range. For comparison, a skin-to-electrode impedance measurement was performed on a human with the OpenBCI board and was found to be in the range of 1291 Ω to 3240 Ω, which is also in the same range as the textile-based and gelatin-based head phantoms. The lower impedance means the long-lasting and lightweight textile-based head phantom can collect somewhat better-quality signals than the gelatin-based head phantom which would make it preferable for validating EEG electrodes in particular and other bio-potential electrodes in general. The head phantom can also potentially be used during modeling and simulation work related to brain neurological activities.

Table 6.1: The phantom-to-electrode impedance of the textile-based head phantom in the EEG alpha band power.

Time (s)	Textile-Based Head Phantom			Gelatin-Based Head Phantom		
	V_{avg} [1]	Z_{raw} [2]	Z_{act} [3]	V_{avg}	Z_{raw}	Z_{act}
30	41.18	6183.18	1183.18	43.93	6596.10	1596.10
60	43.81	6578.08	1578.08	43.98	6603.60	1603.60
90	42.66	6405.41	1405.41	44.54	6687.69	1687.69
120	42.92	6444.44	1444.44	43.87	6587.09	1587.09
150	43.13	6475.98	1475.98	42.49	6379.88	1379.88
180	42.44	6372.37	1372.37	44.12	6624.62	1624.62
210	41.33	6205.71	1205.71	43.72	6564.56	1564.56
240	42.72	6414.41	1414.41	43.63	6551.05	1551.05
Mean	42.52	6384.38	1384.38	43.79	6575.08	1575.08
STDEV	0.88	132.78	132.78	0.59	88.9	88.9

[1] Raw average voltage [μV]. [2] Raw average phantom-to-electrode impedance [Ω]. [3] Actual phantom-to-electrode impedance [Ω].

II. Electroencephalogram (EEG) Signal

The textile-based head phantom allowed for the injection of well-defined synthetic waves using a digital oscilloscope, and collection of the EEG waveform using an OpenBCI board, strongly similar and matching to the gelatin-based one. The EEG wave collected from the textile-based head phantom predominantly lays in the alpha band, the same as the injected sine wave. Whereas, from the ballistic gelatin, a very small theta band was observed where an injected band power was generated. From the EEG band powers in Figure 6.6, the noise in the textile-based head phantom was less, however, statistically, the root-mean-square voltages (Vrms) from the time series in Figure 6.6 in both phantoms were

not significantly different at 95% of confidence interval according to one-way ANOVA. The frequency vs FFT (Fast Fourier Transform) plot showed that the amplitude and frequencies were strongly similar and in the same range, in addition, the head plot was also quite similar. Therefore, this textile-based head phantom can potentially replace the gelatin-based head for validating EEG electrodes.

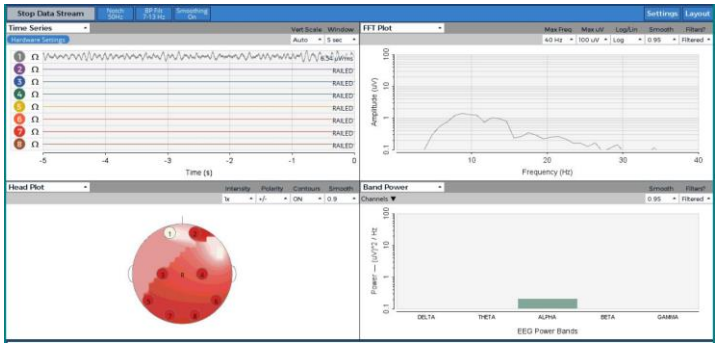

a)

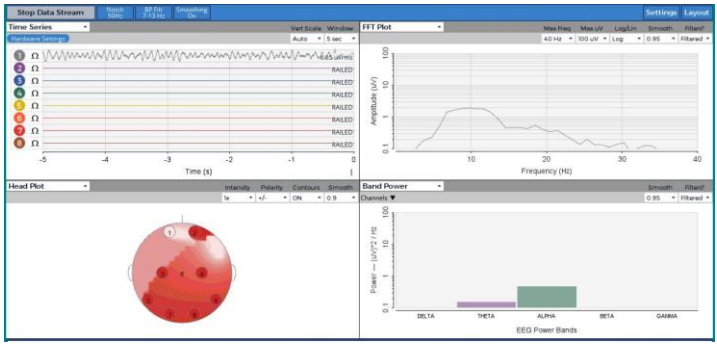

b)

Figure 6.6: EEG signal from OpenBCI board: **a**) textile-based head phantom; **b**) gelatine-based head phantom. In both cases, the peak is around 9.925 Hz, similar to the frequency of the injected sine wave.

III. ITC and ERSP

The frequency and time ranges are plotted on the y-axis and x-axis, respectively, and a color scale is used, with green representing non-significant ITC and red representing significant ITC at a 99% confidence interval. The averaged ERSP response for that person (in blue) is plotted beneath each ITC plot. Although, the ERSP response amplitude scale for both phantoms is different in this study. For the ballistic gelatin, it was 0.1 to 50 Hz frequency whereas for the textile-based

phantom it is -40 to 40 Hz, the main bandwidths of an EEG are within. However, the distribution of spectral powers was more uniform in the textile-based main phantom. The ITC and ERSP plots of the textile-based and gelatin-based head phantoms are shown in Figure 6.7.

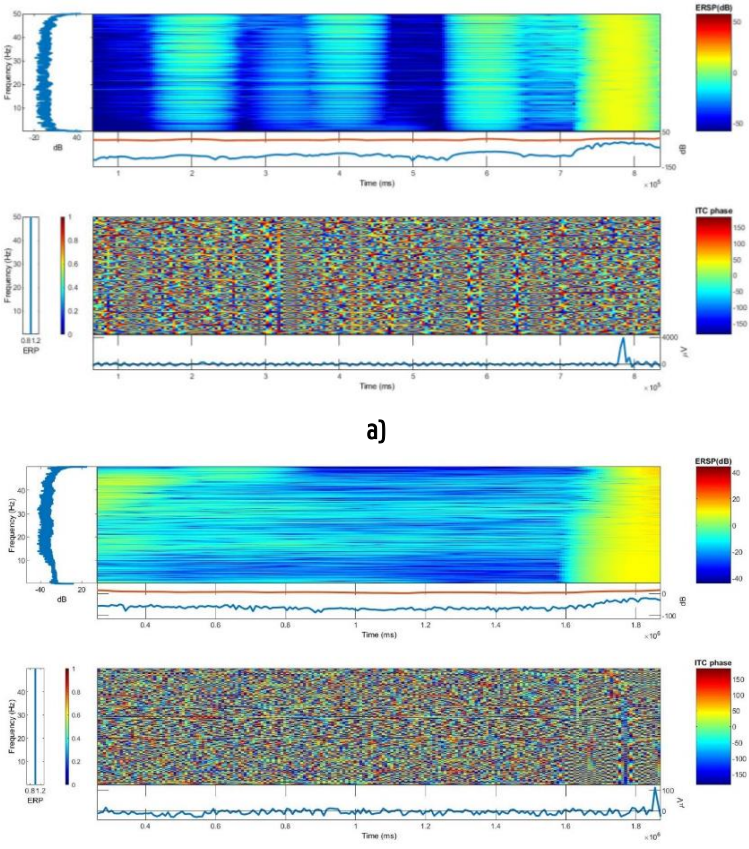

Figure 6.7: ITC and ERSP: **a**) gelatin-based head phantom; **b**) textile-based head phantom

IV. SNR Analysis

From Table 6.2, the SNR of the textile-based head phantom was found to be significantly greater at 33.6 dB (+11.26%) than the gelatin-based one where the marginal error was 30.2 dB ± 1.67 (±10.45%) with a 95% confidence interval. Therefore, textile-based head phantoms are preferable.

Table 6.2: Injected wave, acquired signal, and SNR of the head phantoms.

	Wave	V Max (mV)	V Min (mV)	V Pk-Pk (mV)	SNR (dB)
Raw Signal	Undenoised	168.00	−192.00	360.00	
Gelatin-based head phantom	Denoised Signal	164.92	−184.30	349.22	30.2
	Noise	3.08	−7.701	10.78	
	Signal/Noise	0.054	0.024	0.032	
Textile-based head phantom	Denoised Signal	166.83	−185.80	352.63	33.6
	Noise	1.17	−6.20	7.37	
	Signal/Noise	0.142	0.03	47.84	

6.3.2. Validating the Textile-Based Electrode

I. Phantom-to-Electrode Impedance

Table 6.3 shows the average voltage and respective raw and actual phantom-to-electrode impedance of the textile and dry Ag/AgCl electrodes. The phantom-to-electrode impedance of the textile-based electrode is statistically not significantly different from the commercial dry Ag/AgCl EEG electrode with an *f*-ratio and *p*-value of 0.84 and 0.37, respectively, at a 95% confidence interval based on a one-way ANOVA. On top of that, the mean phantom-to-electrode impedance, 1329.95 Ω, is less than half of the required value to detect an EEG signal, i.e., 5000 Ω [19]. Therefore, the textile-based electrode can be potentially used to acquire EEG signals in a wearable application.

Table 6.3: The phantom-to-electrode impedance of the textile-based head phantom in the EEG alpha band power.

Time (s)	Dry AgAgCl electrode			Textile Electrode		
	V_{avg} [1]	Z_{raw} [2]	Z_{act} [3]	V_{avg}	Z_{raw}	Z_{act}
30	41.18	6183.18	1183.18	40.22	6039.04	1039.04
60	43.81	6578.08	1578.08	41.36	6210.21	1210.21
90	42.66	6405.41	1405.41	42.57	6391.89	1391.89
120	42.92	6444.44	1444.44	42.38	6363.36	1363.36
150	43.13	6475.98	1475.98	42.99	6454.95	1454.95
180	42.44	6372.37	1372.37	42.36	6360.36	1360.36
210	41.33	6205.71	1205.71	42.5	6381.38	1381.38
240	42.72	6414.41	1414.41	42.88	6438.44	1438.44
Mean	42.52	6384.38	1384.38	42.16	6329.95	1329.95
STDEV	0.88	132.78	132.78	0.92	138.81	138.81

[1] Raw average voltage [μV]. [2] Raw average phantom-to-electrode impedance [Ω]. [3] Actual phantom-to-electrode impedance [Ω].

II. EEG Signal Analysis: Amplitude and Frequency

The EEG signals in Figure 6.8 indicate that the textile electrodes are capable of acquiring EEG signal quality equivalent to Ag/AgCl electrodes. All five textile electrodes have collected the wave predominantly at the alpha band as in the injected sine wave. The amplitudes and band powers collected by the five textile electrodes are equivalent to the Ag/AgCl electrode. Therefore, the textile electrodes give reliable EEG signal amplitude and band power that are important for long-term monitoring of brain activity.

III. ERSP and ITC

The event-related spectral perturbation (ERSP) plots mean event-related spectral power fluctuations at each frequency and time during the epoch [20]. The ERSP quantifies the average time course of relative changes in the spontaneous EEG amplitude spectrum caused by a series of similar experimental events. Meanwhile, intertrial coherence (ITC) refers to the degree to which EEG activity in single trials is phase-locked at a given time and frequency (not phase-random with respect to the time-locking experimental event) [21]. It is a measure of oscillatory phase consistency across a group of trials for comparing phase synchronization between trials. At a given point in time, it is the circular sum of phases (length of the red arrow). It achieves a maximum of 1 for perfectly phase-aligned signals, indicating perfect intertrial coherence (i.e., the same phrase on every trial), and then drops to 0 as the phase distribution becomes more uniform, indicating no intertrial coherence at all. ERSP and ITC responses of the textile-based electrodes were equivalent. Moreover, the ERSP and ITC of the textile-based EEG electrodes were also similar, as shown in Figure 6.9. Thus, the PEDOT:PSS/PDMS-printed cotton fabric textile electrodes can be used to monitor brain activity. The textile electrode requires no conductive gel, taking advantage of wet electrodes, and has flexible, lightweight, and washable characteristics that makes it advantageous over commercial dry metallic electrodes too. In addition, it possesses the characteristics of normal textile materials, which means it is suitable to be attached to any textile substrate and structure the way conventional textile materials are attached to each other.

At a 99% confidence interval, the frequency and time ranges are plotted on the y-axis and x-axis, respectively, and a color scale is used, with green representing non-significant ITC and red representing significant ITC. Under each ITC plot, the averaged ERSP response for phantom (in blue) is plotted. The ERSP response amplitude scale for both textile and dry Ag/AgCl electrodes is somewhat similar, as shown in Figure 6.9. The log power spectral density (PSD) for both the textile and dry Ag/AgCl electrodes was 90 dB and the distribution of spectral powers

was also similar. In the range of 1 to 5 Hz frequency, generally, the ERSP and ITC responses of the textile and dry Ag/AgCl electrodes are almost identical.

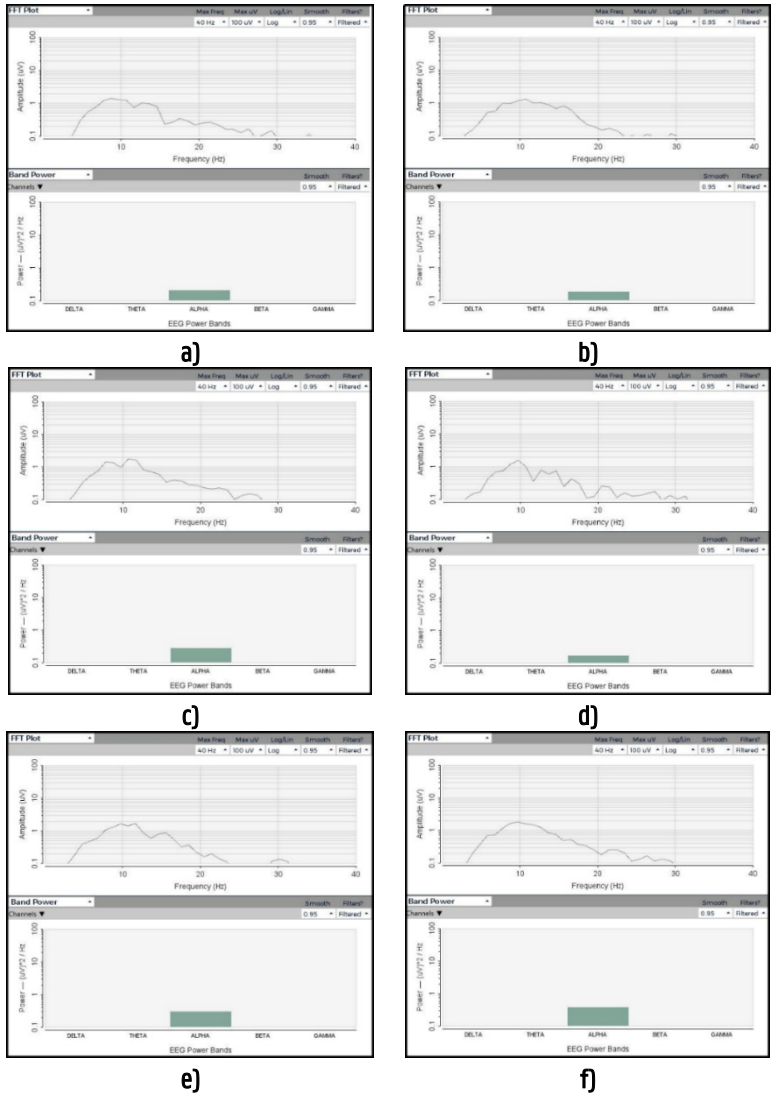

Figure 6.8: EEG signals from OpenBCI board on textile-based head phantom: **a**) dry Ag/AgCl; **b**) textile electrode (TE) 1; **c**) TE 2; **d**) TE 3; **e**) TE 4; and **f**) TE 5.

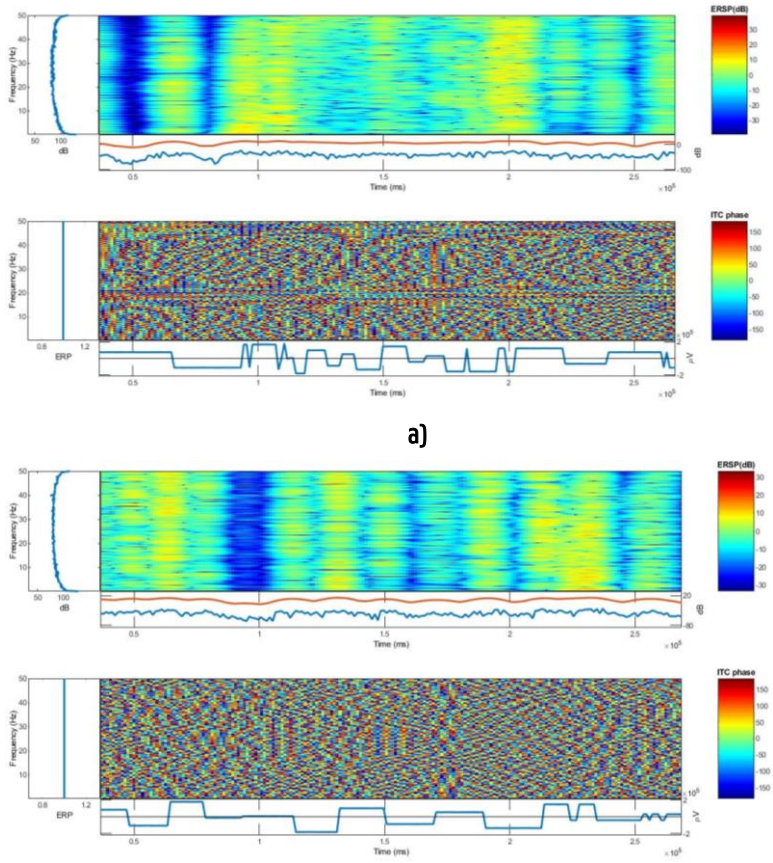

Figure 6.9: The event-related spectral perturbation (ERSP) and intertrial coherence (ITC) plots: (a) textile electrode and (b) dry Ag/AgCl electrode.

IV. SNR Analysis

External noise or artifacts in EEG are defined as any signal picked up by the sensors but not generated by the brain; in this case, by the phantom. Noise or artifacts in EEG data can come from a variety of sources. Anything that uses electricity emits an electromagnetic field, which your measuring equipment may be able to detect. The signal-to-noise ratio (SNR) is the ratio of desired signal power to undesired information or background noise power, which is often expressed in decibels [22]. SNR is a scientific and engineering measurement that compares the level of the desired signal to the level of background noise.

From Table 6.4, the average SNR of five replicas has been found to be 34.73 dB ± 0.14 (±0.41%) at a 95% confidence interval, which shows the values are not significantly different. In addition, the SNR of the textile electrodes is higher (+3.36 %) than the Ag/AgCl electrode. Therefore, the sensing reputability of the textile-based EEG electrode is excellent. In this work, only three active electrodes were used to measure the EEG. Using more active electrodes, increasing the duration of measurement, increasing the size of the electrode, and using a clinical EEG machine would also enhance the SNR to a higher level. On the other side, if the EEG measurement was performed with humans, the SNR would be affected by motion artifacts and other physiological activities. Further study on the SNR correlation of the brain and the textile head phantom would be important to find out the actual values.

Table 6.4: Injected synthetic wave, acquired signal, and SNR of the textile-based electrodes.

	V Max (mV)	V Min (mV)	V Pk-P (mV)	SNR (dB)
Synthetic Wave	168.00	192.00	360.00	–
Ag/AgCl electrode	166.83	−185.80	352.63	33.6
Textile electrode 1	165.62	−187.82	353.44	34.64
Textile electrode 2	165.67	−187.87	353.56	34.68
Textile electrode 3	165.60	−187.80	353.39	34.56
Textile electrode 4	165.60	−188.00	353.58	34.82
Textile electrode 5	165.69	−188.00	353.69	34.98

6.4. Sustainability Concerns

The sustainability concerns of this chapter focus on the textile head phantom rather than the textile EEG electrodes because the sustainability concerns of the EEG textrode validated in this chapter have already been addressed in Chapter 1. As keeping the human brain constant is hardly possible, anatomically realistic head phantoms are used to validate bio-potential electrodes. In this work, we explored a long-lasting and lightweight head phantom that allows synthetic wave injection and measuring at a performance similar to the commonly used ballistic gelatin-based head phantoms. It was found to perform similarly, and for some parameters like the SNR even better than the gelatin-based one. The result proved that the textile-based head phantom can accurately mimic body-electrode frequency responses which makes it suitable for the controlled validation of new electrodes. While the textile-based phantom was designed for

EEG, it can also be adapted to electrocardiogram, electromyogram, electrooculogram, and other related studies as well.

The new textile-based head phantom has a much lighter weight than the gelatin-based i.e., 0.5 and 6 kg, respectively. Therefore, the weight reduction is 91.67% which makes it more suitable for handling and moving from place to place. In addition, it is not delicate as the ballistic gelatin-based one, where the shape of ballistic gelatin could be distorted and decayed fast even when kept in a refrigerator. In our case, the gelatin-based head phantom began decaying after a week of its construction which may also depend on the weather where it is placed during testing. In contrast, the textile-based head phantom does not decay for years. All these will play an enormous role from an economic and sustainability point of view.

6.5. Conclusions

In this study, we have validated a PEDOT:PSS/PDMS-based textile EEG electrode that has the properties of regular textiles and acceptable skin-to-electrode resistance. In addition, it can receive EEG signals comparable to conventional dry electrodes and shows a PSD similar to that of a dry Ag/AgCl electrode with ERSP and ITC equivalent plots. Thus, this validated textile electrode can be used to monitor brain activity in wearable devices.

A textile-based electrode that has a lower representation than metallic electrodes in EEG measurement and textile phantom is a completely new approach. Thus, this work also investigates the potential performance of textile electrodes and head phantoms, where emerging methods of applying conductive polymers to textile substrates may outperform the approach to exploiting conductive textiles.

Bibliography

[1] H. Hallez *et al.*, "Review on solving the forward problem in EEG source analysis," *J. NeuroEngineering Rehabil.*, vol. 4, no. 1, p. 46, Dec. 2007, doi: 10.1186/1743-0003-4-46.

[2] A. S. Oliveira, B. R. Schlink, W. D. Hairston, P. König, and D. P. Ferris, "Induction and separation of motion artifacts in EEG data using a mobile phantom head device," *J. Neural Eng.*, vol. 13, no. 3, p. 036014, Jun. 2016, doi: 10.1088/1741-2560/13/3/036014.

[3] S. Kohli and A. J. Casson, "Removal of Gross Artifacts of Transcranial Alternating Current Stimulation in Simultaneous EEG Monitoring," *Sensors*, vol. 19, no. 1, p. 190, Jan. 2019, doi: 10.3390/s19010190.

[4] C. Richardson, S. Bernard, and V. A. Dinh, "A Cost-effective, Gelatin-Based Phantom Model for Learning Ultrasound-Guided Fine-Needle Aspiration Procedures of the Head and Neck," *J. Ultrasound Med.*, vol. 34, no. 8, pp. 1479–1484, Aug. 2015, doi: 10.7863/ultra.34.8.1479.

[5] M. S. Md Said, N. Seman, N. R. Sulaiman, and T. Abd Rahman, "Modeling of Gelatin-Based Head Phantom Based on its Electrical Properties for Wideband Microwave Imaging Application," *Appl. Mech. Mater.*, vol. 781, pp. 608–611, Aug. 2015, doi: 10.4028/www.scientific.net/AMM.781.608.

[6] E.-R. Symeonidou, A. Nordin, W. Hairston, and D. Ferris, "Effects of Cable Sway, Electrode Surface Area, and Electrode Mass on Electroencephalography Signal Quality during Motion," *Sensors*, vol. 18, no. 4, p. 1073, Apr. 2018, doi: 10.3390/s18041073.

[7] A. Y. Owda and A. J. Casson, "Electrical properties, accuracy, and multi-day performance of gelatine phantoms for electrophysiology," Bioengineering, preprint, May 2020. doi: 10.1101/2020.05.30.125070.

[8] M. S. M. Said and N. Seman, "Preservation of gelatin-based phantom material using vinegar and its life-span study for application in microwave imaging," *IEEE Trans. Dielectr. Electr. Insul.*, vol. 24, no. 1, pp. 528–534, Feb. 2017, doi: 10.1109/TDEI.2016.006029.

[9] E. Tsizin, T. Mund, and A. Bronstein, "Printable anisotropic phantom for EEG with distributed current sources," p. 18.

[10] T. J. Collier, D. B. Kynor, J. Bieszczad, W. E. Audette, E. J. Kobylarz, and S. G. Diamond, "Creation of a Human Head Phantom for Testing of Electroencephalography Equipment and Techniques," *IEEE Trans. Biomed. Eng.*, vol. 59, no. 9, pp. 2628–2634, Sep. 2012.

[11] W. E. Audette, J. Bieszczad, L. V. Allen, S. G. Diamond, and D. B. Kynor, "Design and Demonstration of a Head Phantom for Testing of Electroencephalography (EEG) Equipment," 2020.

[12] J. Xiaopei Wu and L. Li, "An Introduction to Wearable Technology and Smart Textiles and Apparel: Terminology, Statistics, Evolution, and Challenges," in *Smart and Functional Soft Materials*, X. Dong, Ed. IntechOpen, 2019. doi: 10.5772/intechopen.86560.

[13] L. Van Langenhove, "Smart Textiles: Past, Present, and Future," in *Handbook of Smart Textiles*, X. Tao, Ed. Singapore: Springer Singapore, 2014, pp. 1–20. doi: 10.1007/978-981-4451-68-0_15-1.

[14] A. Yu and W. D. Hairston, "Open EEG Phantom." https://osf.io/qrka2/ (accessed Oct. 08, 2020).

[15] A. B. H. Musa, B. Malengier, S. Vasile, L. Van Langenhove, and A. De Raeve, "Analysis and Comparison of Thickness and Bending Measurements from Fabric Touch Tester (FTT) and Standard Methods," *Autex Res. J.*, vol. 18, no. 1, pp. 51–60, Mar. 2018, doi: 10.1515/aut-2017-0011.

[16] W. Jia, J. Wu, D. Gao, M. Sun, and R. J. Sclabassi, "Characteristics of skin-electrode impedance for a novel screw electrode," in *2014 40th Annual Northeast Bioengineering Conference (NEBEC)*, Boston, MA, USA, Apr. 2014, pp. 1–2. doi: 10.1109/NEBEC.2014.6972825.

[17] J. L. Vargas Luna, M. Krenn, J. A. Cortés Ramírez, and W. Mayr, "Dynamic Impedance Model of the Skin-Electrode Interface for Transcutaneous Electrical Stimulation," *PLOS ONE*, vol. 10, no. 5, p. e0125609, May 2015.

[18] TEXAS INSTRUMENTS, "ADS1299-x Low-Noise, 4-, 6-, 8-Channel, 24-Bit, Analog-to-Digital Converter for EEG and Biopotential Measurements." 2017. [Online]. Available: https://www.ti.com/lit/ds/symlink/ads1299.pdf

[19] T. C. Ferree, P. Luu, G. S. Russell, and D. M. Tucker, "Scalp electrode impedance, infection risk, and EEG data quality," *Clin. Neurophysiol.*, vol. 112, no. 3, pp. 536–544, Mar. 2001, doi: 10.1016/S1388-2457(00)00533-2.

[20] Q. Zhao and L. Zhang, "Temporal and Spatial Features of Single-Trial EEG for Brain-Computer Interface," *Comput. Intell. Neurosci.*, vol. 2007, pp. 1–14, 2007, doi: 10.1155/2007/37695.

[21] A. Nash-Kille and A. Sharma, "Inter-trial coherence as a marker of cortical phase synchrony in children with sensorineural hearing loss and auditory neuropathy spectrum disorder fitted with hearing aids and cochlear implants," *Clin. Neurophysiol.*, vol. 125, no. 7, pp. 1459–1470, Jul. 2014, doi: 10.1016/j.clinph.2013.11.017.

[22] M. Welvaert and Y. Rosseel, "On the Definition of Signal-To-Noise Ratio and Contrast-To-Noise Ratio for fMRI Data," *PLoS ONE*, vol. 8, no. 11, p. e77089, Nov. 2013, doi: 10.1371/journal.pone.0077089.

7. Hook Fabric EEG Textrode for Brain Activity Monitoring without Shaving the Head

In this chapter, new electroencephalogram (EEG) electrodes that can detect quality EEG signals without the need for conductive gels or skin treatments and shaving the head locally have been fabricated from an electrically conductive hook fabric with surface resistivity of 1 Ω/sq. A knitted-net EEG bridge cap featuring a shutter mechanism that separates the hair and ensures good contact between the hook fabric electrode and the scalp has been constructed.

Some part of this chapter is redrafted from a proceeding paper:

G.B. Tseghai, B. Malengier, K.A. Fante, and L. Van Langenhove, "Velcro Hook Electroencephalogram Textrode for Brain Activity Monitoring", 2022 IEEE International Conference on Flexible and Printable Sensors and Systems (FLEPS), IEEE Xplore, 2022. DOI: 10.1109/FLEPS53764.2022.9781526.

Table of Contents

7.1. Introduction

As discussed in Chapters 3, 5, and 6, the associated problems with the Ag/AgCl wet electrodes (Figure 7.1a) led to the development of dry electrodes made of a conductive substance that mechanically interfaces with the skin, avoiding the skin preparation procedure and the use of conductive paste. They can work without any physical contact on pure capacitive coupling (Figure 7.1b) or with a dry sensor-skin contact (Figures 7.1c&d). Capacitive EEG electrodes [1], [2] are unlikely to be appropriate for recording spontaneous EEG signals as the amplitude levels are so low, moreover, the high impedance of these electrodes, on the other hand, necessitates the use of an ultra-high impedance on-site amplifier [3]. In addition, the "floating" fixation on the scalp causes motion artifacts. Skin contact dry EEG electrodes were also introduced [4]–[6]. However, the flat skin contact dry electrodes cannot be used on hairy regions, so shaving is required. Whereas the needle-based dry electrodes can be used on hairy regions, they still are heavy in weight and stiff in structure, while penetration of the skin risks infection. Thus, all the aforementioned EEG electrodes are inappropriate for wearable purposes. These limitations caused the emergence of textile-based EEG electrodes. With this in mind, in Chapter 5, we have successfully developed dry EEG electrodes from PEDOT:PSS/PDMS-printed cotton fabric that collected EEG signals comparable to Ag/AgCl dry EEG comb electrodes. However, placing such an electrode on the hairy part of the head is not possible as it is a completely flat electrode. Thus, shaving the head locally is a compulsory step before using this electrode. Moreover, tens or hundreds of electrodes are required to monitor brain activity with EEG electrodes where any part of the head would be shaved each time the measurement is intended because the hair grows rapidly which in turn increases the skin-to-electrode contact impedance and affects the signal quality. Therefore, this trend is not suitable for long-term monitoring. In addition, shaving the hair off is an extra burden for the expert and time-consuming. In addition, shaving the head would not be liked by the patients. As a result, developing a textile-based dry EEG electrode that can be used even on hairy skin undoubtedly provides a significant advantage in addressing the limitations of the existing electrode. In this chapter, a dry EEG electrode was made from conductive hook fabric and compared to a dry EEG comb electrode, which has a comb structure to also allow it to be used on hairy regions, see Figure 7.1.

a) **b**) **c**) **d**)

Figure 7.1: Types of EEG electrodes: **a**) Gold cup EEG electrode [7]; **b**) Capacitive EEG electrode [8]; **c**) dry EEG comb electrode [9]; **d**) PEDOT:PSS/PDMS-printed cotton EEG flat electrode.

7.2. Experiment

7.2.1. Materials and Methods

A Velcro® hook tape made of 100% silver-plated fiber durable material and high cycle life having a surface resistivity of 1 Ω/sq obtained from (Light Stitches, UK) was used to construct electrodes. Circular electrodes with a diameter of 1 cm (a surface area of π/4 cm^2), the same size as the comb Ag/AgCl dry EEG electrode, were constructed. The schematic illustration, photographic and microscopic images of the hook fabric electrode are shown in Figure 7.2.

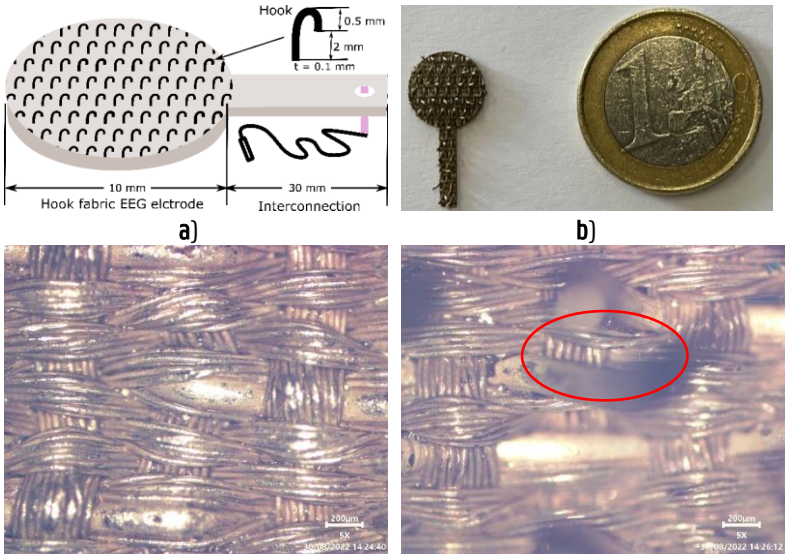

Figure 7.2: a) Schematic illustration of hook fabric textrode; **b**) actual hook fabric EEG textrode; **c**) optical microscopic view of the back side of EEG textrode **d**) optical microscopic view of the face EEG textrode with the red circle indicating a hook.

7.2.2. Impedance Measurement

As addressed in Chapters 5 and 6, when electrodes are used to monitor biopotentials, the system's impedance is made up of the impedance of the electrode and the skin together. As a result, the skin-to-electrode impedance is crucial. The impedance of the skin-electrode combination was measured using an IVIUM potentiostat set-up with three electrodes configuration according to [15]. For the IVIUM instrument, conventional wet electrodes were employed as counter and reference electrodes. To allow impedance stability at the contact interface, they were positioned 10 cm apart on the skin/phantoms and kept in place for 30 min before starting the measurements. IVIUM's working and sensing cables of the IVIUM were attached to the electrode under test, which was next to the reference electrode. The hook fabric electrodes were employed as the working electrodes, but a dry Ag/AgCl comb and standard wet gold cup electrodes were also characterized to compare this result with the results of the other hook fabric electrodes. The potentiostat controlled a 25 mV AC signal between the working and reference electrodes during the experiments, with a signal frequency ranging from 0.1 Hz to 60 Hz. The current traveled mostly

through the working and counter electrodes, as well as the skin and tissue between them because the internal impedance of the IVIUM's voltage meter is above 1000 GΩ. In the schematic illustrated in Figure 7.3, the corresponding impedances are labeled as ZWE (impedance of skin-to-working electrode), ZRE (impedance of skin-to-reference electrode), and ZCE (impedance of skin-to-counter electrode). Z1 represents the impedance of the tissue between WE and RE), Z2 represents the impedance of the tissue between RE and CE, and Z3 represents the impedance of the tissue between WE and CE.

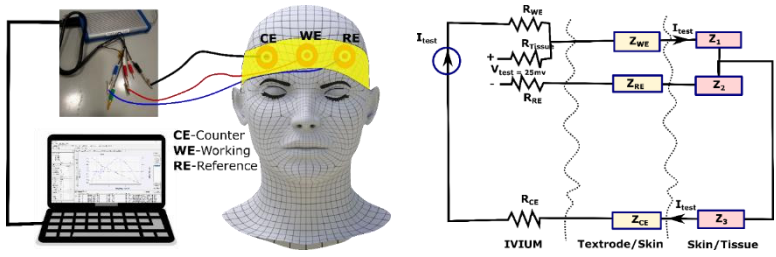

a) b)

Figure 7.3: Impedance measurement: (a) schematic illustration of the impedance measurement; (b) circuitry of the impedance measurement [10].

7.2.3. Knitted Net EEG Electrode Bridge/EEG Cap Construction

A multifilament polyester yarn was used to create a knitted net EEG electrode bridge by hand knitting. The knitted net EEG electrode bridge could simultaneously support up to 21 electrodes. Felt foam with a diameter of 13.5 cm was placed on the knitted net bridge. The felt foam exerts pressure on the electrode, preventing it from sliding and allowing for better skin-to-electrode contact. Its side towards the electrode has an adhesive that maintains the electrode in place. In addition, felt foam, which is a permanent part of the bridge, can be used as a guideline for electrode placement using the 10-20 electrode placement system. The knitted net EEG electrode bridge is adjustable, allowing the user to tighten or loosen it, depending on the size and shape of the subject's head. The positions of the felt foams were also adjustable within the knitted net EEG electrode bridge. The schematic illustration of the knitted net EEG electrode bridge is shown in Figure 7.4.

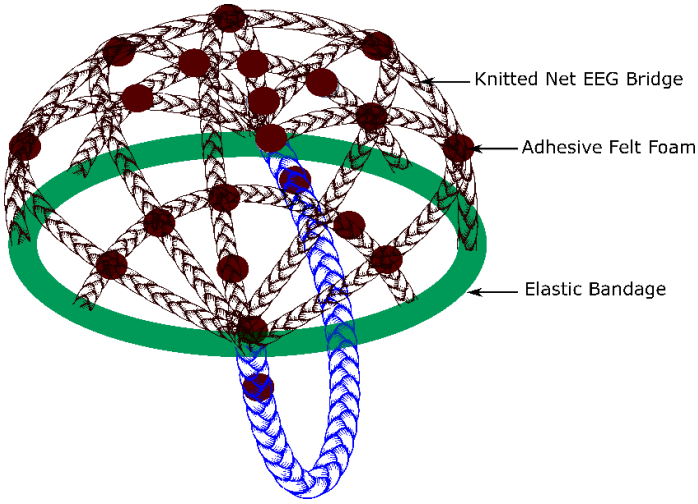

Figure 7.4: A hand-knitted net EEG electrode bridge (EEG cap)

7.2.4. EEG Measurement

The EEG measurement was performed at the Department of Neurology in UZ Gent, Ghent University Hospital. waveforms were recorded using a Brain Quick® Clinical EEG Line [12], the device supports Micromed - SystemPLUS Evolution software. 12 hook fabric electrodes, 10 active, and two reference electrodes were placed on the hairy region of the head according to the 10-20 EEG placement system as shown in Figure 7.5a (chapter 5). The 10 and 20 in the system indicate the distance of the electrodes from each other in proportion to the size of the head. The letters in the indicated positions represent the corresponding position of the head with even numbers representing the right position and odd numbers the left. The schematic illustration of the EEG measurement setup used in this work is shown in Figure 7.5b.

The knitted net EEG electrode bridge/EEG cap (Figure 7.4) was used to keep the electrode in the required positions according to the 10-20 system, preventing them from sliding. The EEG cap has non-conductive foams placed on top of the electrodes to ensure the electrode is sufficiently pressed against the skin. The performance of the knitted net EEG electrode bridge was compared with a universal EEG cap [13]. Figures 7.5b are photographic images of the EEG measurement at the clinical level using the hook fabric EEG textrodes. Figures 7.5c and d are photographic images of the knitted net EEG electrode bridge and universal EEG cap, respectively.

The collected signals were also analyzed using EEGLab software. A Florida Research Instrument Inc product reusable Ag/AgCl dry EEG comb electrode (TDE-20-15 reusable EEG electrode) [9] obtained from OpenBCI, shown in Figure 7.1c, was used as a comparison electrode.

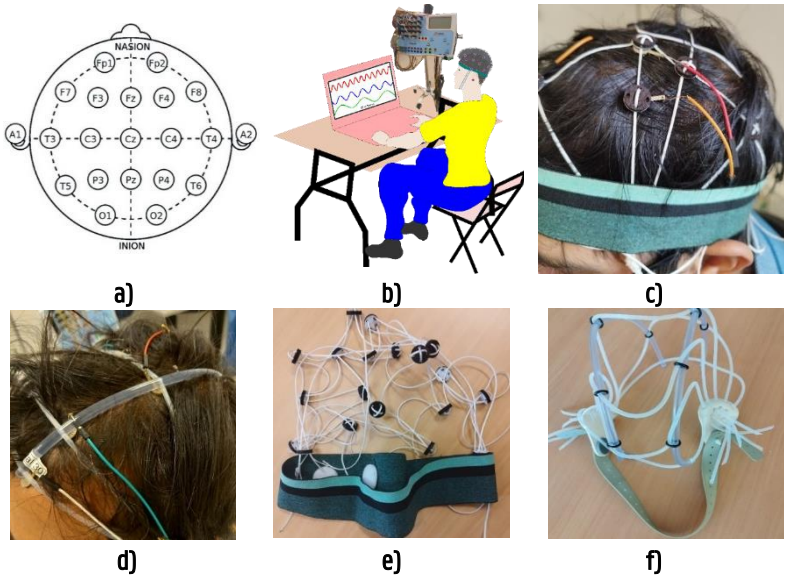

Figure 7.5: **a**) 10-20 EEG placement system; **b**) schematic illustration of EEG measurement setup; **c**) photographic image of the EEG measurement at a clinical level using the knitted net EEG electrode bridge; **d**) photographic image of the EEG measurement at a clinical level using Universal EEG cap; **e**) photographic image of the knitted net EEG electrode bridge; **f**) photographic image of the Universal EEG cap.

7.2.5. ITC, ERSP, and PSD Analysis

An EEGLAB software [11]was used to perform data treatment and statistics offline. The EEGLAB allows for to generation of time-frequency images and for calculating event-related spectral perturbation (ERSP) and intertrial coherence (ITC). ERSP measures how much the power at various frequencies in signal changes in proportion to a certain time point [12], whereas, ITC measures the consistency of the oscillatory phase throughout a set of trials [13]. A 250 Hz low pass filter, 256 Hz sampling rate, and a 0.5 Hz high pass filter were used in the beginning. ERSP was obtained for the time domain analysis by averaging

baseline-corrected epochs taken from 0 to 9.996 s after the target apparition event. From the initial 2560 epochs (5% discarded), a total of 2432 epochs remained after artifact rejection. Meanwhile, ITC was obtained for wave cycles from 3 to 0.5, epoch time limit from 0 to 9.996, and frequency limit from 0.5 to 250 Hz. The power spectral density (PSD) of the textrode was also compared to wet gold cups and dry Ag/AgCl electrodes.

7.2.6. Signal-To-Noise Ratio (SNR) Analysis

For the SNR analysis, a single active electrode was used. a function generator (Chapter 6, Figure 6.3a) and Micsig TO1104 Handheld Tablet Digital Oscilloscope (Chapter 6, Figure 6.3b) were used to generate a synthetic sine wave (360 mV peak to peak voltage, 9.925 Hz frequency, 50 ms time). The generated synthetic sine wave (Chapter 6, Figure 6.3c) was then injected into a textile-based head phantom (Chapter 6, Figure 6.5. To impersonate events according to [14], the EEG phantom signal parameters were set in the alpha wave range and varying the amplitude from 0.2 to 1V to mimic a neurological event. Then the EEG wave was compared to waves from Ag/AgCl dry comb electrode under the same conditions using an OpenBCI board. Next, the EEG signals were denoised using EEGLAB. Finally, the quality of signals collected was analyzed mathematically in terms of Signal-to-Noise Ratio (SNR) using (6.1).

7.3. Results and Discussion

7.3.1. Performance of the knitted net bridge EEG cap

The EEG channel data collected by Ag/AgCl dry comb electrodes using a universal EEG cap and the knitted net bridge EEG cap are equivalent as shown in Figure 7.6. Fpz, Fp2, and Fz were kept railed in both EEG bridges and the effect has appeared in the knitted net bridge EEG cap similar to the universal EEG cap. This shows that the knitted net bridge EEG cap can be used in its present form at the clinical level as a replacement for currently used caps.

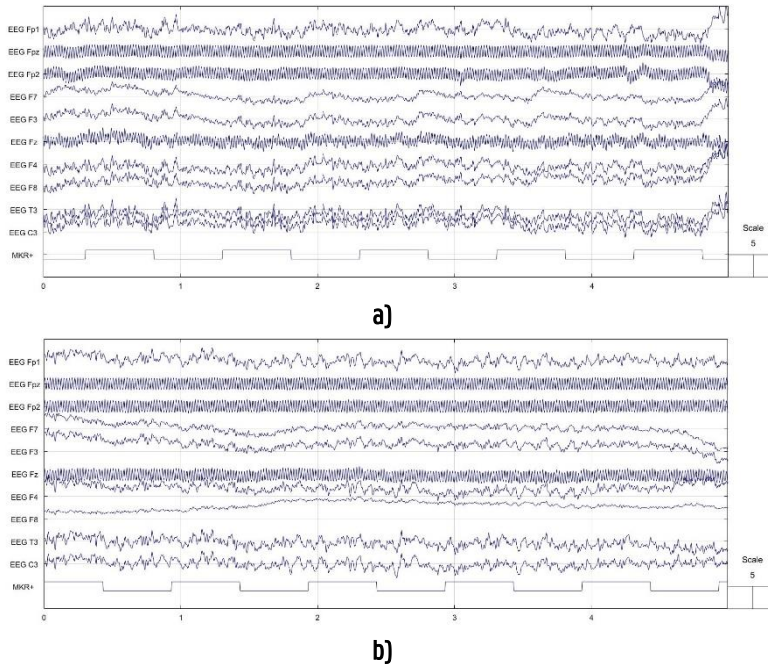

Figure 7.6: EEG channel data from (a) universal EEG cap; (b) knitted net bridge EEG cap

The output graph of ERSP and ITC EEG signals collected by the knitted net bridge EEG cap and universal EEG cap were compared using EEGLAB software. In each plot, the frequency range and the time range are placed on the *y*-axis and *x*-axis, respectively, and a color scale is used where green is for non-significant, and red represents significant ITC at a 99% CI. Beneath each ITC plot is the averaged ERSP response for that individual (in blue), in microvolts.

The amplitude scale for the ERSP response is equivalent for both the knitted net bridge EEG cap and universal EEG cap with a maximum value of 99 μV. To the left of each ITC plot, the average power is shown for that electrode at each frequency, while a black dotted line shows the significance threshold at each frequency relative to the baseline period at a 95% confidence level. The ERSP and ITC phases, and channel time frequencies for Fp1, of both bridges are shown in Figure 7.7. From the EEGLAB software analysis, the maximum log power distribution for both bridges also equally ranged from -50 to 50 dB. The maximum log PSD for both electrodes was ~40 $\mu V^2/Hz$. Therefore, the knitted net bridge EEG cap can replace the universal EEG cap providing weight, price, and accessibility advantages.

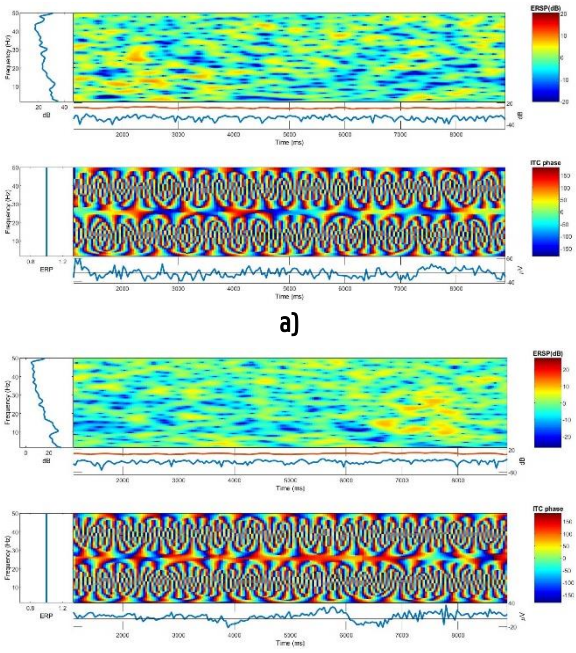

Figure 7.7: ERSP and ITC Phases: **a**) universal EEG cap; **b**) knitted net bridge EEG cap

7.3.2. Skin-to-Electrode Contact Impedance of the Hook Fabric EEG Textrode

Throughout all frequencies, the skin-to-electrode contact impedance of the hook fabric textrode was significantly lower than the Ag/AgCl dry comb electrode as shown in Figure 7.8. The one-way ANOVA at a 95% CI showed the skin-to-electrode contact impedance of the hook fabric textrode and Ag/AgCl dry comb electrode is significantly different providing an *f*-ratio value of 2.81 and *p*-value of 0.01. These results could be because the hook fabric textrode has more contact points than the Ag/AgCl dry comb electrode. Thus, the hook fabric textrode could have a technical advantage over the Ag/AgCl dry comb electrode EEG monitoring, especially for wearable applications, as the impedance is lower.

At alpha, beta, and gamma frequencies, the skin-to-electrode contact impedance of the hook fabric texture was lower than that of the dry Ag/AgCl comb electrode, as shown in Figure 7.8. The one-way ANOVA at a 95% CI showed that the skin-to-electrode contact impedance of the hook fabric textile and dry Ag/AgCl comb

electrode was significantly different, providing an *f*-ratio value of 2.81 and a *p*-value of 0.01. These results could be because the hook fabric electrode has more contact points than the dry Ag/AgCl comb electrode. Thus, the hook fabric textrode could have a technical advantage over dry Ag/AgCl comb electrode EEG monitoring, particularly for wearable applications. However, the impedance was higher than that of standard wet gold cup electrodes, which agrees with the existing literature that states that wet electrodes provide lower skin-to-electrode impedance than commercial dry electrodes [15]. However, the impedance increases with time due to dehydration, even at room temperature, as a conductive gel or electrolyte is employed to lower the impedance. Therefore, hook fabric textrodes are potential candidates for the detection of cardiac and neural activity.

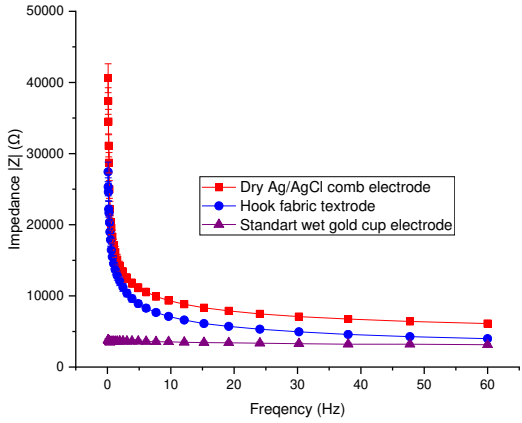

Figure 7.8: Skin-to-electrode impedance from IVIUM Potentiostat

7.3.3. EEG Waves from the Hook fabric Textrode

The EEG signals recorded by the textrode were comparable to those of standard gold cups and dry Ag/AgCl comb electrodes. The amplitude of the signal was as high as that of the standard wet gold cup and dry Ag/AgCl comb electrodes in all head regions. In addition, the textrode provides a similar bandwidth range. The EEG signals from the textrode, standard wet gold cup, and dry Ag/AgCl comb electrodes from a healthy subject with no history of brain health problems are shown in Figure 7.9. In addition, blinking and mouth opening artifacts were clearly recognized and identified in the novel hook fabric textrode in the same manner as in the standard wet gold cup and dry Ag/AgCl comb electrodes, as marked in red in the images in Figure 7.9. This textrode is, therefore, a promising alternative to the existing EEG electrodes, offering weight, flexibility, and

economic benefits. The EEG signals collected with the hook fabric textrode had a similar EEG pattern to those collected by the standard wet gold cup and dry Ag/AgCl comb EEG electrodes. When comparing the images, there is no doubt that the EEG waves from a human cannot be exactly identical, even within the same electrode, as the human brain cannot be in a constant state. Hence, for commercial use, these electrodes should be validated using head phantoms.

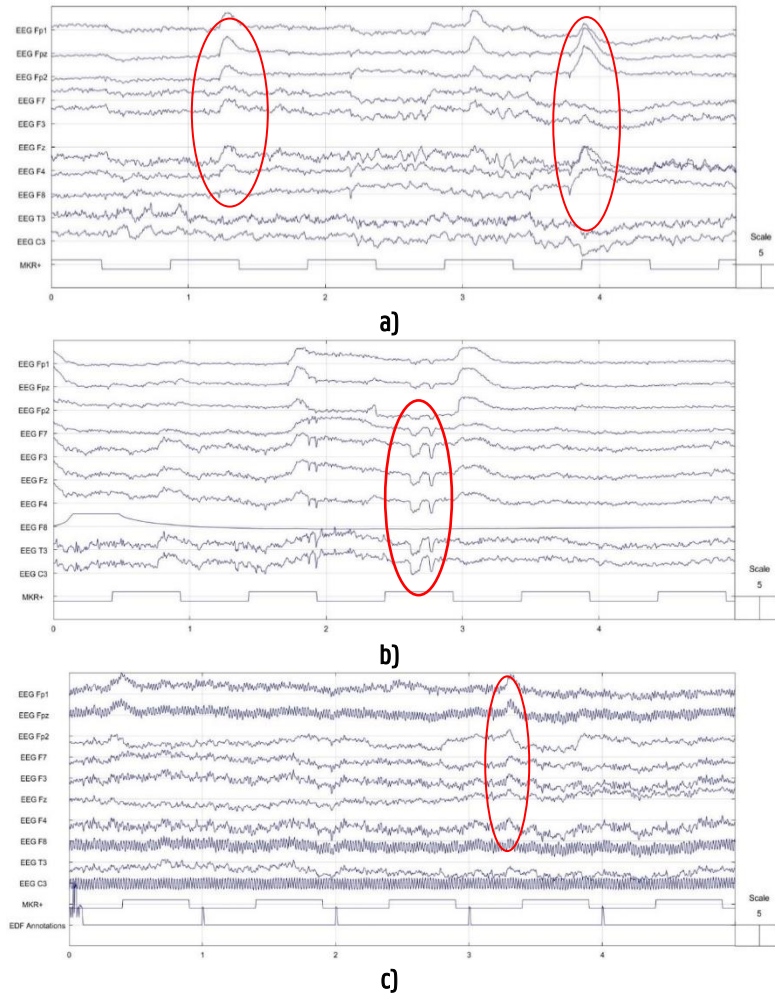

Figure 7.9: EEG signals using knitted net EEG bridge: **a**) hook fabric textrode; **b**) Ag/AgCl dry comb electrode; **c**) standard wet gold cup electrode

7.3.4. EEG Signal Analysis

The European Data Format (EDF) file types of the EEG waves in Figure 7.9 were analyzed using EEGLAB software. The ITC, ERSP, and PSD graphs generated from the hook fabric, dry Ag/AgCl, and wet gold cup electrodes are discussed below.

I. ERSP

Figure 7.10 shows mean event-related changes in spectral power at each time during the epoch and at each frequency, < 50 Hz. The amplitude scale for the ERSP response is 20 dB to 60 dB and similar for hook fabric textrode, dry Ag/AgCl comb, and wet gold cup electrodes. As marked with white and red on the images in Figure 7.10, the spectral power was found fairly similar in both the dry Ag/AgCl and the hook fabric electrodes across the frequency domain. For both, the ERSP envelope, low and high mean dB values relative to baseline, were ~17 dB at any time in the epoch. Visual observation shows that green, yellow and blue are evenly distributed over the region and are similar for both electrodes.

II. ITC

Figure 7.11 shows the ITC phases of the hook fabric test, standard wet gold cup, and dry Ag/AgCl comb electrodes at all frequencies. In the ITC, the ratio of the spectral power distribution similarly ranges between -50 and 50 dB, as marked with a white arrow in the images in Figure 7.11. Most importantly, the ITC plots were equivalent. Therefore, the ITC plots prove that the hook fabric EEG textrode can be used without a doubt to monitor brain activity in its present form, even at a clinical level. Further design improvements would, of course, make the textrode a better choice than existing electrodes for the proposed application.

III. PSD

The PSD representing the power distribution of EEG series in the frequency domain was also used to evaluate the hook fabric EEG textrode against standard wet gold cup and dry Ag/AgCl comb electrodes across 0.1 to 50 Hz covering all EEG bandwidths. Specifically, the log PSD decreased linearly with an increase in the frequency domain, and the maximum log PSD for all electrodes was in the delta EEG bandwidth of ~35 $\mu V^2/Hz$, as shown in Figure 7.12. Therefore, the hook fabric EEG textrode can be used exactly in its present form, as per this comparison.

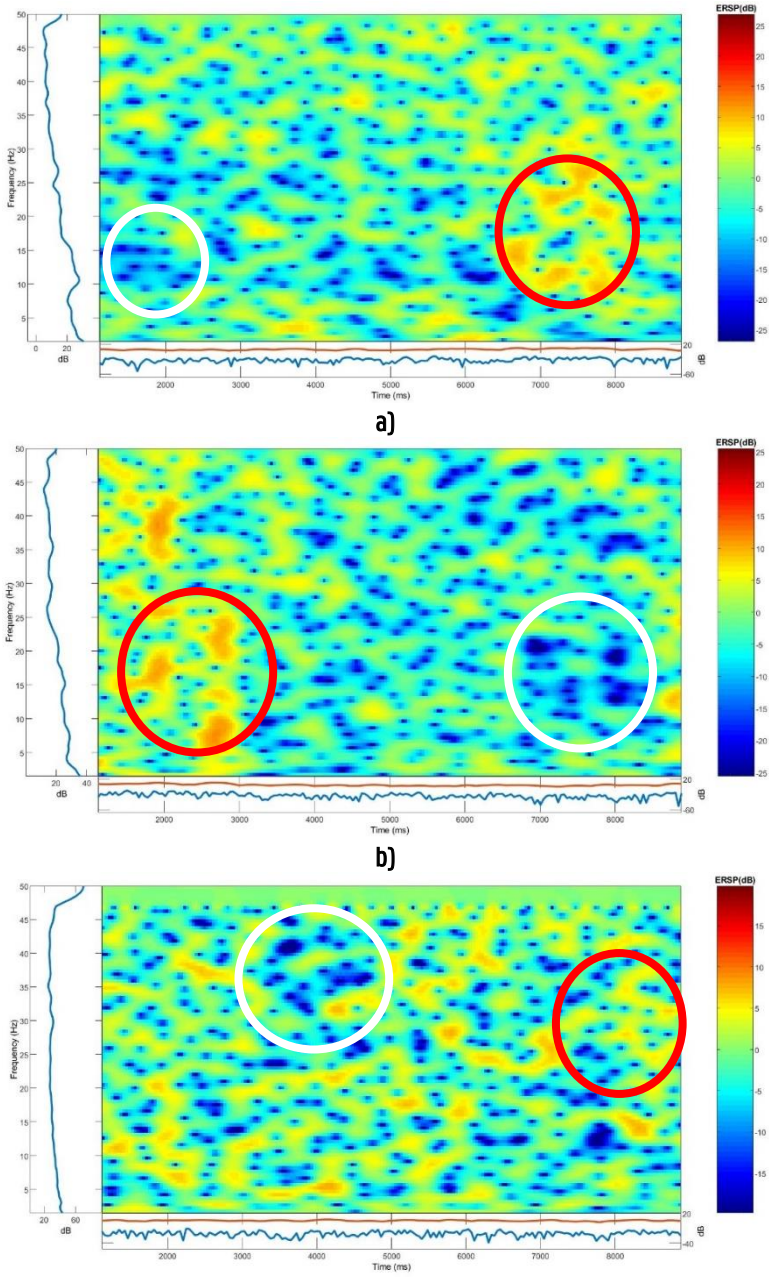

Figure 7.10: ERSP phases: **a**) hook fabric textrode; **b**) Ag/AgCl dry comb electrode; **c**) standard wet gold cup electrode

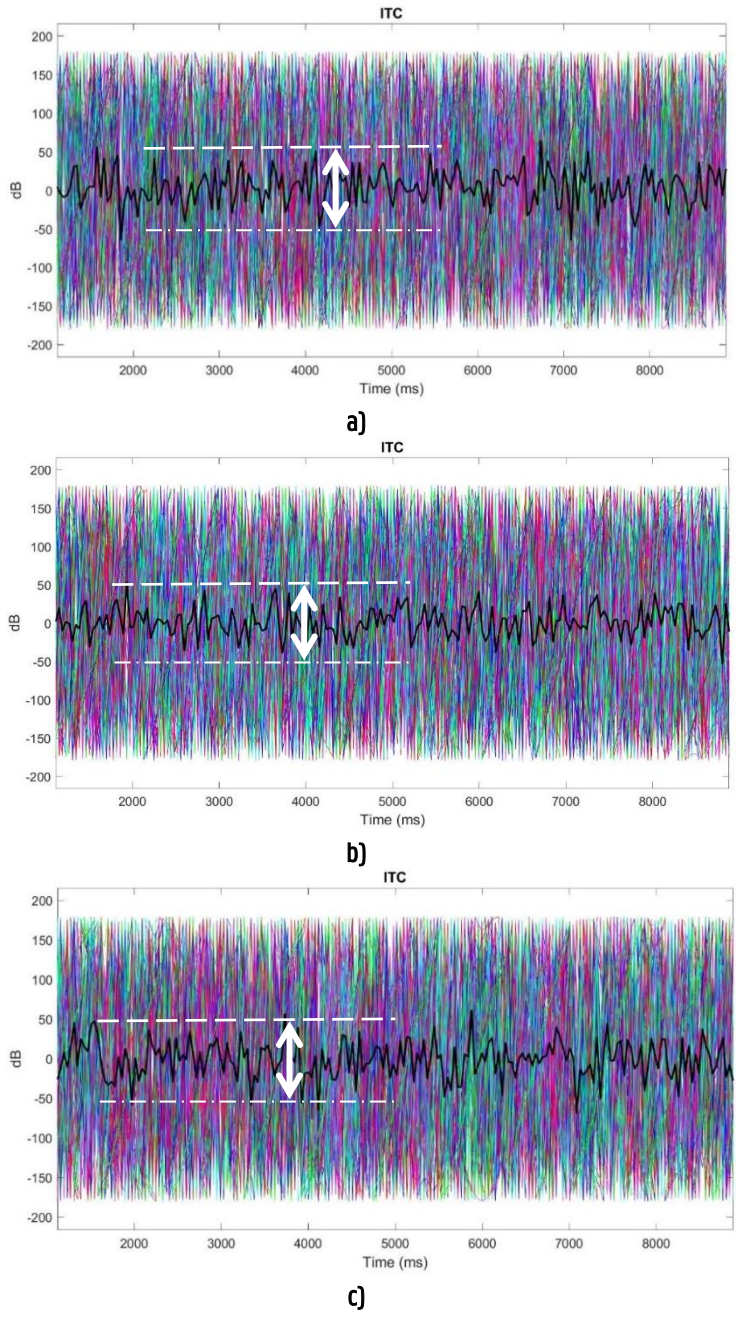

Figure 7.11: ITC phases. **a**) hook fabric textrode; **b**) Ag/AgCl dry comb electrode; **c**) standard wet gold cup electrode

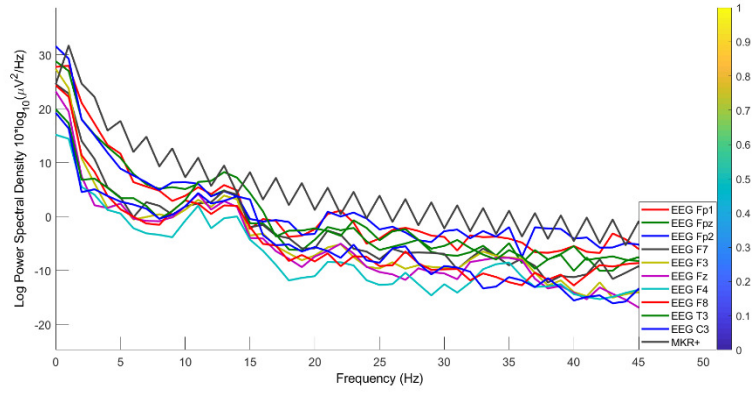

a)

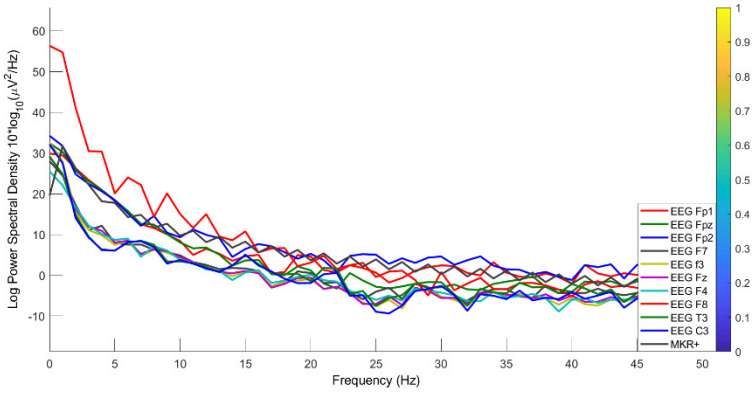

b)

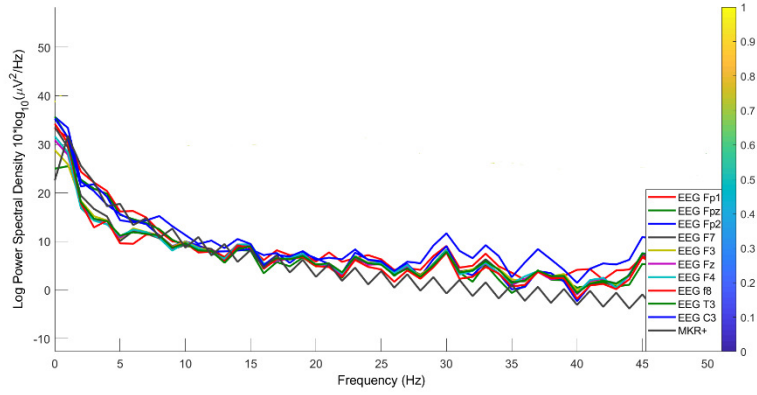

c)

Figure 7.12: Channel spectra of the PSD. **a**) hook fabric textrode; **b**) Ag/AgCl dry comb electrode **c**) standard wet gold cup electrode

7.3.5. Signal-To Noise-Ratio (SNR)

The average SNR of the textrode was 33.6 dB ±0.14 (±0.41%) at a 95% confidence interval, which shows that the values are not significantly different. Therefore, the sensing ability of the textile-based EEG electrode is excellent. Moreover, the SNR of the textrode was higher than that of the standard wet gold cup electrodes (+4.2%), as shown in Figure 7.13 However, the SNR of the hook fabric textrode was slightly lower (-2.98%) than that of the Ag/AgCl dry comb electrode, indicating that the textrode still needs some improvement. This effect could be due to the fact that signals are collected from many narrower scalp contact points in the hook fabric textrode than in the dry Ag/AgCl comb electrode. In addition, the height of the hook was shorter than the length of the comb by 3 folds. Thus, improving the length and thickness of the hook can increase SNR.

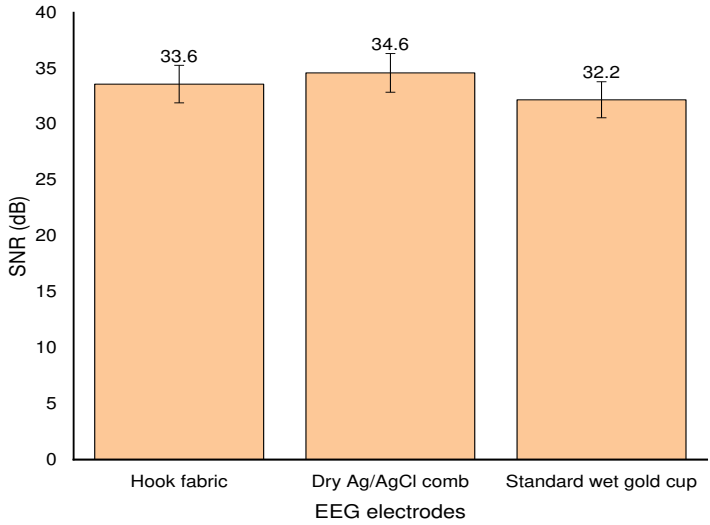

Figure 7.13: Signal-to-Noise ratio comparison

7.4. Sustainability Concerns

The raw material from which the novel hook fabric EEG electrode was constructed and its structural design were set apart from those of other commercial electrodes. Furthermore, they provide additional functions and applications. An optimized hook fabric electrode provides a sustainable benefit over commercial electrodes, as shown below.

Avoids Conductive Gel: At the clinical level, a conductive adhesive gel is used to bridge the EEG electrode with the skin and scalp. To apply the gel, skin preparation and scratching steps are compulsory, which in turn consumes more time. In addition, the scratching of skin leaves skin lesions. Users may also be allergic to gel. The gel must be washed off afterward. This novel hook-fabric electrode completely avoids the use of conductive gel.

Avoid shaving the head: This electrode has hooks that keep it in the right area as the hooks are entangled with the hair. The end tips of the hook were in contact with the skin and the scalp. Therefore, the EEG measurements were performed without shaving the head.

Convenient for long-term monitoring: Although commercial dry flat electrodes are made of metal, their weight and rigidity render them unsuitable for portable purposes. Dry flat electrodes do not work in the hairy region. Although commercial spike/comb electrodes made of metals and conductive plastics were later introduced for use in hairy areas, they are still heavy and rigid in structure, making them unsuitable for portable purposes. In addition, they can penetrate the skin and cause infections. The hook fabric electrode prevents hair from shaving. In addition, it is lightweight and flexible with textile softness, making it a suitable candidate for long-term monitoring for wearable purposes.

Simple to construct and economical: The hook fabric electrodes can be produced much cheaper than existing dry EEG comb electrodes, i.e. ~1.5 Euro per electrode, while the hook fabric can be produced for less than 1 Euro. In addition, as a textile-based electrode, the hook fabric electrodes give you more freedom to easily design the desired size and shape.

Integrable to textile structures: Hook fabric electrodes can be easily integrated into textile structures, for example, by sewing. Therefore, electrodes are suitable for wearable purposes, where people need them for their daily activities. The electrodes were then washed.

Versatile application: The hook fabric electrode can be used as an EEG, ECG, or EMG electrode. They can also be used by both humans and animals. This versatile application would certainly be useful for the existing electrodes.

Lesser environmental burden: Because a large proportion of their constituents are textiles with the potential to evolve from biodegradable substances and conductive polymers, the introduction of such textile-based electrodes could play a role in minimizing the burden of metallic electrode waste.

7.5. Conclusion

The EEG electrodes currently available on the market are not suitable for long-term monitoring or wearable applications. The introduction of textile electrodes could solve these associated issues. As a result, this research examined textrodes to track brain activity. A textile-based EEG electrode was constructed from a silver-plated hook fabric that collected good-quality EEG signals comparable to standard wet gold cups and Ag/AgCl dry comb electrodes. The hook fabric textrode avoids the use of adhesive conductive gel, and no shaving of the hair is necessary. The skin-to-electrode impedance was lower than that of the dry Ag/AgCl comb electrodes. Moreover, the hook fabric textrode yielded a higher signal-to-noise ratio than the standard wet gold cup electrode. A knitted net bridge EEG cap was also developed and compared with universal EEG bridges. Both the hook fabric textrode and knitted net bridge EEG cap were tried at the clinical level using the Brain Quick® Clinical EEEG Line.

Overall, the hook fabric EEG spectrum gave comparable EEG signals, and ITC, ERSP, and log PSD plots across all main EEG bandwidths. The signal-to-noise ratio was higher than that of standard wet gold cup electrodes. However, the signal-to-noise ratio was slightly lower than that of the Ag/AgCl dry-comb electrode. This can be further solved by improving the hook properties, such as length and thickness. The use of a conductive polymer to explore a new type of hook fabric may boost the signal-to-noise ratio.

Bibliography

[1] T. J. Sullivan, S. R. Deiss, and G. Cauwenberghs, "A Low-Noise, Non-Contact EEG/ECG Sensor," in *2007 IEEE Biomedical Circuits and Systems Conference*, Montreal, QC, Canada, Nov. 2007, pp. 154–157. doi: 10.1109/BIOCAS.2007.4463332.

[2] H. J. Baek, H. J. Lee, Y. G. Lim, and K. S. Park, "Conductive Polymer Foam Surface Improves the Performance of a Capacitive EEG Electrode," *IEEE Trans. Biomed. Eng.*, vol. 59, no. 12, pp. 3422–3431, Dec. 2012, doi: 10.1109/TBME.2012.2215032.

[3] M. Lopez-Gordo, D. Sanchez-Morillo, and F. Valle, "Dry EEG Electrodes," *Sensors*, vol. 14, no. 7, pp. 12847–12870, Jul. 2014, doi: 10.3390/s140712847.

[4] P. Salvo, R. Raedt, E. Carrette, D. Schaubroeck, J. Vanfleteren, and L. Cardon, "A 3D printed dry electrode for ECG/EEG recording," *Sens. Actuators Phys.*, vol. 174, pp. 96–102, Feb. 2012, doi: 10.1016/j.sna.2011.12.017.

[5] J. Lofhede, F. Seoane, and M. Thordstein, "Soft textile electrodes for EEG monitoring," in *Proceedings of the 10th IEEE International Conference on Information Technology and Applications in Biomedicine*, Corfu, Greece, Nov. 2010, pp. 1–4. doi: 10.1109/ITAB.2010.5687755.

[6] W. E. Audette, J. Bieszczad, L. V. Allen, S. G. Diamond, and D. B. Kynor, "Design and Demonstration of a Head Phantom for Testing of Electroencephalography (EEG) Equipment," 2020, doi: 10.13140/RG.2.2.12078.25920.

[7] Wolfram Droh GmbH, "Gold Cup Electrode," *Ternimed*. https://www.ternimed.de/Three-Gold-Cup-Electrodes-with-50-cm-cable (accessed Jan. 02, 2022).

[8] Y. M. Chi, P. Ng, E. Kang, J. Kang, and J. Fang, "Wireless Non-contact Cardiac and Neural Monitoring," p. 9.

[9] Florida Reserach Institute, "Disposable/reusable dry EEG Electrode," *Florida Reserach Institute*. https://fri-fl-shop.com/products/new-longer-5mm-spike-disposable-reusable-dry-eeg-electrode-tde-210?pr_prod_strat=copurchase&pr_rec_id=d440f28f3&pr_rec_pid=6710085845045&pr_ref_pid=6710083321909&pr_seq=uniform (accessed Nov. 04, 2020).

[10] Y.-H. Chen *et al.*, "Soft, Comfortable Polymer Dry Electrodes for High Quality ECG and EEG Recording," *Sensors*, vol. 14, no. 12, pp. 23758–23780, Dec. 2014, doi: 10.3390/s141223758.

[11] A. Delorme and S. Makeig, "EEGLAB: an open source toolbox for analysis of single-trial EEG dynamics including independent component analysis," *J. Neurosci. Methods*, vol. 134, no. 1, pp. 9–21, Mar. 2004, doi: 10.1016/j.jneumeth.2003.10.009.

[12] Q. Zhao and L. Zhang, "Temporal and Spatial Features of Single-Trial EEG for Brain-Computer Interface," *Comput. Intell. Neurosci.*, vol. 2007, pp. 1–14, 2007, doi: 10.1155/2007/37695.

[13] A. Nash-Kille and A. Sharma, "Inter-trial coherence as a marker of cortical phase synchrony in children with sensorineural hearing loss and auditory neuropathy spectrum disorder fitted with hearing aids and cochlear implants," *Clin. Neurophysiol.*, vol. 125, no. 7, pp. 1459–1470, Jul. 2014, doi: 10.1016/j.clinph.2013.11.017.

[14] S. T. Brinker, C. Crake, J. R. Ives, E. J. Bubrick, and N. J. McDannold, "Scalp sensor for simultaneous acoustic emission detection and electroencephalography during transcranial ultrasound," *Phys. Med. Biol.*, vol. 63, no. 15, p. 155017, Aug. 2018, doi: 10.1088/1361-6560/aad0c2.

[15] L. Yang *et al.*, "Insight into the Contact Impedance between the Electrode and the Skin Surface for Electrophysical Recordings," *ACS Omega*, vol. 7, no. 16, pp. 13906–13912, Apr. 2022, doi: 10.1021/acsomega.2c00282.

8. General Conclusion and Future Work

This chapter addresses the general conclusion of the entire Ph.D. work and future works.

Table of Contents

8.1. General Conclusion

An EEG electrode is a small conductive electronic material that is attached to the scalp with wires to track and record electrical impulses in the brain and send brain wave pattern signals to a computer. EEG results show brain activity to diagnose brain conditions and seizure disorders. Electrodes can be categorized as polarizable or non-polarizable. In perfectly non-polarizable, the electrodes require electrically-conductive skin interfacing materials to improve their performance. Whereas in perfectly polarizable, the electrodes work based on the capacitive coupling technique between a conductive material and the skin.

The development of EEG electrodes has attracted many researchers in producing flexible, lightweight, and washable wearable electronics. Some attempts have been reported to develop textile-based EEG electrodes ranging from the use of metal-coated to conductive polymer-coated textile fabrics, and through different techniques.

In this dissertation, entirely textile-based EEG electrodes have been developed. The ultimate objective was to explore flexible, lightweight, and washable textile-based EEG electrodes from a PEDOT:PSS-printed textile fabric for wearable applications.

The work started with producing a fabric that conducts electrically and owns characteristics of normal textile fabric, suitable as bio-potential electrodes, and ended up with constructing textile-based dry EEG electrodes. Based on the comprehensive literature reviews of Chapters 2 and 3 the concept of the textile-based electrode (textrode) was chosen. It consists of a PEDOT:PSS/PDMS conductive polymer printed on a cotton fabric via screen printing. This allows the development of flexible, lightweight, and washable electrodes thus collecting EEG signal qualities comparable to commercial dry electrodes.

Chapter 4 was aimed at the development of conductive textile fabric. It is interesting to note that from the experiment a wide range of sheet resistance (67.72 Ω/sq to 90.8 kΩ/sq) has been obtained by varying PDMS to PEDOT:PSS ratio and PEDOT:PSS/PDMS add-on. The research looked into the use of conductive polymer composites to achieve adequate flexibility and conductivity at the same time. The fabrics stayed conductive after washing and stretch to their infliction point. PDMS improved surface resistance recovery after stretching release, and PEDOT:PSS/PDMS-printed fabrics remained electrically conductive for more stretching cycles than PEDOT:PSS-printed fabric. We also discovered that increasing the add-on of the conductive polymer composite can reduce surface

resistance even further. These various electrical resistance characteristics could be chosen based on the application, such as sensors, interconnections, antennas, storage, and so on. The inference from this experiment is that a PEDOT:PSS/PDMS-printed conductive fabric can be used to develop different formats of textile-based sensors. As a proof of concept, entirely textile-based strain, moisture, ECG, and EEG electrodes were developed.

For example, a conductive fabric was used to create a washable strain and moisture sensor that provided fairly stable sensing stability up to 40% elongation and 150% moisture regain. These sensors could be used to detect stretching in bicyclists, sweat and urine in babies and the elderly, and the extent of swelling in peripheral edema, among other things. Furthermore, an ECG signal comparable to the dry Ag/AgCl electrode has been investigated for use in a wearable application.

Besides, the physical property of the conductive fabric like tensile strength and elongation at break, bending length, and its respective flexural rigidity were evaluated. The fabric owns normal textile characteristics and behaves as a twill ¼ cotton fabric or a twill 2/1 kermel/viscose. The presence of the conductive polymer composite on the fabric was confirmed by SEM and FT-IR.

Chapter 5 has addressed the construction of EEG textrodes and the comparison of impedance and signal quality against commercial dry electrodes. Since the focus of this work was to create a textile-based EEG textrode, a fabric with possible lower sheet resistance from Chapter 4 was selected. And then, BTCA was added to the conductive polymer composite to improve the washing fastness. The skin-to-electrode impedance and signal qualities have been achieved strongly comparable to commercial dry electrodes. An analysis using EEGLAB gave a dB of 95, the same as the commercial dry electrode.

This chapter also describes the robustness of the textrode to washing and bending, as well as multiple and continuous use. The effect of textrode size and shape on signal quality has been also evaluated. It was achieved that the textrode is able to collect clear EEG waves comparable to commercial dry EEG electrodes up to 15 washes, 60 bending cycles, 5 multiple uses, and 8 hours of continuous use. A 2 cm diameter circular electrode was found to provide optimum size and shape.

Chapter 6 was focused on the validation of the EEG textrode via head phantoms. An anatomically realistic gelatin-based and textile-based head phantoms were constructed. It was found that the textile-based head phantom has a good

agreement with the gelatin-based. From the validation via head phantoms, the textrode has given stable and reproducible impedance and EEG signals at all the EEG bandwidths.

The new textile-based head phantom is significantly lighter (-91.67%), than the gelatin-based counterpart, weighing 0.5 and 6 kg, respectively. This makes it easier to handle and move from one location to another. Furthermore, it is not as delicate as the ballistic gelatin-based one, where the shape of the ballistic gelatin can be distorted and decayed quickly even when kept in a refrigerator. In our case, the gelatin-based head phantom began decaying after a week of construction, which could also be influenced by the weather where it is tested. The textile-based head phantom, on the other hand, does not decay for years. All of this will play a huge role in terms of economics and sustainability.

Chapter 7 presents a different approach with a dry EEG textrode constructed from a silver-plated hook fabric that can be used on a hairy scalp without shaving the head. The skin-to-electrode impedance was found to be better than commercial dry Ag/AgCl comb electrodes. The signal qualities collected at a clinical level were promising and comparable to commercial dry Ag/AgCl comb electrodes. Moreover, the novel hook fabric EEG textrode has flexibility, a low weight, and economical advantage over commercial dry Ag/AgCl comb electrodes.

Hook fabric electrodes are significantly less expensive than existing dry EEG comb electrodes, which cost 1.5 Euros per electrode, while hook fabric electrodes cost less than 1 Euro. Furthermore, as a textile-based electrode, hook fabric electrodes allow you to easily design the desired size and shape. It is suitable for use as an EEG, ECG, or EMG electrode. It is also suitable for both humans and animals. This versatile application would undoubtedly be beneficial to the existing electrodes.

The use of such textile-based electrodes may help to reduce the burden of metallic electrode waste because the base material is textiles with the potential to evolve from biodegradable substances and conductive polymers. Furthermore, the hook fabric electrodes' flexibility and low weight make them suitable for integration into textile structures and convenient for long-term monitoring. Overall, this study opens the way for long-term EEG monitoring and the use of wearable application devices.

8.2. Future Work

The ultimate objectives of this dissertation, the development of textile-based dry EEG electrodes to monitor brain activity, have been already achieved, however, the work has explored many aspects suited for further research work. The following could be taken into consideration for future work:

8.2.1. PEDOT:PSS/PDMS-Printed Cotton EEG Textrode

This dissertation has been predominantly focused on the use of PEDOT:PSS/PDMS-printed cotton fabric for producing the EEG textrode. The electrical conductance of the fabric drops fast over time however, therefore, improving the stability of conductivity over time would be future work to bring better textrodes for wearable applications. The PEDOT:PSS-based textrodes are flat and can only be placed on hair-free skin or scalp, so, developing PEDOT:PSS/PDMS-printed textile-based textrodes with hooks could be considered for this technique. Further work can also address the effect of the textile substrate and the fabric construction on the performance of the skin-to-electrode impedance and EEG signal. Another future work possibility could be to improve the washing cycle and multiple uses of the electrodes by incorporating long-lasting fixing agents with less/no impact on signal qualities.

8.2.2. Hook Fabric EEG Textrode

The hook fabric EEG textrode gave comparable EEG signals and ITC, ERSP, and log PSD plots across all main EEG bandwidths. However, the signal-to-noise ratio was found to be slightly lower than that of the dry Ag/AgCl comb electrode. This could be further solved by improving the hook properties such as its length and thickness. The use of conductive polymer to explore a new type of hook fabric may also boost the signal-to-noise ratio. Therefore, the future work is to optimize the design of the hook fabric textrode and also use it for ECG and EMG measurements with humans and animals.

8.2.3. Textile Head Phantom

We used conductive textile fabric to mimic the scalp and the brain activity on the scalp. However, in order to complete the head phantom, the hair, skull, and brain must also be mimicked. Therefore, another future work is to create a complete set of long-lasting head phantoms.

8.2.4. Clinical Validation

To commercialize biopotential electrodes, clinical validation involving a large number of test subjects is required. Furthermore, in order to use the electrodes for clinical diagnosis, it may be necessary to conduct tests on patients. Therefore, future work is to conduct an in-depth clinical validation with the optimized electrodes.

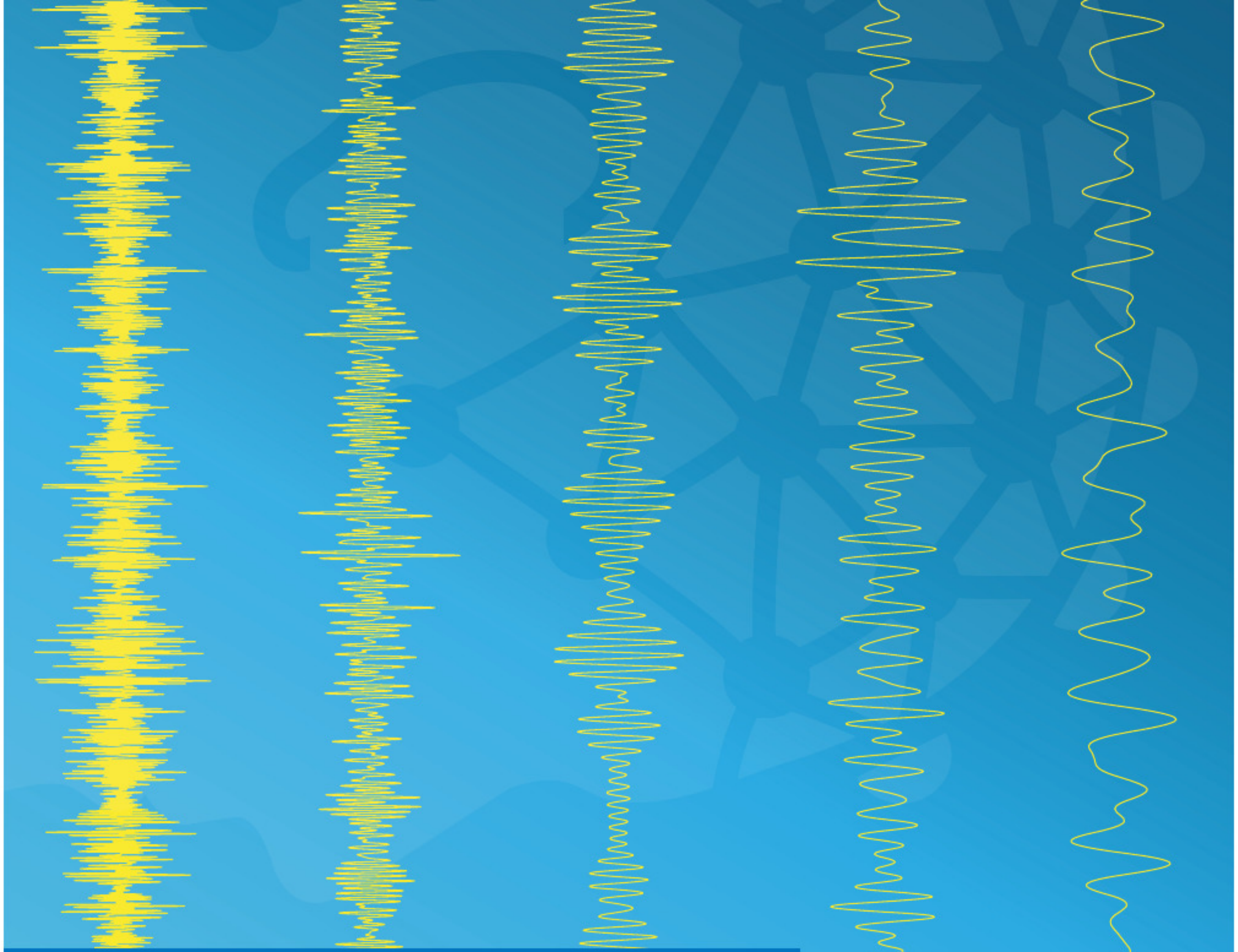

EEG measures the electrical activity of neurons that extend to the scalp to detect abnormalities in brain waves.